Nmr studies of zeolites and related materials

Appleyard, Ian Peter

NMR STUDIES OF ZEOLITES AND RELATED MATERIALS

by

IAN PETER APPLEYARD, B.Sc. (Hons), G.R.S.C.

(Collingwood College)

A thesis submitted for the degree of Doctor of Philosophy of the University of Durham.

September 1986

MEMORANDUM

The work for this thesis has been carried out in the School of Chemical Sciences at the University of East Anglia between October 1983 and September 1984, and in the Department of Chemistry at the University of Durham between October 1984 and September 1986. It is the work of the author unless otherwise stated. None of the work has been submitted for any other degree.

To my parents and Karen

ACKNOWLEDGEMENTS

I would like to thank my supervisors, Professor R.K. Harris and Dr. F.R. Fitch (Laporte Industries Limited, Widnes) for their guidance and patience during the course of this research. I would like also to thank Pete Croskerry (Laporte) for the preparation of samples and Mr. John Dwyer (UMIST) for supplying me with two Ti-ZSM-5 samples. I am indebted to the people working in the Analytical Section at Laporte for numerous powder XRD traces and chemical analyses.

Much laughter has been shared with present and past members of the NMR Research Groups at UEA and Durham. For their friendship and encouragement, I would like to thank them all.

I would also like to thank the BZA Committee for providing the financial support to enable me to attend three excellent and informative conferences.

Finally, I would like to thank the SERC and Laporte Industries Limited for financial support under the CASE studentship scheme and my typist for his excellent work.

NMR STUDIES OF ZEOLITES AND RELATED MATERIALS

by

Ian Peter Appleyard

ABSTRACT

Magic-angle spinning NMR has been used for the first time to investigate two new classes of molecular sieve-type materials.

Firstly, various substituted high-silica (ZSM-5-type) molecular sieves have been studied. The substituting elements (B, Fe, Cr, Ti, La) are (with the exception of boron) unobservable by NMR and so the effects of their substitution are observed indirectly by ^{29}Si NMR. Calcination (thermal treatment in air) affects the ^{29}Si NMR spectra of several of the samples. Substitution of paramagnetic elements (Fe, Cr) affects the ^{29}Si NMR spectra causing substantial line broadening and the appearance of spinning sidebands. The use of other spectroscopic methods of investigation combined with NMR measurements yields a considerable amount of information concerning the environment(s) of the substituting elements.

Secondly, several members of a new class of crystalline microporous molecular sieves based on three-dimensional frameworks of phosphorus and aluminium have been studied. Heteroatom substitution (Si, B) into molecular sieves possessing novel and zeolite-related structures has been investigated and the general mode of silicon substitution has been elucidated. Again, calcination produces significant changes in the NMR spectra of these samples. Ordering of the aluminium and phosphorus framework tetrahedra is normally one of direct alternation in which case unique resonances are observed in the ^{27}Al and ^{31}P NMR spectra. For several framework structures, crystallographically inequivalent sites exist, and ^{31}P NMR (also ^{29}Si NMR) is particularly sensitive to this phenomenon. ^{31}P CP NMR provides information on the interaction of the organic template with the framework and on the possible sources of proton reservoir necessary for the CP experiment.

KEY TO ABBREVIATIONS USED

AlPO = aluminophosphate
SAPO = silicoaluminophosphate
SBU = secondary building unit
CP = cross-polarization
CSA = chemical shielding anisotropy
efg = electric field gradient
ZSM = Zeolite Sircony Mobil
TPD = temperature programmed desorption
FTIR = Fourier transform infrared
SEM = scanning electron microscopy
MES = multi-element scan
SF = spectrometer frequency
CT = CP contact time
RD = recycle delay
NT = number of transients
FID = free induction decay
SW = spectral width
SI = number of data points acquired
TD = time domain points
SS = spinning speed
SR = reference frequency
LB = line broadening
PD = pulse duration
PA = pulse angle
NMR = nuclear magnetic resonance
MAS = magic-angle spinning
SSB = spinning sideband
HPD = high-power proton decoupling
SPE = single-pulse excitation
ESR = electron spin resonance
XRF = X-ray fluorescence
XRD = X-ray diffraction
UCC = Union Carbide Corporation

CONTENTS Page No.

CHAPTER ONE - INTRODUCTION

1.1 A brief history of zeolite discovery and synthesis 2

1.2 The scope of the work 4

1.3 Background: NMR 6

CHAPTER TWO - SOLID-STATE NMR THEORY

2.1 Introduction 8

2.2 Magnetic Dipole-Dipole Coupling 9

2.3 Magnetic Shielding (Chemical Shift) 13

2.4 Nuclear Electric Quadrupole Coupling 15

2.5 Cross-Polarization 22

CHAPTER THREE - LITERATURE REVIEW OF NMR STUDIES OF ZEOLITES AND RELATED MATERIALS

3.1 Introduction 29
3.1.1. Definition of a zeolite 29
3.1.2. Structure and properties of natural and synthetic zeolites 30
3.1.3. Techniques for structural characterisation 41

3.2 Solid-state NMR of silicates and aluminosilicates 43
3.2.1. ^{29}Si studies 46
3.2.2. ^{27}Al studies 63
3.2.3. Monitoring of chemical modifications of zeolites 67
3.2.4. Precursors in zeolite synthesis 77

3.2.5. Other NMR studies of zeolites 79

3.3 Isomorphous framework substitution in zeolites 82
3.3.1. Framework substitution by elements other than Si or Al as studied by NMR 88

3.4 Novel zeolite related molecular sieve type materials and their study by solid-state NMR 91
3.4.1 Aluminophosphate molecular sieves 92
3.4.2 Silicoaluminophosphate molecular sieves 96
3.4.3 Other substituted $AlPO_4$ molecular sieves 98

CHAPTER FOUR - EXPERIMENTAL

4.1 Introduction 100

4.2 Sample Synthesis and Procurement 100
4.2.1. Substituted ZSM-5-type molecular sieves 102
4.2.2. Aluminophosphate and substituted aluminophosphate molecular sieves 102
4.2.3. Natural minerals and other samples. 103

4.3 Sample Analysis 103
4.3.1. X-ray diffraction (XRD) 104
4.3.2. Chemical analysis 104
4.3.3. Other techniques
(a) Scanning electron microscopy (SEM) 105
(b) Magnetic susceptibility measurements 105
(c) ESR measurements 105

4.4 Sample Handling and Treatment 105
4.4.1. Calcination 106
4.4.2. Dehydration/rehydration 106

4.5 NMR Instrumental Considerations 106
4.5.1. General (a) Pulse sequences 107
(b) Magic-angle spinning (MAS) 109

(c) Hartmann-Hahn matching in the CP experiment 110
(d) Recycle times 111
(e) Chemical shift referencing and errors 111
(f) Linewidth measurement 113
(g) Spectral manipulation 113
4.5.2. Quadrupolar nuclei: ^{27}Al
(a) Problems encountered 114
(b) Establishment of the correct "setting-up" procedure. 124

CHAPTER FIVE - NMR RESULTS FOR VARIOUS SUBSTITUTED ZSM-5-TYPE MOLECULAR SIEVE MATERIALS

5.1 Introduction 129

5.2 High-silica zeolites 129
5.2.1. B-ZSM-5 (Boralite) 130
5.2.2. Fe-ZSM-5 (Ferrisilicate) 137
5.2.3. Cr-ZSM-5 (Chromosilicate) 151
5.2.4. Ti-silicalite/Ti-ZSM-5 155
5.2.5. La-ZSM-5 160

5.3 Viséite 162

5.4 Conclusions and Recommendations for Further Work 170

CHAPTER SIX - NMR RESULTS FOR VARIOUS MOLECULAR SIEVE TYPE MATERIALS BASED ON ALUMINOPHOSPHATE FRAMEWORKS.

6.1 Introduction 174

6.2 Aluminophosphates ($AlPO_4$-n) 174
6.2.1. $AlPO_4$-5 175
6.2.2. $AlPO_4$-11 184

6.3 Silicoaluminophosphates (SAPO-n) 192
6.3.1. SAPO-5 193
6.3.2. SAPO-20 209
6.3.3. SAPO-34 216

6.4 Other substituted aluminophosphate molecular sieves 224
6.4.1. BAPO-5 224

6.5 General Discussion of Results 231

6.6 Conclusions and Recommendations for Further Work 235

PUBLICATIONS, COLLOQUIA, AND CONFERENCES 238

REFERENCES 246

CHAPTER ONE - INTRODUCTION

1.1 History of zeolite discovery and synthesis

For over thirty years synthetic molecular sieve zeolites have been an important class of industrial materials.[1] They were introduced in 1954 as adsorbents for industrial separations and purifications. Since that time, this unique class of materials has generated a mass of scientific literature describing their synthesis, properties, structure, and applications.

The theme in research on molecular sieve zeolite materials has been the quest for new structures and compositions, the idea being that novel and useful properties would result from the discovery of these new compositions and structures. The first generation materials were "low-silica" or aluminium-rich zeolites. The discovery of zeolites A and X represented a fortunate optimum in composition, pore volume, and channel structure, guaranteeing these two zeolites their lasting commercial prominence out of more than 120 synthetic species known and discovered since the middle 1950's. The next evolution in zeolite materials was the impetus to synthesise more siliceous zeolites, primarily to improve stability characteristics. Zeolite type Y was the first of these "intermediate silica" zeolites to be synthesised, and was commercially introduced in 1959 in catalytic applications involving hydrocarbon conversion. The most recent stage in the quest for more siliceous molecular sieve compositions was achieved in the late 1960's and early 1970's with the synthesis of the "high-silica zeolites", compositions exemplified by ZSM-5 discovered by Argauer and Landolt. Subsequently many other ZSM-zeolites have been described. These compositions are molecular sieve zeolites with Si/Al ratios of 10 to 100 or higher, the end member of this pentasil series being silicalite, essentially

aluminium-free ZSM-5.

An alternate method for producing highly siliceous zeolite compositions had its beginnings in the mid-1960's when thermochemical modification reactions that lead to framework dealumination were first reported. Thus "ultrastable" and other dealuminated forms of zeolites emerged, the focus in the late 1960's being on their improved stability characteristics and catalytic applications.

More recently,[2] chemical modification of "high-silica zeolites" has led to the production of materials with some chemical compound incorporated in the channels. For instance, in the case of ZSM-5 type zeolite, the introduction of compounds of P, Mg, B, Zn, Sb, Si... has resulted in an improvement of selective *p*-xylene formation by toluene alkylation with methanol.

In an attempt to synthesise novel zeolite materials with different catalytic or thermal properties, zeolitic structures again related to ZSM-5 have been obtained. Isomorphous substitution into this high-silica zeolite has resulted in the preparation of B-ZSM-5 (borosilicate), Fe-ZSM-5 (ferrisilicate), Cr-ZSM-5 (chromosilicate) and many other related materials.

The Union Carbide Corporation has in the last few years pursued the synthesis of molecular sieves containing other elements apart from silicon. Phosphorus is known to form tetrahedrally coordinated oxide frameworks and this line of investigation culminated in the synthesis of aluminophosphate molecular sieves (acronym AlPO), which were patented in 1982. The pentavalency and trivalency of P and Al respectively do not result in a supplementary negative charge as is observed in aluminosilicate zeolites, and consequently no acidity is to be expected. However, the substitution of silicon or another metallic oxide (or combination of metallic oxides) into the aluminophosphate framework

resulted in the discovery of a family of structures parallel to that of the aluminophosphates, with variable Al and P contents. These materials are expected to have catalytic and molecular sieve properties similar to those observed for zeolites, and indeed, are beginning to find applications in catalysis and other important ares of the chemical process industry.

1.2 The scope of the work

The first publications concerning solid-state NMR (silicon-29) and zeolites (both natural minerals and synthetic aluminosilicates) appeared in 1980. Since then, solid-state NMR has made many important contributions to our knowledge of various zeolite structures and zeolite chemistry as a whole. However, prior to 1983 (the beginning of the work presented here), the major drive was in the area of aluminosilicate structure determination.

With the advent of isomorphous substitution in zeolites and the synthesis of aluminophosphate and later silicoaluminophosphate (SAPO) molecular sieves comes the possibilty of using multinuclear solid-state NMR for their investigation and structural characterization. The work reported herein is an attempt to determine the applicability of existing solid-state NMR techniques when used for the analysis of novel zeolite-related materials.

A variety of structures have been studied, both novel and zeolite-type, and wherever possible other analytical techniques have been used to provide supplementary information to that obtainable from solid-state NMR. Development work has included the use of various benign nuclei and

the establishment of correct procedures for the observation of quadrupolar nuclei, (specifically aluminium-27). The synthetic zeolite-related samples were all synthesised at Laporte Industries Limited, Widnes. Several natural minerals and zeolites have been studied whose structures are related to those of molecular sieves of interest.

Chapter Two outlines the various magnetic interactions present in solid-state NMR and describes the effects of line-narrowing and sensitivity enhancing techniques that have been developed to allow the production of high-resolution NMR spectra of solids.

Chapter Three is a literature review chapter. It deals with the more familiar aspects of zeolite chemistry and the important contributions solid-state NMR has made to zeolite science. Special attention is paid to the relatively new areas of isomorphous substitution in high-silica zeolites and the synthesis of novel zeolite-related molecular sieve type materials. To date, there have been very few reported NMR studies on either isomorphous subsitution in tectosilicates or on novel molecular sieve materials.

Chapter Four is the experimental chapter. It includes sample synthesis and general sample characterisation procedures as well as solid-state NMR instrumental considerations. Details are given of problems encountered with the observations of quadrupolar nuclei, and the methods adopted for the solution of those problems.

Chapters Five and Six are devoted to the presentation and discussion of NMR results obtained for various samples belonging to two related areas (1) isomorphous substitution in ZSM-5, and (2) aluminophosphate and related novel zeolite-like molecular sieve materials.

1.3 Background: NMR

The theory of the NMR experiment and the techniques and equipment necessary for achieving high-resolution spectra of solids are now well established.[3-5] Consequently in the following chapter only the interactions present in the solid-state, and how the solid-state NMR spectroscopist selectively averages the interactions to yield useful information will be reviewed. Expressions for the magnetic interactions will be presented and discussed with special emphasis on the aspects relevant to the study of aluminosilicates and other zeolite-like materials.

CHAPTER TWO - SOLID-STATE NMR THEORY

2.1 Introduction

The NMR spectra of solids are very much broader than those of liquids. The origin of this difference lies in the anisotropic interactions to which the nuclei are subject. In mobile fluids, the rapid isotropic motions of the nuclei average the anisotropic interactions and effectively remove them from the spectrum. As a consequence, NMR spectra of mobile liquids are of high-resolution and are often of great value to the structural and dynamical analysis of molecules. Complementary information to that obtainable for liquids is available for solids, such as polycrystalline materials, for instance zeolites, using solid-state NMR. However, several, now well-established, line-narrowing techniques have to be employed, and these are:

(i) high-power (dipolar) decoupling of abundant spins (protons) to eliminate heteronuclear dipolar interactions as a source of broadening;

(ii) magic-angle rotation [magic-angle spinning (MAS)] to reduce shielding constants (and scalar heteronuclear coupling constants) to their isotropic averages, and to eliminate homonuclear (rare spin) dipolar interactions (and weak dipolar interactions of rare spins to heteronuclei other than protons);

(iii) multi-pulse decoupling of abundant spins to eliminate strong homonuclear dipolar interactions (if any).

To overcome inherent sensitivity problems associated with the observation of rare spins, cross-polarization (CP) between protons and the rare spin systems by heteronuclear double resonance under the Hartmann-Hahn condition can be performed in favourable cases where high abundances of protons are present. This chapter outlines the important

anisotropic nuclear interactions that are of interest in solid-state NMR, and considers how these interactions are selectively removed to yield spectra comparable with those from fluids. The theory of cross-polarization is also discussed. For a more thorough treatment of the phenomena associated with NMR, the reader is referred to the monographs of Abragam,[6] Slichter,[5] Haeberlen,[4] Mehring,[3] Harris,[7] and articles by Andrew.[8]

2.2 Magnetic Dipole-Dipole Coupling

Classically, two magnets a distance, r, apart have an energy of interaction as expressed in Equation 2.1.

$$U = \left\{ \frac{\underset{\sim}{\mu_1} \cdot \underset{\sim}{\mu_2}}{r^3} - 3.\frac{(\underset{\sim}{\mu_1} \cdot r)(\underset{\sim}{\mu_2} \cdot r)}{r^5} \right\} \frac{\mu_0}{4\pi} \quad \ldots \quad (2.1)$$

where $\underset{\sim}{\mu_1}$ and $\underset{\sim}{\mu_2}$ are the two magnetic dipole moments and $\underset{\sim}{\mu_0}$ (the permeability constant) is $4\pi \times 10^{-7}$ kg m s^{-2} A^{-2}. Such an interaction can also occur between two nuclear spin magnetic moments. The appropriate quantum mechanical expression, Equation 2.2, is obtained by using $\hat{\underset{\sim}{\mu}}_i = \gamma\hbar\hat{\underset{\sim}{I}}_i$ where i = 1,2:

$$\hat{\mathcal{H}}_{DD} = \gamma_1\gamma_2\hbar^2.\left\{ \frac{\hat{\underset{\sim}{I}}_1 \cdot \hat{\underset{\sim}{I}}_2}{r^3} - 3.\frac{(\hat{\underset{\sim}{I}}_1 \cdot r)(\hat{\underset{\sim}{I}}_2 \cdot r)}{r^5} \right\} \frac{\mu_0}{4\pi} \quad \ldots \quad (2.2)$$

where γ is the magnetogyric ratio [defined as the ratio of the magnetic moment $(\underset{\sim}{\mu})$ to the angular momentum $(\underset{\sim}{P})$] and $\hat{\underset{\sim}{I}}_1$ is the nuclear spin operator for nucleus 1. Equation 2.2 may be written in polar coordinates (r, θ, ϕ) and by evaluating the scalar products and introducing $\hat{\underset{\sim}{I}}_{1+}$ and $\hat{\underset{\sim}{I}}_{1-}$ (the "raising" and "lowering" spin operators), Equation 2.3 is obtained, where the six terms A to F are given in equations 2.4 to 2.9.

$$\hat{\mathcal{H}}_{DD} = r^{-3}\gamma_1\gamma_2\hbar^2.[A + B + C + D + E + F].\frac{\mu_o}{4\pi} \quad \ldots \quad (2.3)$$

$$A = -\hat{I}_{1_z}.\hat{I}_{2_z}.(3\cos^2\theta - 1) \quad \ldots \quad (2.4)$$

$$B = 1/4\ [\hat{I}_{1_+}.\hat{I}_{2_-} + \hat{I}_{1_-}\hat{I}_{2_+}]\ (3\cos^2\theta - 1) \quad \ldots \quad (2.5)$$

$$C = -3/2\ [\hat{I}_{1_z}.\hat{I}_{2_+} + \hat{I}_{1_+}.\hat{I}_{2_z}]\ \sin\theta.\cos\theta.\exp(-i\phi) \quad \ldots \quad (2.6)$$

$$D = -3/2\ [\hat{I}_{1_z}.\hat{I}_{2_-} + \hat{I}_{1_-}.\hat{I}_{2_z}]\ \sin\theta.\cos\theta.\exp(i\phi) \quad \ldots \quad (2.7)$$

$$E = -3/4.\hat{I}_{1_+}.\hat{I}_{2_+}\sin^2\theta.\exp(-2i\phi) \quad \ldots \quad (2.8)$$

$$F = -3/4.\hat{I}_{1_-}.\hat{I}_{2_-}.\sin^2\theta.\exp(2i\phi) \quad \ldots \quad (2.9)$$

For non-viscous fluids, the dipolar interaction does *not* affect the transition energies or the intensities of an NMR spectrum as the isotropic average, $\overline{\cos^2\theta} = 1/3$, due to thermal motion of molecules in fluids, averages the dipolar interaction to zero. This allows the chemically important chemical shifts and splittings due to scalar couplings, both of which are usually smaller than the dipolar interaction strengths, to be revealed. Equation 2.3 can be rewritten in a truncated form involving only secular terms. Equation 2.10 shows the (truncated) dipolar Hamiltonian expressing the dipolar interaction between two like spins:[8]

$$\hat{\mathcal{H}}_{DD} = R(1 - 3\cos^2\theta)[\hat{I}_{1_z}.\hat{I}_{2_z} - 1/4(\hat{I}_{1_+}.\hat{I}_{2_-} + \hat{I}_{1_-}.\hat{I}_{2_+})] \quad \ldots \quad (2.10)$$

where $R = \left[\frac{\mu_o}{4\pi}\right].\gamma^2.\left[\frac{\hbar^2}{2\pi}\right].r^{-3}$

For the case of two unlike spins, I and S (heteronuclear case), the expression for the (truncated) dipolar interaction reduces to Equation 2.11:

$$\hat{\mathcal{H}}_{IS} = -\frac{\mu_o\hbar^2\gamma_I\gamma_S}{4\pi}\frac{}{r_{IS}^3}\hat{I}_z.\hat{S}_z.(3\cos^2\theta_{IS} - 1) \quad \ldots \quad (2.11)$$

The dipolar interaction can be eliminated by: (i) random rotation of molecules in fluids or of adsorbed molecules such as water in the pores of zeolites, averaging the dipolar interaction $\hat{\mathcal{H}}_{DD}$ to zero, as the

isotropic average, $\cos^2\theta = 1/3$; or (ii) rapid specimen rotation with an angular velocity, ω_r, about an axis, β, to the static magnetic field, $\underset{\sim}{B_o}$, (see Figure 2.1).

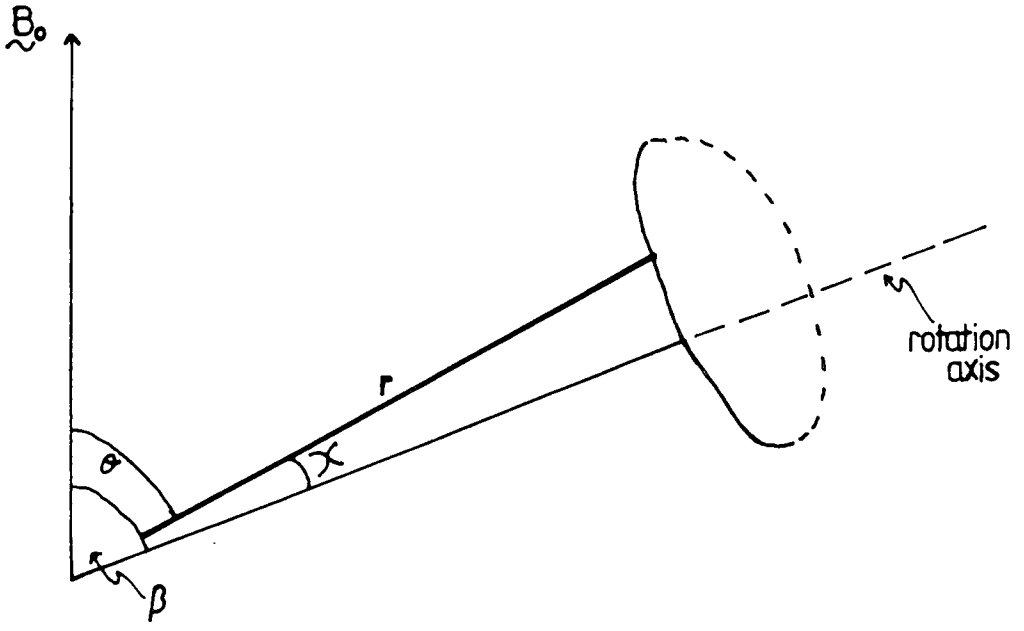

Figure 2.1

Macroscopic sample rotation at an angle to the applied magnetic field, $\underset{\sim}{B_o}$.

It has been shown that:[8]

$$\langle 3\cos^2\theta - 1\rangle = 1/2(3\cos^2\beta - 1)(3\cos^2\chi - 1) \quad \ldots \quad (2.12)$$

The parameter, χ, is fixed for a rigid solid, though (like θ) it takes all possible values if the material is a powder. The term $1/2(3\cos^2\beta - 1)$ therfore acts as a scaling factor on dipolar powder patterns. The angle β is under the control of the experimentalist. If $\beta = 0$, $1/2(3\cos^2\beta - 1) = 1$, so there is no net effect on the spectrum. If $\beta = \pi/2$, $1/2(3\cos^2\beta - 1) = -1/2$, so the powder pattern is scaled by a factor of two, and a mirror image is obtained. However, the dipolar pattern for the two spin case is symmetrical, and so only the scaling is

observable. Rotation about an axis making an angle $54^{o}44'$ (the so-called "magic-angle") is the most interesting case, since then $\cos\beta = 1/\sqrt{3}$ and $1/2(3\cos^{2}\beta - 1) = 0$, so that $\langle 3\cos^{2}\theta - 1\rangle = 0$ for all orientations (*i.e.* all values of χ). Thus, just as for isotropic tumbling, the dipolar interaction is averaged to zero, and so dipolar broadening is eliminated, giving much higher resolution. In principle, because both equations 2.10 and 2.11 (relating to homo- and heteronuclear dipolar interactions respectively) contain the geometric term $(3\cos^{2}\theta - 1)$, the technique of magic-angle rotation (MAR), [or magic-angle spinning (MAS)], applies in both cases. However, the rate of rotation has to be of the order of, or greater than, the static bandwidth expressed in Hz. For heteronuclear dipolar interactions even if the spinning frequency is less than the static bandwidth, line broadening can be eliminated, and spinning sidebands (SSB) appear equidistant from the resonance line at multiples of ω_{r}. For homonuclear interactions where the static bandwidth can be as large as 50 kHz, MAS cannot, at present, be used to narrow the resonance line. (In the case of dilute spins such as ^{13}C or ^{29}Si, homonuclear dipolar interaction between these spins is small due to the large internuclear distances). High-power (dipolar) decoupling of abundant spins (protons), I, coupled to rare spins, S, is achieved by irradiating the I nuclei at their resonance frequency while observing the resonance of nucleus, S. This technique is completely analogous to the low-power decoupling used in liquid-state NMR. Obviously, as the strength of the interaction is greater in solids, greater r.f. power (several hundred watts) is necessary to achieve decoupling in solid-state NMR.

(iii) When the dominant dipolar interactions are homonuclear, for instance with ^{1}H or ^{19}F, neither MAS nor high-power decoupling can be used to achieve line-narrowing. In such instances, multiple-pulse-cycle

sequences are used to time-average the scalar product spin terms in the Hamiltonian (Equation 2.10) not affected by rotation.[3-5] Multi-pulse decoupling is, in general, not necessary for the study of zeolites or related materials, as due to -OH mobility, MAS is sufficient to eliminate dipolar interactions.

2.3 Magnetic shielding (Chemical Shift)

Nuclear spins are shielded from the applied field, $\underset{\sim}{B}_o$, by the surrounding electrons, such that the field experienced by a nuclear moment, i, is expressed by Equation 2.13:

$$\underset{\sim}{B}_i = (1 - \underset{\approx}{\sigma}_i).\underset{\sim}{B}_o \quad \ldots \quad (2.13)$$

where $\underset{\approx}{\sigma}_i$ is the shielding tensor for spin i. The tensor nature of $\underset{\approx}{\sigma}$ expresses the fact that the resonance frequency of a nucleus in a non-cubic site of a molecule, depends on the orientation of that molecule with respect to $\underset{\sim}{B}_o$. Generally speaking, a nuclear environment will have its shielding characterised by two (for the case of axial symmetry) or three unique values (for symmetry lower than axial). The three values are referred to as the principal components and occur for orientations specified by the principal axes in a molecule-fixed system. In the general case, the observed shielding constant is denoted σ_{zz} and is given by Equation 2.14:

$$\sigma_{zz} = \{\sigma_{iso} + \delta/2[(3\cos^2\theta - 1) + \eta.\sin^2\theta.\cos2\theta]\} \quad \ldots \quad (2.14)$$

where $\sigma_{iso} = 1/3.\mathrm{Tr}\ \underset{\approx}{\sigma} = 1/3(\sigma_{xx} + \sigma_{yy} + \sigma_{zz})$;

δ (the chemical shift anistropy) is $(\sigma_{zz} - \sigma_{iso})$;

η (the asymmetry parameter) $= \sigma_{yy} - \sigma_{xx}/(\sigma_{zz} - \sigma_{iso}) = \sigma_{yy} - \sigma_{xx}/\delta$

using the convention $|(\sigma_{zz} - \sigma_{iso})| \geq |(\sigma_{xx} - \sigma_{iso})| \geq |(\sigma_{yy} - \sigma_{iso})|$.[4] In solution, with molecules tumbling rapidly and isotropically, substantial averaging of $\underset{\approx}{\sigma}$ occurs, so that only one third of the trace ($1/3$ Tr $\underset{\approx}{\sigma}$) is observed ($\sigma_{iso}$).

For a microcrystalline powder sample, the distribution of nuclear orientations of the crystallites results in all possible frequencies of chemical shift being observed simultaneously, giving a powder pattern. The magnitude of the shielding anisotropy is such that overlapping of powder patterns is likely to occur if more than one resonance line is present in the NMR spectrum. However, inspection of Equation 2.14 shows us that the equation for the observed shielding constant consists of an isotropic and an anisotropic part. The latter contains the $1/2(3\cos^2\theta - 1)$ term, that we have already seen can be made zero by spinning the sample at the magic-angle. Spinning at rates lower than the shielding anisotropy (expressed in Herz), results in the formation of spinning sidebands. According to the Hamiltonian for chemical shift (Equation 2.15), shielding anisotropy varies linearly with static

$$\hat{\mathcal{H}}_{cs} = \gamma\hbar\sigma_{zz}\underset{\sim}{B_0}\hat{\underset{\sim}{I}}_z \quad \ldots \quad (2.15)$$

magnetic field. At lower magnetic field strengths, relatively modest MAS speeds are needed to average the CSA, at higher magnetic field strengths however, achievable MAS speeds (3-5 kHz) are no longer of the order of the shielding anisotropy, and so the spectra can be cluttered with spinning sidebands. This of course depends on the size of the CSA interaction present in the sample.

2.4 Nuclear Electric Quadrupole Coupling (for I = n/2; n = 3,5,7,9).

Nuclei with spin quantum numbers greater than 1/2 have an ellipsoidal charge distribution (Figure 2.2). Because of this ellipsoidal charge, nuclei with spin > 1/2 possess a quadrupole moment

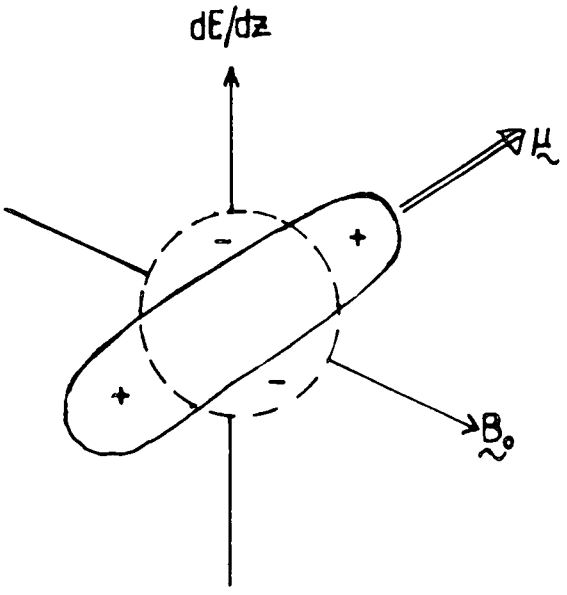

Figure 2.2

A nuclear electric quadrupole moment showing the equivalent sphere of charge. Compression results in the formation of two antiparallel electric dipoles. The magnetic moment is shown as colinear with the major axis of the charge ellipsoid.

(eQ) which may interact with electric field gradients (efg) present in the solid. Quadrupolar nuclei also possess angular momentum, the nuclear magnetic moment being parallel to one of the axes of the ellipsoid. Thus the nucleus is subject to two opposing forces when placed in an external magnetic field. The magnetic moment wishes to align itself along $\underset{\sim}{B_0}$, the quadrupole moment along the efg. Therefore the nuclear spin energy of a quadrupolar nucleus depends both on the orientation of the nuclear spin relative to $\underset{\sim}{B_0}$ and on its orientation relative to its electronic environment (characterised by the efg

tensor).

The Hamiltonian describing the inhomogeneous broadening of an NMR resonance of quadrupolar nuclei in a powder due to the interaction between the nuclear quadrupole moment and an electric field gradient at the nuclear site is given by Equation 2.16:[4,9]

$$\hat{\mathcal{H}}_Q = \sum_i [eQ_i/6\hat{I}_{\sim i}(2I - 1)]\hat{I}_{\sim i} \cdot \underset{\approx}{V}_i \cdot \hat{I}_{\sim i} \quad \ldots \quad (2.16)$$

where $\underset{\approx}{V}_i$ is the electric field gradient tensor of nucleus i.

This Hamiltonian can be written in terms of the parameters V_{zz} and η [= $(V_{xx} - V_{yy})/V_{zz}$] (the asymmetry parameter which is a measure of the deviation of the field gradient tensor from axial symmetry), where V_{xx}, V_{yy}, and V_{zz} are the principal elements of the tensor $\underset{\approx}{V}$. The quadrupole Hamiltonian for a single spin is then:

$$\hat{\mathcal{H}}_Q = \frac{e^2qQ}{4I(2I-1)}.[3\hat{I}_z^2 - \hat{I}^2 + \eta(\hat{I}_x^2 - \hat{I}_y^2)] \quad \ldots \quad (2.17)$$

where the spin operators are evaluated in the principal axis system (P.A.S.) of $\underset{\approx}{V}$.

Three cases are now possible: (i) $\hat{\mathcal{H}}_z \simeq \hat{\mathcal{H}}_Q$; (ii) $\hat{\mathcal{H}}_z < \hat{\mathcal{H}}_Q$; and (iii) $\hat{\mathcal{H}}_z > \hat{\mathcal{H}}_Q$. Only the usual "high-field" case in which $\hat{\mathcal{H}}_z >> \hat{\mathcal{H}}_Q$ will be considered here. The effect of the quadrupole interaction on the energy levels, m, created by the Zeeman interaction can be treated by perturbation theory. Various energy levels are obtained using perturbation theory. The frequency of the transition $m \longleftrightarrow m-1$ appears according to first order perturbation theory at:[10]

$$\nu_{m \longleftrightarrow m-1} = \nu_0 - \nu_Q[1/2(3\cos^2\theta - 1) + \eta/2.\sin^2\theta.\cos2\phi](m - 1/2) \quad \ldots \quad (2.18)$$

where $\nu_Q = 3e^2qQ/2I(2I - 1)h$, where ν_0 (Larmor frequency) = $\gamma\underset{\sim}{B}_0.(1 - \underset{\approx}{\sigma})/2\pi$, and θ and ϕ are the angles of the magnetic field $\underset{\sim}{B}_0$ with

respect to the pricipal axis of q, the electric field gradient, and χ, the nuclear quadrupole coupling constant ($\chi = e^2 q_{zz} Q/h$).

Figure 2.3 shows the Zeeman energy levels for a spin I = 5/2 nucleus (such as ^{27}Al) and the change of these levels by the first-order

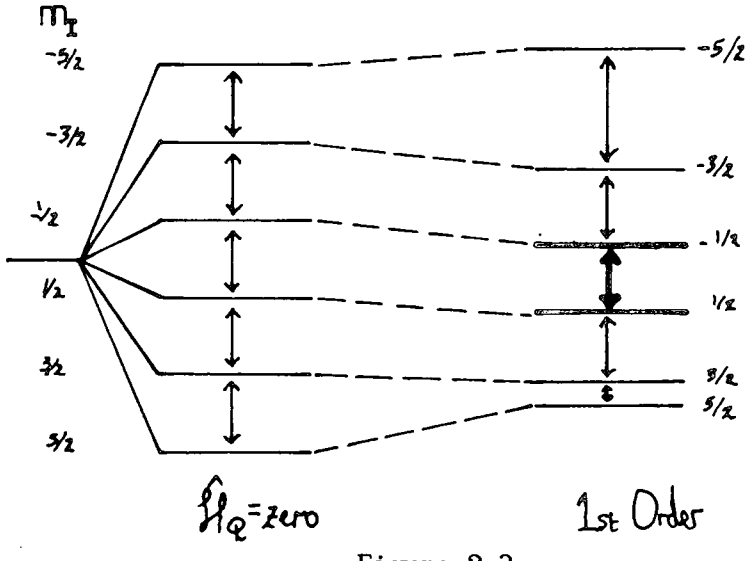

Figure 2.3

Energy level diagram for a spin 5/2 nucleus showing the effect of the first-order quadrupolar interaction on the Zeeman energy levels. Frequency of the central transition (emboldened) is independent of the quadrupolar interaction to first order.

contribution of the quadrupole interaction.

The frequency of the (1/2 $\leftrightarrow$ -1/2) transition is not perturbed by the quadrupole interaction to first order (Equation 2.18, m = 1/2). The frequency shift of the other transitions is of the order of the quadrupole coupling constant, χ, which in many cases can be quite large (MHz range). The magnitudes of the shifts are dependent on the direction of the magnetic field with respect to the symmetry axes and the asymmetry parameter. Consequently only the central (1/2 $\leftrightarrow$ -1/2) transition is normally observable in solid-state NMR spectra of quadrupolar nuclei in non-cubic environments.

The quadrupole interaction contributes to the (1/2 $\leftrightarrow$ -1/2) transition in second order perturbation theory and the frequency of the central transition is:[11]

$$\nu_{1/2\leftrightarrow -\nu_{1/2}} = \nu_0 - F/\nu_0[A(\phi).\cos^4\theta + B(\phi)\cos^2\theta + C(\phi)] \quad \ldots \quad (2.19)$$

where $F = \nu_Q^2/6.[I(I + 1) - 3/4]$, and

$$A(\phi) = -27/8 - 9/4\eta.\cos 2\phi - 3/8\eta^2.\cos^2 2\phi$$

$$B(\phi) = 30/8 - \eta^2/2 + 2\eta.\cos 2\phi + 3/4\eta^2.\cos^2 2\phi$$

$$C(\phi) = -3/8 + \eta^2/3 + 1/4\eta.\cos 2\phi - 3/8\eta^2.\cos^2 2\phi \quad \ldots \quad (2.20)$$

and θ, ϕ are the angles mentioned with Equation 2.18.

For a single crystal, the principal axes of the efg tensor can be determined as well as their orientations relative to the crystal axes. For powders, however, the orientations of the efg tensor are randomly spread and a powder pattern results. In this case, the information about the orientation of the efg tensor relative to the crystal frame is lost. The position of the Larmor frequency, ν_0, is not distinguished in the powder spectrum. The centre of gravity, $\nu_{c.g.}$, and the Larmor frequency, ν_0, do not coincide in the powder pattern:[12]

$$\nu_{c.g.} - \nu_0 = -1/5(1 + \eta^2/3)F/\nu_0 \quad \ldots \quad (2.21)$$

Whereas the quadrupole broadening to first-order of the $(1/2 \leftrightarrow -1/2)$ transition can be eliminated by MAS [Equation 2.18 contains the $(3\cos^2\theta - 1)$ term], the equation for quadrupole broadening to second-order (Equation 2.19) is not of the form $(3\cos^2\theta - 1)$ and therfore MAS does not eliminate second-order quadrupolar broadening. (It does however narrow the central transition.) The equation for the central transition under fast MAS conditions has been written in a form analogous to Equation 2.19 for the static term. Terms A, B, and C now become:[12]

$$A^{MAS}(\phi) = 21/16 - 7/8\eta.\cos 2\phi + 7/48\eta^2.\cos^2 2\phi$$

$$B^{MAS}(\phi) = -9/8 + \eta^2/12 + \eta.\cos 2\phi - 7/24\eta^2.\cos^2 2\phi$$

$$C^{MAS}(\phi) = 15/16 - 1/8\eta.\cos 2\phi + 7/48\eta^2.\cos 2\phi \quad \ldots \quad (2.22)$$

Equation 2.21 allows the true (corrected) chemical shift to be obtained

(in both static and rapidly spun cases) provided η and χ are known for the sample.

The quadrupole-induced shift[13] (QIS)-$\upsilon_{c.g.}$-υ_0- depends on the ratio υ_Q^2/υ_0. It is clear that at high magnetic fields, this ratio is low and consequently the QIS is reduced. The centre of gravity is then shifted to higher frequency closer to the true isotropic chemical shift of the nucleus under investigation. It is relevant to note here that more efficient line-narrowing may be achieved by spinning at angles other than the conventional "magic-angle",[14] although the magic-angle has the advantage that dipolar and chemical shift anisotropy effects are eliminated simultaneously.

To recapitulate, there is always a discrepancy between the location of the peak in the MAS spectrum of quadrupolar nuclei and the position of the isotropic chemical shift. For a determination of the actual chemical shift value either the MAS spectrum has to be simulated or the QIS has to be corrected for. The actual chemical shift value can be obtained by the following methods:

(i) comparison of the experimental central ($1/2 \leftrightarrow -1/2$) transition line shapes with the calculated MAS NMR powder pattern lineshapes;[12,15]

(ii) evaluation of the quadrupolar shifts from several MAS NMR spectra, registered at different magnetic field strengths (assuming $\eta = 0$);

(iii) from the arithmetic mean of the corresponding spinning sidebands of the first or second spinning sidebands of the least shifted first satellite ($\pm 3/2 \leftrightarrow \pm 1/2$) transition;[16,17]

(iv) by adding a correction term according to Equation 2.21 to the experimental (field-dependent) chemical shift value of the MAS spectrum:[12] (without the knowledge of the values of χ and η, a rough approximation of the correction term $\delta_{corr} \simeq 0.85\ \delta\upsilon$, where $\delta\upsilon$ is the linewidth at half-height, assuming a Gaussian lineshape, has been

proposed);[18]

(v) determination of quadrupolar interaction parameters by fitting the experimental MAS NMR excitation spectra to the numerically simulated nutation spectra.[19,20] [The nutation spectrum is measured using incrementally increasing pulses of resonant rf radiation of duration t_1, to influence all transitions, with registration of the FID signal of the central transition during t_2. It is assumed that $\hat{\mathcal{H}}_z >> \hat{\mathcal{H}}_Q$, but that $\hat{\mathcal{H}}_Q$ is large enough to broaden all transitions beyond detection except the $m = 1/2 \leftrightarrow -1/2$ transition. This permits the use of two-dimensional Fourier transform (FT) NMR techniques with simultaneous measurement of the isotropic chemical shift and the corresponding second-order quadrupole interaction parameters. Following FT in the t_1 and t_2 directions the central transition excitation spectrum is displayed along the F_1 axis, the chemical shift anisotropy (if present) and second-order quadrupole interaction along the F_2 axis. The total nutation spectrum (along the F_1 axis) can be simulated as a function of the ratio between the quadrupole coupling constant, χ, and the rf field parameter, γB_1.]

While each of the methods of chemical shift refinement has its merits, none is universally applicable. Table 2.1 lists the various methods and discusses their relative advantages and drawbacks.

For polycrystalline samples, characteristic lineshapes (powder patterns) exist for the central ($1/2 \leftrightarrow -1/2$) transition. The lineshapes are functions of both the asymmetry parameter and the quadrupole coupling constant. The lineshape has both shoulders and singularities and analytical expressions exist for the positions of these shoulders and singularities for both stationary[10,11] and spinning samples.[12] These expressions can be used for the estimation of quadrupole interaction parameters if the first- and second-order quadrupole interaction terms dominate as perturbations to the Zeeman

Method	Discussion
(i)	Can be used with χ values in the 3-9 MHz range. Linewidths often obscured by other line broadening mechanisms such as distribution of chemical shifts due to chemical inhomogeneity, dipolar interactions, and anisotropy of magnetic susceptibility.
(ii)	Yields useful results with small χ values, but requires the use of several magnetic fields. Measurements at lower fields unavoidably lead to diminished sensitivity and lowered resolution often with overlapping of broad lines.
(iii)	Appears to be the method of choice for nuclei with sufficiently strong NMR signals such as ^{27}Al. ($\pm 3/2 \leftrightarrow \pm 1/2$) transition MAS NMR linewidth smaller by a factor 24/7 compared with ($1/2 \leftrightarrow -1/2$) central transition for I = 5/2 nucleus. Demands very high precision in setting of magic-angle and ultra-high, very stable sample spinning (7-9 kHz). Error in determination of isotropic chemical shift reported to be < 1ppm.[17]
(iv)	Stationary samples at low magnetic field strengths used for determination of χ and η values. Errors due to other linewidth contributions and intensity problems as for methods (1) and (2) respectively.
(v)	Simultaneous measurement of isotropic chemical shifts and corresponding quadrupole interaction parameters. Useful for simple systems with no overlapping lines. Requires time-consuming and precise experiments with lengthy computations. Sample not spun, so method applicable over a wide temperature range.

Table 2.1

Comparison of methods of shift refinement used for determination of isotropic chemical shifts for quadrupolar nuclei, such as ^{27}Al.

energy levels. This, however, is not always the case and the powder patterns may lack all characteristic quadrupole features due to otherinteractions, such as dipolar line broadening, large chemical shift anisotropies, and inhomogeneous broadening. Inhomogeneous broadening of structural or magnetic origin cannot be suppressed by MAS techniques. In such cases, the central transition centre of gravity is the only parameter which can be reasonably determined.

2.5 Cross-polarization

NMR is an inherently insensitive technique due to the small Boltzmann factor at normal temperatures. A second problem is the fact that spin-lattice relaxation times can be very long, so that multiple-pulse methods are not very efficient. This is particularly so for studying systems with intrinsically very weak signals, such as ^{29}Si, where many repetitions of the experiment must be added to achieve an acceptable signal-to-noise ratio.

The abundant spins (^{1}H) on the other hand have a very strong signal by comparison. In addition, the spin-lattice relaxation times of the protons will generally be shorter than the corresponding ^{29}Si values. Both of these factors make it sensible to generate the dilute-spin signal from the abundant spins. In order to achieve this *cross-polarization*[21] process, it is necessary to irradiate simultaneously both spin species with resonant or near resonant radiation, the amplitudes of these two rf fields satisfying a particular relationship (*vide infra*).

In order to exchange polarization, the different spin species must

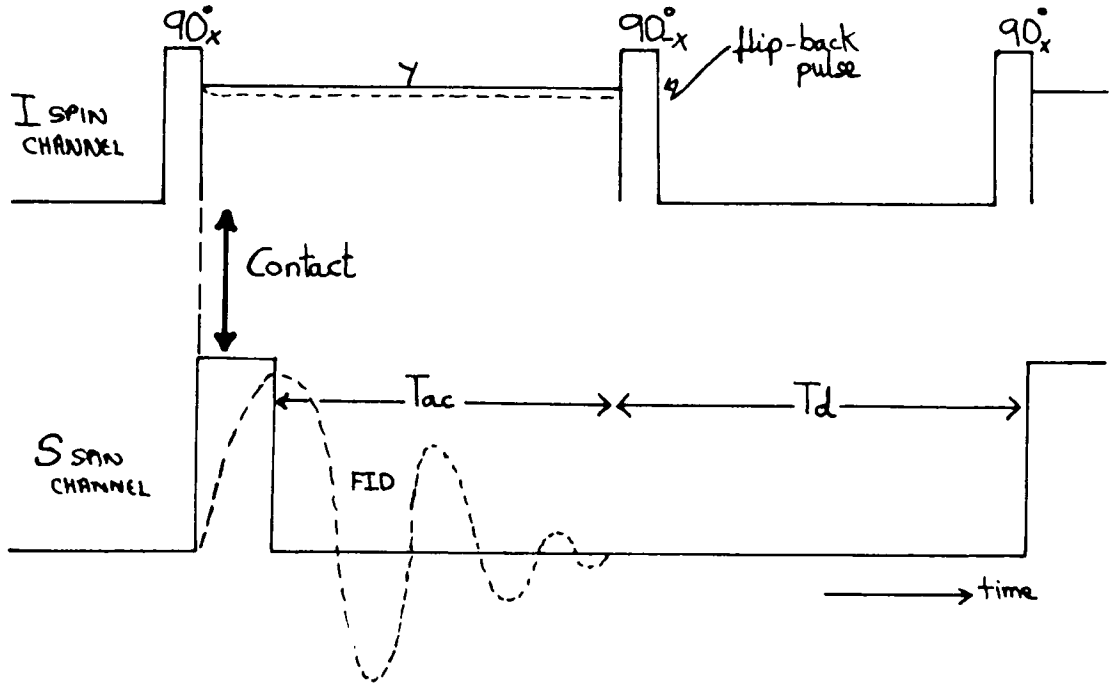

Figure 2.4

The pulse sequence for cross-polarization with flip-back (*vide infra*) acquisition and recycle delay times are indicated T_{ac} and T_d respectively.

be able to undergo mutual flip-flop transitions, the maximum exchange occurring in the double resonance (amplitudes matched) experiment. The pulse sequence used is shown in Figure 2.4. The first step is to apply a 90° pulse in the proton channel and to spin-lock the ^1H magnetization in the y direction of the rotating frame. At this point the rf in the other channel is switched on, and the amplitude of the magnetic field (B_{1S}) adjusted so that the Hartmann-Hahn matching condition,[22] Equation 2.23, is fulfilled:

$$\gamma_I \underset{\sim}{B}_{1I} = \gamma_S \underset{\sim}{B}_{1S} \quad \ldots \quad (2.23)$$

This condition implies that in their respective rotating frames of reference, the protons and carbons precess at equal frequencies and that the effective energies (also in the rotating frames) are comparable,

thus allowing a rapid transfer of magnetization induced by the flip-flop term (term B, Equation 2.5) in the dipolar Hamiltonian. In practice, several adjustments are made to the basic CP sequence, one of which (flip-back[23]) is illustrated in Figure 2.4. The process involves flipping of the proton magnetization back into the z ($\underset{\sim}{B_o}$) direction with a 90^o pulse reversed in phase with respect to the preparation pulse preceding the spin-lock pulse, immediately following S-spin acquisition (Figure 2.4). This allows the proton rf field to be switched off during the recycle delay times (T_d), and also makes maximum use of the available proton magnetization.

The second adjustment made to the basic CP sequence is the use of spin temperature inversion (STI) plus data routing.[24] STI removes signal artefacts such as those arising from phase irregularities, or those due to imperfect matching of parts of the electrical equipment. STI relies on the simple fact that artefacts are independent of phase. The spin temperature (*vide infra*) and the sign of the data acquisitiion for protons are alternated every second transient. The data collected in the observed channel are then added or subtracted from data memory according to the sign of the spin temperature expected. This results in the accumulation of the desired portion of the signal and the rejection of the phase independent artefacts. The spins in the S channel are also phase cycled to remove pulse phase irregularities and imperfections.

The pulse sequence incorporating both the above improvements to the basic CP sequence is shown in Figure 2.5 (for the ^1H channel only as the S-spin channel pulse sequence remains the same). The CP experiment can be described thermodynamically as follows: originally the I spins have spin order in the $\underset{\sim}{B_o}$ field and a spin temperature of, say, 300 K. These spins are spin-locked in the $\underset{\sim}{B_1}$ field causing cooling of the I spin

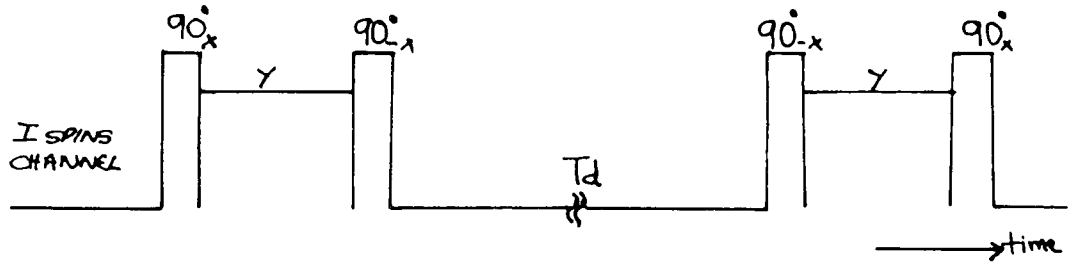

Figure 2.5

I-Channel (^{1}H) irradiation for the phase-alternated (STI) version of the flip-back CP experiment (single contact).

system (as $\underset{\sim}{B}_1 \lll \underset{\sim}{B}_0$; typically $\underset{\sim}{B}_0$ = 2 T = 20 kG, $\underset{\sim}{B}_1$ = 20 G), so now theI spins have a spin temperature of $\simeq$ 0.3 K. The S spins have no spin order and hence an infinite spin temperature. Contact of the two spin systems causes rapid transfer of energy (magnetization) which is only possible under conditions of total energy conservation, *i.e.* only in the rotating frame of reference by the establishment of matching energy levels. This is, of course, the Hartmann-Hahn condition where $\omega_{1S} = \omega_{1I}$. The transfer of energy can be visualised thermodynamically as follows: the ^{1}H magnetization, produced in the laboratory frame by equilibration with the lattice, is given by the Curie Law of Paramagnetism as:

$$M_0(I) = C_I \underset{\sim}{B}_0 / T_L \quad \ldots \quad (2.24)$$

where $C_I = 1/4\gamma_I^2 \hbar^2 N_I / K$ and T_L is the lattice temperature. Since $\underset{\sim}{B}_1 \lll \underset{\sim}{B}_0$, the I spin magnetization in the rotating frame following spin-locking is no longer at equilibrium. The situation can be expressed in terms of a spin temperature in the rotating frame, T_S. Thus:

$$C_I \underset{\sim}{B}_0 / T_L = C_I \underset{\sim}{B}_1 I / T_S$$

$$i.e. \quad T_S = (\underset{\sim}{B}_1 I / \underset{\sim}{B}_0).T_L \quad \ldots \quad (2.25)$$

The I spins are at a very low temperature and their total spin energy is $-C_I B_0^2/T_S$. The S spin temperature at this point is infinite (zero magnetization in their rotating frame). Thus, on contact, the spin energy will be repartitioned between the two spin systems to give a common spin temperature T_S', as in Equation 2.26:

$$C_I B_1 I^2/T_S = (C_I B_1 I^2 + C_S B_1 S^2)/T_S' \quad \ldots \quad (2.26)$$

where $C_S \ll C_I$, so $T_S' \simeq T_S$. Thus the protons only lose a very small part of their magnetization, whereas the resulting magnetization of the S spins is:

$$M(S) = C_S B_1 S/T_S' \simeq C_S B_1 S/T_S \quad \ldots \quad (2.27)$$

Substitution from Equations 2.23 and 2.25 gives:

$$M(S) = C_S(\gamma_I/\gamma_S).B_0/T_L \quad \ldots \quad (2.28)$$

The normal S spin magnetization in the laboratory frame (given by the equivalent of Equation 2.24) is:

$$M_0(S) = C_S B_0/T_L \quad \ldots \quad (2.29)$$

Comparing Equations 2.28 and 2.29, a gain of γ_I/γ_S is apparent. For the ^1H, ^{13}C system, this ratio is approximately four. For the ^1H, ^{15}N system the gain is approximately ten. The enhanced magnetization in the S spins is detected by monitoring the FID following cross-polarization (see Figure 2.4).

In principle, this process of double resonance with the Hartmann-Hahn condition in operation, can be repeated with no waiting time being required between the end of the FID and the re-establishment of the matched amplitudes condition. In cases where the proton spin-lattice relaxation in the rotating frame ($T_{1\rho}$ ^1H) is long, this process can be repeated many times (the so-called "multiple-contact" CP experiment). However, eventually the proton reservoir becomes substantially attenuated because of (a) the small but significant amount

of magnetization transferred, and also (b) the ^{1}H $T_{1\rho}$. At this stage a waiting time of T_1 (^{1}H) is necessary before the sequence can be repeated.

Thus as mentioned in the beginning of this section on cross-polarization, we have a way of circumventing both the long T_1's of many dilute nuclei and also of improving the S/N ratio of the experiment. Moreover, as the rate of cross-polarization, T_{CH}^{-1} (the CP efficiency) is directly proportional to the internuclear I-S distance, we also have a discriminatory technique (see Chapter Four for further details).

CHAPTER THREE - LITERATURE REVIEW OF NMR STUDIES OF ZEOLITES AND RELATED MATERIALS

3.1 Introduction

This chapter reviews the important contributions solid-state NMR has made to zeolite chemistry to date. It is divided into three areas, (1) aluminosilicates, (2) isomorphous substitution to high-silica zeolites, and (3) the aluminophosphate molecular sieves (and their various substituted analogues). The latter two areas form the body of the results to be described in Chapters Five and Six. For a more complete discussion of all matters concerning zeolites and NMR, the reader is referred to several review articles published recently.[25-27] For a comprehensive treatment of zeolite structures and properties the reader is referred to the monographs by Breck and Barrer.[28-30]

3.3.1. Definition of a zeolite

The name "zeolite" [from the Greek "ζεω" (boiling) and "λιθοσ" (stone)] was coined by Cronstedt[31] in 1756 to describe the behaviour of the newly discovered mineral stilbite. When heated, stilbite loses water rapidly and thus seems to boil. Zeolites are microporous, crystalline aluminosilicates built from corner-sharing SiO_4^{4-} and AlO_4^{5-} tetrahedra linked to each other by sharing all of the oxygens. The so-formed infinitely extending three-dimensional network contains regular systems of intracrystalline cavities and channels of molecular dimensions. The net negative charge of the aluminosilicate framework, equal to the number of the constituent aluminium atoms, is balanced by exchangeable cations, M^{n+}, located in the channels which normally also contain water. The void space may be up to 50% of the total crystal volume. The cations are quite mobile and exchange can take place to

varying degrees with other cations. In many cases, the intracrystalline water may be reversibly removed. In many other zeolites, natural and synthetic, cation exchange or dehydration may produce structural changes in the framework. Zeolites may be represented by the general oxide formula

$$M^{n+}_{x/n}(AlO_2)_x(SiO_2)_y.m\ H_2O$$

In all zeolite structures studied to date, it has been found that $y \geq x$. The simplest interpretation of this, given that each silicate and aluminate tetrahedron is linked, *via* oxygen bridges to four other tetrahedra, is that aluminate tetrahedra cannot be neighbours in a zeolite framework, *i.e.* that Al-O-Al linkages are forbidden. This requirement, known as Loewenstein's rule,[32] will be discussed later in this chapter.

3.1.2. Structure and properties of natural and synthetic zeolites.

There are at present around 40 identified species of zeolite minerals and at least 120 synthetic species. There are more than 35 different known framework topologies. Zeolites can be classified into groups related through the occurrence of shared structural features. Breck has classed zeolites and tectosilicates into groups, (1) Analcime Group, (2) Natrolite Group, (3) Heulandite Group, (4) Phillipsite Group, (5) Mordenite Group, (6) Chabazite Group, (7) Faujasite Group, (8) Laumontite Group, (9) Pentasil Group, and (10) Clathrate Group. The members of a zeolite group fall into two categories:

(1) Those which have the same framework topology, but have different chemical compositions (cations or Si/Al ratios) and in which as a result there may be minor framework adjustments and also differences in chemical, crystallographic, and physical properties. Thus all the

members of the analcime group are considered to have the same framework topology, but often differ widely in chemical composition.
(2) Those members of a group which have frameworks containing one or more common structural elements, linked together in different ways, so resulting in different topologies. Examples in the faujasite group are faujasite itself and zeolite A, and zeolite ZK-5 and zeolite RHO.

It is more convenient however, to describe and classify zeolite structures in terms of fundamental building units, as listed in Table 3.1. These building units include the primary building unit TO_4 tetrahedra, so-called secondary building units (SBU) which consist of both single rings of 4, 5, 6, 8, 10, and 12 tetrahedra and double rings of 4, 6, and 8 tetrahedra (according to Meier), and larger symmetrical polyhedra described in terms of Archimedean solids. Several of the secondary building units and the larger symmetrical polyhedra are shown in Figure 3.1. The secondary building units are the smallest number of such units from which known zeolite topologies can be built (see Table 3.2). In the SBU, Al or Si is present at each corner but the oxygens are not shown. They are located near the mid-points of the lines joining each pair of T atoms. The zeolites natrolite, thompsonite, and scolecite have tectosilicate frameworks that can be constructed using only the 4-1 units of the figure. Sometimes more than one SBU is involved. Thus zeolite A can be made from 4-, 6-, and 8-rings and 4-4 cubic units; faujasite from 4-, 6-, and 8-rings together with 6-6 hexagonal prisms. Various other ways of formulating zeolite framework topologies have been developed involving structural units of greater complexity than the SBU in the polyhedra. Stacking of these polyhedral cages with other cages, like or unlike the first can generate various structures as shown in Figure 3.2. Several methods are used to depict structural models in zeolites and Figure 3.3 shows three ways of

Primary Building Unit - Tetrahedron (TO_4)

Tetrahedron of four oxygen ions with a central ion (T) of Si^{4+} or Al^{3+}. All oxygens shared between two tetrahedra, $(TO_2)_n$.

Secondary Building Unit (SBU)

Rings: S-4, S-5, S-6, S-8, S-10, S-12

Double Rings: D-4, D-6, D-8.

Larger Symmetrical Polyhedra

Truncated Octahedron or Sodalite Unit (β-cage)

11-Hedron or Cancrinite Unit (ϵ-cage)

14-Hedron II or Gmelinite Unit

18-Hedron (γ-cage)

Truncated cuboctahedron (26-hedron of type 1)(α-cage)

Zeolite Structure

Packing of SBU's and polyhedra in space

Table 3.1

Building Units in Zeolite Structures

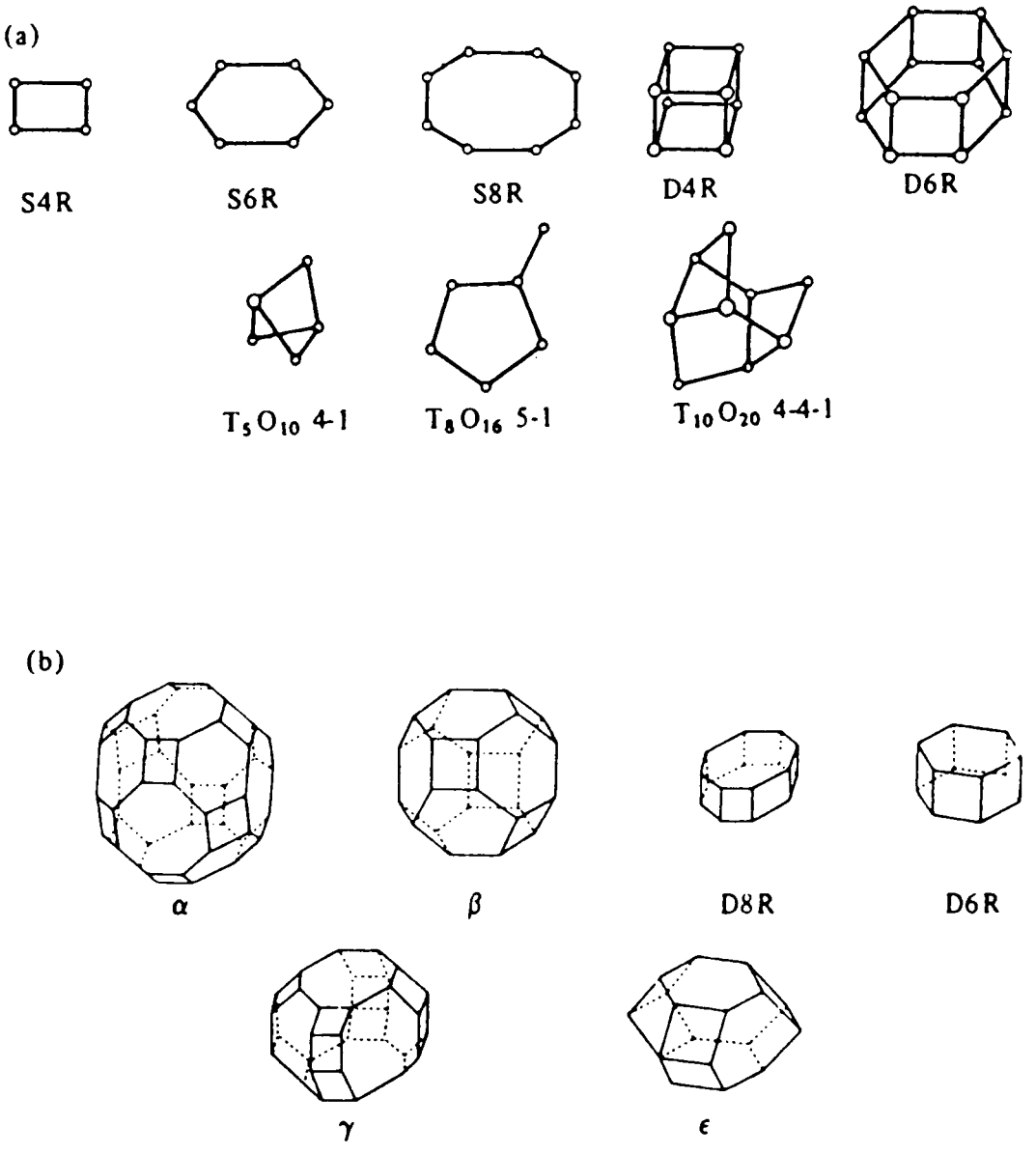

Figure 3.1

a) The secondary buiding units (SBU) in zeolite structures according to Meier

b) Some polyhedra in zeolite frameworks

S4R	phillipsite	8	0.39 x 0.44	D6R	chabazite	8	0.42
	gismondine	8	0.28 x 0.49		gmelinite	12	0.70
					faujasite	12	0.74
					type X (syn)	12	0.74
S6R	erionite	8	0.36 x 0.52		type Y (syn)	12	0.42
	offretite	12	0.69		type ZK-5 (syn)	8	0.39
	levyne	8	0.32 x 0.51		type L (syn)	12	0.71
	mazzite	12	0.74				
	omega (syn)	12	0.74	5-1	mordenite	12	0.67 x 0.70
	losod	6	0.22		dachiardite	10	0.37 x 0.67
					ferrierite	10	0.43 x 0.55
D4R	type A (syn)	8	0.42		ZSM-5 (syn)	10	0.54 x 0.56
	type ZK-4 (syn)	8	0.42		silicalite (syn)	10	0.52 x 0.58
4-1	natrolite	8	0.26 x 0.39	4-4-1	heulandite	10	0.44 x 0.72
	scolecite	8	0.26 x 0.39		clinoptilolite	10	0.44 x 0.72
	thompsonite	8	0.26 x 0.39		stilbite	10	0.41 x 0.62
					barrerite	10	0.41 x 0.62

(syn): synthetic

Table 3.2

Classification of zeolites according to SBU. The number of atoms forming the main channel system in each zeolite is given together with the free aperture of the channels in nanometres.

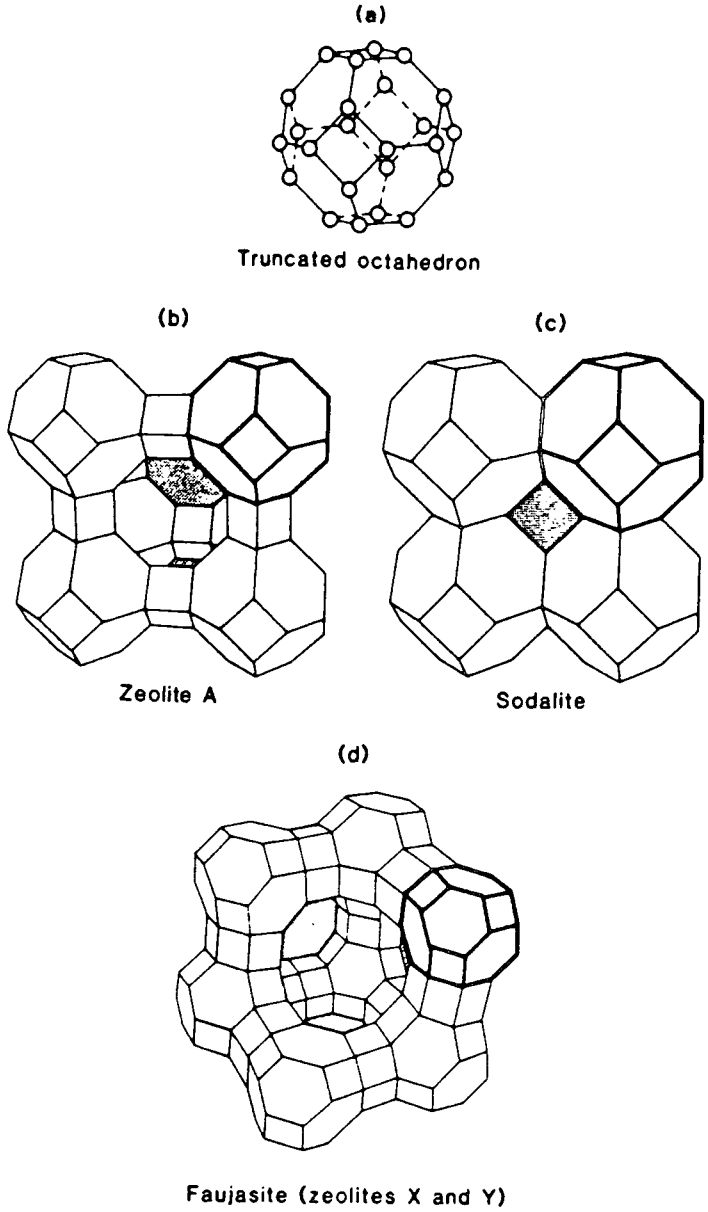
(a)
Truncated octahedron
(b)
(c)
Zeolite A
Sodalite
(d)
Faujasite (zeolites X and Y)

Figure 3.2

representing the truncated octahedron (or sodalite unit). Figure 3.4 shows the framework structure of chabazite (the polyhedron in the Figure is the 20-hedron). Figure 3.5 shows the structure of ZSM-5. The framework of ZSM-5 contains the two intersecting tunnel systems; one sinusoidal 10-ring tunnel system runs along the *a* axis, and the other 10-ring tunnel runs straight along the *b* axis. The basic building brick is the novel 8-5 ring (pentasil unit) shown in Figure 3.5a. In the ZSM-5 framework these units link up as illustrated in a simplified *ac* projection (Figure 3.5b). In Figure 3.5b, sections marked A correspond to the 8-5 ring unit and have the same orientation. The section B corresponds to a mirror image of the 8-5 unit. Similarly, the sections marked C are 8-5 units in 180^{o} horizontal orientation in relation to Figure 3.5c, and the section marked D has mirror image orientation in relation to section C. This link-up gives rise to 10-ring cavities in the *ac* plane, and the sinusoidal 10-ring tunnels in the *a* direction.

Zeolites display a number of interesting physical and chemical properties. The three classes of phenomena which are of greatest practical importance are the ability to sorb organic and inorganic substances, to act as cation exchangers and to catalyse a wide variety of reactions. The most important aspects of these are described below.

The zeolite channel systems are normally filled with water. Removal of this zeolitic water allows other molecular entities such as CO_2, CS_2, ammonia, alkali metal vapours, hydrocarbons, alcohols, and other organic and inorganic species to be accommodated in the intracrystalline cavities. Depending on the pore diameter and molecular dimensions (see Table 3.2), this process is often highly selective, and

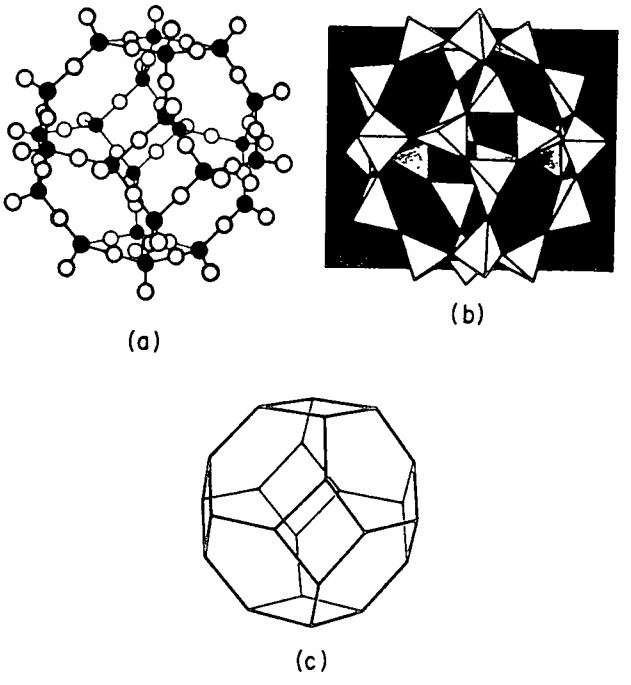

Figure 3.3

Three ways of depicting the sodalite unit in aluminosilicate frameworks

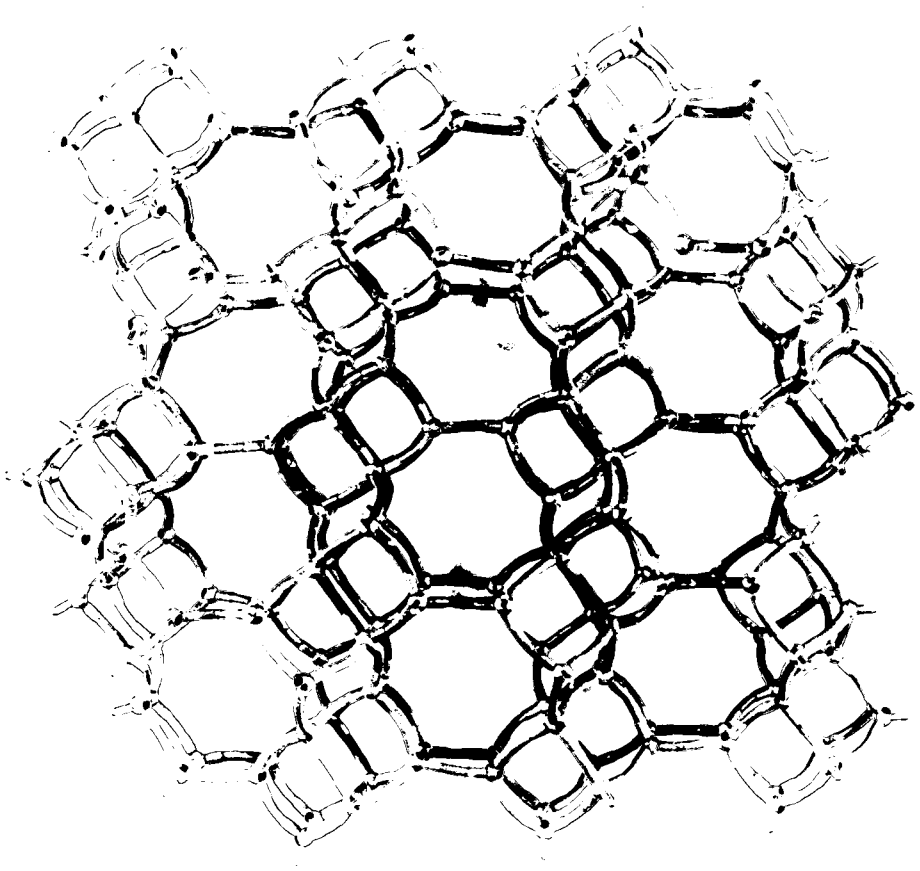

Figure 3.4

Chabazite framework structure

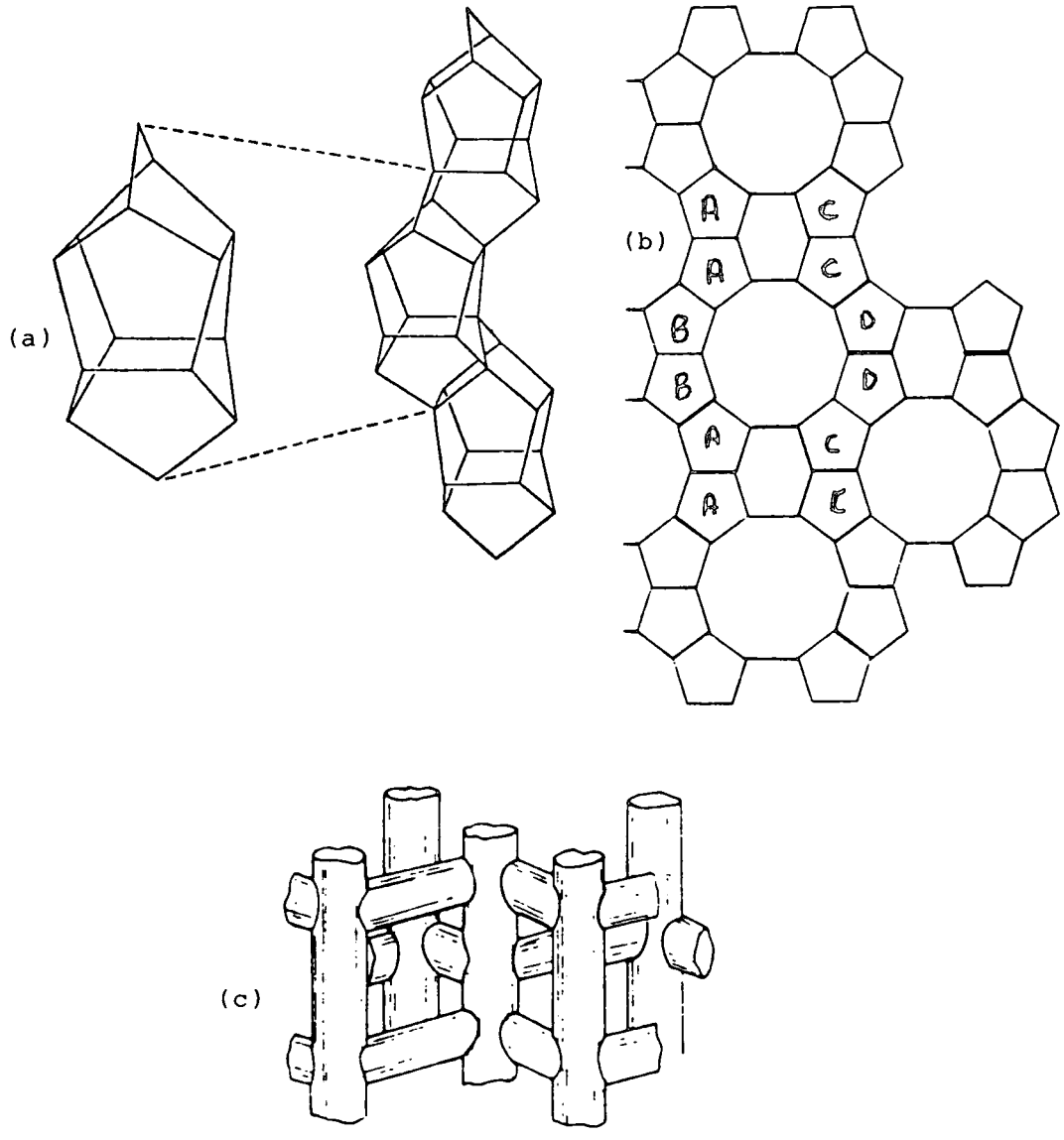

Figure 3.5

The structure of ZSM-5. (a) The pentasil unit (b) *ac* Projection (c) Channel structure.

gives rise to an alternative name for zeolites: molecular sieves. Thus dehyrated chabazite, with pore openings less than 0.5 nm wide, can sorb water, methanol, ethanol and methanoic acid but not acetone, ether, or benzene. Thus zeolitic sorption is a powerful method for the resolution of mixtures. For example, Ca-exchanged zeolite A (the so-called 5A) can separate *n*-paraffins from other hydrocarbons. Moreover, as zeolite crystals are usually highly polar, polar molecules are in general selectively sorbed in the presence of non-polar molecules. Commercial applications of molecular sieving are wide and include thorough drying of organics, separation of hydrocarbons and of N_2 and O_2 in air and the removal of ammonia and CS_2 from industrial gases.

Cations neutralising the electrical charge of the aluminosilicate framework can be exchanged for other cations from solution. Zeolites often possess high ion-exchange selectivities for certain cations and this is used for their isolation and concentration. Thus zeolites can act as sieves for ions just as they do for molecules in the course of sorption. For example, NH_4^+ is efficiently removed from solution by clinoptilolite. Other applications are the collection of harmful products of nuclear fission (such as ^{137}Cs and ^{90}Sr), water softening, the treatment of brackish water and the recovery of precious metals (as complex cations). Finally, the molecule sieving properties of zeolites can be modified by ion-exchange. Thus Na-A sorbs both N_2 and O_2, while Ca-A sorbs nitrogen preferentially to oxygen (at room temperature).

However, most importantly, zeolites, particularly those with relatively high Si/Al ratios and rich in free protons (prepared indirectly by thermal decomposition of the ammonium exchanged form), exhibit impressive activity and selectivity as catalysts for the cracking, hydrocracking and isomerization of hydrocarbons. In these

functions rare-earth exchanged and hydrogen forms of faujasite zeolites are amongst the most widely used of all commercial catalysts: they far surpass the performance of their silica-alumina gel predecessors, and possess the useful property of being sufficiently thermally stable to withstand regeneration at high temperatures. Zeolite based catalysis was first discovered in 1960 and two years later cracking catalysts based on zeolite Y were introduced. The synthetic zeolite ZSM-5, introduced in 1972, is an even more powerful catalyst. Its high silica content (Si/Al is typically 30) gives it high thermal stability, while the channel diameter, *ca.* 0.55 nm, is very convenient for many applications, particularly in the petroleum industry. The 10-membered channels of ZSM-5 are responsible for its remarkable shape selectivity. Various types of shape selectivities can be distinguished depending on whether pore size limits the entrance of the reacting molecule, the departure of the product molecule, or the formation of certain transition states. Ion-exchange or chemical modification of ZSM-5 (for instance impregnation with phosphoric acid or boron compounds) can further fine tune this shape selectivity.

3.1.3. Techniques for structural characterization

The overall framework structure of most zeolites can be satisfactorily determined by conventional X-ray diffraction (XRD) methods. However, the detailed Si,Al ordering within the tetrahedral framework itself cannot, in general, be readily extracted from X-ray crystallography. This arises partly because of the similar scattering powers of Si and Al (due to the small difference in relative atomic

number between Si and Al), but also because of the difficulty in obtaining single crystals of sufficient quality and dimension. [Zeolites are normally obtained as a fine powder, the average crystallite size being between 0.5 and 20 μm (80 to 100 μm are needed for a single-crystal study).]

Until recently, most of the methods employed for zeolite structure determination (except for single crystal XRD when available) were indirect in nature. Vibrational spectroscopy, more specifically mid-IR spectroscopy (a direct method of analysis) has been used to determine the location of loosely bonded protons in zeolite catalysts, however, the vibration bands assigned to internal tetrahedral linkages are, in general, structure insensitive. Significant progress has however recently been made in structural elucidation of zeolites because of the introduction of three powerful new techniques:

(1) High-resolution electron microscopy (HREM), is capable of determining the structural characteristics of solids in real space. Dealuminated samples are used so as to extend the life of the zeolite under electron irradiation. Coupled with optical diffractometry, HREM has elucidated the nature of the intergrowths that may form between ZSM-5 and its closely related analogue ZSM-11. The strategy employed in studying zeolites by HREM is as follows. From the coordinates obtained in the X-ray structure determination, a series of images is calculated as a function of specimen thickness and objective lens setting. The images are then computer simulated for specific crystallographic projections. A matching of HREM image and computed image confirms the correctness of the X-ray determined structure.

(2) Rietveld neutron scattering diffraction (powder) profile analysis, can completely determine the Al, Si ordering and cation position in

dehydrated zeolites. Neutrons are used for diffraction as the scattering intensity of neutrons is independent of angle and the peaks produced are accurately gaussian. Provided long-range order may be assumed and some preliminary model is known in broad outline, refinement of the observed and calculated line-profiles (intensity of scattering *versus* 2θ) permits the structure to be fully determined.

(3) High resolution solid-state magic-angle spinning NMR (MAS NMR), has had perhaps the greatest single impact in the structural elucidation of aluminosilicate zeolites. The use of MAS allows spectra to be obtained which are comparable to those displayed by species in solution. The information obtainable from MAS NMR spectra is summarized in the next section.

3.2 Solid-state NMR of silicates and aluminosilicates.

The first high-resolution (*i.e.* magic-angle spinning) ^{29}Si NMR publication appeared in 1978[33] and described results for two organosilanes, as well as two siloxanes and two silicates. The first applications of these techniques to the investigation of solid silicates and aluminosilicates were due to Engelhardt *et al.*[34] and to Lippmaa *et al.*.[35]

In solids of known composition containing more than one type of Q unit, separate lines were observed in the requisite intensity ratio. For instance, the spectrum of xonotlite, $Ca_6(OH)_2(Si_6O_{17})$, a double-chain silicate branched at every third silicon contains two ^{29}Si signals, at -86.8 and -97.8 ppm, in the 2:1 intensity ratio.

$$\begin{bmatrix} - Q^3 - Q^2 - Q^2 - \\ - Q^3 - Q^2 - Q^2 - \end{bmatrix}_n$$

Lippmaa *et al.*[35] concluded originally that the ranges of chemical shift corresponding to each kind of Q^n unit were narrow and non-overlapping. Subsequent work involving a large number of silicates of various types[36] revealed that chemical shift ranges in silicates do in fact overlap significantly, with the exception of those for Q^3 and Q^4 units. Figure 3.6a shows the information available at present for silicates.

The "Q notation" used above comes from ^{29}Si work on silicate solutions where silicon atoms in monosilicates, *i.e.* in isolated SiO_4^{4-} groups, are denoted by Q^0, disilicates and chain end groups by Q^1, middle groups in chains by Q^2, chain branching sites by Q^3, and fully cross-linked framework sites by Q^4. This notation is not sufficient to describe the basic building units in aluminosilicates such as zeolites. While in framework silicates the environment of each silicon atom is always Q^4 (4Si), in framework aluminosilicates there are five possibilities described by the formula Q^4 [nAl, (4-n)Si] where n = 0, 1, 2, 3, 4. These five basic units are normally referred to as Si(nAl) units, which expresses the fact that each silicon atom is linked, *via* oxygens, to n aluminium and (4-n) silicon neighbours.

Lippmaa *et al.*[35] found that when one or more Si atoms in a Q^4 unit are replaced by Al atoms, a significant paramagnetic shift results, *i.e.* the ^{29}Si chemical shift becomes less negative. In general, the substitution Si[(n-1)Al] $\longrightarrow$ Si(nAl) brings about a high-frequency shift of *ca.* 5 ppm (see Figure 3.6b). The spectra of aluminosilicates were in good agreement with known crystal structures.[35,37]

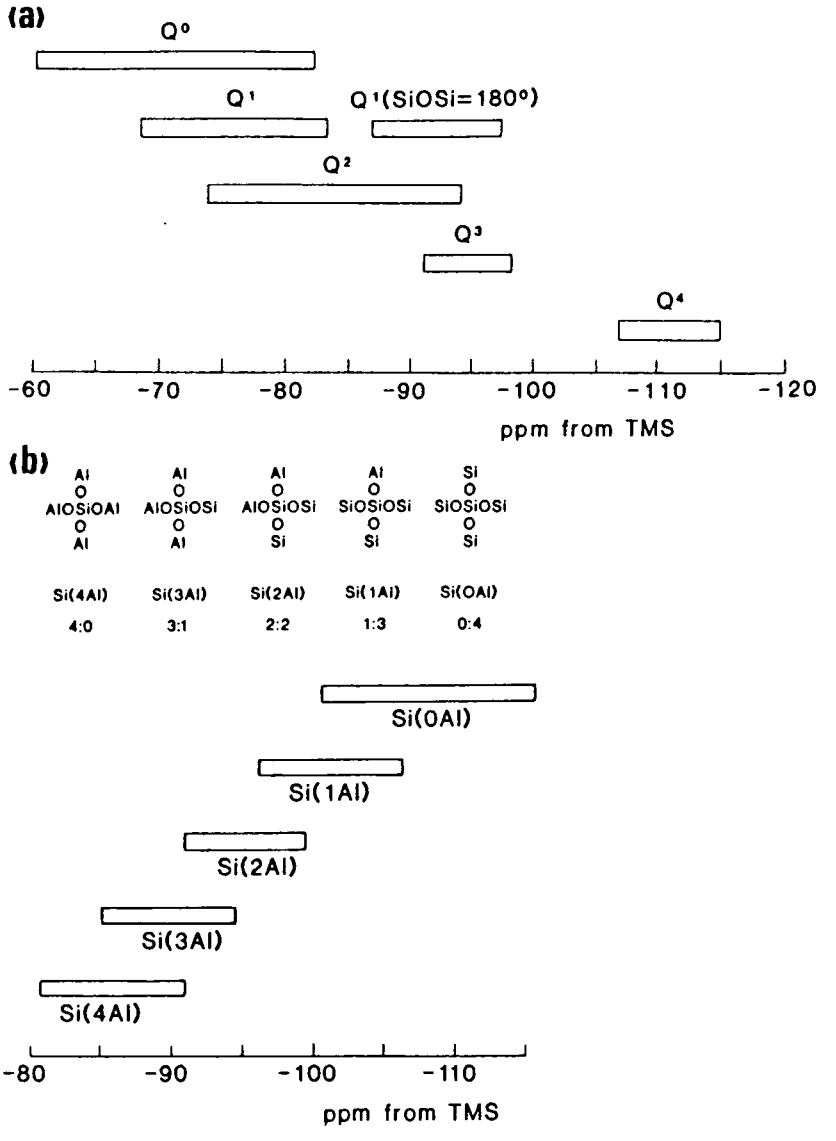

Figure 3.6

a) Ranges of ^{29}Si chemical shifts in silicates

b) Ranges of ^{29}Si chemical shifts in zeolites

For instance, the spectrum of the natural zeolite thompsonite, $Na_4Ca_8(Al_{20}Si_{20}O_{80}).24H_2O$, in which all Si atoms are crystallographically equivalent and alternate with Al atoms in the framework, contains a single signal at -83.5 ppm, assigned to Si(4Al); while the spectrum of natrolite, $Na_2Al_2Si_3O_{10}.2H_2O$, which is known to contain two kinds of Si atoms, Si(3Al) and Si(2Al) in the ratio 2:1, shows two signals in the same ratio of intensity. The spectra of zeolites X and Y (synthetic faujasites) show, depending on composition, all five Si(nAl) signals, while the spectrum of zeolite A (Si/Al = 1.00) has just one signal which indicates that the environment of each Si atom is identical, *i.e.* that there is ordering in the zeolite framework.

In the years since the pioneering work of Lippmaa and Engelhardt,[34,35] many research groups worldwide have become interested in the application of MAS NMR to the structural elucidation of zeolites. This is reflected in the huge body of work published as well as the number of reviews of the subject available in the literature. Consequently, no attempt will be made here to review the entirety of the literature published. However, in the light of results obtained for a variety of zeolite systems, the most important points raised will be discussed in some detail.

3.2.1. ^{29}Si studies

a) The structure of zeolite A (see Figure 3.2)

The most surprising result of the early ^{29}Si MAS NMR experiments on zeolites was the observation[34] that in the spectrum of zeolite A there is a single sharp resonance at -89.0 $\pm$ 1 ppm. On the basis of the chemical shift ranges found by Lippmaa *et al.*,[35] this result pointed to

a 3:1 ordering rather than the expected 4:0 ordering, corresponding to, instead of Si(4Al) units *i.e.* strict alternation of Si and Al atoms in the zeolitic framework, Si(3Al) units, where each Si atom in the structure is linked to three Al atoms and one Si atom and *vice versa*. Thus each Al is linked to three Si and one other Al, breaking the Loewenstein rule[32] which forbids Al-O-Al linkages.

X-ray structural investigations[38,39] of hydrated and dehydrated single crystals of Na-exchanged zeolite A (Si/Al = 1.00) led to the conclusion that the (cubic) space group of the zeolite is $Fm\bar{3}c$, and that the Si and Al atoms alternate throughtout the structure (see Figure 3.7a). The presence of a single ^{29}Si resonance in the spectrum of zeolite A proves the existence of Si,Al ordering but the chemical shift of the signal coincides with the Si(3Al) signal in zeolite X which is also built of sodalite units. Thus the ^{29}Si NMR results appeared to be at odds with the findings of the X-ray studies. The suggested non-Loewensteinian structure of zeolite A[35] involved alternating Si,Al distribution within the cubooctahedral sodalite cages, but Al-O-Al bridges in the double four-membered rings joining the cages. Since each tetrahedral atom is part of one such ring, each Al atom would be involved in an Al-O-Al linkage. However, this structure was rejected on the grounds of incorrect unit cell repeat.

Bursill *et al.*[40] having confirmed the NMR results of Lippmaa *et al.*,[35] re-examined the structure of zeolite A using HREM and neutron diffraction. They discovered[41] that dehydrated Na-A exhibited a small rhombohedral distortion and therefore the space-group assignment ($Fm\bar{3}c$), which had been used for the structural refinement for the 4:0 structure, was not valid. They also found that many of their electron diffraction patterns appeared[40] to be irreconcilable with a 4:0 ordering scheme.

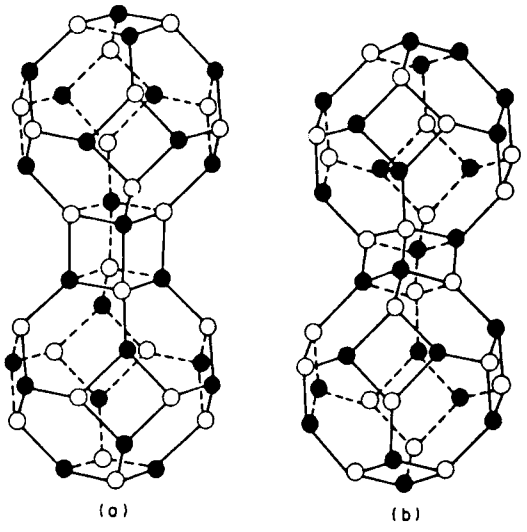

Figure 3.7

(a) The original model for the structure of zeolite A

(b) The alternative model

They therefore concluded that Al-O-Al linkages were probably responsible for the rhombohedral distortion, and were able to show that a cubic structure (space group Pn3n) for zeolite A could be assembled from rhombohedral units. They also found[41] that encouraging structural refinement of their neutron diffraction data could be obtained in space group $R\bar{3}$. All this led Bursill *et al.*[40,41] to propose an alternative structure for zeolite A (see Figure 3.7b).

However, Rayment and Thomas[42] showed by powder XRD, that the crystal symmetry of Na-A is a function of the degree of hydration and of temperature. In the hydrated condition the structure is perfectly cubic. Next, using neutron diffraction, Cheetham *et al*[43,44] found that

the rhombohedral distortion in dehydrated Tl-A and Ag-A is extremely small and that $Fm\bar{3}c$ was a more appropriate space group than Pn3n to interpret their powder diffraction data.

The controversy was finally resolved by the results of two independent ^{29}Si MAS NMR experiments by Thomas *et al.*[45] and Melchior *et al.*[46] who examined the spectra of zeolite ZK-4, the high-silica variant of zeolite A (*i.e.* Si/Al > 1.00). The ^{29}Si MAS NMR spectrum of ZK-4 must contain more than one resonance, signals corresponding to the same type of Si(nAl) unit in zeolite A and zeolite ZK-4 should therefore coincide. [For a given aluminosilicate structure the ^{29}Si chemical shifts for each kind of Si(nAl) unit are only marginally affected by variation in Si/Al ratio.] Also the correctness of the assignment of peaks in the latter zeolite can be checked by comparing the Si/Al ratio as obtained from the spectrum with the results of chemical analysis (*vide infra*). It was found that the ^{29}Si spectrum of ZK-4 does indeed contain several peaks, and that when the resonance at -89.0 $\pm$ 1 ppm is assigned to Si(4Al) rather than Si(3Al), good agreement between $(Si/Al)_{NMR}$ and $(Si/Al)_{XRF}$ ratios is obtained.

To summarise, the ordering in zeolite A is Si(4Al). Thomas *et al.*[45] suggested that the unusually low chemical shift in zeolite A is due to the presence of strained double four-membered rings (see Figure 3.2 and Table 3.2) with Si-O-Al angles of 129, 152, 152, and 177°. It is assumed that the presence of nearly linear linkages modifies the bonding, which in turn affects the values of the chemical shift. The influence of T-O-T angles on chemical shift values will be considered in part (e) of this section on ^{29}Si NMR.

The point to note here is that the assignment of a single ^{29}Si resonance line, as in zeolite A, to a particular Si(nAl) environment is ambiguous. This is in contrast to the zeolites to be discussed next,

faujasites, where a range of compositions are available within the same crystal framework.

b) Si,Al ordering in Zeolites X and Y (faujasites) and determination of the composition of the aluminosilicate framework.

Faujasites with Si/Al ratios between 1.0 and 1.5 are, by convention, designated zeolite X; beyond that ratio, faujasitic zeolites are designated zeolite Y. Figure 3.8 shows ^{29}Si spectra of zeolites X and Y of different compositions.[47] As the Si:Al ratio approaches unity, the spectra converge to a single Si(4Al) line, *i.e.* towards strict ordering within the aluminosilicate framework, the Al and Si atoms alternating as occupants of the tetrahedral sites. In other words, Loewenstein's rule[32] is strictly obeyed. Engelhardt *et al.*[48] used this fact to derive Si/Al ratios from ^{29}Si MAS NMR spectra. They recognised that the first-order neighbourhood of every Al atom is Al(4Si) so that each Si-O-Al linkage in a Si(nAl) structural unit is equivalent to Al/4 atoms, it follows that the Si/Al ratio in the tetrahedrally bonded anionic framework is given by:

$$(Si/Al)_{NMR} = \frac{\sum_{n=0}^{4} ISi(nAl)}{\sum_{n=0}^{4} 0.25n\ ISi(nAl)} \quad \ldots \quad (1)$$

This equation is only valid if no Al-O-Al linkages are present. Moreover, when for a particular zeolite, the ratio derived by ^{29}Si MAS NMR does not coincide with the ratio measured either by conventional X-ray fluorescence (XRF), analytical electron microscopy or by wet chemical methods, it means that either the Loewenstein rule is inapplicable or non-framework Al or Si (such as detrital silica or

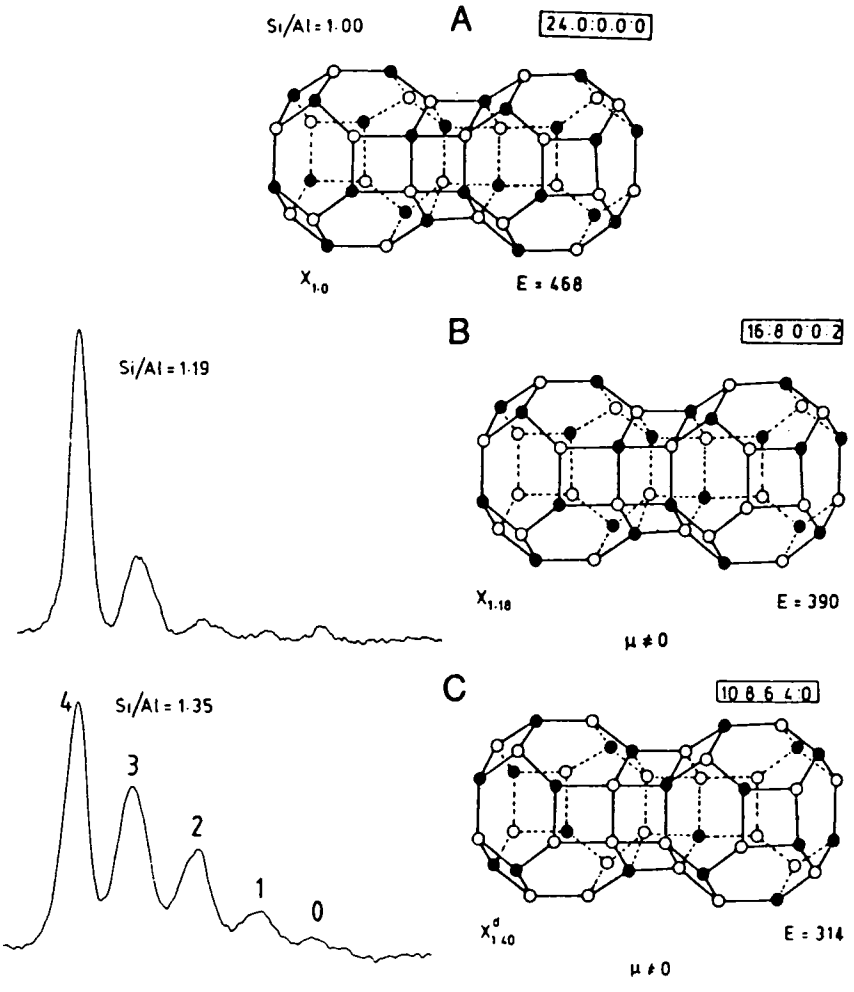

o = Si

• = Al

E = calculated electrostatic energy for the double cage [units $(qe)^2/a$]

Figure 3.8

A) Si,Al ordering scheme in a hypothetical zeolite X with Si/Al = 1.00. Ratios of populations of basic Si(nAl) units Si(4Al) ⟶ Si(0Al), corresponds to the scheme given in upper right hand corner of the Figure.

B) and C) Left hand side: ^{29}Si MAS NMR spectra of the two zeolites Na-X with Si/Al ratios of 1.19 and 1.35 respectively. Right hand side: most probable structures based on electrostatic and other considerations for the nearest "ideal" Si/Al ratio. $\mu \neq 0$ denotes net dipole moment in double sodalite cage.

hydrated Al^{3+} ions) is present. Very good agreement has been found between composition determined using this equation and by conventional analytical techniques.[47] Thus Loewenstein's rule is obeyed in faujasites.

The ^{29}Si MAS NMR spectra provide a way of determining Si,Al ordering in the lattices of microcrystalline aluminosilicates where X-ray diffraction methods are not applicable. It should be remembered that the NMR spectra do not themselves provide evidence for Si,Al ordering beyond the first tetrahedral coordination shell (as NMR is a technique that yields spatially averaged *i.e.* short-range information). Structural models may be constructed which are compatible with the NMR-determined ratio of the populations of Si(nAl) units (as deconvoluted using computer-simulated spectra based on Gaussian peak shapes), bearing in mind the need for any such model to comply with the requirements of crystal symmetry and with Loewenstein's rule. Sometimes more than one ordering scheme is compatible with a set of spectral intensities. In these cases, additional arguments must be invoked and the choice between the competing ordering schemes is finally made on the basis of three criteria: a goodness of fit of experimental and model-generated Si(nAl) intensities; compliance with the correct crystal symmetry and unit cell repeat as determined by X-ray crystallography; and minimal electrostatic repulsion within the aluminosilicate framework. The most likely ordering scheme in zeolites X and Y for the compositions corresponding to the spectra on the left-hand side of Figure 3.8 are given on the right-hand side of the Figure.

Equation (1) works well for materials with framework Si/Al ratios below *ca.* 10. For more siliceous zeolites, the ^{29}Si MAS NMR spectrum is dominated by the Si(4Si) signal and the estimation of composition

becomes inaccurate.

(c) ^{29}Si MAS NMR of gallosilicate zeolites

Vaughan *et al.*[49] and Thomas *et al.*[50] have recently reported ^{29}Si MAS NMR studies of the sodium forms of (Si,Ga)-sodalites and (Si,Ga)-faujasites. Their findings are summarized below:

1) $(Si/Ga)_{NMR}$ ratios calculated from a formula similar to eq. (1) agreed closely with chemical analysis *i.e.* the gallosilicate equivalent of the Loewenstein rule applies (no Ga-O-Ga linkages are present).

2) The composition of (Si,Ga)-sodalite was Si/Ga > 1, so more than one ^{29}Si signal was observed. It was found that the distribution of signal intensities corresponding to various Si(nGa) units in gallo-sodalite was different from that measured in aluminosilicate zeolites ZK-4 and X of similar Si/T ratio (T = Al or Ga).

3) The ^{29}Si chemical shifts in gallium zeolites span a wider range than the corresponding aluminosilicates (25.1 ppm *vs.* 18.5 ppm).

4) The Si(nGa) atoms are deshielded in comparison with Si(nAl) silicons with the same n in aluminium zeolites. Vaughan *et al.*[49] suggest that this effect may be related to the magnitude of the T-O-T angle. The "non-bonded radius" approach by O'Keefe and Hyde[51] indicates that Si-O-Ga angles would generally be smaller than Si-O-Al angles, and consequently gallium substitution would tend to deshield the silicon atom.

Thomas *et al.*[50] also recorded the ^{71}Ga MAS NMR spectra of gallosilicate zeolites. However, the single resonance was too broad for ready interpretation. Hayashi *et al.*[52] in a study of various Ga-substituted zeolites produced results similar to those of Vaughan *et al.*[49] and Thomas *et al.*.[50] Recently, Xin-Sheng and Thomas[52] have reported the synthesis and characterization of a variety of gallium

substituted silicate zeolites, specifically Ga-silicalite II (ZSM-11). They used IR spectroscopy and ^{71}Ga MAS NMR to prove that Ga has entered the framework.

d) ZSM-5/Silicalite and other pentasil zeolites

The structure of ZSM-5 was discussed in section 3.1.2. Silicalite is a thermally stable, crystalline, microporous silica. It is a synthetic material and is topologically identical to ZSM-5, except that it has a lower aluminium content.

In the light of what has been said about the appearance and interpretation of ^{29}Si MAS NMR spectra of zeolites, one might expect the spectrum of a highly siliceous zeolite to be uncomplicated and to display a single Si(4Al) signal, sometimes with a smaller Si(3Si) resonance, depending on the Si/Al ratio. The typical spectrum of ZSM-5 is indeed featureless[53] (Figure 3.9). However, Fyfe *et al.*[54] have shown that the ^{29}Si MAS NMR spectrum of a sample of silicalite with a particularly low aluminium content shows considerable fine structure (Figure 3.10) arising from the crystallographically inequivalent tetrahedral environments of the Si(4Si) sites. The spectrum may be simulated by a minimum of nine Gaussian signals, the intensities of which are approximately in the ratio 1:3:2:3:10:1:1:2:1. Using the intensities of the well resolved lowest- and highest-frequency signals as base units of one, the total intensity of the component peaks in the multiplet is 24. This result suggests that the space group of silicalite is not Pnma, which provides for 12 non-equivalent sites in the structural repeat unit, but some other space group (such as Pn2, $P2_1/n$ or $P2_12_12_1$) providing for 24 such sites. No attempt has been made to assign individual ^{29}Si signals to specific crystallographic sites,

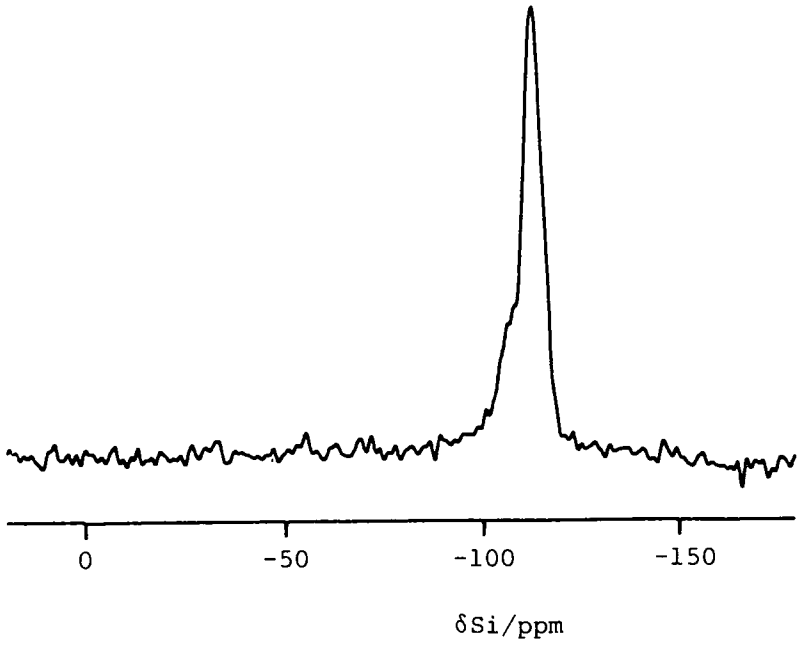

Figure 3.9

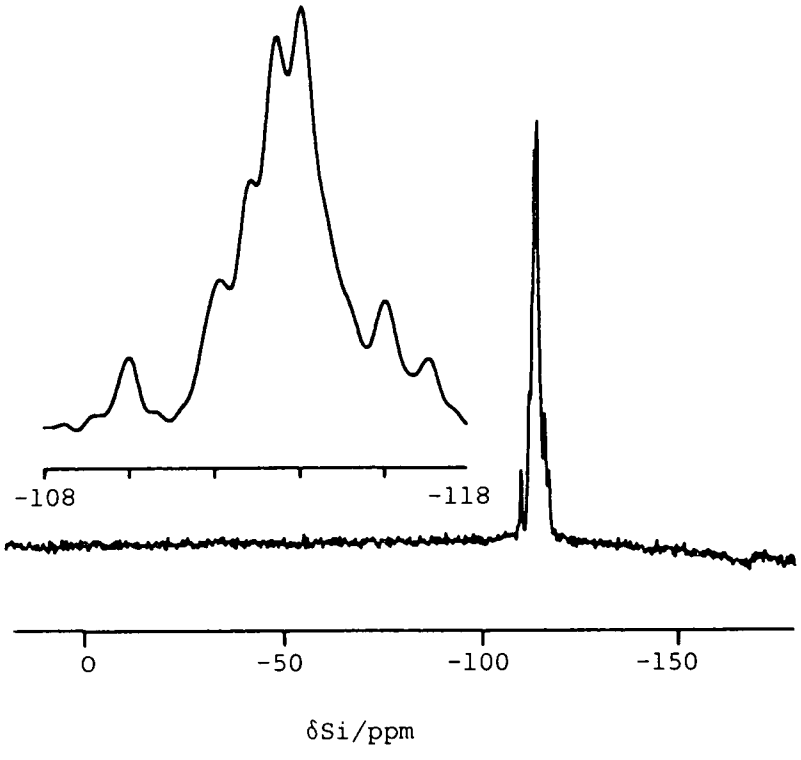

Figure 3.10

mainly because the details of the structure of silicalite are not sufficiently well established.

Apart from silicalite, the spectra of synthetic zeolites do not in general reveal signals which may be assigned to non-equivalent silicon sites.

Hay *et al.*[55] and Fyfe *et al.*[56] have used variable temperature ^{29}Si MAS NMR, together with powder XRD, to monitor the reversible change with temperature of silicalite (highly siliceous ZSM-5) from monoclinic to orthorhombic phase. The ^{29}Si NMR spectrum of the orthorhombic material was successfully deconvoluted into 24 identical Gaussian peaks, suggesting that the orthorhombic space group for silicalite at 353 K is $Pn2_1a$ with 24 unique tetrahedral Si atom sites in each cell.

Fyfe *et al.*[57] and West[58] independently reported on the changes which occur in the ^{29}Si MAS NMR spectrum of highly siliceous ZSM-5 (silicalite) when sorbate molecules are present in the channel system. The changes, also monitored by XRD, indicate that structural changes causing lattice distortion are occurring which are characteristic of the sorbate used. West also reported that addition of excess ethanol, propanol, or decane caused a loss of signal intensity which was attributed to an increase in ^{29}Si spin-lattice relaxation time (T_1). Although there has been no systematic study of T_1 in aluminosilicates, to date, it was generally assumed that spin diffusion from paramagnetic centres was the controlling mechanism. Barron *et al.*[59], however, found little correlation between the total Fe^{3+} content and their respective T_1 values for ^{29}Si and ^{1}H in layer silicates. Watanabe *et al.*[60a] investigated the influence of paramagnetic impurities on the ^{29}Si MAS NMR spectra of 12 clay minerals. They found T_1 to be inversely proportional to the concentration of paramagnetic species and that the

linewidth increased with Fe^{3+} concentration, demonstrating that dipolar interactions between ^{29}Si and the electron spin of the Fe^{3+} ion is largely responsible for line broadening. Iwamiya and Gerstein[60b] have recently measured the ^{29}Si T_1 values of a number of offretite samples. The results of their NMR and ESR studies indicate that the T_1 of offretite is dominated by dipolar couplings to a specific type of paramagnetic centre in the framework. This centre is some type of Fe^{3+} species located in the framework and/or in the channels and cages of the zeolite.

Debras *et al.*[60c] in an investigation of both precursors and calcined forms of pentasil type materials have shown that the ^{29}Si T_1's vary in the range 10-150 s and 5-8 s, respectively. The T_1 values for the precursor materials depend strongly on the H_2O, Al, and Na contents. The opposite was found to be true for the calcined materials.

Following on from the work of Fyfe *et al.*[57] and West,[58] Cookson and Smith[61] have reported that gaseous (paramagnetic) molecular oxygen significantly affects the ^{29}Si T_1 of silicalite. They found that a plot of $1/T_1$ against atmospheric oxygen content was linear and that under ambient conditions, the effect of paramagnetic oxygen accounts for over 95% of the observed ^{29}Si spin-lattice relaxation rate ($1/T_1$). They proposed that the effects noticed by Fyfe *et al.*[57] and West[58] on sorption of organics are due to the organic species displacing gaseous oxygen from the channels with the consequent increase in ^{29}Si relaxation times.

^{29}Si NMR cross polarization (CP) experiments have been used to detect the presence of defects in the zeolite lattice. In a study of ZSM-5 type zeolites, Nagy *et al.*[62] identified the silanol group (Si-OH) at -103 ppm. Silanol groups have also been observed[63] in faujasite-type structures at -100 ppm using ^{29}Si CP/MAS NMR. Boxhoorn *et al.*[64] and

more recently Woolery *et al.*[65] have used ^{29}Si CP MAS NMR and FTIR to show the presence of internal silanols in highly siliceous ZSM-5. Engelhardt *et al.*[66] have studied ^{29}Si-enriched forms of ZSM-5 by ^{29}Si MAS NMR. They detected a new signal at -98 ppm in the ^{29}Si spectrum and again detected SiOH groups (in the proton containing form of ZSM-5) using CP ^{29}Si NMR.

ZSM-11 (another highly siliceous zeolite belonging to the pentasil family) has been studied by Nagy *et al.*[67] and Fyfe *et al.*.[68] No fine structure could be detected in the ^{29}Si MAS NMR spectrum of ZSM-11 (Si/Al = 1000)[67] in contrast to that observed for ZSM-5. Fyfe *et al.*[68] studied a highly siliceous ZSM-11 sample that had been prepared by hydrothermal dealumination. The ^{29}Si MAS NMR spectrum of the dealuminated ZSM-11 revealed crystallographically inequivalent sites, as has been observed for silicalite.

(e) Relationship between the ^{29}Si isotropic chemical shift(δ) and T-O-T angle(θ) or T-T distance in aluminosilicate zeolites.

Thomas *et al.*[49] have suggested that a correlation exists between the ^{29}Si isotropic chemical shift value and averaged T-O-T angle in zeolites. The Si(3Al) signal in zeolites X and Y is coincidental with the Si(4Al) signal in zeolites A and ZK-4, and they suggested that this related to the larger value of the Si-O-Al angle in the latter structures. Grimmer *et al.*[69] found the isotropic ^{29}Si chemical shift(δ) of the non-zeolitic mineral zunyite to be -128.5 ppm (from TMS) and commented on the apparent relationship between δ and the Si-O-Si angle which is almost 180^{o}. Jarman[70] considered the quantitative relationship between δ and θ for several dealuminated zeolites. The average values of θ for hydrothermally dealuminated zeolite Y and dealuminated acid-washed mordenite are very close to those in non-

dealuminated materials. Thomas *et al.*[71] assumed this to be true for other dealuminated zeolites and proposed the following linear correlation between θ (degrees) and δ (ppm) from TMS:

$$\delta = -25.44 - 0.5793\ \theta \quad \cdots \quad (2)$$

Equation (2) correlates the chemical shift of the Si(OAl) signal with the magnitude of the T-O-T angle. In an attempt to extend the correlation to all five Si(nAl) signals, Ramdas and Klinowski[72] used the accumulated NMR data on many zeolites to derive a semi-empirical relationship between δ of a Si(nAl) signal and Σd_{TT} the total (non-bonded) Si...T distance (T = Si or Al) in Ångstroms calculated from the T-O-T angle, assuming constant Si-O and Al-O bond lengths of 1.62 and 1.75 Å respectively:

$$\delta = 143.03 - 20.34\ \Sigma d_{TT} \quad \ldots \quad (3)$$

where $\Sigma d_{TT} = [3.37n + 3.24(4-n)] \sin \frac{\theta}{2}$. Theoretical lines were drawn for Si(nAl) units with n = 1, 2, 3, and 4 assuming the same slope as for Si(OAl) but including an additional term to account for the paramagnetic contribution of n tetrahedral aluminium atoms to the chemical shift of the central silicon. The experimental data were found to be in close agreement with the theoretical lines and Ramdas and Klinowski suggested that their work might serve as a basis for estimation of the T-O-T angle for each kind of silicon in an aluminosilicate of unknown structure from ^{29}Si MAS NMR data.

Radeglia and Engelhardt[73] have attempted to explain the empirical correlation between δ and mean Si-O-T bond angles in aluminosilicates by using a semi-empirical quantum mechanical model. They derived a linear correlation of δ and cos α/cos(α - 1), whereby the number, n of the Al atoms in the five $Si(OSi)_4$ - $n(OAl)_n$ structural units has to be taken into account by an additive term. The linear correlation was confirmed by an extended set of experimental data. Their theoretical treatment

also offered a general explanation for the empirical correlations of Thomas *et al.*,[71] Ramdas and Klinowski,[72] and Smith and Blackwell.[74] This same approach has most recently been applied by Engelhardt *et al.*[75] to highly dealuminated ZSM-5. With moderate resolution enhancement, Engelhardt *et al.*[75] identified 17 separate signals in the ^{29}Si MAS NMR spectrum due to crystallographically non-equivalent silicons in the zeolite framework. Each of these signals could be assigned a mean Si-O-Si angle from the equation:

$$\delta/(\text{ppm}) = -247.05 \times \frac{\cos \bar{\alpha}}{\cos(\bar{\alpha} - 1)} + 2.19 \quad \cdots \quad (4)$$

where $\bar{\alpha}$ is the mean Si-O-Si angle.

From the range of bond angles determined, in comparison to those obtained by Olsen *et al.*[76] for orthorhombic ZSM-5, they assigned their dealuminated ZSM-5 a monoclinic symmetry.

Grimmer[77] has attempted to use all the information available from ^{29}Si NMR concerning the chemical shift. He compared the ^{29}Si shielding tensor data for solid silicates with structural data for the corresponding SiO_4 tetrahedra, and demonstrated a linear relationship between individual Si-O bond lengths and the "bond direction related" shielding along the directions of the four Si-O bonds. He interpreted the result in terms of the fractional s character of the silicon and oxygen hybrid orbitals in the Si-O bonds.

Janes and Oldfield[78] have used group (fragment) electronegativities to predict ^{29}Si shifts in silicates and aluminosilicates. When all types of silicon were considered, their empirical approach was found to have a good correlation between some 99 sites in 51 different silicate and aluminosilicate compounds.

(f) Effect of cation on ^{29}Si isotropic chemical shift.

The influence of cation type and position on the ^{29}Si isotropic

chemical shift has been recognised from the outset of ^{29}Si NMR work on zeolites,[34] and solid silicates.[36] Thomas *et al.*[45] observed a wide chemical shift range for zeolite A depending on cationic form *e.g.* Li-A (-85.1 ppm), Ba-A (-90.5 ppm). This effect coupled with the fact that dealuminated samples yield information about non-equivalent crystallographic (^{29}Si) sites, led Jarman[70] and others to dealuminate samples in work concerning the relationship between δ and θ, and so remove the charge-balancing cations. Grobet *et al.*[79] have investigated the effect of dehydration on the ^{29}Si MAS NMR spectrum of Ca-Y zeolite. The spectrum is more complicated than the hydrated spectrum showing at least two extra lines attributed to distortion effects on the lattice silicons of the cations being more localized than in the hydrated state.

Fyfe *et al.*[80] monitored, using powder XRD and ^{29}Si MAS NMR, the exchange of cationic species that can occur between different zeolite crystals on simple physical contact of the crystallites. Li- and Na-A zeolites were chosen for the investigation as they both give well-defined XRD patterns and a simple sharp absorption line in their ^{29}Si MAS NMR spectra. On immediate contacting of the two cationic forms of zeolite A, changes were observed in both the XRD pattern and the ^{29}Si MAS NMR spectrum. The replacement of Li^+ for Na^+ causes unit cell shrinkage to occur, and this was detectable in the XRD trace. The XRD pattern of the mixture showed the superposition of the two patterns giving a "doublet" splitting of many of the peaks and indicating clearly that the sample consists of a simple physical mixture of the two sets of crystallites. This was confirmed by the ^{29}Si MAS NMR spectrum which initially showed two lines and then at equilibrium a single line.

(g) Factors determining line-shape and resolution in zeolites.

Substantial improvement in resolution is achieved on going to

higher field in the study of zeolites. Resolution generally increases until fields of 4.7 T are reached, and beyond this, no further improvement is observed. Melchior[81] suggested that the likely cause of this improvement in resolution was due to ^{29}Si-^{27}Al dipole-quadrupole interaction (an effect not averaged to zero by MAS). To test this theory, Fyfe *et al.*[82] prepared a variety of highly siliceous zeolites. A very marked decrease in linewidths was noticed on going from low Si/Al zeolites to highly siliceous forms of the same zeolites. When no aluminium was present the line-broadening was removed. Further, as seen in zeolite A [Si(4Al)], when aluminium is present but it is in a very symmetrical environment, a very narrow line is again observed. Clearly, the line-broadening mechanism involves the aluminium atoms in the lattice. If this effect were due to direct magnetic interactions which would depend mainly on the nearest neighbours, a decrease in linewidth would be apparent in the ^{29}Si MAS NMR resonances due to Si(3Al) to Si(2Al) to Si(1Al) to Si(0Al). The fact that all absorptions have residual broadening of the same magnitude, suggests that although the aluminiums are responsible for this residual broadening in these systems, it is by a less direct route than direct magnetic interactions. An alternative mechanism is that a large number of silicon environments for each of the different Si(nAl) first coordination sphere absorptions is created by the distribution of aluminium atoms in the second and furthest coordination spheres. This effect may be manifest both by the proximity of different atoms and by distortions of bond angles and bond lengths. The substantial low-frequency shift of the Si(0Al) signal upon removal of aluminium atoms is seen as experimental proof of this alternative line-broadening mechanism. Thus, the placing of a single aluminium atom may affect many silicons. If the line-broadening is indeed due to the distribution of aluminium in second and further

nearest coordination spheres, then narrow ^{29}Si resonances are predicted for any perfect ordered system, whatever the first coordination sphere may be. This is borne out by the sharp resonance for zeolite A attributed to perfect ordering.

3.2.2. ^{27}Al NMR studies of zeolites.

Details concerning the experimental procedures and potential problems to be encountered in the observation of a quadrupolar nucleus, such as ^{27}Al, are given in Chapter Four. The NMR theory pertaining to nuclei with nuclear spin $I > 1$ (non-integer) is delineated in Chapter Two.

^{27}Al has a nuclear spin of 5/2, is 100% abundant, and has, in solution-state, a large chemical shift range. Being a quadrupolar nucleus *i.e.* possessing a quadrupole moment, the symmetry of the environment of the nucleus is very sensitive to distortions and this is directly reflected in the linewidth of the ^{27}Al resonance. Useful chemical information can be obtained from observation of ^{27}Al nuclei in the NMR experiment provided quadrupole-coupling and chemical shift effects can be separated. In solids, this can be achieved with magic-angle rotation of the sample. The ($1/2 \longleftrightarrow -1/2$) transition (normally observed) is independent of quadrupolar effects to first order, but is affected by second-order quadrupolar effects which are inversely proportional to the magnetic field strength. Thus, the best spectra will be obtained at very high magnetic field strengths (11.7 T is the largest commercially available field strength).

Solution-state studies[83] have shown that four-coordinated aluminium (with respect to oxygen) resonates at 60-80 ppm and six-coordinated aluminium at around 0 ppm {relative to six-coordinated Al in

$[Al(H_2O)_6]^{3+}$}. Thus, ^{27}Al NMR is a sensitive tool for determining the coordination of aluminium.

Müller *et al.*[84] were the first to carry out a systematic investigation of ^{27}Al MAS NMR spectra of polycrystalline aluminates. Their results showed that aluminium in the solid-state mirrored the results obtained for aluminium in solution-state *i.e.* that tetrahedral Al could be distinguished from octahedral Al on the basis of the chemical shift with magic-angle spinning at high-field strengths.

The first ^{27}Al MAS NMR study of zeolites was carried out by Freude and Behrens.[85] They measured chemical shifts and linewidths of signals from both stationary (broad-line) samples and spinning samples at two different magnetic field strengths. They then calculated the quadrupole frequencies and the centre of gravity of each line due to the observed shifts. They showed that at 70 MHz there was several ppm difference between the quadrupole corrected (calculated) chemical shift and that observed for Na-A, Tl-A, Na-Y, and Tl-Y zeolites. Fyfe *et al.*[86] measured high-resolution ^{27}Al MAS NMR spectra of a number of natural and synthetic zeolites at 104.22 MHz (400 MHz proton). All the spectra contained one peak, the chemical shifts of which fell within the 50-70 ppm range reported for four-coordinated Al by Müller *et al.*[84] and by Freude and Behrens.[85] In dealuminated zeolites an additional signal was observed corresponding to six-coordinated Al in the zeolitic channels. Fyfe *et al.*[86] reported that on increasing the magnetic field strength from 23.45 MHz (90 MHz proton) to 104.22 MHz, very substantial improvement in the quality of the ^{27}Al MAS NMR spectrum of zeolite Na-A was apparent. The resonance lineshape of the four-coordinate Al at the lower field strength was severely distorted and had a linewidth of 10's of ppm. At 104.22 MHz, the resonance appeared symmetric, possessed spinning sidebands equidistant from the main peak, and had a linewidth

of *ca.* 6 ppm. The improvement was due to the reduction of second-order quadrupolar interaction at higher field.

Thus, ^{27}Al MAS NMR is a sensitive probe for the determination of the coordination of Al. It is relevant to note here that a change in Si coordination from four to six leads to an 80 ppm shift.[87a] (Cruickshank *et al.*[87b] have recently reported that the chemical shift of aluminium in penta-coordinated aluminates as determined by high-field ^{27}Al MAS NMR is approximately 35 ppm.). As we have already noted, species with different degrees of condensation of the SiO_4 tetrahedra span a 40 ppm shift range,[35] each substitution of Si by Al causes a 5 ppm paramagnetic (deshielded) shift.[37] Effects of a smaller nature could be expected for ^{27}Al NMR spectra as was pointed out by Freude *et al.*.[88] However, the study of these effects has been hampered by the small chemical shift range in zeolites and by the unavoidable second-order quadrupolar line shifts. Most of the ^{27}Al chemical shift data published correspond to the line centres of gravity and are uncorrected for quadrupolar effects. Thus the usefulness of ^{27}Al MAS NMR is limited primarily to coordination number determination. In one of the first systematic studies of Al in various zeolites, Nagy *et al.*[89] found no variation of ^{27}Al chemical shifts with the average T-O-T bond angle.

^{27}Al MAS NMR is however sometimes able to distinguish crystallographically non-equivalent tetrahedral Al atoms. One such example is zeolite omega where two separate types of site are observed at 130.32 MHz,[90] but not at 52.11 MHz due to increased second-order quadrupolar effects. Another example is silicalite. It has been argued[91] that silicalite is not a zeolite but a "porous form of silica", and any aluminium that may be present is in the form of Al_2O_3 impurity in the zeolitic channels. However, Fyfe *et al.*[54] have used ^{27}Al MAS NMR to detect the very small amounts of Al present in silicalite (below

X-ray crystallographic detection limits) and have demonstrated conclusively that there are at least two distinct types of tetrahedral framework sites occupied by Al in silicalite. When dealuminated ZSM-5 (Si/Al $\simeq$ 800) is investigated by ^{27}Al MAS NMR at high fields, the same splitting of the residual tetrahedral ^{27}Al signal is seen in the spectrum. This coupled with the fact that the ^{29}Si MAS NMR spectrum of highly dealuminated ZSM-5 is identical to that of silicalite proves the structural congruence of the two tectosilicates.

Kentgens *et al.*[92] used ^{27}Al MAS NMR to study the effect of hydration/dehydration on the electric field gradient at the ^{27}Al nucleus in zeolites ZSM-5 and H-Y at three different field strengths. They observed an initial decrease in linewidth of the tetrahedral Al signal in the hydrated samples on lowering of the magnetic fields. This suggests that the linewidth at high magnetic fields (300 MHz proton) is governed not by quadrupolar effects but by there being a distribution of ^{27}Al chemical shifts. This effect is dominated at lower fields by the quadrupolar interaction. They found that for dehydrated ZSM-5 samples, the quadrupolar effects were always dominant. In dehydrated samples, quadrupole interactions are so strong that the tetrahedral Al line disappears, to reappear on hydration. Obviously, this observation has important consequences for quantification studies of aluminium and two general points emerge: 1) ^{27}Al MAS NMR studies for the purpose of quantification of tetrahedral sites, or tetrahedral/octahedral ratios should always be performed on fully hydrated samples, and 2) to minimize quadrupolar effects, the highest possible magnetic field strength should always be used.

Recently, Lippmaa *et al.*[17] have addressed the problem of refinement of the ^{27}Al chemical shift data and their correlation with short-range order parameters in aluminosilicates. They report that at present there

are four methods that can be used for the determination of precise isotropic chemical shift values of half-integer quadrupolar nuclei in powder samples of solids:

(1) comparison of the experimental central (1/2,-1/2) transition line shapes with the calculated MAS NMR powder pattern line shapes;[12,15]

(2) evaluation of the quadrupolar shifts from several MAS NMR spectra, registered at different magnetic strengths;[85]

(3) measurement of the first or second spinning sidebands of the least shifted satellite ($\pm$3/2,$\pm$1/2) transition;[16]

(4) determination of the first-order quadrupolar interaction parameters by fitting the experimental MAS NMR excitation spectra[19,20,93] to the numerically simulated nutation spectra.

Lippmaa *et al.*[17] used all the above methods to determine the quadrupole corrected isotropic chemical shifts (with <1 ppm error) of a variety of natural framework zeolites (also synthetic Na-X and Na-Y zeolites). They found the most convenient shift refinement method to be registration of the ($\pm$3/2,$\pm$1/2) satellite transition spectra. Using the corrected (field-independent) isotropic chemical shifts obtained from such experiments, Lippmaa *et al.* found that there was a linear dependence of the ^{27}Al chemical shift on the mean Al-O-Si bond angles in the framework aluminosilicates studied.

3.2.3. Monitoring of chemical modification of zeolites.

Recently MAS NMR has been used to monitor the course of several important zeolite modifying processes whereby the composition of a zeolite is changed while the topology and crystallinity of the parent structure are retained. Results of particular interest are obtained using a process known as "ultrastabilization", which involves the

thermal treatment of NH_4-Y zeolite to produce an extremely effective cracking catalyst with high thermal stability. Another important reaction involves isomorphous replacement of framework Al with Si using $SiCl_4$ vapour at elevated temperatures.

(a) Decationation and ultrastabilization

Dehydration and thermal treatment of NH_4-Y zeolite under high vacuum at temperatures of up to 600^{o}C is known as "decationation". During this process water is removed, while the cation decomposes to give off ammonia; crystalline zeolite in the "hydrogen" (acidic) form is left behind. McDaniel and Maher[94-96] were the first to report that thermal treatment of NH_4-Y resulted in a considerable increase in stability of the zeolite. The following summarises the most important observations:

(i) thermally treated NH_4-Y has a greatly increased thermal stability;

(ii) the process is facilitated by low sodium content of the zeolite;

(iii) the process is facilitated by the presence of water vapour;

(iv) the properties of the product depend on the bed geometry during treatment;

(v) due to loss of Al, the unit cell dimension of the ultrastable zeolite is smaller than in the parent molecule;

(vi) if a thick layer of zeolite is gradually heated under atmospheric pressure the zeolite has a greatly reduced ion-exchange capacity;

(vii) framework vacancies created by the removal of Al are subsequently re-occupied by Si.

The proposed course[97] of ultrastabilization is shown below:

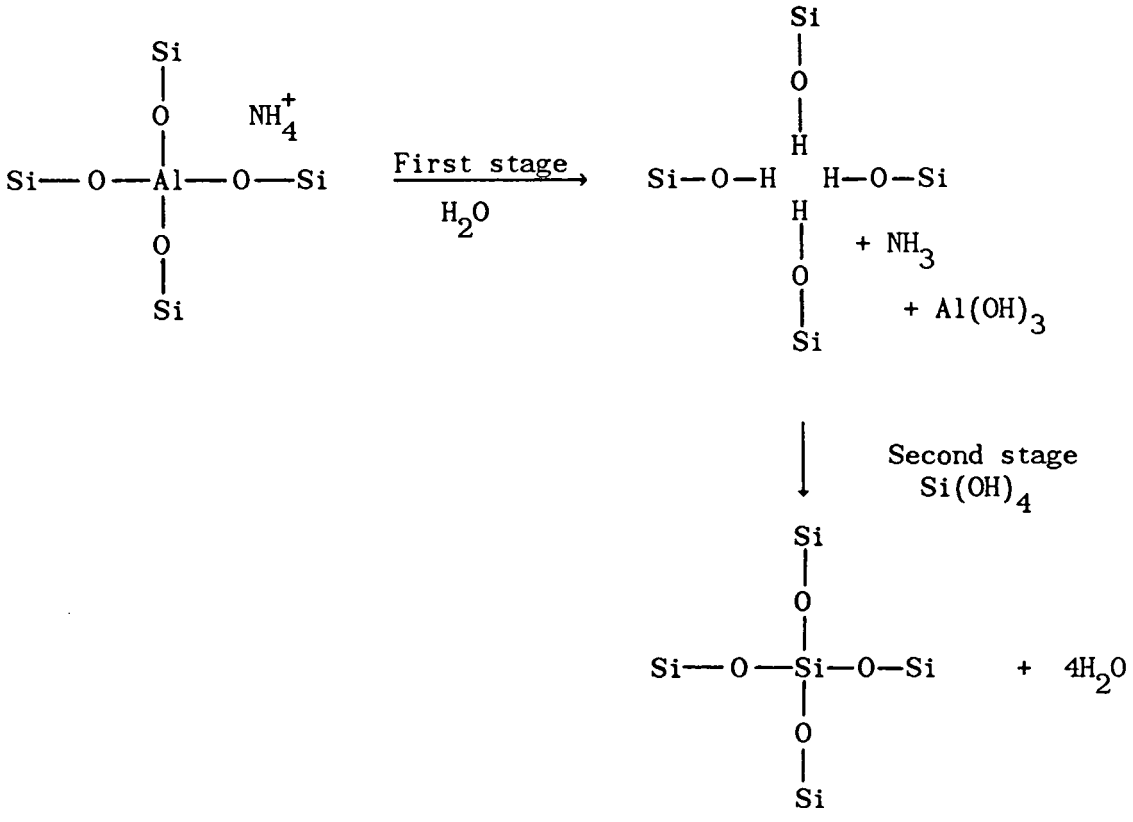

Ultrastabilization has been studied using solid-state NMR by several research groups.[63,98-105] ^{29}Si and ^{27}Al MAS NMR are used in tandem to follow the reaction. ^{29}Si MAS NMR spectra show[98] how the parent sample with a typical zeolite Y Si/Al ratio of 2.6 is transformed during the reaction to an ultrastable zeolite with Si/Al > 50 (by chemical analysis). The ^{29}Si spectrum shows one sharp Si(0Al) peak at -106.9 ppm and a small broad residual Si(1Al) peak at *ca.* -101.3 ppm. Clearly framework vacancies have been reoccupied as, if this were not the case, a range of Si environments including one, two, or three neighbouring hydroxyl groups would be apparent in the ^{29}Si spectrum. ^{27}Al MAS NMR shows directly[98] how the occluded six-coordinate Al builds up at the expense of the four-coordinate Al in the framework.

Engelhardt *et al.*[63] used ^{29}Si MAS NMR with cross-polarization in order to detect "surface" Si atoms (defect sites) attached to one or two hydroxyl groups. Si(3Si)(OH) groups were detected at -100 ppm, and

$Si(2Si)(OH)_2$ groups at -90.5 ppm, although the former signal coincides with that of Si(0Al) groupings. The absolute amounts of defect sites could not be determined because the enhancement factor (CP efficiency) was not known.

In another ^{29}Si MAS NMR study, Engelhardt *et al.*[101] considered the problem of Si,Al ordering in dealuminated Y zeolites in the range of compositions $2.5 \leq Si/Al \leq 5.8$. They found that the relative spectral intensities depended only on the final Si/Al ratio. Although this does not necessarily mean that the ordering is the same, this is a strong possibility. This is because "random" distribution and various different ordering schemes may in principle give rise to the same relative spectral intensities.

Freude *et al.*[85] carried out a systematic study of the relative amounts of 4- and 6-coordinated Al in thermally treated zeolite Y using wide-line and MAS ^{27}Al NMR at 16.0 and 70.34 MHz, respectively. The results showed the loss of ^{27}Al line intensity which takes place on treating zeolites (in comparison with the parent material) was due to extra-framework Al being in an environment of low symmetry. This "invisible" aluminium could be present as $Al(OH)_3$, $Al(OH)^{2+}$, $Al(OH)_2^+$, Al_2O_3, or some polymeric aluminous species.

Corbin *et al.*[106] used ^{27}Al MAS NMR to examine commercial samples of K-A, Na-A, and (Ca,Na)-A, as received. For K-A and Na-A only framework tetrahedral Al species were observed. However, in (Ca,Na)-A an additional intense resonance at 78 ppm, typical of $Al(OH)_4^-$ was found. Freude *et al.*[107] and Pruski *et al.*[108] came to very similar conclusions in their NMR and IR studies of heat-treated zeolite Ca-A. It appears that octahedral Al is produced in NH_4^+-exchanged (acid) zeolites on heating, and tetrahedral Al in Ca- (and Sr-) exchanged (basic) zeolites.

(b) ^{1}H MAS NMR studies of zeolite acidity

In zeolites Brønsted acidity arises because of the presence of accessible hydroxyl groups associated with framework aluminium ("structural hydroxyl groups") and can therefore be studied using ^{1}H and ^{27}Al MAS NMR. Brønsted acidity (and Lewis acidity) are conveniently monitored by observing the ^{1}H, ^{13}C, ^{15}N, and ^{31}P resonances from adsorbed molecules. NMR studies of the acidity of solid surfaces have been extensively reviewed.[109,110]

High-resolution ^{1}H MAS NMR is the most advanced tool for the measurement of zeolitic acidity. It is, however, a technique fraught with difficulties. Briefly the difficulties are: (i) the strong homonuclear dipolar interactions which necessitate the use of multiple-pulse line narrowing (spin-averaging) techniques and (ii) the narrow chemical shift range of protons. As a result, only a small number of lines can be expected to be resolvable. Despite these not inconsiderable problems, the Leipzig group in particular, led by Prof. H. Pfeifer, was able to obtain very important information on the chemical state of hydroxyls in zeolites[110b] and gels.

Freude *et al.*[111] obtained ^{1}H MAS NMR spectra of deep-bed (DB) treated zeolite Y (thick layer of zeolite thermally treated at atmospheric pressure) at 60 MHz and considered the magnitude of the proton chemical shift as a measure of Brønsted acidity. By comparing the spectra of their zeolite samples with those of various inorganic materials, they concluded that terminal Si-O hydroxyls and hydroxyls attached to extra-framework Al resonate at *ca.* 2 ppm from TMS, and the acidic hydroxyls at 6-10 ppm.

In another study, Freude *et al.*[104] used ^{1}H MAS NMR at 270 MHz with the WHH-4 pulse sequence to obtain high-resolution spectra of thermally treated zeolites. Three distinct lines are present and the authors

assign their chemical shifts as follows:

(i) 2.0 ppm - terminal OH groups and hydroxyl groups attached to extra-framework Al.

(ii) 4.2 - 5.0 ppm
(iii) 6.8 - 8.0 ppm
} due to structural hydroxyl groups

In addition, a signal at 7.1 ppm was observed in some samples. This was assigned as residual NH_4^+ cations. The sum of the intensities of (ii) and (iii) minus the intensity due to residual NH_4^+ cations gave the true total content of acidic hydroxyl groups.

Scholle *et al.*[112,113] used ^1H MAS NMR to study the acidity of the hydroxyl groups in zeolite H-ZSM-5 and H-boralite with various water contents. Without the use of multiple-pulse techniques they were able to distinguish terminal and water hydroxyls from acidic hydroxyl groups in the framework. H-ZSM-5 was found to be more acidic than boralite.

Other studies[114-117] of zeolite activity have involved the use of probe molecules and the observations of nuclei such as ^{15}N, ^{31}P, and ^{13}C. The molecules are sorbed on the zeolites and bind (chemisorption/physisorption) with the surface Brønsted and/or Lewis sites.

(c) The mechanism of dehydroxylation of zeolites.

When H-Y zeolite is subjected to further thermal treatment at higher temperatures, water is irreversibly lost from the framework in a process known as "dehydroxylation". The resultant zeolite Y displays both Brønsted and Lewis acid properties. The now well established mechanism for this process was suggested by Uytterhoeven *et al.*[118] and is depicted as follows:

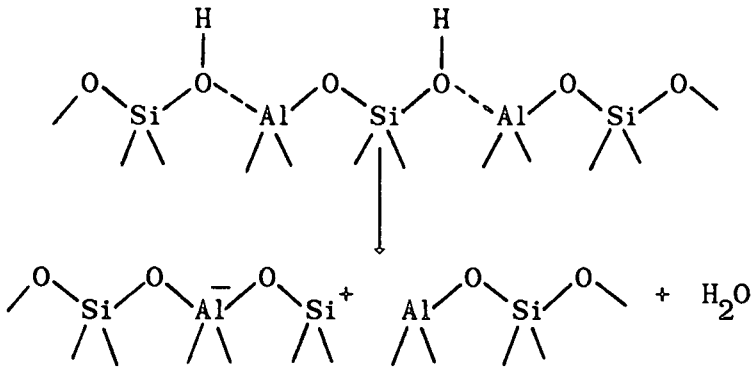

The scheme requires that:

(i) a defect structure involving 3-coordinated Si and Al is formed, with Lewis acidity being due to the latter;

(ii) the amount of 4-coordinated Al decreases with increasing degree of dehydroxylation. After complete dehydroxylation half the Al atoms remain 4-coordinated.

(iii) The number of 4-coordinated Al atoms is always greater than or equal to the number of structural hydroxyl groups (because two OH groups disappear for each framework Al atom).

The scheme has been repeatedly questioned in the light of X-ray and IR spectroscopic results which do not support it. However, the strongest arguments against this scheme come from NMR work.[102,104] No 3-coordinated Si or Al were observed; the amounts of structural hydroxyls and 4-coordinated Al are always equal; and much less than half of 4-coordinated Al was found after complete dehydroxylation.

It is therefore clear that dehydroxylation is always accompanied by the release of Al from the framework. It seems that when the Al atom in the vicinity of a structural OH group is lost from the framework, the group is simultaneously dehydroxylated. In a recent study of the dehydroxylation and dealumination of zeolite H-Y, Shannon *et al.*[119] using distribution functions obtained from X-ray intensity data and infrared spectoscopy, identified the non-framework Al species formed

during the dehydroxylation of zeolite H-Y as a boehmite (-AlOOH)-like species.

(d) Chemical dealumination using $SiCl_4$ vapour.

Beyer and Belenykaja[120] reported a new method of dealuminating synthetic faujasites by reaction of $SiCl_4$ vapour at elevated temperatures. The aluminium was successively substituted in the zeolite framework by silicon and removed in part from the crystals in the form of volatile $AlCl_3$ observed as white vapours. The reaction occurs without collapse of the crystal structure (although it is now known from sorption measurements that for ultrastable faujasites, a secondary mesopore system is formed, signifying that the Si that re-occupies empty tetrahedral sites comes from the bulk of the crystals as well as from the surface of their amorphous parts)[121] as can be shown by powder XRD, IR spectroscopy, and HREM. Klinowski *et al.*[90,122-125] and Hays *et al.*[126] applied ^{29}Si and ^{27}Al MAS NMR to the study of this reaction in a number of zeolites. The overall reaction may be written:

$$Na_x(AlO_2)_x(SiO_2)_y + SiCl_4 \longrightarrow Na_{x-1}(AlO_2)_{x-1}(SiO_2)_{y+1} + AlCl_3 + NaCl$$

^{27}Al MAS NMR indicates that Al is also present in the form of $Na^+(AlCl_4)^-$ ion pairs in the zeolitic channels. Upon washing this dealuminated zeolite with water, all the extra-lattice Al is converted to $Al(H_2O)_6^{3+}$ which can be removed by repeatedly washing with aqueous acid.

Zeolite Na-Y (Si/Al = 2.61), with the characteristic ^{29}Si MAS NMR spectrum of a range of Si(nAl) resonances goes to a single Si(0Al) resonance after complete dealumination (Si/Al = 55). The progress of the same reaction can also be monitored by ^{27}Al MAS NMR.

Beyer *et al.*[127] have recently shown that in order to obtain highly crystalline materials in a reproducible manner, a very specific dealumination and washing procedure has to be followed. This is because when dehydrated Na-Y is brought into contact with $SiCl_4$ vapour above 750 K, a violent exothermic reaction occurs which may produce a partially amorphous material. Thus, direct contact of the zeolite sample with $SiCl_4$ vapour will provoke a very significant temperature increase. Beyer *et al.*[127] subsequently designed a reactor for which the temperature of the reaction bed could be carefully monitored and controlled.

Grobet *et al.*[128] have used ^{29}Si CP/MAS NMR and ^{27}Al MAS NMR, together with infrared spectroscopy to characterise the products of chemical dealumination (Na-Y with Si/Al = 50) and chemical dealumination followed by treatment with HCl then steaming (Si/Al = 200). They show that the two techniques are capable of identifying hydroxyl nests at aluminium deficient spots in the lattice, and that these nests contribute to the observed intensities of the ^{29}Si NMR resonance lines at -107 ppm and that hydroxyls associated with lattice or extra-lattice aluminium enhance the intensity of the line at -100.6 ppm. Thus, isomorphous substitution of silicon for aluminium only occurs partially since, *via* a consecutive reaction, hydroxyl nests and octahedral aluminium are formed. A subsequent acid treatment was able to remove the extra-lattice aluminium and to dealuminate further the zeolite. All the hydroxyl nests created by this treatment could be healed by the migration of silicon atoms into the lattice vacancies during the steaming process. The authors state that had NMR been used alone, erroneous conclusions would have been reached.

Other zeolites, notably mordenite,[126,90] zeolite omega,[90] ZSM-5,[129] and zeolite ZK-4[130] are also dealuminated in a similar fashion to

faujasite and ^{27}Al MAS NMR proves this beyond doubt.

(e) Aluminium insertion into highly siliceous zeolites.

The dealumination of zeolite frameworks without collapse of the crystal superstructure is a well documented phenomenon.[131] The possibility of the reverse reaction of Al substitution into zeolite frameworks was first addressed by Breck and Skeels, who in a recent publication[132] presented data which they interpreted as evidence for realumination during stabilization[133] of zeolite Y. Their interpretation was rejected by Engelherdt and Lohse,[134] who used ^{29}Si MAS NMR and IR spectroscopy to show that after dealumination has taken place, no change of $(Si/Al)_{NMR}$ ratio is apparent from the intensities of the ^{29}Si NMR spectra (as would be expected if up to 20% reinsertion of the total Al content into the framework had occurred). Thus no realumination had taken place. More recently, the framework alumination of the highly siliceous zeolite ZSM-5 has been achieved by reaction with aluminium halides.[135-137] Anderson *et al.*[137] used ^{27}Al MAS NMR to show that when ZSM-5 (Si/Al >400) is treated with $AlCl_3$ vapour at 400°C for 12 h, aluminium is isomorphously substituted for silicon in the zeolitic framework and also enters six-coordinated intrazeolitic positions. $AlCl_3$ vapour reacts with surface hydroxyl groups in the parent zeolite and with structural faults involving hydroxyl nests. Reaction of $AlCl_3$ with these defects followed by ion exchange would result in the creation of Brønsted sites. The incorporation of Al into the zeolite framework as a tetracoordinate species generates a negative framework charge. The octahedral signal has approximately 1/3 of the intensity of the tetrahedral one. This intensity ratio is preserved even after prolonged washing of the sample with water. It seems that the six-coordinate Al neutralizes the negative framework charge according to the following

reaction:

$$(SiO_2)_x + 4AlCl_3 \longrightarrow Al^{3+}[(AlO_2)_3(SiO_2)_{x-3}] + 3SiCl_4$$

Chang *et al.*[135] and Dessau and Kerr[136] have also described the insertion of aluminium into highly siliceous ZSM-5 by reaction with aluminium halides and their conclusions are similar to those of Anderson *et al.*.[137]

In a related development, Shihabi *et al.*[138] have reported that the ion-exchange capacity and acid-catalytic activity of high-silica ZSM-5 was markedly increased when the zeolite was extruded with alumina binders. Chang *et al.*[139] have further investigated this observation with both Al-ZSM-5 and B-ZSM-5 zeolites. They found that the aluminium was transported as an aquo-species from Al_2O_3 into the zeolite and entered the framework as tetrahedral aluminium. The presence of framework boron induced enhanced activation due to the hydrolytic instability of framework boron and hence its ready substitution by Al.

3.2.4. Precursors in zeolite synthesis.

Solid-state MAS NMR has also been used to study solid aluminosilicate gel precursors. Engelhardt *et al.*[140] first used ^{27}Al and ^{29}Si MAS NMR to investigate the mechanism of crystallization of zeolite A. They showed, using ^{29}Si and ^{27}Al MAS NMR that the properties of the aluminosilicate gels formed as intermediates from reactant mixtures of equal composition in zeolite Na-A synthesis depend highly on the chemical composition of the starting silicate and aluminate solutions. They concluded from the NMR spectra and chemical analysis that after mixing 1M sodium silicate solution with a molar Na/Si ratio of 1.9 and 1M sodium aluminate solution with a molar Na/Al ratio of

1.45, initially a gel with a molar Si/Al ratio of 1.0 and alternating Si,Al ordering is formed. With increasing time of heating of the reaction mixture the transformation of the amorphous gel phase into highly crystalline zeolite A could be monitored by the NMR spectra. The same authors[141] then considered two different starting sodium silicate solutions. They found that using a sodium silicate solution of C_{SiO_2} >1M and molar Na/Si ratio of 2 an aluminosilicate gel of Si/Al = 1.0 precipitates, whereas a silica-rich initial aluminosilicate gel of Si/Al = 2.4 is formed from a silicate solution of C_{SiO_2} = 1.7M and Na/Si = 0.6. Thus the two solutions when mixed with sodium aluminate so as to give reaction mixtures with the same overall composition, gave rise to very different intermediate solid samples. The nature of the reaction intermediate is thus seen to depend greatly on the nature of the initial silicate solution. The composition of zeolite A (with Si/Al = 1.00) is achieved *via* structural rearrangements in the amorphous precursors and is dictated by the final structure itself.

Scholle *et al.*[142,143] used ^{27}Al (at 130.3 MHz) MAS NMR to study the intermediates of zeolite ZSM-5 containing tetrapropylammonium hydroxide (TPAOH) as template as a function of crystallization time. For the samples with crystallization times of 12 h, 1 d, and 3 d, two distinct ^{27}Al resonances were observed, both corresponding to tetrahedrally coordinated aluminium. Low-field ^{27}Al (78.2 MHz) spectra of TPA-ZSM-5 did not show the fine structure seen at 130.3 MHz. They assigned the two aluminium resonances to aluminium atoms in the framework near TPA^+ and aluminium atoms next to (hydrated) sodium atoms. On calcination of the TPA-ZSM-5, only one signal is observed, as TPA^+ is removed and neutralization of the framework is achieved by hydrated sodium ions or protons (H^+) alone.

^{13}C MAS NMR has been used to study the organic template molecules present in the pores of many highly-siliceous zeolites. In the first study of this kind, Boxhoorn *et al.*[144] observed that the methyl carbon resonance from the TPA^+ cation enclathrated in the framework of ZSM-5 in the course of synthesis is split into two components of near equal intensity. The explanation for this is that the carbon is located at the cross-section of the two non-equivalent channels with two propyl groups lodged in each channel. Nagy *et al.*[145] who used thermogravimetry in combination with ^{13}C MAS NMR to study TPA^+ as well as tetrabutylammonium (TBA^+) and tetrabutylphosphonium (TBP^+) species in ZSM-5 and ZSM-11, also observed the split signal in the ZSM-5/TPA^+ system.

Jarman and Melchior[146] used ^{13}C MAS NMR to investigate the state of TMA^+ cations in zeolite TMA-A. They found they could distinguish between TMA^+ cations trapped in the α and β (sodalite) cages in the course of crystallization from a precursor gel. This and other ^{13}C MAS NMR studies[147] have shown that for trapped organic amines involved in zeolite synthesis, the linewidths and chemical shifts of the ^{13}C resonances are extremely sensitive to the zeolite structure.

3.2.5. Other NMR studies of zeolites.

It is outside the scope of this review which is primarily concerned with solid-state NMR, to give an in-depth survey of the areas to be considered in this section. Only a very general discussion will be given here of the following topics (a) NMR studies of exchangeable cations, and (b) NMR studies of guest molecules in zeolites.

(a) Exchangeable cations.

The sorptive and catalytic properties of zeolites depend to a large extent on the precise position, mobility, and environment of the cations. These properties can be studied effectively using wide-line NMR techniques and a number of studies have been made in the past few years.[148-152] For systems where quadrupole effects dominate, information is obtained about electric field gradients at the cation site.[148-150] Chemical shifts have been observed in some cases and this has provided information about site occupancy and covalent effects.[151,152] The variation in linewidth often gives information about the mobility of the cation.

West[153] and Freude *et al.*[151,152] have studied thallium exchanged zeolite A and faujasites respectively, using ^{205}Tl NMR. ^{205}Tl is a very favourable nucleus for solid-state studies: it has I = 1/2, high natural abundance (70.50%) and high sensitivity. Its large chemical shift range makes it possible to observe individual environments of the nucleus. Thallium can be easily introduced into zeolites by cation exchange. Both West and Freude *et al.* observed fine structure in the thallium resonance line from association with specific cation sites. Other cations that have been studied by NMR techniques include sodium (^{23}Na),[154,155] and lithium (^{7}Li).[156,157]

(b) Guest molecules in zeolites.

There have been several reviews of this area of zeolite science and the reader is referred to these for fuller details.[150,158-161,109,110]

(i) Water sorption and mobility: early work centred on the behaviour of water adsorbed on zeolites and the determination of T_1 and T_2 values as a function of temperature and surface coverage in various zeolites, particularly of the faujasite type.[162-164] Kasai and Jones[165] applied

MAS NMR to the study of water in zeolites A, X, Y, mordenite, ZSM-5, and silicalite. They found that although the signals are sometimes broad, their chemical shifts are characteristic of the zeolite. They interpret this as the effect of the disruption of hydrogen bonding in bulk water by the zeolitic framework and of the interaction of water molecules with framework oxygens. An inverse relationship was found between the chemical shift and the Si/Al ratio. They showed that interparticle diffusion occurs at ambient temperature, while the intraparticle diffusion depends on the number and size of the cations. For highly-siliceous zeolites (ZSM-5 and silicalite), they found that while water molecules are located interstitially in ZSM-5, they are located on the extracrystalline surface of silicalite.

(ii) Multinuclear studies of sorbed species. Multinuclear work involving ^{13}C, ^{15}N, and ^{129}Xe in particular began in the early 1970's with the advent of FT NMR spectrometers.

The usefulness of ^{13}C NMR to the study of sorption of various hydrocarbons adsorbed in zeolites has been demonstrated by Deininger and Michel[166] and Michel.[167,168] More recent work involving ^{13}C NMR studies of sorbed species has centred on adsorption of organic bases to study Bronsted acidity.[169] Michel *et al.*[114,115] and Jünger *et al.*[116] have shown the potential of ^{15}N NMR for studying the interactions of various sorbate molecules (ammonia, trimethylamine, pyridine, and acetonitrile) with cations and Brønsted and Lewis acid sites.

Xenon has also proved to be a very useful probe for adsorption studies. ^{129}Xe is a spin 1/2 nucleus of 26.44% natural abundance and a very wide range of chemical shifts. The atomic diameter of xenon is 4.6 Å *i.e.* comparable to the size of zeolitic channels. Ito and Fraissard[170] were the first to take advantage of these useful properties of ^{129}Xe for the study of zeolites Ca-A, Na-X, Na-Y, H-Y, and Ca-Y.

They interpreted the observed chemical shifts/density gradients in terms of collisions between Xe atoms and the cavity walls. De Menorval *et al.*[171] studied xenon adsorbed on zeolite Y containing particulate platinum with or without pre-chemisorbed hydrogen. They conclude that chemisorption of hydrogen occurs homogeneously on all particles of similar size and claim to be able to determine the mean size of platinum particles from their results. Ripmeester[172] used MAS NMR to study xenon adsorbed on zeolites Na-A and H-mordenite. For H-mordenite two broad ^{129}Xe resonances are ob served *ca.* 62 ppm apart, one line being attributable to xenon in side pockets in the structure, the other to xenon in the main channels. In a further paper,[173] Ripmeester determined the distribution of xenon in various cationic forms of mordenite. Most recently, de Menorval *et al.*[174] and Primet *et al.*[175] have used ^{129}Xe as an NMR-detectable probe to determine quantitatively the distribution of CO molecules sorbed on small platinum particles located in the supercages of Na-Y zeolite. (It appears that ^{129}Xe NMR can determine directly the surface area of zeolite samples, which may be of considerable practical importance.)

3.3. Isomorphous framework substitution in zeolites.

Isomorphous anionic framework substitution of elements such as Ga, Ge, B, Fe, Cr, P, and Mg for Si or Al in tectosilicate frameworks has been recently reviewed by Barrer.[30] Minerals whose silica frameworks contain substituents other than Al are found in nature,[30] examples include substitution of B in datolite[176] [$CaBSiO_4(OH)$] and danburite[177,178] ($CaB_2Si_2O_8$) although boron usually occurs in three-fold coordination with oxygen and forms structural units which are not part

of the silicate framework.[179,180] At least two examples of P substitution are reported in the literature, in the minerals viséite[181] and perhamite.[182] Substituted tectosilicates can also be prepared in the laboratory, either by crystallization[30] or framework modification by various reagents.[183]

It is well known that in zeolites catalytically active sites are associated with the aluminium cations, whose coordination environment determines the character of the catalytic action.[184] Based on the known ideas about the nature of acid-base properties of binary oxide systems[185,186] *i.e.* that acid-base catalytic action results from incomplete compensation of cation charges by oxygen atoms of the environment, one may expect that by modification of the cation which substitutes for Si in the framework, it is possible to change the activity and selectivity of the latter.

Consequently in recent patent literature a whole variety of modified silicates with medium pore size and high-silica content has been claimed (Table 3.3). Table 3.3 shows that apparently numerous possible substitutions can occur in these high-silica materials. Generally speaking, these new materials are claimed based upon their novel chemical composition or XRD or both. This novelty does not necessarily mean that the new materials contain the new element substituted in the zeolite framework.

Tielen *et al.*[192] have attempted to predict the catalytic implications of isomorphous substitution in zeolites using general chemical principles. They cite four possible modes of different valency state substitution in a crystalline microporous silica polymorph: (i) for a substitution with a tetravalent cation the framework remains electrically neutral; (ii) for every trivalent cation incorporated, a negative charge will have to be compensated for; (iii) with incorporation

of a bivalent cation, the creation of two negative charges is associated if tetrahedral coordination is strictly obeyed, otherwise oxygen defect sites will make the lattice electroneutral; (iv) when a pentavalent cation is incorporated an excess positive charge exists. In order to behave as a cation exchanger, T-atoms with formal charge of 2 or lower will have to be present at the same time.

The scheme shows that incorporation of M^{2+} forms silanol groups in close proximity (4), which are expected to be very susceptible to dehydroxylation(5), and result possibly in elimination of $M\text{-}O_x$ and structural rearrangements. Thus substitution of M^{3+} T atoms gives an increased number of Brønsted acid sites (1), the strength of which can be varied by substitution with M^{4+} of different nature (2).

Nature of Silicate	Si/M	Si/Al	Remarks	Reference
AMS-1B borosilicate	>40	>1000	Specific XRD	187
Iron-aluminosilicate	>40	>150	MFI	188
AMS-ICr chromosilicate	>40	>1000	MFI	189
TS-1 titanium silicate	>20	-	MFI	190
TRS-27 beryllium silicate	12	-	-	191 ex.1
TRS-66 zinc silicate	15	-	-	191 ex.3
TRS-64 titanium silicate	3	-	-	191 ex.3
TRS-48 vanadium silicate	17	-	MFI: ZSM-type structure	191 ex.7

Table 3.3

(Non-exhaustive) survey of different metallosilicates in the parent literature

Cation	Pauling[a]	Goldschmidt[b]	Schannon[c]	R[d]
Si^{4+} *	0.41	0.38	0.40	0.37
Ge^{4+} *	0.53	0.54	0.53	0.43
Cr^{4+}	-	-	0.55	-
Ti^{4+}	0.68	0.60	0.56	0.55
Sn^{4+}	0.71	0.71	0.69	0.55
Zr^{4+}	0.80	0.77	0.73	0.62
Hf^{4+}	-	-	0.72	-
B^{3+} *	0.20	0.20	0.25	0.20
Al^{3+} *	0.50	0.45	0.53	0.41
Fe^{3+} *	-	0.53	0.63	0.45
Cr^{3+}	-	0.55	-	-
Ga^{3+} *	0.62	0.60	0.61	0.46
Be^{2+} *	0.31	0.30	0.41	0.25
Mg^{2+}	0.65	0.65	0.71	0.47
Zn^{2+}	0.74	0.69	0.74	0.50
As^{5+}	-	-	0.475	0.40
P^{5+}	-	-	0.31	0.34
V^{5+}	-	-	0.495	0.5
Cr^{5+}	-	-	0.485	-
La^{3+}	1.15	1.04	-	-

* Evidence exists for their incorporation into zeolite frameworks.

a) Ref. 185, p.514. b) Ref. 193. c) Ref. 194. d) Derived from ref. 185, p.545.

Table 3.4

Ionic radii (Å) of elements for substitution into a zeolite framework and their minimum radius ratio, "R", in a M-O matrix

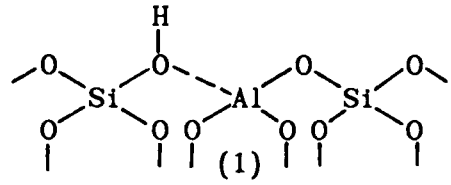

(1)

—: chemical bond

---: formal coordination link

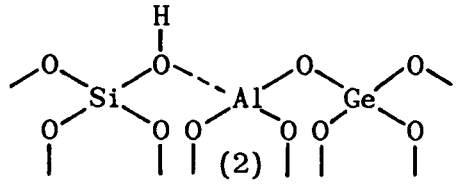

(2)

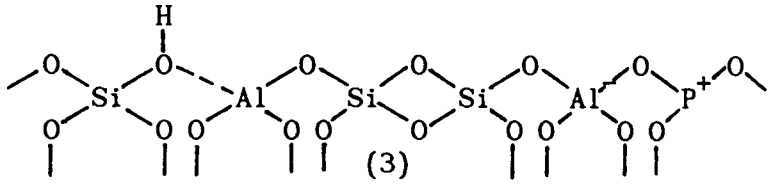

(3)

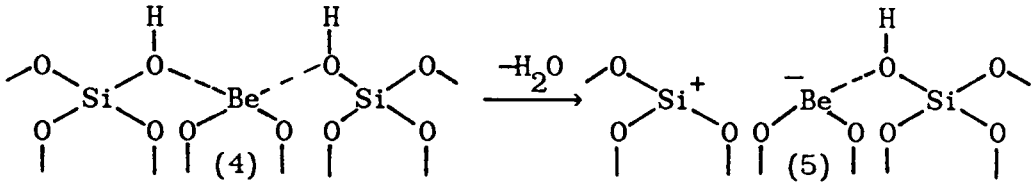

(4) (5)

Tielen *et al.*[192] then consider the requirements for stable tetrahedral coordination. One possible measure for this can be the ionic radius (although it should be remembered that zeolite structures show an appreciable amount of covalency). Ionic radii from several literature sources for pertinent cations are given in Table 3.4. Tielen *et al.*[192] conclude that elements with ionic radii between 0.20 Å (0.020 nm) and 0.61 Å (0.061 nm) are potential candidates for incorporation into a silicate framework.

A more accurate estimate of the potential of a given cation to be tetrahedrally coordinated in an oxygen matrix of anions is provided by the minimum radius ratio, R, introduced by Pauling.[185] The minimum radius ratio determines the stability of various coordination polyhedra or the preferred ligancy of a cation. In the simplified version, R =

r_c/r_o , where r_c is the cation radius and r_o is the radius of the oxygen anion. According to Pauling, stable tetrahedral coordination can be formed for cations for $0.414 > R > 0.225$. This group of cations includes only Al^{3+}, Mn^{4+}, Ge^{4+}, V^{4+}, Cr^{6+}, Si^{4+}, P^{5+}, Se^{6+}, and Be^{2+}. However, any cation can be occluded in the isomorphous position by inorganic compounds, provided the concentration of this cation is low.[195]

Romannikov *et al.*[196] state that the probability of isomorphous substitution is high when the values of radii (r) and electronegativities (X) of mutually substituting cations are nearly the same. For the BeO-SiO_2 systems they report values of r and X for Be^{2+} and Si^{4+} as 0.035 nm and 0.042 nm, and 210 and 260, respectively.

Meyers *et al.*[197] report that based on studies of alloys,[198] substitution of a heteroatom into a tetrahedral site of a crystalline silica structure might occur if the Si-O and heteroatom-oxygen bond distances differ by $\lesssim$ 10%. Since a Si-O bond distance is 1.61 Å[199,200] substitution by both Al and B atoms should be permissible (bond distances of 1.74 Å[200,201] and 1.47 Å[200,201,203] respectively).

Several methods have been used to prove the existence of the replacement of T-atoms by isomorphous cations:

(1) XRD - the change of unit cell dimensions with the degree of substitution. For example, incorporation of Al would result in lattice expansion whereas substitution by B would result in a contraction of the lattice;[197]

(2) IR - the gradual shifts of the lattice vibrations with the degree of substitution. This correlation has been established by Flanigen[204] for faujasites with different Si/Al ratios;

(3) MAS NMR - this will be discussed with reference to various

isomorphously substituted cations in the next section.

3.3.1. Framework substitution by elements other than Si or Al as studied by MAS NMR

Ga-substituted aluminosilicate zeolites have already been discussed in section 3.2 (^{29}Si) and will not be referred to extensively here.

ZSM-5 has been frequently mentioned in the recent patent literature, and much interest has been shown in the question of isomorphous substitution of B atoms into high-silica zeolites of the ZSM-5-type,[195,205-207] and in its catalytic activity.[195,208-212]

Gabelica *et al.*[205] were the first to investigate ZSM-5 using ^{11}B MAS NMR. They used three methods to introduce boron into the zeolite: (1) direct synthesis following the patent;[187] (2) impregnation of crystalline H-ZSM-5 with H_3BO_3;[213] and (3) synthesis in Pyrex tubes.[214] They found in all cases a single resonance line at -3.3 ppm (*vs.* $BF_3.OEt_2$) with a linewidth of *ca.* 80 Hz, characteristic of tetrahedral BO_4 units in an ordered structure.[215,216] On the basis of ^{11}B NMR chemical shift, they could also distinguish between BO_4-lattice, BO_4-extra-lattice, and BO_3 units. In a fuller account of their studies concerning the incorporation of B into tetrahedral sites of ZSM-5 framework during crystallization, Gabelica *et al.*[206] identified two signals in the precursor gel of B-ZSM-5. One line (at -0.5 ppm) was due to tetrahedral BO_4 units randomly distributed in the precursor gel, the other due to BO_4 units incorporated in the framework. The variation of the relative intensities of these lines is quantitatively related to the % crystallinity of each intermediate phase.

Scholle *et al.*[207] investigated the effect of hydration and dehydration on the coordination of boron in H-boralite (H-B-ZSM-5) by

^{11}B MAS NMR. Their experiments showed that in the hydrated state, the quadrupole interaction ($\upsilon_Q = e^2qQ/h$) of boron is negligible, implying a highly symmetrical electric field gradient around the boron due to the four oxygens to which boron is tetrahedrally coordinated. In dehydrated samples (vacuum drying at 10^{-4} Torr, 280°C for 30 h - shallow bed treatment), a substantial quadrupole interaction (υ_Q = 2.55 MHz, η = 0) for boron is found. Scholle *et al.*[207] interpreted this change as being due to a change in coordination of the boron from highly symmetric BO_4 units to lower symmetry BO_3 units on dehydration. No change of symmetry is found for Al in deydrated ZSM-5[50] and it can be concluded that boron is not as stable as tetravalent aluminium in tetrahedral positions in the zeolite lattice.

On the basis of FTIR and TPD ammonia results,[211] the Brønsted acidity of B-ZSM-5 was found to be very weak (on a par with that for SiOH groups). The decreased catalytic activity of the substituted zeolite was attributed to ppm levels of Al arising from impurities in the commercial silica sample used for synthesis of the zeolite.

Romannikov *et al.*[196] studied the synthesis and catalytic properties of beryllium substituted silicates having ZSM-5 type structure. ^9Be MAS NMR spectra showed that Be^{2+} cations are located in a tetrahedral coordination different from that for Be^{2+} in BeO and $[Be(H_2O)_4]^{2+}$. Zeolites of beryllium-silicate chemical composition with molar ratio SiO_2/BeO equal to 30, 60, and 90 were investigated and in all three cases, a chemical shift of -5.8 ppm (vs. 0.5M aqueous solution of sodium beryllate) was found. Since the tetrahedral oxygen surrounding is known to be the most thermodynamically stable coordination of Be^{2+} in oxide systems, and given that isomorphous substitution is possible for many silicate minerals, Romannikov *et al.*[196] concluded that $[BeO_4]^{6-} \longleftrightarrow (SiO_4)^{4-}$ substitution had taken place.

Ione *et al.*[195] have investigated the possibility of isomorphous heterocharged substitution of Si^{4+} by one $n+$ cation of elements of Groups I - VIII, where $n \neq 4$, in crystalline non-aluminium silicates with ZSM-5 structure. Solid-state MAS NMR was used to characterise those silicates substituted by B^{3+}, Be^{2+}, Al^{3+}, and Ga^{3+} cations. ESR spectra were recorded for Cu^{2+}, Eu^{3+}, Cr^{3+}, Fe^{3+}, Mn^{2+}, and V^{4+} substituted silicates. For the borosilicates, the ^{11}B spectra contained one narrow line at δ = -23.3 ppm (vs. 1M H_3BO_3) before catalytic testing and a broad line centred at = -23.1 ppm after catalytic testing. They attributed the narrow line to boron in tetrahedral coordination and the broad line which exhibits a quadrupole splitting of the second order, to boron in the trigonal oxygen environment. The ^{9}Be MAS NMR spectra of beryllium-silicate having a ZSM-5 type structure consisted of a single line, the chemical shift of which was -5.8 ppm [vs. 1M $Na_2Be(OH)_4$]. They suggest that the major portion of Be^{2+} in the synthesised silicates is coordinated in the crystalline silicon-oxygen framework. The ^{71}Ga NMR spectrum of gallium-substituted ZSM-5 has a single broad line with a chemical shift of 155 ppm [vs. 1M $Ga(NO_3)_3$]. The value of the chemical shift corresponded to one of gallium nuclei in a tetrahedral oxygen environment. Thomas *et al.*[50] reported a value of 182.5 ppm [vs. $Ga(NO_3)_3$] for gallosodalite, although again the resonance line was very broad. ESR measurements carried out by Ione *et al.*[195] on the metallosilicates established that only for Fe^{3+} substitution was there any evidence for incorporation into the zeolite framework.

Artoli *et al.*[217] have determined the crystal structure of a synthetic phosphorus-substituted analcime, originally synthesised by Flanigen and Grose in 1971.[218] The framework structure has alternation of 24 Al and (13Si + 11P) over the tetrahedral sites. No evidence was found for ordering of Si and P. Insufficient sample was available to

test for short-range ordering by MAS NMR.

3.4 Novel zeolite-related molecular sieve type materials and their study by NMR

Silicon and aluminium are not unique in their ability to form tetrahedrally coordinated oxide networks. Phosphorus, which lies to the right of silicon in the Periodic Table, frequently assumes tetrahedral coordination with oxygen (PO_4^{3-} units). Indeed, aluminium phosphate ($AlPO_4$) possesses many structural similarities to silica: (i) $AlPO_4$ is isoelectronic with Si_2O_4; (ii) the average ionic radii of Al^{3+} (0.39 Å) and P^{5+} (0.17 Å) is 0.28 Å, very close to the ionic radius of Si^{4+} (0.26 Å);[193] (iii) $AlPO_4$ and SiO_2 form isomorphous dense phases with Al^{3+} alternating with P^{5+} in a tetrahedral oxide network. Despite isomorphism between $AlPO_4$ and certain of the crystalline silicas, there is little evidence of silica-bearing $AlPO_4$ in which Si substitutes for the other elements. Nevertheless, two naturally occurring phosphatic minerals, viséite and keheoite, are reported to have the analcime structure.[181,219]

The structural analogies between $AlPO_4$ and SiO_2 served as one stimulus for examining aluminophosphates as a potential source of microporous frameworks. A second stimulus was the extensive aluminophosphate synthesis literature and, in particular, the ease of hydrothermal synthesis. Wilson *et al.*[221-223] embarked on a systematic programme for hydrothermal synthesis of framework aluminophosphates using the same types of organic templating agents so useful in the synthesis of high-silica zeolites. They discovered a large number of

aluminophosphate (acronym AlPO) molecular sieves of different structures, as determined by powder XRD. They assigned each new structure type a number. About 20 three-dimensional structures have been reported of which 14 are microporous.

The pentavalency and trivalency of the P and Al respectively do not result in a supplementary negative charge and subsequently no acidity is expected in these materials. However, if the phosphorus is (in part) replaced by a tetravalent metal, or the aluminium by a divalent metal, acid character is expected to be generated. Following this line of thought, Lok *et al.*[224,225] synthesised another new class of microporous crystalline inorganic solids, the silicoaluminophosphate molecular sieves (acronym SAPO). The SAPO materials exhibit structural diversity with some 13 three-dimensional microporous structures having been identified.

More recently, Flanigen *et al.*[226] have reported the synthesis of various microporous molecular sieves which have the following empirical chemical composition:

$$mR : (M_xAl_yP_z)O_z$$

where "R" represents at least one organic templating agent present in the intracrystalline pore system and "M" represents at least one element capable of forming framework tetrahedral oxides and selected from the group consisting of arsenic, beryllium, boron, chromium, gallium, germanium, lithium, and vanadium.

3.4.1. Aluminophosphate molecular sieves.

Table 3.5 shows the properties of selected $AlPO_4$-n molecular sieves.[221]

$AlPO_4$-n	Structure	Approx. free diameter of windows (nm)	ring size[i]	Pore volumes ($cm^3\ g^{-1}$)[ii]	
				O_2 (-183°C	H_2O (25°C)
$AlPO_4$-5	determined and novel[a]	0.8	12	0.18	0.3
$AlPO_4$-11	unknown	0.61	10 or puckered 12	0.11	0.16
$AlPO_4$-12	determined and novel[b]	-	-	-	-
$AlPO_4$-14	unknown	0.41	8	0.19	0.28
$AlPO_4$-15	determined[c,d]	-	-	-	-
$AlPO_4$-16	unknown	0.3	6	0	0.3
$AlPO_4$-17	erionite type[e]	0.46	8	0.27	0.35
$AlPO_4$-20	sodalite type	0.3	6	0	0.24
$AlPO_4$-21	determined and novel[f,g]	-	-	-	-
$AlPO_4$-31	unknown	0.8		0.09	0.17
$AlPO_4$-33	unknown	0.41	8	0.23	0.23

i. Number of tetrahedral atoms (Al or P) in ring that controls pore size

ii. Determined using the McBain-Bakr gravimetric techniques after calcination

a) Ref. 227; b) ref. 228; c) ref. 229; d) ref. 230; e) ref. 231;
f) ref. 232; g) ref. 233.

Table 3.5

Properties of Selected $AlPO_4$-n Molecular Sieves

Blackwell and Patton have reported[234] initial solid-state NMR studies of four $AlPO_4$-n molecular sieves: $AlPO_4$-5, $AlPO_4$-11, $AlPO_4$-17, and $AlPO_4$-31. Their ^{27}Al and ^{31}P MAS NMR measurements were performed at a magnetic field strength of either 4.7 T or 9.4 T. Both "as-synthesised" and calcined forms of the molecular sieves were investigated. A summary of their findings is presented in Table 3.6. The ^{31}P MAS NMR spectra generally showed symmetrical lines in the chemical shift range -19 to -30 ppm, consistent with tetrahedral phosphorus (as PO_4) in the framework of the materials. The ^{27}Al MAS NMR spectra are generally more complicated than the ^{31}P spectra. Two ranges of chemical shifts were observed, one corresponding to tetrahedral Al (between 30 and 40 ppm) and one to octahedral Al (between -11 and -20 ppm). Blackwell and Patton also investigated several forms of microporous aluminophosphates. In several cases, the observation of asymmetrical lines and multiple peak maxima necessitated the use of a high field (9.4 T) and ^{27}Al cross-polarization (^{1}H-^{27}Al) to assign the unusual chemical shifts. The molecular sieve spectra are generally consistent with their known framework structures (alternating AlO_4 and PO_4 tetrahedra). The state of hydration/dehydration and calcination of the molecular sieves was shown to affect the ^{27}Al MAS NMR spectra considerably.

Müller *et al.*[235] have studied both the as-synthesised and calcined forms of Pr_3N-$AlPO_4$-5 using both high-resolution MAS NMR and conventional wide-line ^{27}Al NMR techniques. Their results are summarised in Table 3.7. The chemical shift values are in agreement with those of Blackwell and Patton.[234] The occurrence of a single line in both the ^{31}P and ^{27}Al NMR spectra of $AlPO_4$-5 indicates that all the P and Al atoms in the structure are located at sites of an identical

sample	^{27}Al Chemical Shift[a] /(ppm) MAS	CP/MAS	magnetic field (T)	^{31}P MAS NMR/(ppm) chemical shift[b]
$AlPO_4$-5 (TPA)	35.3	-	4.7	-
	-11.7	-		
$AlPO_4$-5 (TEA)	34.4	-	4.7	-28.6
$AlPO_4$-5	35.3	37.5	4.7	-27.8
calcined	-15.5	-16.3		
$AlPO_4$-11	33.3	33.3	4.7	
$AlPO_4$-11 calcined	34.4	31.4	4.7	-
$AlPO_4$-17	31.2	33.7	4,7	-24.2
$AlPO_4$-17	44.9	45.9	4.7	-29.9
calcined	-15.5	-14.3		
	43.8	-	9.4	
	36.9	-		
	-18.7	-		
$AlPO_4$-31	40.7	41.3	4.7	-30.2
	30.1	32.9		
	38.0		9.4	
	30.1			
$AlPO_4$-31	29.4	32.4		-29.6
calcined	-15.9	-13.0		

a) With reference to aqueous $Al(NO_3)_3$ as 0 ppm.

b) With reference to 85% H_3PO_4 as 0 ppm.

Table 3.6

Abridged Summary of Blackwell and Patton's ^{27}Al and ^{31}P NMR Chemical Shifts for $AlPO_4$-5, $AlPO_4$-11, $AlPO_4$-17, and $AlPO_4$-31.

	chemical shift/(ppm)	Half-width (Hz)	δ_{exp} b,c	δ_{corr} d	Line-width (Hz)	e^2qQ/h (MHz)	η
Pr_3N-$AlPO_4$-5	-30.6	980	36	44	1100	2.3	0.95
$AlPO_4$-5	-29.2	650	32	40	950	2.3	0.95

a) With reference to 85% H_3PO_4; b) With reference to $[Al(H_2O)_6]^{3+}$;
c) Experimental (uncorrected) values; d) Corrected values.

Table 3.7

Summary of ^{27}Al and ^{31}P NMR Data Collected by Müller *et al.* of $AlPO_4$-5 and its Pr_3N precursor.

chemical environment *i.e.* AlO_4 and PO_4 sites alternate throughout the structure. This is in agreement with the crystal structure determined for $AlPO_4$-5.[227] Information about the electric field gradient at the Al sites was obtained from static low field ^{27}Al NMR spectra. Müller *et al.* also suggest a mean angle (Al-O-P) of 150° for $AlPO_4$-5 using an empirical correlation between chemical shift and mean bond angle derived previously for dense $AlPO_4$ phases.[236]

3.4.2. Silicoaluminophosphate molecular sieves.

Table 3.8 shows the properties of selected SAPO-n molecular sieves.[224]

To date, only one solid-state NMR investigation of SAPO molecular sieves has been reported.[238] The work was carried out by the author and will be described in Chapter Six.

SAPO-n n=	typical template	structure type	pore size (nm)	ring size	pore volumes ($cm^{-3}g^{-1}$)	
					O_2	H_2O
5	tri-n-propylamine (Pr_3N)	$AlPO_4$-5	0.8	12	0.23	0.31
11	di-n-propylamine	$AlPO_4$-11	0.6	10 or puckered 12	0.13	0.18
16	quinuclidine	$AlPO_4$-16	0.3	6	-	-
17	quinuclidine	erionite	0.43	8	0.25	0.35
20	tetramethylammonium ion (TMA^+)	sodalite	0.3	6	0	0.40
31	di-n-propylamine	$AlPO_4$-31	≃ 0.7	10 or puckered 12	0.13	0.21
34	tetraethylammonium ion	determined chabazite[a]	0.43	8	0.32	0.42
35	quinuclidine	levynite	0.43	8	0.26	0.48
37	tetrapropylammonium ion + TMA^+	faujasite	0.8	12	0.37	0.35
40	tetrapropylammonium ion	novel	≃ 0.7	10 or puckered 12	0.31	0.31
41	tetrabutylammonium ion	novel	0.6	10 or puckered 12	0.10	0.22
42	TMA^+ + Na	Zeolite A	0.43	8	-	-
44	cyclohexylamine	novel	0.43	8	0.28	0.34

a) Reference 237.

Table 3.8.

Typical Template, Structure Type and Adsorptive Properties of SAPO-n Molecular Sieves

3.4.3. Other substituted aluminophosphate molecular sieves.

Bond *et al.*[239] and Tapp *et al.*[240] have reported on the substitution of zinc and divalent cobalt respectively into $AlPO_4$-5 and $AlPO_4$-11 (Tapp *et al.*). In both cases, new acid sites were created. No MAS NMR studies on these new materials have been published.

CHAPTER FOUR - EXPERIMENTAL

4.1 Introduction

The first half of this chapter is concerned with zeolite synthesis, sample characterization (prior to NMR investigation), and sample post-synthesis treatment. Zeolite synthesis is discussed in some detail with special emphasis on the synthesis of zeolites in the presence of organic compounds. Traditional methods of zeolite analysis are adumbrated. Other techniques that have been used to characterize specific samples, for instance magnetic susceptibility measurements for the ferrisilicates, are also mentioned. Conditions for calcination are discussed and storage conditions are outlined.

The second half of this chapter deals with the practicalities and general instrumental factors involved in obtaining high-resolution NMR spectra of solids. Correct experimental procedures are seen to be extremely important when one is observing quadrupolar nuclei, specifically ^{27}Al, and several problems that came to light during the course of this study are discussed in detail.

4.2 Sample synthesis and procurement

Generally, synthetic zeolites are metastable species that crystallise from alkaline aluminosilicate gels at low temperature and pressure. High-silica zeolites, exemplified by the ZSM series, are generally prepared using organic molecules, such as amines and quaternary ammonium salts, (although ZSM-5 has been synthesised without organic molecules of any kind). The rôle of the organic component is by no means clear but it is believed to exert a "templating effect" (the

crystalline framework grows around the template) and/or a "chemical effect" (solubilising and stabilising the silicate species in the starting solution). A wide range of high silica zeolites are known or have been claimed to have been made using different template molecules. Other important variables are the free OH^-/SiO_2 and SiO_2/Al_2O_3 ratios, as well as temperature, time, agitation, and pH.

The aluminophosphate ($AlPO_4$) molecular sieves are prepared hydrothermally from reactive gels containing an alumina source, a phosphate source, an organic templating agent (R), and water. A large number of different structure-types have been synthesised, and each has been characterized by x-ray powder diffraction. Despite the structural diversity in the $AlPO_4$ series, the product compositions are very similar:

$$xR \cdot Al_2O_3 \cdot 1.0 \pm 0.2\ P_2O_5 \cdot yH_2O$$

Each product as synthesised consists of a crystalline framework composed of essentially equimolar amounts of AlO_2^- and PO_2^+ tetrahedra. The organic R and the H_2O are trapped or clathrated within the framework .

The synthesis of $AlPO_4$ molecular sieves exhibits some similarities with the synthesis of zeolite molecular sieves. Zeolites are synthesised hydrothermally from reactive aluminosilicate gels in alkaline conditions while $AlPO_4$ molecular sieves crystallize from reactive aluminophosphate gels in mildly acidic conditions. Templating agents appear to aid the synthesis of both types of molecular sieve.

Both zeolite and $AlPO_4$ structures apparently avoid Al-O-Al bonds. Zeolites can exhibit variable Si/Al ratios, as Si-O-Si bonds are formed at Si/Al ratios greater than one. The corresponding P-O-P bonds do not appear to be stable in $AlPO_4$ molecular sieves crystallised hydrothermally.

The existence of Si-O-Si bonds makes aluminosilicate structures

with both even- and odd-numbered rings possible with Si/Al ratios of > 1. In $AlPO_4$ frameworks, the avoidance of Al-O-Al and P-O-P bonds necessitates the formation of structures containing only even-numbered rings.

The large diversity of $AlPO_4$ structures results from the addition of various organic species to a narrow gel composition range.

4.2.1. Substituted ZSM-5-type molecular sieves

The substituted ZSM-5 samples were prepared according to methods already established for the synthesis of ZSM-5,[220] with the addition of the appropriate source of substituting heteroatom, for example, boric acid for boron, iron (III) sulphate for iron, and titanium tetrachloride for titanium. Exact methods and reagents cannot be given as they are proprietary. Typical reagents used for the silica source are colloidal silica or various precipitated or fumed silicas. Typical aluminium sources for zeolites are sodium aluminate or aluminium sulphate.

4.2.2. Aluminophosphate and substituted aluminophosphate molecular sieves

These samples were synthesised following U.S.P. 4 310 440 and 4 440 871. Once again exact synthesis conditions cannot be given, but generally phosphoric acid solution was used as the source of phosphorus and a hydrated aluminium oxide was used as the source of aluminium. Various organic molecules were used as templates. For silicon substituted aluminophosphate molecular sieves (acronym SAPO), the synthesis methods are similar to those used for the synthesis of AlPO

molecular sieves. Typical silica sources are as listed for substituted ZSM-5-type molecular sieves.

4.2.3. Natural minerals and other samples

(a) Natrolite - supplied by Gregory, Bottley, and Lloyd, 8-12 Rickett Street, London, SW6 1RU.

(b) Datolite and danburite - Gregory, Bottley, and Lloyd.

(c) Tourmaline - Gregory, Bottley, and Lloyd.

(d) Metavariscite - Gregory, Bottley, and Lloyd.

(e) Viséite (impure) - supplied by Cureton Mineral Co., Tucson, Arizona, U.S.A.. Two small samples also supplied by NMNH (#106384, R18164).

(f) TMA-sodalite and zeolite 4A supplied by Laporte Industries Limited, Widnes.

(g) $AlCl_3.6H_2O$ (solid), B_2O_3, and boric acid supplied by Aldrich Chemical Co. Inc., (research grade purity).

(h) $NaBH_4$ supplied by BDH (research grade purity).

(i) Aluminium ammonium/potassium sulphate alums supplied by Alfa Products (research grade purity).

All minerals with the exception of viséite run without characterization (XRD) or purification.

4.3 Sample Analysis

All aluminosilicates, substituted tectosilicates, and novel zeolite-related materials were identified from their x-ray diffraction patterns. Crystallinity and phase purity were also judged from the XRD traces. In the larger preparations, scanning electron microscopy (SEM)

was used to determine the morphology of the crystalline samples. All samples were subjected to elemental analysis. In certain instances, magnetic susceptibility measurements and ESR measurements were used to characterize further certain samples.

4.3.1. X-ray diffraction

Recorded on a Philips PW 1710 automatic diffractometer. The source was Cu Kα, with a nickel filter. The scanning range was typically 5-50^{o}. Some traces were recorded with a fixed and some with a variable width divergence slit. Approximately 0.2 g of sample was required. Traces recorded at Laporte Industries R & D site, Widnes, Cheshire. The XRD traces presented in Chapters Five and Six were all recorded with a variable width divergence slit. The line intensities extracted from these traces were converted to those obtained with a fixed slit before tabulation, because the use of a compensating slit distorts the real line intensities.

4.3.2. Chemical Analysis

Normal 10 multi-element scan (MES) analyses (K, Ca, Ba, Ti, Fe, Sr, Mg, Na, Si, Al) were performed on a Philips PW 1400 x-ray fluorescence spectrophotometer. The instrument is calibrated *versus* multiple standards and corrects for inter-element interferences. It has an automatic sample changer and borax bead maker. Normally 1 g of calcined sample (at 1000^{o}C to remove water) is combined with 5 g of spectroflux 100 (a lithium metaborate/lithium tetraborate mixture). The resultant mixture is fused and cast into a mould to give a glass bead. The precision of the technique is $\pm$ 0.1 mass %. Instrument sited at Widnes.

4.3.3. Other techniques

(a) Scanning electron microscopy

Used on mainly the larger scale zeolite preparations to check for good crystallite formation, presence of other zeolite phases (co-crystallization) and agglomeration. The Camscan series 4 scanning electron microscope is located at Laporte's R & D site, Widnes, Cheshire.

(b) Magnetic susceptibility measurements

Measured for the Fe- and Cr-substituted ZSM-5 zeolites on an automatic type Johnson-Matthey magnetic susceptibility balance. Measurements were performed at 303 K in Durham.

(c) ESR measurements

Recorded on a Varian X-Band ESR spectrometer with the kind permission of Dr. J. Thorp, Applied Physics Department, University of Durham. Selected Fe-ZSM-5 samples were investigated in both precursor and calcined forms.

4.4 Sample Handling and Treatment

In general the samples were investigated by NMR in two forms: "as-synthesised" (precursor) and calcined. Unless otherwise stated, no ion-exchange procedures were carried out on the zeolite samples. Several samples were however chemically treated. The experimental methods used will be described in the results sections related to the

samples in question. Prior to thermal treatment, the samples were studied by NMR in their "as-delivered" state. Their thermal history was always thorough washing after filtration and drying in air at 140°C for several hours prior to packaging.

4.4.1. Calcination

In order to remove the clathrated organic species from the zeolitic channels, the molecular sieve samples were subjected to temperatures of between 500 and 550°C for several hours under deep bed conditions in a muffle furnace. No attempt was made to control the humidity of the air in the furnace. The heating rate of the furnace was *ca.* 5°C min^{-1}.

4.4.2 Dehydration/rehydration

Sample dehydration was carried out either in an oven at 140°C for extended periods or on a vacuum line at 10^{-3} Torr and 120°C. Samples that had been dehydrated on a vacuum line were stored in a nitrogen filled glove-box and packed into a NMR rotor inside the glove-box. Sample rehydration was achieved by placing the sample in a moisturiser [a desiccator containing a saturated solution of $NaNO_2$ (66% relative humidity)] for several hours.

4.5 NMR Instrumental Conditions

All MAS NMR experiments were performed using a Bruker CXP-200 spectrometer (4.7 Tesla) unless otherwise specified in the text. The spectrometer has three conventional type high-resolution probes

associated with it: (1) a low-frequency broad-banded (^{29}Si - ^{27}Al) probe using Andrew-Beams mushroom shaped rotors capable of *ca.* 3 kHz spinning frequency; (2) a high-frequency broad-banded (^{27}Al - ^{31}P) Andrew-Beams type probe; and (3) a double-bearing broad-banded (^{15}N - ^{31}P) probe using bullet-shaped rotors capable of *ca.* 5 kHz spinning frequency. This last probe has only alumina rotors, the other two have rotors fashioned from Delrin, Kel-F, and Macor.

The observation frequencies and spectral acquisition parameters for the various nuclei studied will be given with the relevant spectra in Chapters Five and Six.

4.5.1. General

(a) Pulse sequences

All NMR measurements were performed at room temperature (293 K). Cross-polarization (CP) experiments[21] (where applicable) were performed with high-power decoupling (HPD), using single contacts with flip-back[23] and spin-temperature inversion.[24] Otherwise single-pulse excitation[241] (SPE) was used (a $\leq \pi/2$ pulse with HPD) or SPE without HPD (SPE - no HPD). In specific cases, the spin lattice relaxation times (T_1)(dilute spin nuclei only) were measured using the inversion-recovery method, with HPD[242] however, in general the T_1's were not determined. The recycle times were altered so as to give no appreciable loss of signal intensity between transients whilst setting up a particular experiment. Where CP was possible and more than one resonance observed in the NMR spectrum, the possible sources of proton spins were investigated by performing the variable contact CP experiment . In this experiment, signal intensity (S) is measured from a CP experiment as a function of

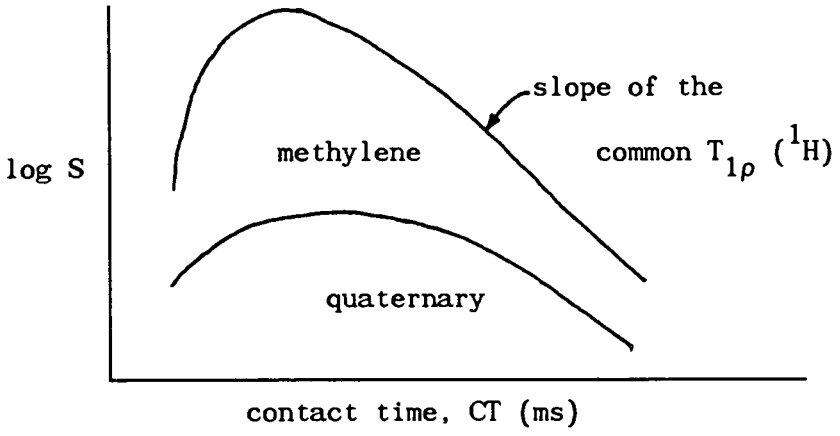

Figure 4.1

contact time (CT). The signal intensity is then plotted on a logarithmic scale against the contact time. The diagram shown (Figure 4.1) is typical of a homogeneous system with a single-exponential value of the spin-lattice proton relaxation time in the rotating frame [$T_{1\rho}$ (^{1}H)]. The example chosen is for ^{13}C NMR of a sample containing equal numbers of methylene and quaternary carbons.

In order to explain the importance of this experiment in the work that follows, it is necessary to discuss briefly the dynamics of the experiment using [as shown in the idealised diagram below (Figure 4.2)] the above schematic as an illustration. During the contact-time *i.e.* while the Hartmann-Hahn condition is established, proton magnetization in the y direction in the rotating frame (parallel to B_{1H} at the relevant time) relaxes to the lattice at the rate of $T_{1\rho}^{-1}$ (^{1}H) at the same time as it is being partially transferred into the carbon spins at the rate of T_{CP}^{-1} (T_{CP} is the cross-polarization relaxation time).

For the experiment to succeed, $T_{CP}^{-1} < T_{1\rho}^{-1}$ (^{1}H), so the spins reach a common spin temperature, and then relax to the lattice *via* $T_{1\rho}^{-1}$ (^{1}H). The rate $T_{1\rho}^{-1}$ (^{13}C) is ignored in this discussion.

The rate of cross-polarization depends on the dipolar interactions

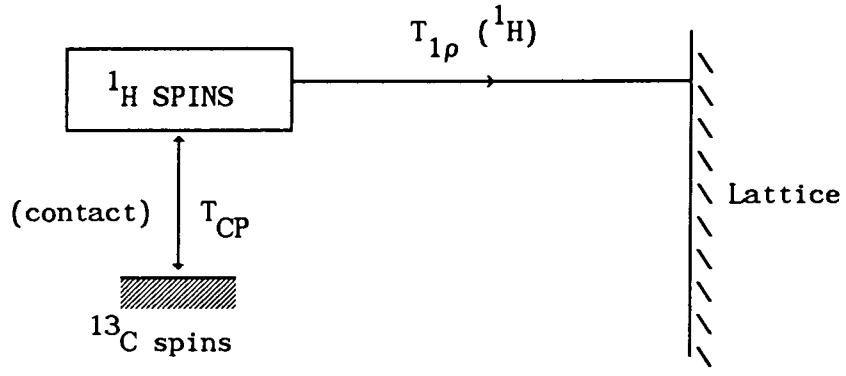

Figure 4.2

between ^{13}C and ^{1}H, as expressed by[21] the (C,H) second moment, $M_2^{C,H}$, in the following equation:

$$T_{CP}^{-1} = C_{CH}.M_2^{CH}/(M_2^{HH})^{1/2}$$

where C_{CH} is a geometry-dependent term and M_2^{HH} is the (H,H) second moment. Thus for an ideal system, such as that depicted in the schematic plot, quaternary carbons will cross-polarize more slowly than protonated carbons, but then lose polarization at a common rate due to spin diffusion.

However, the differential plot of T_{CP} for different dilute spin systems can serve as a discriminatory device. Moreover, the $T_{1\rho}$ (^{1}H) values and hence slopes of the plots may not be equal, implying either incomplete spin diffusion or more than one source of proton reservoir, and the $T_{1\rho}$ (^{1}H) may be multi-exponential, as often occurs for heterogeneous systems.

Other pulse sequences used in suppression of baseline-roll effects will be discussed later in this chapter with reference to early work on ^{27}Al MAS NMR.

(b) Magic-angle Spinning (MAS)

The magic-angle was determined and monitored using the ^{79}Br signal from spectroscopic grade powdered KBr.[243] The twenty or so spinning

sidebands (SSB) present in the spectrum at the magic-angle ($\pm$ 0.1°) allow accurate determination of the spinning speed. In general, for the Andrew-Beams system the magic-angle was set for a particular air pressure. The samples of interest were then run KBr-free assuming reproducibility of the magic-angle at the set (known) air pressure. For spin I > 1 nuclei, precise setting of the magic-angle is not so important as with I = 1/2 nuclei, as signals for quadrupolar nuclei *e.g.* ^{27}Al, are often broad and featureless. For ^{31}P (I = 1/2) especially, the magic-angle was constantly checked for every sample as the linewidths achievable are very sensitive to (mis)adjustment of the magic-angle. With the double-bearing probe, the angle is set once, and because of the design of the system, change of sample and/or spinning speed does not affect that setting of the angle. For systems where several spinning speeds are required in order to establish the position of the centreband from spinning sidebands, this is a distinct (time saving) advantage.

(c) Hartmann-Hahn matching in the CP experiment

The Hartmann-Hahn condition[22] (contact between the dilute spin system, S, and abundant spin system, I, such that $\gamma_S B_{1S} = \alpha\gamma_I B_{1I}$ (where α = 1) was achieved in the accepted manner using Q_8M_8 (a trimethylsilyl ester of double four-ring octameric silicate) for ^{29}Si measurements (contact time 10 ms, recycle time 10 s), or the sodium salt of 3-(trimethylsilyl)-1-propanesulphonic acid (contact time, 10 ms, recycle time 30 s), brushite (hydrated calcium hydrogen phosphate) for ^{31}P (contact time 1 ms, recycle time 5 s), sodium borohydride for ^{11}B (contact time 5 ms, recycle time 10 s), and adamantane for ^{13}C (contact time 10 ms, recycle time 5 s).

To achieve the Hartmann-Hahn matching condition, a 90° pulse is

first found for the high-frequency nucleus (^1H) using silicon gum. The field is then adjusted to bring the ^1H signal on-resonance. The low-frequency transmitter output is then adjusted until the maximum signal enhancement (γ_I/γ_S) is observed (judged by maximum FID area on the oscilloscope).

(d) Recycle times

Recycle times were generally between 10 and 60 s for spin 1/2 nuclei, and 1 or 2 s for quadrupolar nuclei. Unless the spin-lattice relaxation time (T_1) was known for a specific sample, either (1) the recycle times were made sufficiently long so as not to saturate the FID ($\simeq 5\ T_1$), or (2) the effective flip angle was cut down from $\pi/2$ to a smaller value. ^{31}P spin-lattice relaxation times were measured for all samples containing phosphorus, and T_1 values were found to vary between 10 and 50 s. T_1 values for ^{27}Al nuclei are generally accepted to be in the order of milliseconds, although the inversion-recovery method will yield incorrect values for quadrupolar nuclei. Due to the low weight percentage of Si in the SAPO molecular sieves, T_1 values for the ^{29}Si nuclei were not determined. Long recycle times coupled with low flip angles were used in an effort to ensure quantitative measurements.

Proton T_1 measurements were performed for a number of ZSM-5 type zeolites. Millisecond values for proton T_1 appear to be typical and so short recycle times can be used for CP experiments.

(e) Chemical shift referencing and errors

Chemical shifts are reported in parts per million and positive values correspond to low-field, high-frequency, paramagnetic, or deshielded shifts.

The following referencing materials were used: for ^{29}Si,

tetramethylsilane (TMS), ^{31}P, 85% H_3PO_4 solution; for ^{27}Al, a solution of $Al(NO_3)_3.6H_2O$ in water $\{[Al(H_2O)_6]^{3+}\}$; for ^{11}B, a solution of $BF_3.OEt_2$; for ^{13}C, TMS. All of the isotropic chemical shifts were measured using the method of replacement. In some cases (^{29}Si, ^{13}C) a secondary (external) reference was taken with a known shift relative to TMS. Where solutions were used for the measurement of reference frequencies, MAS was not employed as the solutions were contained in sealed glass ampoules. No correction was made for susceptibility effects.

For spin I = 1/2 nuclei, the errors in determination of the isotropic chemical shifts should be minimal, the limit of resolution being the spectral digitization rate.

For spin I > 1 nuclei, *e.g.* ^{27}Al, one has to take into account the quadrupolar character of the nucleus, with the associated shift and broadening of the resonance lines. As the second-order quadrupolar interaction which causes the broadening and shift of the central (1/2, -1/2) transition is inversely proportional to the magnetic field, B_o, the experimental chemical shift will only approach the true isotropic chemical shift at high magnetic field strengths, and will always be shifted to high frequency of the true chemical shift. Thus, unless the experimental chemical shift can be corrected for the presence of the quadrupolar interaction, as is the case when η, the asymmetry parameter, and e^2qQ/h, the quadrupolar coupling constant, are known, then, at medium magnetic field strengths, the experimentally determined chemical shift may be substantially different from the true isotropic chemical shift.[17]

The various methods for determining the parameters necessary for conversion of experimental to true isotropic chemical shift are discussed in Chapter Two. One example of the kind of quadrupolar

induced shift encountered at 4.7 T is given for $AlPO_4$-5 in Chapter Six. As is to be expected, ^{27}Al NMR spectra of $AlPO_4$-5 at 7.05 T have narrower lines and the experimental chemical shift is closer to the true isotropic chemical shift. Ideally, in order to minimise the correction factor, all ^{27}Al NMR spectra should be run at 130.3 MHz (11.7 T), however this magnetic field strength was not available during the course of this research. The typical linewidth found for ^{27}Al at 4.7 T is *ca.* 1000 Hz (20 ppm). The error in the reported chemical shift is estimated to be $\pm$ 4 ppm.

(f) Linewidth measurement

Resonance linewidths were measured directly from the oscilloscope of the CXP-200 spectrometer. Typically a spectrum was first zero-filled to increase the number of data points, then Fourier transformed. In expand and phase mode, the peak in question was then set to a certain height. Half that height was then found using the cursor and set to zero Hz. The corresponding point on the other side of the peak gave the width of the peak which was then read off the screen. In cases of broad signals or bad signal-to-noise ratios (S/N), the time domain (TD) was reduced and again the spectrum was zero-filled and the process repeated.

(g) Spectral manipulation

For most nuclei, first-order phase correction proved enough to phase the spectrum correctly. However, in the cases where the resonance line was broad, the first few points (in pairs) of the FID were often zero-ed, otherwise the baseline appeared sinusoidal in shape ("baseline roll") and the spectral information was often lost. For some of the ^{27}Al NMR spectra presented, the only way that sensible information could

be extracted from the spectra was to left-shift (LS) the first n pairs of points (real and imaginary). This has the effect of removing the spurious points from the FID prior to Fourier transformation. First-order phase correction would then be sufficient to phase the spectrum correctly. How many points are left-shifted is largely a matter of trial and error and varies from spectrum to spectrum. One way of partially circumventing this problem is to leave a delay in the pulse programmed sequence before data acquisition. This is done for instance where HPD is employed, however, the use of HPD is not desirable for the majority of ^{27}Al NMR spectra as (1) it is not generally needed, and (2) because of duty cycle considerations one cannot then recycle as fast as the typical quadrupolar dominated T_1 value of ^{27}Al nuclei will allow *i.e. ca.* every 0.5 s. Another possible way of alleviating the problem somewhat is by using the spin-echo technique. This works well for static CP/HPD spectra of solids but proper refocusing only occurs when the 90^{o}-180^{o} pulse interval of the sequence corresponds to an integral number of sample rotations. When this is not the case, the intensities of the resonances in the MAS spectrum are often distorted.[244]

4.5.2. Quadrupolar nuclei: ^{27}Al.

Instrumental considerations relating to the observation of NMR active spin I = 1/2 nuclei have been dealt with in the preceding experimental section. The observation of quadrupolar nuclei (spin I > 1) can present much more of a problem to the NMR spectroscopist and specific problems encountered with ^{27}Al MAS NMR during the course of these studies will be discussed in this section. A detailed theoretical treatment of quadrupolar nuclei of half-integer spin in NMR is presented in Chapter Two.

(a) The problems encountered.

The problems encountered in the attempt to obtain high-resolution ^{27}Al MAS NMR spectra of solids were of two sorts (1) hardware problems, and (2) problems intrinsic to a quadrupolar nucleus such as ^{27}Al.

The observation frequency of ^{27}Al at 4.7 T (CXP-200) is 52.1 MHz. Thus, either probe (Andrew-Beams design) could in theory be used for this purpose. The ^{29}Si-MAS probe was tried first. At that time, shimming (as well as setting of the $\pi/2$ pulse) was performed on a static sample (sealed in a cylindrical glass vial) of a solution of $AlCl_3$ $\{[Al(H_2O)_6]^{3+}\}$. There are several fundamental reasons why this approach is incorrect (1) MAS may not be necessary for a liquid sample, however the inductance tuning will not be the same for a glass vial as for a spinning rotor and the vial will always touch the sides of the coil, (2) the sample does not possess similar quadrupolar effects as are likely to be observed in solids where ^{27}Al nuclei are not in perfectly cubic environments. However, it is still possible to "set-up" (incorrectly, as will be shown) for the observation of ^{27}Al nuclei using this method, and the first ^{27}Al MAS NMR spectra were obtained in this manner.

The first spectra obtained on a series of $SiCl_4$-vapour-dealuminated and acid-extracted zeolite HY samples provided by Dr. R. Rudham, University of Nottingham, were of poor quality, marred by distorted baselines. An example of the quality of ^{27}Al NMR spectra obtained is shown in Figure 4.3. The distortions, due to "pulse feed-through", that is, to ringing somewhere in the combination of receiver coils, cables, and pre-amplifier,[245] induced by the rf pulse, results in the accumulation of invalid data early in the FID which, in turn, produces distortions of the baseline upon Fourier transformation. Thus, the interpretation of such spectra as shown in Figure 4.3 is often

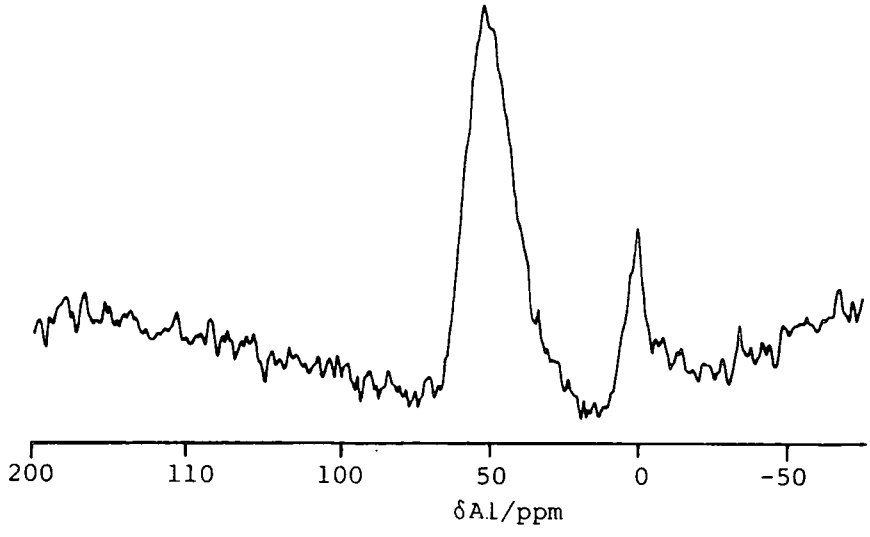

Figure 4.3

HY(b) ^{27}Al MAS NMR on ^{29}Si probe

complicated and certainly, the original aim of obtaining octahedral Al to tetrahedral Al NMR ratios is impossible.

Since this ringing is frequency specific, to eliminate the ringing requires extensive probe modification. The more usual approach is to try to suppress the effects of the ringing in the spectrum itself. There are three well known approaches to the solution of this problem. (1) The insertion of a delay, τ, between the excitation pulse and the beginning of data acquisition[246] ($\pi/2$ - τ - acquire). This delay must be longer than the time required for the extinction of the ringing, and generally entails large first-order phase corrections in the Fourier

transformed spectrum. These invariably lead to rolling baselines. (2) For solids, the detection of "solid-echos" using the sequence $[(\pi/2)_x - \tau - (\pi/2)_y - \tau - \text{acquisition}]^{247}$ (the subscripts x and y refer to a $\pi/2$ rf phase change). This procedure avoids phase correction problems but implies a careful adjustment of the π pulse and a correct rf field homogeneity. Strictly speaking when dealing with quadrupolar nuclei such as ^{27}Al , one cannot in general speak of a π or a $\pi/2$ pulse. However, this method produced reasonable results (Figure 4.4) even though it is subject to severe sensitivity losses.

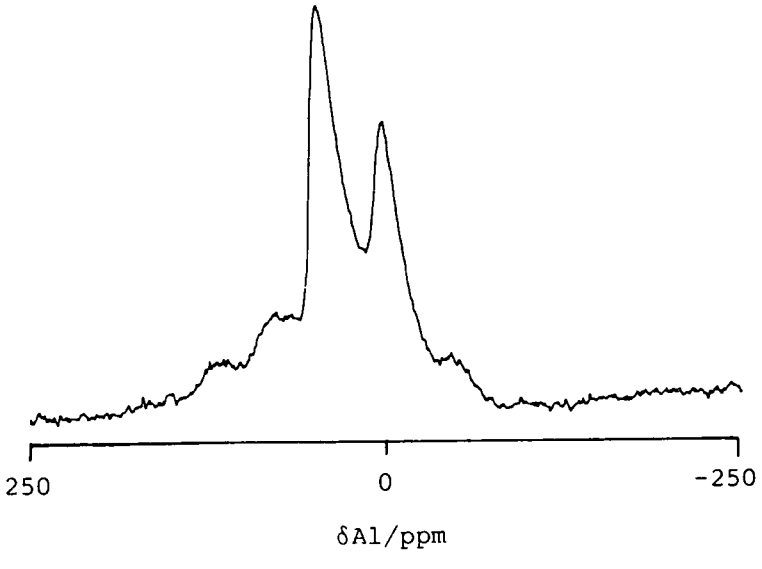

Figure 4.4

^{27}Al Solid-echo experiment on ^{31}P MAS probe

(3) Since ringing is a linear phenomenon (coherent with the pulse), if it is compounded after a series of pulses designed to subtract out the ringing, leaving the FID intact, the signal should be free of the effects of ringdown.[248,249] A suitable pulse sequence as originally implemented on the CXP-200 by Dr. Jane Cox[250] is given below:

$$90_x \underset{(+)}{-} \text{acquire} - \text{delay} - 180_x - \tau - 90_x \underset{(-)}{-} \text{acquire} - \text{delay} -$$

$$90_{-x} \underset{(-)}{\text{- acquire}} \text{ - delay - } 180_{x} \text{ - } \tau \text{ - } 90_{-x} \underset{(+)}{\text{- acquire}} \text{ - delay}$$

This pulse sequence known as the RIDE pulse sequence (RIng - Down Elimination) is illustrated schematically below.

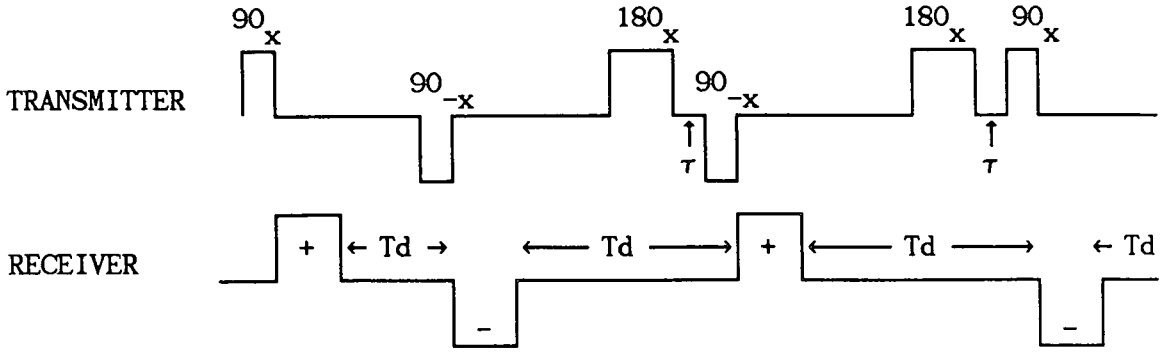

Td - variable delay after acquisition

τ - small delay (negligible w.r.t. the acquisition time)

The ringdown in the receiver cancels, leaving only the FID.

As can be seen in Figure 4.5, the use of RIDE did not solve the problem of the distorted baseline. The first useful ^{27}Al MAS NMR spectra were therefore obtained on the broad-banded ^{31}P MAS NMR probe

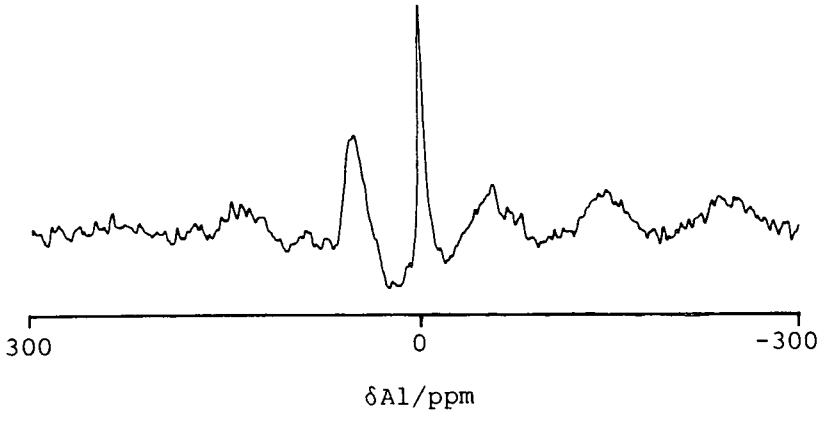

Figure 4.5

Nottingham HY(b) sample (^{29}Si probe - with RIDE)

using a similar set-up procedure to that described earlier. The results for the series of six dealuminated HY zeolites from Nottingham University are shown in Figure 4.6. The samples, (a)-(f), (produced from dealuminated HY zeolites by controlled acid treatments between pH 4.8 and pH 0.0), were used in a study to find the optimum pretreatment conditions for the catalytic dehydration of propan-2-ol. The samples were characterised by MAS NMR (using the CXP-200 at the University of East Anglia), and by pore volume measurements, powder XRD and IR, carried out at the University of Nottingham under the supervision of Dr. R. Rudham. The catalytic measurements and dealumination of the samples were also performed at the University of Nottingham.

The most active catalysts for alcohol dehydration and conversion possess a high concentration of both strong proton donor sites and extra-structural aluminium sites. Thus, aluminium atoms are central to the catalysis process being investigated here. Aqueous pre-treatment at different pH using mineral acid can be expected to remove extra-structural aluminium, and at low pH values, extract aluminium from lattice positions. Thus, acid pre-treatment will affect the catalytic activity of zeolites for the dehydration of propan-2-ol. The samples and their acid pre-treatment conditions are listed below:
(a) was prepared by five successive 2 h treatments of dealuminated zeolite with aqueous NH_4Cl at reflux temperature, followed by extensive water washing, and drying. The acid form of the sample, obtained by deammoniation, was produced during the 650 K treatment of the samples prior to catalytic measurements. Catalysts (b), (c), (d), and (e) were prepared by acid treatment at pH values of 2.5, 2.5, 1.3, and 0.22 respectively, achieved by the addition of 0.5 cm^3 aliquots of 1M hydrochloric acid to an aqueous suspension of 1 g of dealuminated

zeolite over a period of 3 h. Catalyst (f) was prepared at pH 0.0 using 1M hydrochloric acid at 353 K. All catalysts were washed and dried after acid treatment.

The ^{27}Al MAS NMR spectra (Figure 4.6) show the effect of acid treatment on the samples. The progressive removal of extra-structural aluminium (decrease in I_{oct}/I_{tet}) as the pH is reduced from 4.8 to 0.0 is clearly visible.

The ^{29}Si MAS NMR spectra (not shown; carried out by Dr. G. Haines) indicate that samples (a)-(d) have both Si(0Al) and Si(1Al) peaks, whilst samples (e) and (f) only possess a single peak corresponding to Si(0Al). The Si/Al_{NMR} ratio derived from the spectra yield an approximate value of 15 for samples (a)-(d). From the published correlation between the wavenumber for the internal asymmetric TO_4 stretch and the Si/Al ratio of the zeolite framework,[252] the ratio for samples (a)-(d) was estimated to be *ca.* 13. Pretreatment at pH values of 0.22 and 0.0 resulted in a shift of the TO_4 asymmetric stretching band to higher wavenumbers, indicative of framework dealumination.

For catalyst (a), the I_{oct}/I_{tet} value of 0.72 derived from the ^{27}Al MAS NMR spectrum, together with an overall Si/Al ratio of 9.5 determined by chemical analysis, leads to a Si/Al framework ratio of 16. This is in remarkably good agreement with values of 15 from ^{29}Si MAS NMR and 13 from IR spectroscopy.

O_2 pore volumes increased by 20% on decreasing the pH from 4.8 to 1.3, as a consequence of the removal of extra-structural aluminium species. At pH 0.0, framework dealumination occurred with subsequent decrease in porosity and fall in crystallinity.

From results for the catalytic dehydration of propan-2-ol, it was found that decreasing the pH from 4.8 to 1.3 resulted in an increase in

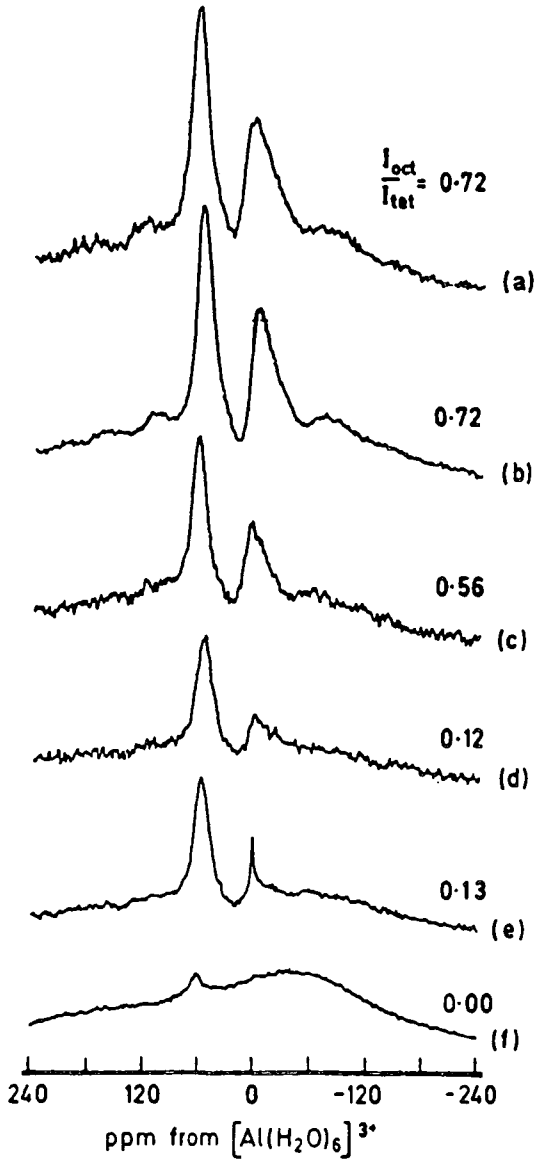

Figure 4.6

^{27}Al on ^{31}P MAS probe: Nottingham dealuminated zeolites.

the rates of formation of propene (r_p) and di-isopropyl ether (r_e), coupled with a decrease in the selectivity for di-isopropyl ether formation [$2r_e/(r_p + 2r_e)$]. This trend is attributed to the removal of extra-structural aluminium. Positively charged aluminium species act as charge balancing cations so that their acid extraction, in the absence of framework dealumination leads to a higher concentration of Bronsted acid centres. An increase in activity is then to be expected since all such centres contribute to an ionic mechanism for propan-2-ol dehydration.[253-256] The removal of the aluminium species may also increase catalytic activity through increasing both pore volume and active site accessibility. There is a rapid fall in catalytic activity following pretreatment at pH < 1.0. This is explained in terms of framework dealumination reducing the concentration of Brønsted acid centres, whilst the loss of crystallinity and porosity may reduce the accessibility of those that remain.

These results form the basis for a paper which has recently been accepted for publication.[251]

The second hardware problem encountered is apparent in all the spectra in Figure 4.6 especially spectrum (f). The broad featureless hump is a residual background signal from the probe itself, as confirmed by running an empty rotor. One could, in principle, subtract this resonance out by running a blank of the same number of transients. However, this process is known to introduce phase errors in the solid-state spectra. After trying either to remove or shield the parts of the probe nearest the coil (for instance, the spin meter assembly) and finding that this had no effect on the ^{31}P MAS NMR probe, some of the HY zeolites were run on the ^{29}Si NMR probe, this time with PTFE tape or thin brass surrounding wrapped around the aluminium-containing

protruding parts of the spinner assembly. This had the effect of detuning the probe so that the probe and its parts no longer acted as part of the tuned tank circuit following the rf pulse. Thus, ringdown no longer occurred in the ^{29}Si MAS NMR probe. However, it was found that there was also an appreciable amount of background aluminium signal from this probe. Following a suggestion that the background signal in the probe came from the ceramic material of the Jennings capacitor,[257] the probe was modified (a glass Jennings capacitor being used - no effects of the replacement were apparent in the ^{29}Si MAS NMR, presumably due to the long ^{29}Si T_1 of silica). The ^{29}Si MAS NMR probe was thus rendered "aluminium-free" for the purposes of qualitative ^{27}Al NMR determination.

Having now established that the probe with which all ^{27}Al MAS NMR measurements are to be made is free from background aluminium signals, the next problem that arises is one of aluminium quantification in ^{27}Al solid-state MAS NMR. For spin I = 1/2 nuclei, it is well known that the initial value of the FID after a $\pi/2$ pulse are proportional to the number of resonant nuclei in the sample coil. Using a reference sample with a known number of resonant nuclei, one is able to determine the absolute number of resonant nuclei in the actual sample (provided the time interval between pulses for both the samples is longer than $5T_1$).

For spin I = n/2 nuclei, where n = 3, 5, 7, *etc.*, quadrupolar coupling is generally, but not always, large enough in the solid-state under MAS conditions so that only the central ($-1/2 \longleftrightarrow 1/2$) transition is observed,[14] as is explained in Chapter Two. Schmidt[258] has calculated that the intensity of the central transition under rf excitation is not a simple fraction of the intensity observed for solutions. Moreover, this intensity depends on both the quadrupole frequency (υ_Q) and excitation frequency (υ_{rf}). For non-selective

excitation (*e.g.* in liquids), the maximum FID signal is measured after a $\pi/2$ pulse, while for selective excitation of the central transition only (assuming $\upsilon_{rf} << \upsilon_Q$) , the maximum is measured after a $\pi/(2I + 1)$ pulse.[6] For short pulses [angles $< \pi/(2I + 1)$], the intensity is proportional to the pulse length and independent of the quadrupole coupling parameter. Under this condition a comparison of the signal intensity of the sample with that of the reference [bearing in mind that the intensity of the ^{27}Al solid-state signal is a factor $4I(I + 1)/3(I + 1/2) = 35/9$ smaller than that of a liquid-state signal of the same number of nuclei][258] gives correct results for the determination of the number of resonant nuclei.

(b) Establishment of the correct "setting-up" procedure.

We are now in a position to discuss the necessary requirements for qualitative determination of ^{27}Al nuclei in aluminosilicate-type samples using solid-state NMR:

(1) We need a sample that closely mimics the behaviour of aluminosilicates when observing aluminium by ^{27}Al MAS NMR.

(2) The sample should allow accurate setting of T_1 (and hence "$\pi/2$") pulses (by the null-method), implying that the sample exhibits a narrow resonance line or lines in the ^{27}Al NMR spectrum. The use of $\pi/6$ pulses is essential.

(3) Ideally the sample should have a small quadrupole coupling constant, be readily and cheaply available and not be hygroscopic.

(4) The sample should be a pure polycrystalline powder.

Several materials were studied including zeolite A (^{27}Al linewidth = 700 Hz); natrolite (^{27}Al linewidth = 400 Hz); metavariscite, $AlPO_4.2H_2O$ (^{27}Al linewidth = 400Hz); solid $AlCl_3.6H_2O$ (^{27}Al linewidth = 100 Hz); and finally two aluminium alums, hydrated aluminium potassium

sulphate and hydrated aluminium ammonium sulphate (both having ^{27}Al linewidths of 70 Hz with HPD). Figure 4.7 shows ^{27}Al MAS NMR spectra of metavariscite, solid $AlCl_3.6H_2O$, and aluminium potassium sulphate.$12H_2O$. Figure 4.8 shows the peak height response to pulse length for aluminium under MAS NMR conditions for solid $AlCl_3.6H_2O$, $AlK(SO_4)_3.12H_2O$, and NH_4^+-ZSM-5. It is obvious from the graph that, in order to have a linear relationship between the signal intensity and the pulse length, small flip angles ($\lesssim \pi/6$) must be used.

Figure 4.7 (see over)

^{27}Al MAS NMR of (a) metavariscite; (b) solid $AlCl_3.6H_2O$; and (c) hydrated aluminium potassium sulphate.

Note: Extensive spinning sidebands observed in (a),(b), and (c) due to modulation of the non-central transitions. These sidebands only appear at the magic angle exactly.

Conditions for Figure 4.7:

(a) SF = 52.1 MHz; RD = 0.5 s; SW = 100 kHz; SI = 2 K; TD = 1 K; NT = 60; SS = 3.3 kHz; PD = 1 μs; PA = $\pi/6$; SR = -2369.

(b) SPE: SF = 52.1 MHz; RD = 5 s; SW = 100 kHz; SI = 2 K; TD = 1 K; NT = 32; SS = 3.3 kHz; PD = 1 μs; PA = $\pi/6$; SR = -2332.

(c) left - SPE (no HPD): SF = 52.1 MHz; RD = 1 s; SW = 50 kHz; SI = 2 K; TD = 1 K; NT = 60; SS = 3.3 kHz; PD = 1 μs; PA = $\pi/6$; SR = -2344.

right - SPE: SF = 52.1 MHz; RD = 1 s; SW = 50 kHz; SI = 2 K; TD = 2 K; NT = 32; SS = 3.3 kHz; PD = 1 μs; PA = $\pi/6$; SR = -2344.

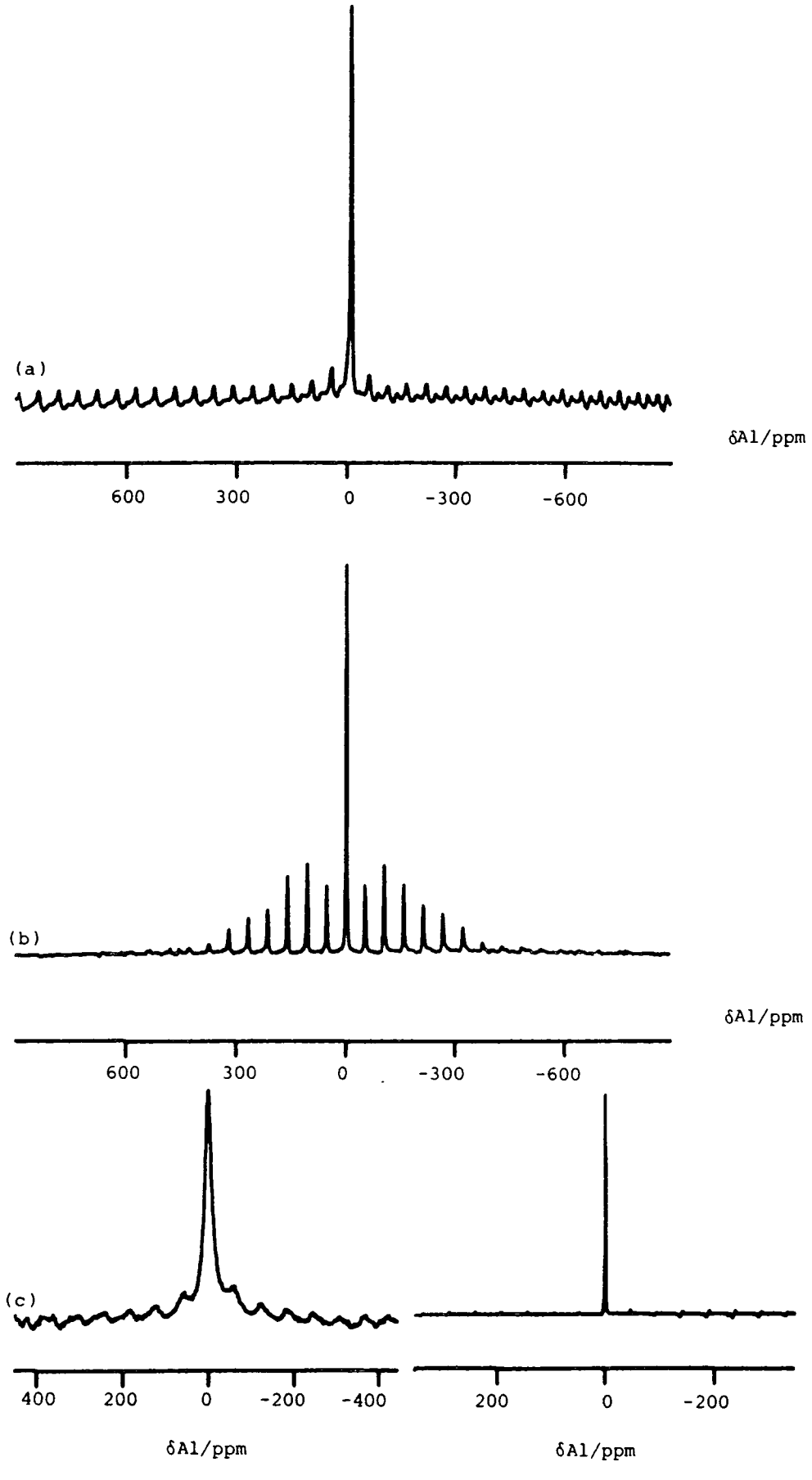
(a)
δAl/ppm
600
300
0
-300
-600
(b)
δAl/ppm
600
300
0
-300
-600
(c)
400
200
0
-200
-400
δAl/ppm
200
0
-200
δAl/ppm

Figure 4.7

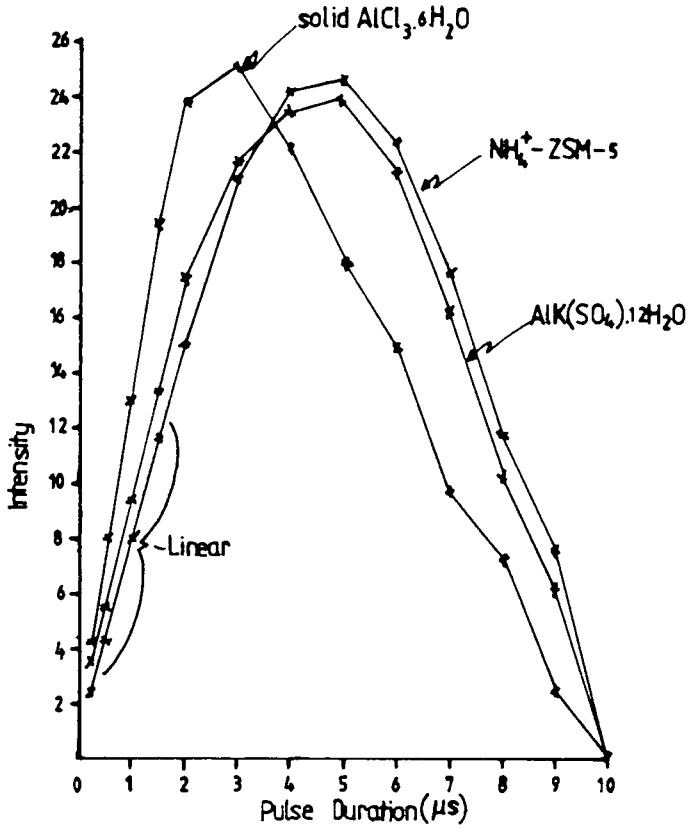

(PD = 5 μs; PA = π/2)

Figure 4.8

Peak heights (arbitrary units) *versus* variation in pulse length (μs).

CHAPTER FIVE - NMR RESULTS FOR VARIOUS SUBSTITUTED ZSM-5 TYPE MOLECULAR SIEVE MATERIALS

5.1 Introduction

The results of NMR investigations into a variety of isomorphously substituted high-silica zeolites having the ZSM-5 structure are presented in this chapter. Only for the case of boron substitution can NMR investigate directly the substituting element with ease. In all other cases (Fe, Ti, Cr, and La), isomorphous substitution of the heteroatom is inferred, or not, from indirect observation of the effect of the heteroatom on the lattice silicons, using ^{29}Si MAS NMR. Where appropriate, samples were also studied using ESR and magnetic susceptibility measurements. For all samples, the effect of thermal treatment on the ^{29}Si MAS NMR spectra and hence the substituting heteroatom, is also investigated.

In the final results section of this chapter, MAS NMR is used, for the first time, to investigate the controversial zeolitic mineral, viséite. Viséite is reported to be a phosphorus substituted mineral with the analcime structure.[181]

5.2 High-silica zeolites

NMR is used to investigate, either directly (as in the case of B-ZSM-5) or indirectly (for La-, Ti-, Cr-, and Fe-ZSM-5) the coordination state of the substituting heteroatom in an attempt to prove that isomorphous substitution does occur in ZSM-5-type molecular sieve materials.

5.2.1. B-ZSM-5 (Boralite)

Two B-ZSM-5 samples were received, HBZ-626 and RD/492/85. There was essentially no difference between the two samples, the SiO_2/B_2O_3 ratios in both samples being approximately 44 (equivalent to four boron atoms per unit cell). Consequently, both samples will be treated together. The powder XRD traces (not shown) identify the samples as being ZSM-5-type, remaining crystalline after calcination (Table 5.1).

(i) As-synthesised Laporte B-ZSM-5			(ii) Calcined Laporte B-ZSM-5
d (Å)	2θ	I/I_{max} x 100	I/I_{max} x 100
11.04	8.00	100	100
10.04	8.81	68	71
5.98	14.82	20	22
5.53	16.03	13	16
4.27	20.80	10	13
3.83	23.23	84	96
3.72	23.92	48	45
3.64	24.46	23	29
3.42	26.06	9	8
3.30	27.02	11	10
3.04	29.38	9	9
2.98	29.99	16	13
2.94	30.41	10	7
2.00	45.34	13	8
1.99	45.59	14	7

Table 5.1

Powder XRD data for as-synthesised and calcined B-ZSM-5 (major lines only)

Figure 5.1 shows ^{11}B and ^{29}Si MAS NMR spectra of both the precursor (TPABr-ZSM-5) and calcined (B-ZSM-5) forms of the sample. The calcined sample was partially rehydrated prior to ^{11}B NMR observation. The NMR data are collated in Table 5.2. The ^{11}B NMR results for the precursor

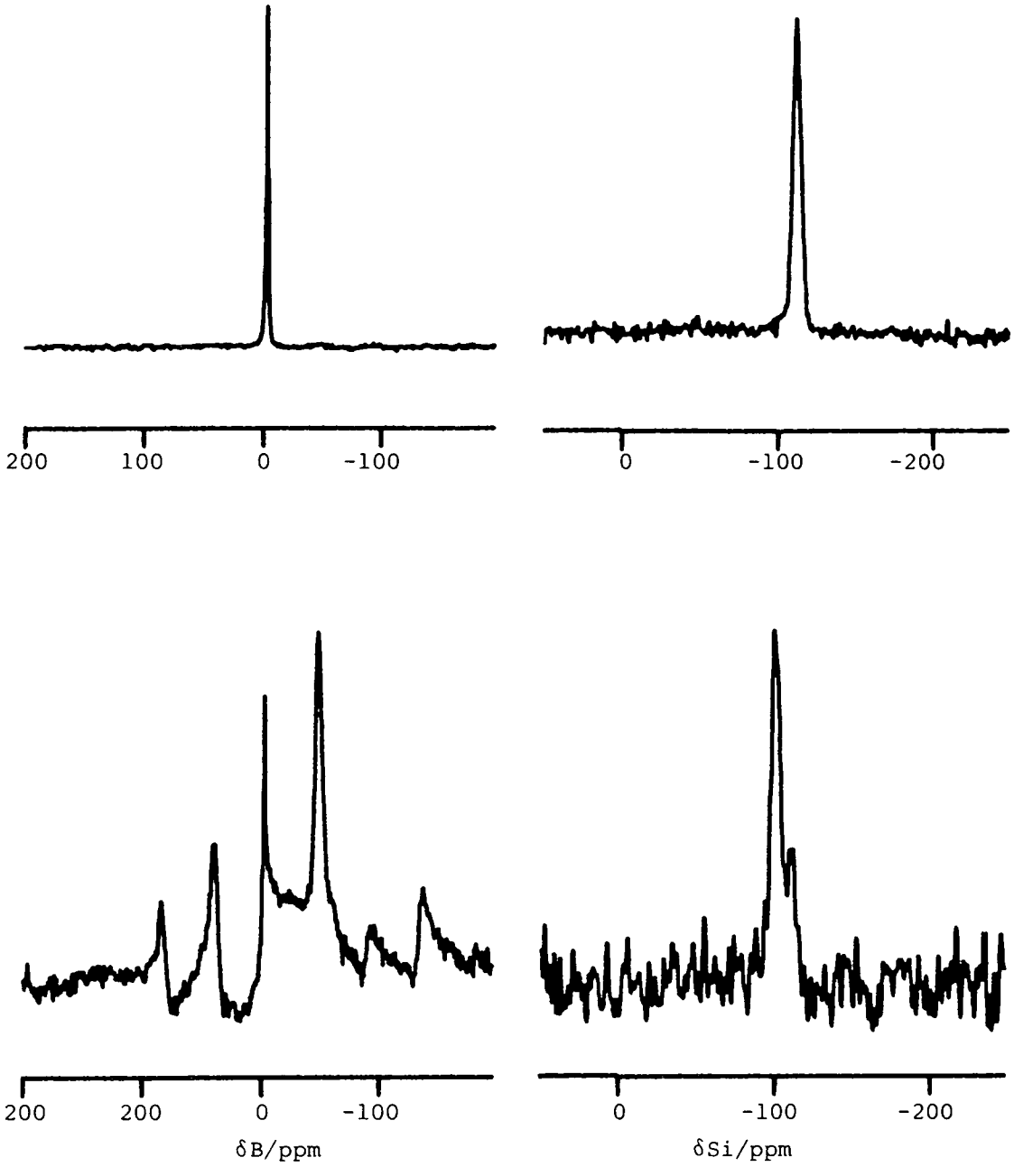

^{11}B SPE (no HPD); SF = 64.2 MHz; RD = 3 s (precursor), 10 s (calcined); NT = 60 (precursor), 3754 (calcined); SW = 50 kHz; SI = 2 K; TD = 2 K; SS = 2.8 KHz; PD = 3 μs; PA = π/4; SR = 42669.

^{29}Si CP/HPD; SF = 39.7 MHz; RD = 10 s; NT = 1208 (precursor), 5824 (calcined); SW = 20 kHz; SI = 2 K; TD = 1 K; CT = 5 ms; SS = 3.0 kHz; SR = 13200.

Figure 5.1

^{11}B (left) and ^{29}Si (right) MAS NMR spectra of the precursor (upper) and calcined partially hydrated (lower) forms of B-ZSM-5

sample	^{11}B NMR		^{29}Si NMR		
	chemical shift/ (ppm)	linewidth (Hz)	chemical shift/(ppm) CP/MAS	SPE	linewidth (Hz)
TPA-B-ZSM-5	-3.7	80	-111.5	-111.5	240
B-ZSM-5	quadrupolar lineshape pattern		-102.0 -111.3	-111.5	250

Table 5.2
^{11}B and ^{29}Si MAS NMR data for B-ZSM-5

form of B-ZSM-5 are in good agreement with those of Gabelica *et al.*[205,206] proving the coordination of boron in Boralite to be tetrahedral. The low level of boron substitution is reflected in the virtual absence in the ^{29}Si NMR spectrum of the precursor compound of a Q^3 resonance [expected at *ca.* -102 ppm due to Si(1B) units]. As boron-11 is a quadrupolar nucleus, it is very sensitive to the symmetry of its nuclear environment. This is evident from the ^{11}B NMR spectrum of calcined, partially rehydrated Boralite. The coordination of the substituting boron atoms has changed from framework tetrahedral (with low quadrupolar coupling constant)[259,260] to trigonal following calcination. The symmetry of the environment is altered (lowered) causing an increase in the nuclear quadrupolar coupling constant with the consequent appearance of a typical quadrupolar powder pattern [with non-zero chemical shift anisotropy (CSA) also] and spinning sidebands in the ^{11}B NMR spectrum. The proposed dehydration mechanism[207] is shown in Figure 5.2.

On dehyration, SiOH units are formed as well as BO_3 units. This is confirmed using ^{29}Si CP/HPD MAS NMR to enhance selectively SiOH groups over Q^4 Si groups (Figure 5.1). Note that CP with a contact time of 5 ms did not produce a Q^3 signal for the precursor Boralite material.

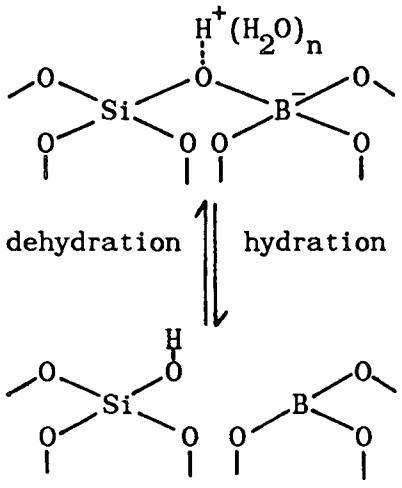

Figure 5.2

The influence of hydration on the coordination of boron atoms in Boralite

At 64.2 MHz (200 MHz proton), the ^{11}B MAS NMR spectrum (not shown) of a fully dehydrated (10^{-3} Torr, 280°C for 10 h) B-ZSM-5 sample is barely visible *i.e.* the quadrupolar effects are sufficiently large to hamper considerably the observation of an NMR signal. Scholle *et al.*[207] who worked at 93.3 and 54.8 MHz, reported that at the lower frequency, the ^{11}B NMR spectrum of the dehydrated Boralite was so broad (due to the increased quadrupole interaction at lower field) that a recognizable lineshape was not observable. The process of dehydration is reversible, complete rehydration taking over 12 hours and yielding an ^{11}B spectrum indistinguishable from that of the as-synthesised sample.

The assignment of the ^{11}B NMR chemical shift for the precursor form of Boralite to tetrahedral BO_4 units is supported by ^{11}B NMR data acquired for several borosilicate minerals. Danburite ($CaB_2Si_2O_8$) contains tetrahedral boron coordinated to silicate tetrahedra and gives rise to a single sharp resonance at *ca.* 0.7 ppm. Datolite [$CaB(SiO_4)(OH)$], also contains tetrahedral boron coordinated to silicate

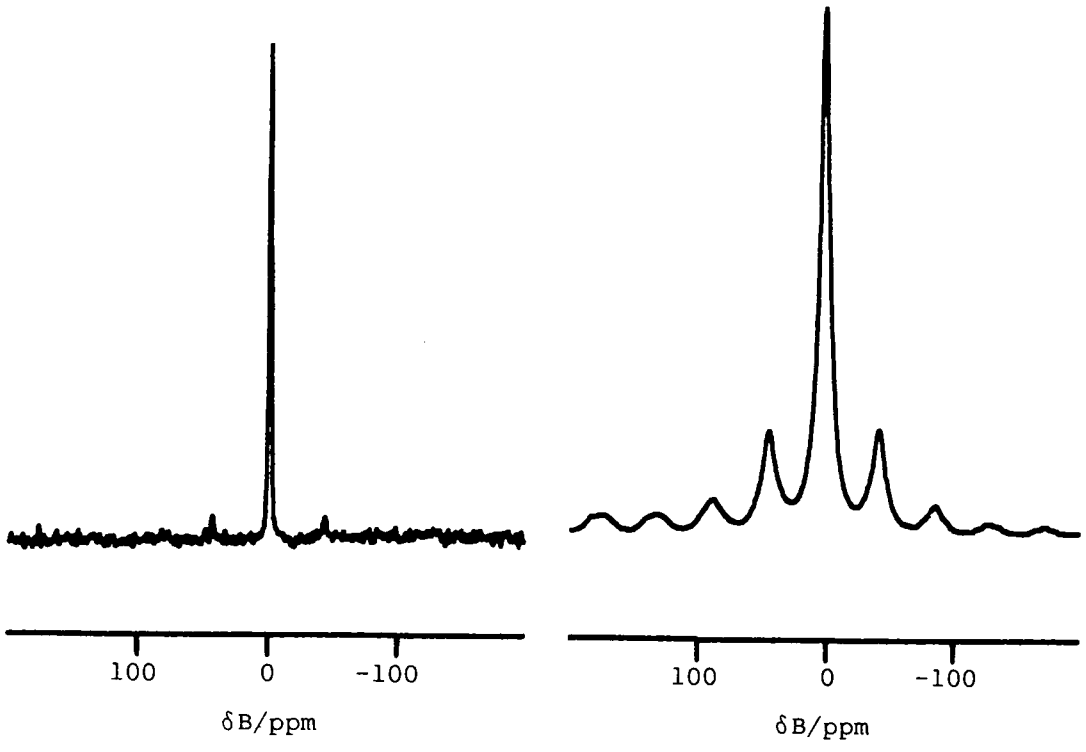

SPE (no HPD); SF = 62.2 MHz; SW = 30 kHz; RD = 5 s; NT = 500 (danburite), 48 (datolite); SI = 2 K; TD = 2 K; PD = 3 μs; PA = π/4; SS = 3.3 kHz; SR = -406.9.

Figure 5.3

^{11}B MAS NMR spectra of danburite (left) and datolite (right)

---

tetrahedra and exhibits a chemical shift of *ca.* 1.0 ppm. The ^{11}B MAS NMR spectra of these two minerals are shown in Figure 5.3. The difference in linewidth and the increased intensity of the spinning sidebands of datolite with respect to danburite simply reflects the extent of boron-hydrogen dipolar coupling in the two samples. In danburite the boron tetrahedra are BO_4 units, in datolite they are (BO_3)-OH tetrahedra. Turner *et al.*[261] have recently shown that rapid ($\geq$ 6 kHz) MAS effectively removes this sideband intensity, and that rapid MAS combined with HPD yields well-resolved ^{11}B NMR spectra for a

variety of borosilicate and borate materials. Turner *et al.* have also proposed that the presence of silicon (rather than boron) as a next-nearest neighbour to boron may cause a slight deshielding for BO_4 units. Tetrahedral BO_4 units appear to be characterised by two different resonance lines.[261] When randomly distributed in a structure (where B-O-B bonds might be expected) they give rise to an NMR line with a chemical shift of between 1-2 ppm as observed by Gabelica *et al.*[205,206] for BO_4 units in the aluminosilicate gel of boralite prior to crystallization. If located in a more ordered sructure (where solely B-O-Si bonds might be expected) this line is shifted to lower frequency to give the typical value of *ca.* -3 ppm observed for BO_4 units in a zeolite framework. However, both danburite and datolite contain B-O-Si bonds and have a chemical shift of *ca.* 1 ppm. Turner *et al.*[261] report that at 11.7 T (160.4 MHz boron-11) the chemical shift range for the BO_3 unit is *ca.* 12.7-190 ppm. They report that tourmaline $[(Na,Ca)(Li,Mg,Al)(Al,Fe,Mn)_6(BO_3)_3(SiO_{18})(OH)_4]$ which contains trigonal boron coordinated to a $(Si_6O_{18})^{-12}$ cyclosilicate, yields a broad resonance centred at *ca.* 12.7 ppm, together with spinning sidebands, which probably originate from the paramagnetic Fe and Mn impurities.[262] A sample of tourmaline was obtained from Gregory, Bottley, and Lloyd, London, for the purposes of ^{11}B NMR investigation. However at 4.7 T (64.2 MHz boron-11), no spectrum was observed, presumably due to the increased quadrupole broadening effects present at this lower magnetic field strength.

Gabelica *et al.*[205,206] reported that tetrahedral boron could be very easily incorporated into growing zeolitic particles during synthesis in Pyrex tubes. Figure 5.4 shows the ^{11}B MAS NMR spectra of a Laporte ZSM-5 (SiO_2/Al_2O_3 = 200) after simple contact with a 1M solution

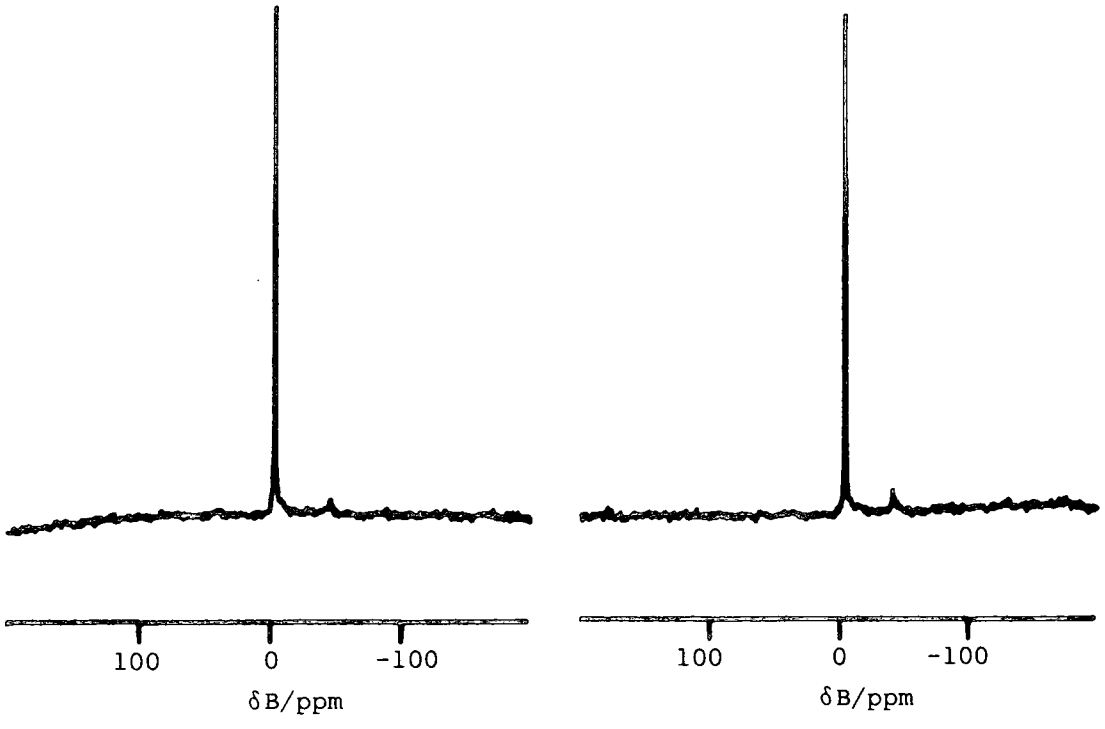

SF = 64.2 MHz; RD = 4 s; NT = 1390; SPE; SW = 30 kHz; SI = 2 K; TD = 2K; PD = 3 μs; PA = π/4; SS = 3.3 kHz; SR = -406.9.

Figure 5.4

ZSM-5 after being heated under reflux with boric acid solution in Pyrex (left) and soda glass (right)

---

of boric acid under reflux. The experiment was carried out in both Pyrex and soda glass vessels to ensure that the BO_4 units entering the zeolite framework resulted from the boric acid solution only. The isotropic chemical shifts and linewidths are identical to that found for Boralite. Thus, it would seem relatively easy to substitute small amounts (less than one B atom per unit cell) of boron simply by contacting the zeolite with a source of boron in either a caustic or an acidic medium.

To summarize, ^{11}B MAS NMR has shown that isomorphous substitution

sample code	SiO_2/Fe_2O_3 [a)]	wt % Fe	Fe/unit cell [b)]	colour
HSZ-719	74.0	2.5	2.6	white
HSZ-707	62.0	2.8	2.9	white
HSZ-708	60.7	2.9	3.0	white
HSZ-591	42.8	4.0	4.2	light beige
HSZ-553	38.0	4.4	4.5	light beige
HSZ-524	16.8	8.6	8.9	beige

a) determined by multi-element scan (MES) XRF
b) assuming all Fe to be isomorphously substituted in the lattice

Table 5.3

Chemical and physical characteristics of the six ferrisilicates studied (in their as-synthesised condition).

of boron atoms into the silicate framework of ZSM-5 does indeed occur. Calcination produces BO_3 units, the change in coordination of the boron atoms being observable by ^{11}B MAS NMR.

5.2.2. Fe-ZSM-5 (Ferrisilicate)

Six ferrisilicate samples were studied using ^{29}Si MAS NMR, powder XRD, ESR, and magnetic (Faraday) susceptibility measurements. The sample codes and SiO_2/Fe_2O_3 ratios plus other chemical and physical characteristics of the six (as-synthesised) samples are listed in Table 5.3.

The powder XRD pattern for sample HSZ-719 (typical of that obtained for the Fe-ZSM-5 samples) is shown in Figure 5.5, and the crystallographic data relevant to the Figure are presented in Table 5.4. Powder XRD confirms that the structure remains intact on calcination. Figure 5.6 shows typical ^{29}Si MAS NMR spectra of both precursor and calcined forms of several of the ferrisilicate samples. The chemical

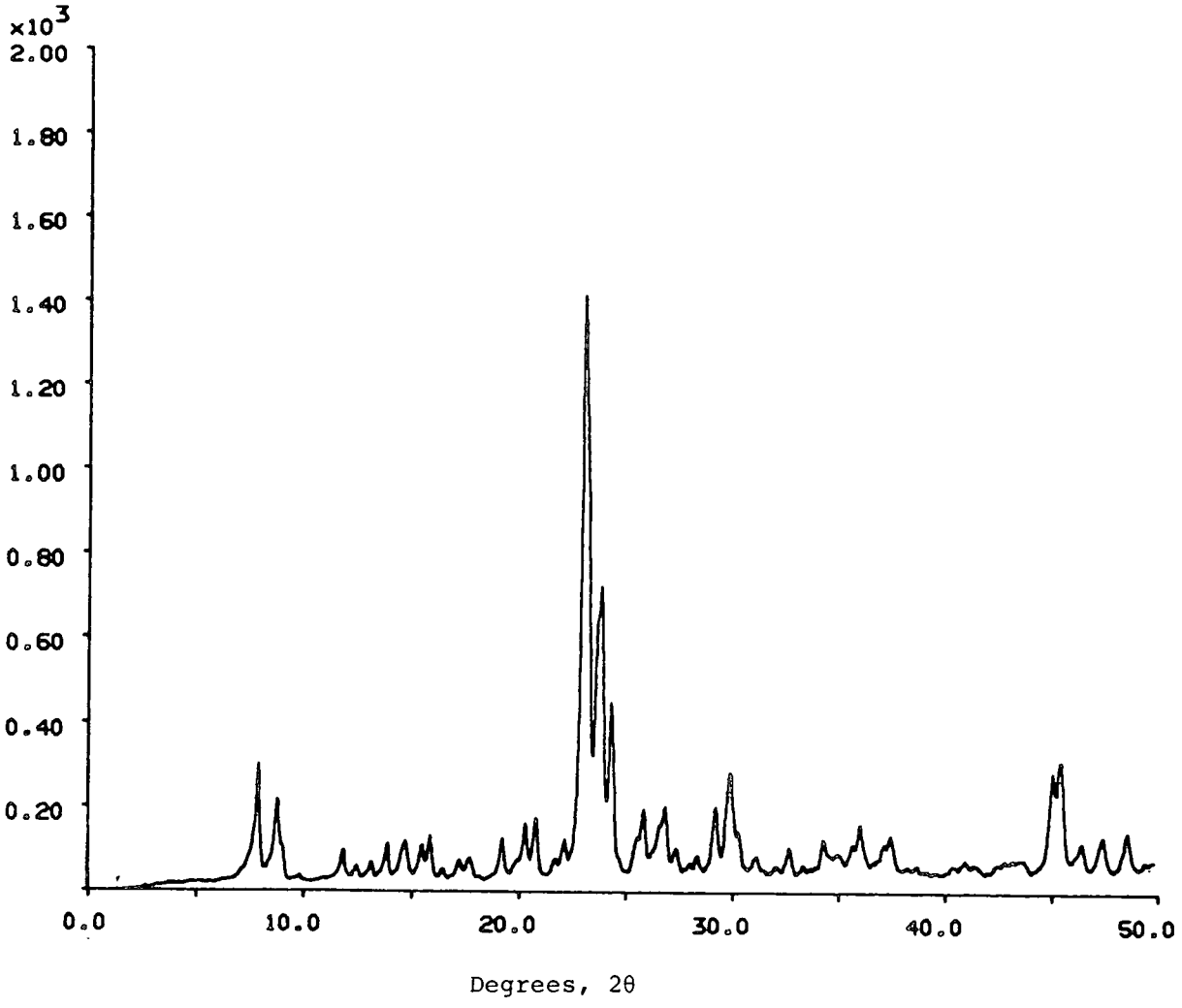

Figure 5.5

Powder XRD trace for Fe-ZSM-5 (HSZ-719)

d (Å)	2θ	I/I_{max} x 100
11.14	7.93	57
10.03	8.81	38
4.26	20.82	12
3.86	23.04	100
3.72	23.90	47
3.65	24.36	29
3.44	25.88	10
3.31	26.90	10
3.06	29.20	9
2.99	29.84	13
2.01	44.98	8
1.99	45.44	10

Table 5.4

Powder XRD data for HSZ-719 (major lines only).

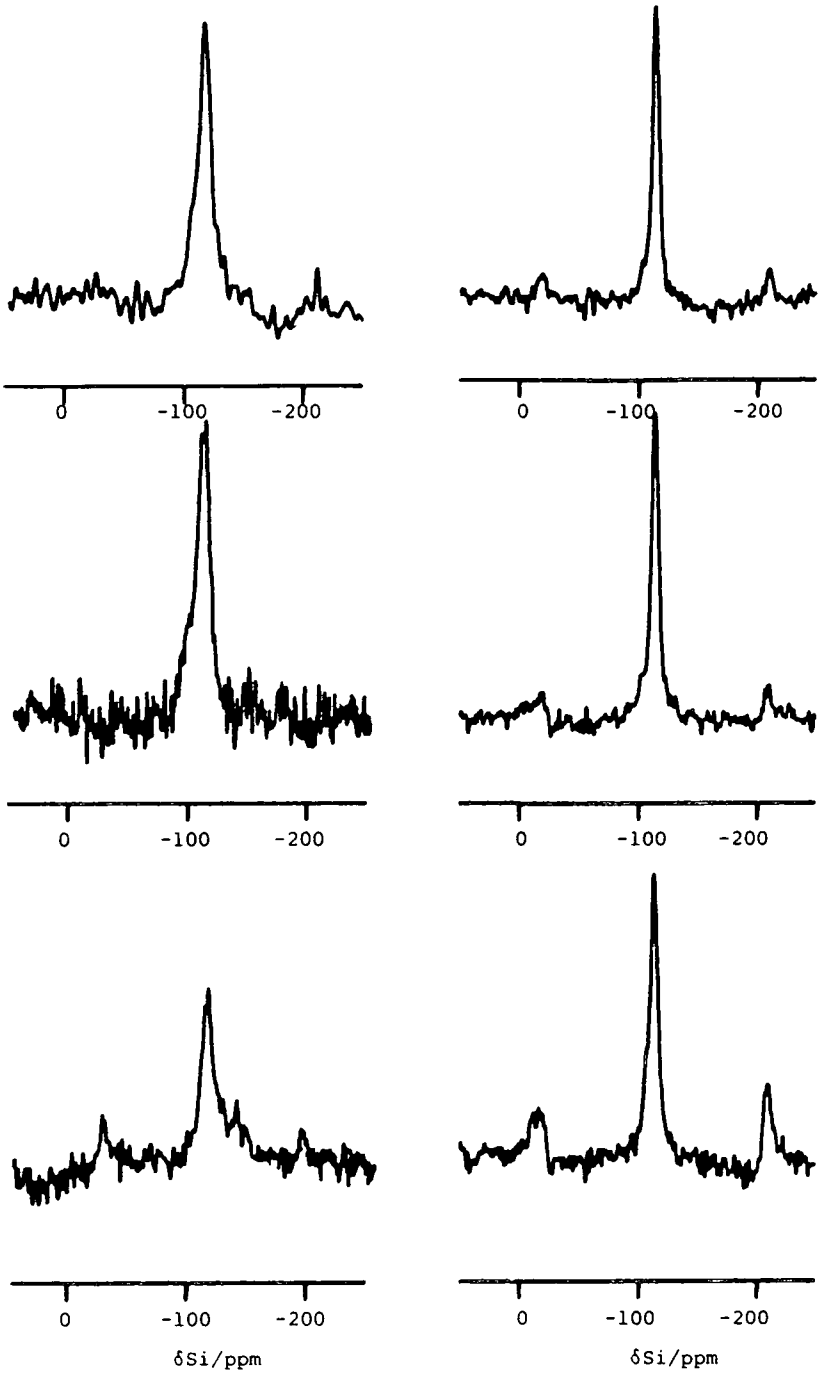

SF = 39.7 MHz; RD = 5 s; NT = 1600 to 3000 (as-synthesised), 300 to 600 (calcined); SW = 20 kHz; SI = 2 K; TD = 1 K; PD = 5 μs; PA = π/2; SS = 3.7 kHz; SR = 13200.

Figure 5.6

^{29}Si MAS NMR spectra of precursor (left) and calcined (right) forms of ferrisilicates HSZ-719 (upper), HSZ-708 (middle) and HSZ-524 (lower).

sample	^{29}Si MAS NMR chemical shift/(ppm) as-synthesised	calcined	linewidth (Hz) as-synthesised	calcined
HSZ-719	-111.9	-112.8	480	270
HSZ-707	-113.0	-113.3	360	260
HSZ-708	-113.0	-112.4	630	280
HSZ-591	-113.3	-112.7	670	400
HSZ-553	-113.0	-113.3	580	330
HSZ-524	-114.0	-112.8	540	260

Table 5.5

^{29}Si MAS NMR data for precursor and calcined ferrisilicates

shifts and linewidths are collated in Table 5.5.

The ^{29}Si MAS NMR spectra of the precursor forms of the samples are broad and featureless. The chemical shift is centred around the typical shift for silicon in a Q^4 [Si(4Si)] environment. The linewidths of these samples are greatly increased over what is normal for a ZSM-5 type zeolite (*ca.* 200 Hz), depending on the Si/Al ratio (see Figure 3.9, Chapter 3). Calcination significantly decreases the linewidths of all the samples, in some cases allowing fine structure (Q^3 resonance at *ca.* -102 ppm) to be observed. The obvious conclusion to be drawn based on the data presented so far is that the ^{29}Si lines are broadened because of the paramagnetic nature of the substituting iron. The line broadening occurs because the distribution of local magnetic fields within the sample is spread due to the large perturbation caused by the unpaired electrons of the paramagnetic species. The degree of broadening reflects the average extent of the interaction between the unpaired electrons and the silicon nuclei. Calcination somehow effects a decrease in the ^{29}Si NMR linewidth. It is interesting to note the presence of spinning sidebands in the ^{29}Si MAS NMR spectra of the

ferrisilicates, especially following calcination. Oldfield *et al.*[262] have suggested that for samples containing magnetic centres, magnetic susceptibility broadening might be the cause of the spinning sidebands. It should be remembered, however, that there are three possible sites for the iron in the zeolite:

(1) in the lattice;

(2) extra-lattice (cation exchange positions);

(3) extra-lattice (oxide/hydroxide phases).

To help to clarify the state of the substituting iron in the samples, magnetic susceptibility measurements (χ_g) and ESR measurements were carried out for all the samples, both in their as-synthesised and calcined forms.

The magnetic susceptibility measurements are presented in Table 5.6. The ^{29}Si NMR and magnetic susceptibility results are presented in a variety of different formats in Graphs 5.1 to 5.5. From the Graphs, it is obvious that before calcination there is a good linear correlation between the weight percentage of iron and χ_g (Graph 5.1), but after

sample	as-synthesised χ_g (cgs units/g) x 10^6	calcined samples χ_g (cgs units/g) x 10^6	colour
HSZ-719	2.04	0.47	light beige
HSZ-707	2.84	0.54	beige
HSZ-708	2.79	0.53	beige
HSZ-591	6.22	0.70	beige
HSZ-553	6.87	0.89	beige
HSZ-524	18.32	2.41	dark beige

Table 5.6

Magnetic susceptibility values for as-synthesised and calcined ferrisilicates

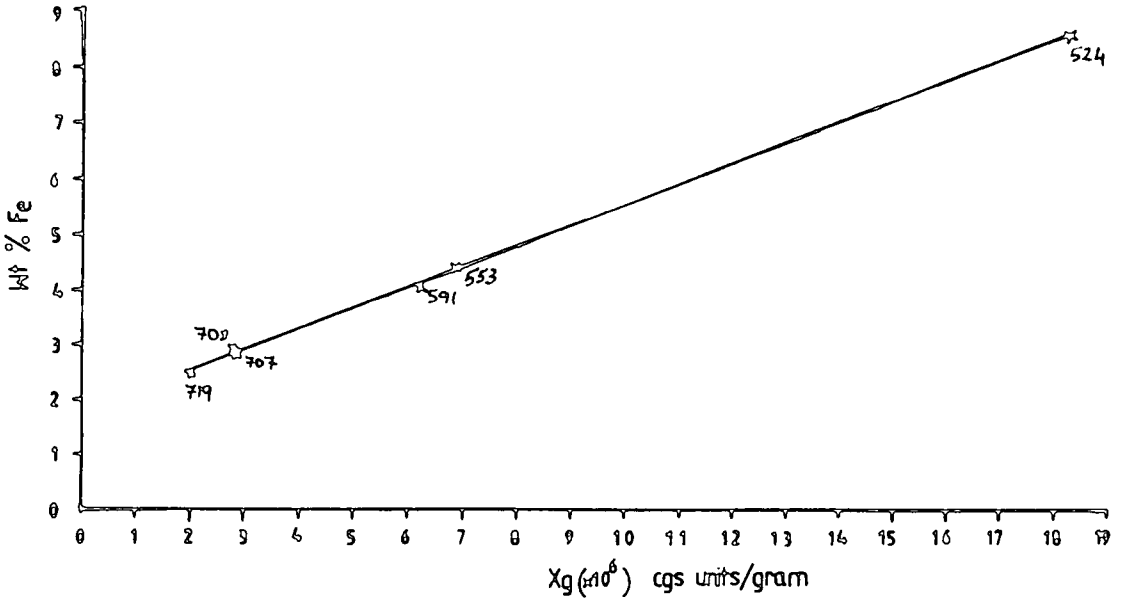

Graph 5.1

Weight % of iron versus χ_g before calcination

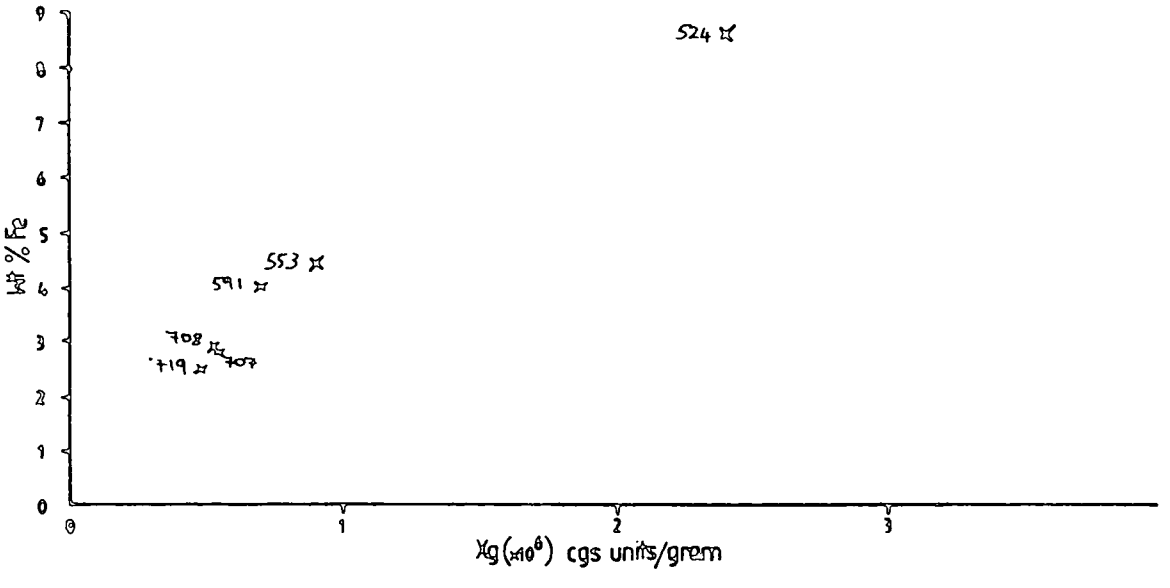

Graph 5.2

Weight % of iron versus χ_g after calcination

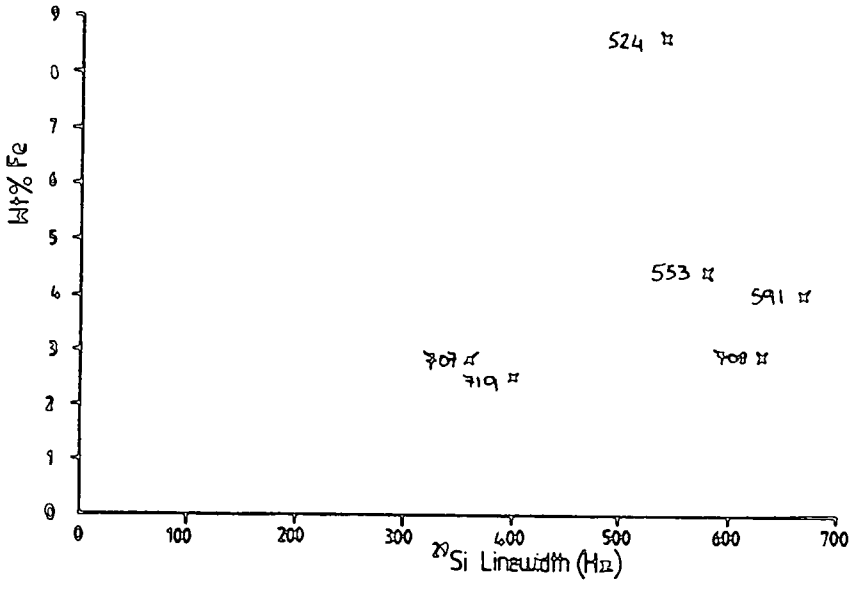

Graph 5.3

Weight % of iron (as-synthesised samples) versus linewidth (^{29}Si)

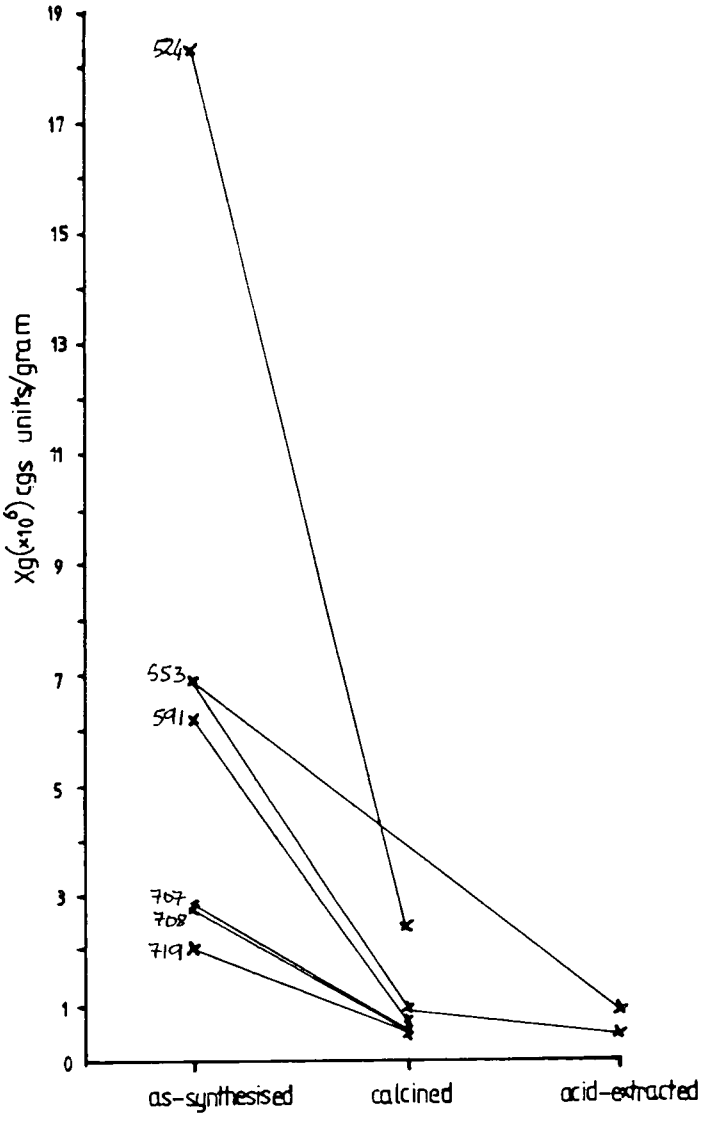

Graph 5.4

χ_g versus state of zeolite

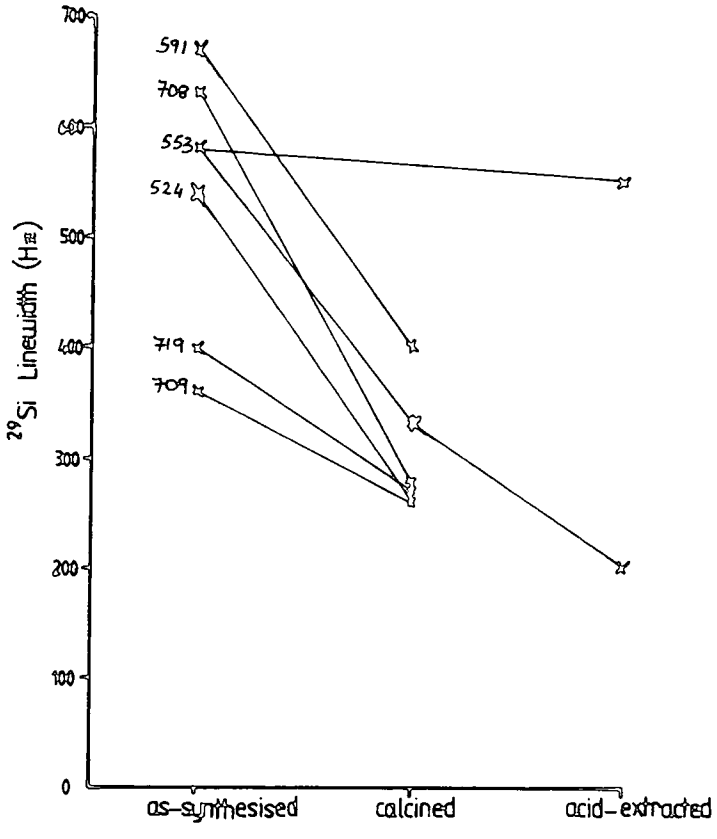

Graph 5.5

^{29}Si linewidth *versus* state of zeolite

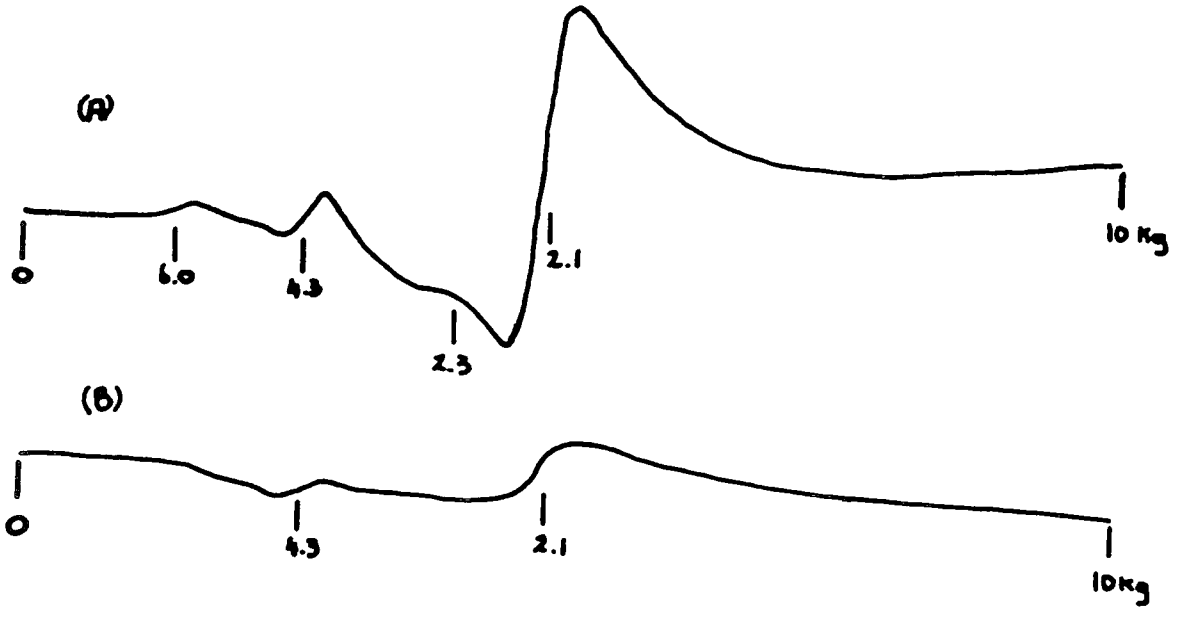

Figure 5.7

X-Band ESR spectra (υ = 9.502 MHz) obtained at 298 K for HSZ-591. (A) As-synthesised, (B) calcined. (A) and (B) have the same vertical and horizontal scales.

calcination, no such correlation exists (Graph 5.2). Also, there appears to be no direct relationship between the weight percentage of iron in the as-synthesised samples and the ^{29}Si NMR linewidth (Graph 5.3), suggesting the existence of more than one type of iron environment in these samples. Following calcination, the χ_g values tend to converge towards a common value (Graph 5.4). The same trend is apparent for the ^{29}Si linewidths following calcination (Graph 5.5).

Two types of ESR spectra were obtained for the six ferrisilicate samples. The first type, obtained for samples HSZ-591, HSZ-553, HSZ-708, and HSZ-707 is shown in Figure 5.7. The experimental g values and their assignments are given in Table 5.7. Figure 5.8 shows

sample	g value	linewidth (mT)	assignment[263]
as-synthesised HSZ-591	2.1	60	Fe^{3+} in cationic positions
	2.3	broad (>100)	Fe^{3+} oxide/hydroxide
	4.3	40	Tetrahedral Fe^{3+} (lattice)
	6.0	48	
calcined HSZ-591	2.1	80	Fe^{3+} in cationic positions
	4.3	40	Tetrahedral Fe^{3+} (lattice)

Table 5.7

g values, their assignments, and linewidths in sample HSZ-591.

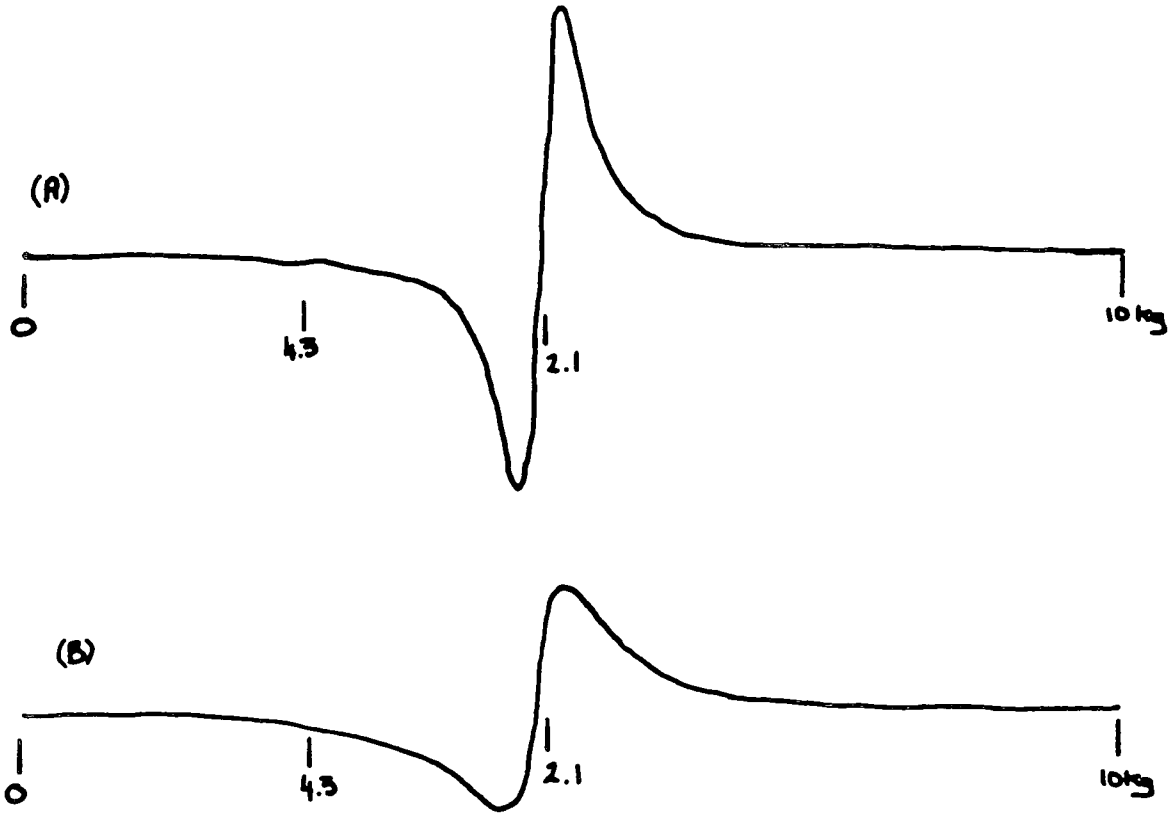

Figure 5.8

X-Band ESR spectra (υ = 9.502 MHz) obtained at 298 K for HSZ-719.

(A) As-synthesised, (B) calcined. (A) and (B) have the same vertical and horizontal scales.

sample	g value	linewidth (mT)	assignment[263]
as-synthesised	2.1	45	Fe^{3+} in cationic positions
HSZ-719	4.3	25	Tetrahedral Fe^{3+} (lattice)
calcined	2.1	60	Fe^{3+} in cationic positions
HSZ-719	4.3	25	Tetrahedral Fe^{3+} (lattice)

Table 5.8

g values, their assignments, and linewidths in sample HSZ-719.

the second type of ESR spectrum obtained for samples HSZ-719, HSZ-524. The g values, together with their assignments and linewidths are collated in Table 5.8.

One further set of experiments was performed on sample HSZ-553. Both as-synthesised and calcined forms of this sample were acid-leached (1M HCl at 95°C for 4 h followed by thorough washing and drying at

	HSZ-553 sample	
	as-synthesised acid-washed	calcined and acid-washed
^{29}Si MAS NMR chemical shift/(ppm)	-112.8	-112.7* -102.8
^{29}Si linewidth (Hz)	550	200*
χ_g (cgs units/g) x 10^6	0.86	0.48
XRF determined weight % Fe	2.31	0.70
SiO_2/Fe_2O_3	77.3	263
Fe/unit cell†	2.4	0.72

*Main resonance

†Assuming all iron to be isomorphously substituted in the lattice

Table 5.9

^{29}Si MAS NMR, χ_g, and XRF data for as-synthesised and calcined, acid-washed HSZ-553.

150°C). The two samples were investigated using ^{29}Si NMR, ESR, XRF, and Faraday balance measurements. The results are presented in Table 5.9.

Powder XRD traces (not shown) indicate that in both cases, following acid-extraction, the silicate lattice remains intact. ESR shows all three possible iron environments exist in both treated samples of HSZ-553 (spectra not shown). Figure 5.9 shows the ^{29}Si MAS NMR spectrum of the calcined, acid-washed HSZ-553 sample.

ESR investigations prove that in all samples (in their as-synthesised and calcined states), iron has substituted isomorphously into the silicate lattice. In all cases, however, only a relatively small (undetermined) proportion of the total iron weight percentage has done so.

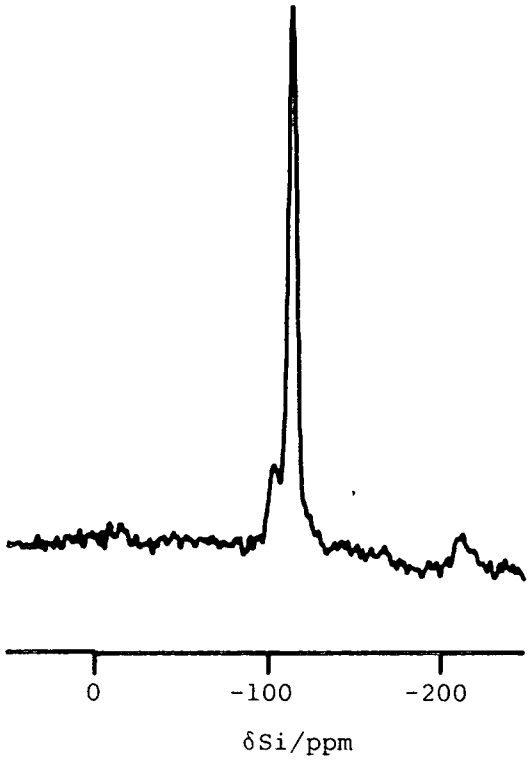

SPE; SF = 39.7 MHz; NT = 210; RD = 5s; SW = 20 kHz; SI = 2 K; TD = 1 K; PD = 5μs; PA = π/2; SS = 3.7 kHz; SR = 13200.

Figure 5.9

^{29}Si MAS NMR of calcined, acid-washed HSZ-553.

For all the samples, most of the iron seems to be present as either an oxide/hydroxide phase or in cationic extra-lattice positions. Calcination is seen to reduce the ESR signal relating to Fe^{3+} in cationic positions and oxide/hydroxide phases, whilst at the same time not significantly affecting the iron tetrahedrally coordinated into the zeolite lattice. The symmetry of the ESR signal (linewidth related) is also seen to be reduced (increase in linewidth) following calcination for the g = 2.1 signal. This is consistent with the removal of water molecules on calcination with the subsequent effect on the Fe^{3+} coordination in extra-lattice positions and hence, the symmetry. On calcination, ^{29}Si MAS NMR linewidths and χ_g values decrease, until at levels of *ca.* 0.53 (cgs units/g x 10^6) or below, the ^{29}Si MAS NMR linewidth has fallen to such an extent as to be able to allow observation of a second (minor) resonance at *ca.* -103 ppm (Q^3). In none of the samples, whether in the precursor or calcined state, could ^{29}Si CP MAS NMR spectra be obtained. This is most likely to be due to the effect of paramagnetic Fe^{3+} ions on the ^1H $T_{1\rho}$ value. [The ^1H $T_{1\rho}$ was measured (directly) at 200 MHz as < 0.1 ms.] Thus it is impossible to use the CP experiment to discriminate between a Q^3 resonance due to ≡SiOR where R = Na^+, TPA^+, or H^+ or a Q^3 resonance due to [3Si(1Fe)].

The decrease in χ_g values and ^{29}Si NMR linewidths noted for the samples after calcination is most likely to be due to the formation of higher levels of iron oxides. The colour change of the samples following calcination is indicative of the formation of an oxide of iron. The relative susceptibility of an oxide of iron is several orders of magnitude less than that for cationic iron (in the silicate lattice and in extra-lattice positions). There is most likely to be less iron-silicon interaction following oxide formation, and so

^{29}Si NMR linewidths will be reduced. Acid-leaching of the sample appears to have a dramatic effect on the χ_g values of, and weight percentages of iron in the samples, but not until the samples have been calcined does acid-leaching appear to have any effect on the ^{29}Si NMR linewidth. Thus, acid-leaching prior to calcination removes extra-lattice iron (probably as oxide/hydroxide phase), and as more of this phase is thought to be produced on calcination of the sample, more is removed with acid-leaching following calcination.

To summarize, we can say that iron does substitute isomorphously into the silicate lattice of ZSM-5 type molecular sieves, although even at very low levels of iron (SiO_2/Fe_2O_3 = 263), the majority of the iron is present as cationic Fe^{3+} in extra-lattice sites. Following calcination, the lattice iron appears to remain predominantly in the lattice, indicating the considerable stability of the ferrisilicate system.

5.2.3. Cr-ZSM-5 (chromosilicate)

Only one chromosilicate sample was obtained (HSZ-705). Table 5.10 lists the physical, chemical, and spectroscopic properties of both the calcined and the precursor form of this substituted zeolite.

The ^{29}Si MAS NMR spectra for the precursor and calcined forms of the chromosilicate sample are presented in Figure 5.10. The ^{29}Si linewidth of the precursor Cr-ZSM-5 is normal for a typical ZSM-5 zeolite. The spectrum shows some fine structure, indicating a reasonably high level of silica, and a low level of any other lattice oxide. It is interesting to note the appearance of spinning sidebands in this spectrum. As noted for the ferrisilicates, the presence of

properties	sample condition	
	as-synthesised	calcined
colour	green	orange
SiO_2/Cr_2O_3	18.9 (equivalent to 8.3 Cr per unit cell)*	-
^{29}Si shemical shift/(ppm)	-112.8	-113.7
^{29}Si linewidth (Hz)	270	150
χ_g (cgs units/g) x 10^6	4.38	$\simeq 0$

*Assuming all Cr to be isomorphously substituted in the lattice.

Table 5.10

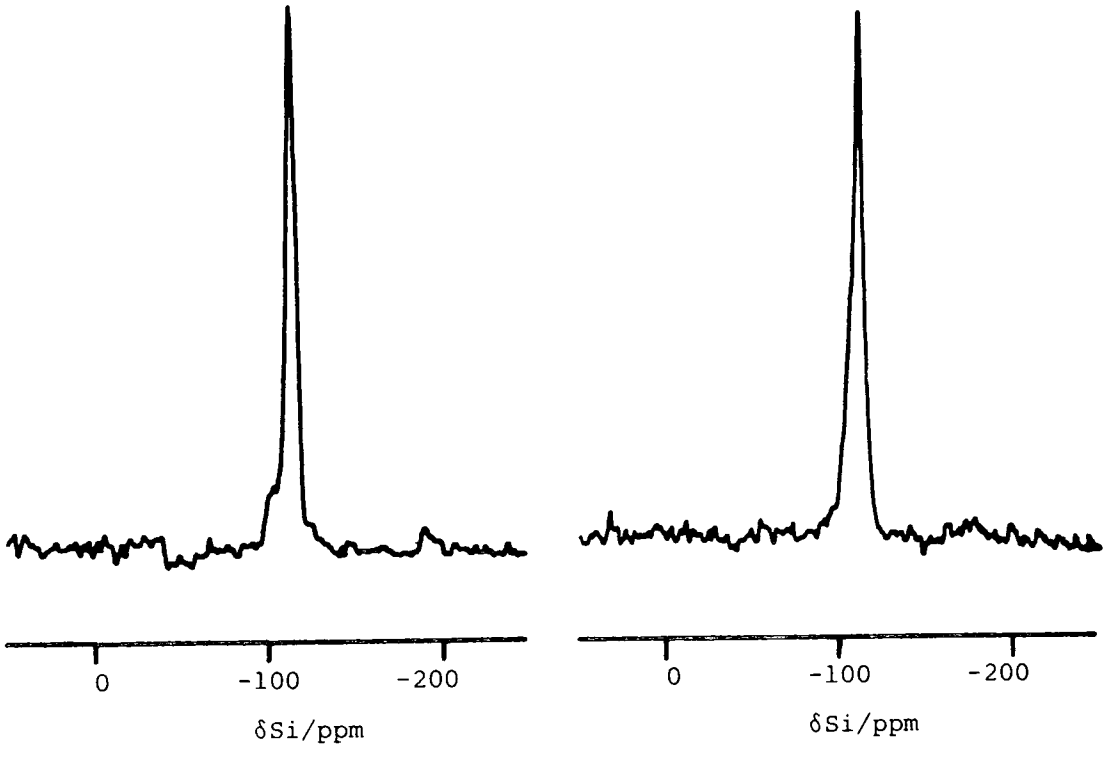

SPE; SF = 39.7 MHz; RD = 5 s; NT = 400 (precursor), 200 (calcined); SI = 2 K; TD = 1 K; PD = 5μs; PA = π/2; SS = 3.0 kHz; SR = 13200; SW = 20 kHz.

Figure 5.10

^{29}Si MAS NMR spectra of the calcined (left) and precursor (right) forms of Cr-ZSM-5

spinning sidebands in samples containing magnetic centres appears not to be due to chemical shift anisotropy, but rather to the presence of large magnetic susceptibility broadenings.[262]

The as-synthesised sample is confirmed as having a non-zero magnetic susceptibility from the Faraday balance measurements. On calcination in air, the ^{29}Si linewidth decreases and consequently even more fine structure becomes apparent in the ^{29}Si MAS NMR spectrum. The sample no longer has a magnetic susceptibility and the colour changes from green (indicative of Cr^{3+}) to orange (indicative of Cr^{6+}).

If chromium were present in the lattice to any appreciable extent it would be expected to have several effects on the ^{29}Si NMR spectrum. The first effect would be a considerable line broadening influence. Although a decrease in ^{29}Si linewidth is observed following calcination, the linewidth prior to calcination is significantly less than the linewidths observed for as-synthesised ferrisilicate samples. The second effect of chromium in the lattice not withstanding the line broadening influence, would be the expected appearance of a different nuclear environment for some lattice silicon atoms with the consequent creation of a separate (Q^3) chemical shift. The situation would then be analogous to a typical aluminium-containing ZSM-5 with both Q^4 [Si(4Si)] and Q^3 [Si(3Si)1Al] peaks being present in the ^{29}Si NMR spectrum. The ^{29}Si spectrum of chromosilicate does indeed exhibit two resonances similar to those observed in an aluminium containing ZSM-5. However, in the chromosilicate ^{29}Si spectrum, the "Q^3" resonance may not be due to substituted chromium, but rather to a combination of impurity aluminium atoms [the presence of tetrahedral aluminium has been confirmed by ^{27}Al MAS NMR (spectrum not shown)] and lattice defect sites. The latter are confirmed by the ability of the chromosilicate sample to cross-polarise

and produce a peak at -102 ppm. [Note: the -102 ppm resonance is attributed to a Q^3-type grouping *i.e.* silicon atoms connected *via* oxygen bridges to three other tetrahedral silicons. This means that this resonance is composed of contributions from ≡SiOR groups in which R can be H^+, but also Na^+ or TPA^+ (XRF confirms the presence of 5.65 weight % Na_2O in the chromosilicate)]. The ^{29}Si CP/HPD MAS NMR spectrum is shown in Figure 5.11. The calcined chromosilicate also cross-polarises (spectrum not shown).

Calcination in air renders the previously paramagnetic Cr^{3+} centres diamagnetic by forming a Cr^{6+} containing compound, most probably an oxide.

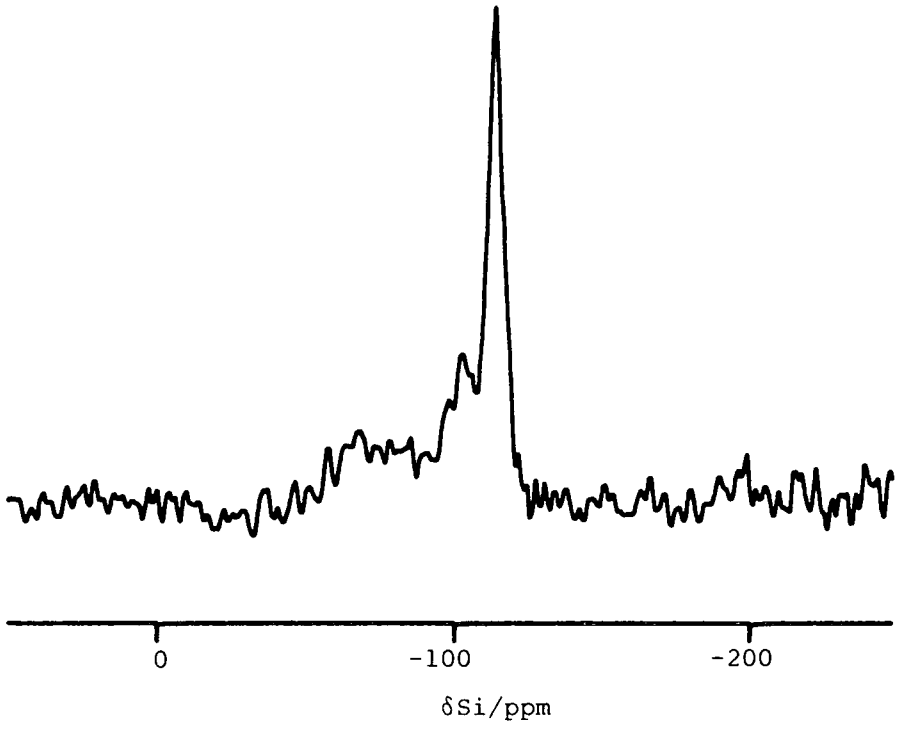

SF = 39.7 MHz; RD = 5 s; NT = 550; CT = 1 ms; SI = 2 K; TD = 1 K;
SS = 3.0 kHz; SR = 13218; SW = 20 kHz.

Figure 5.11

^{29}Si CP/HPD MAS NMR spectra of the as-synthesised chromosilicate

In order for there to be such a large decrease in ^{29}Si linewidth following calcination, at least some of the magnetic Cr^{3+} centres must have been in contact with silicon atoms in the lattice. The diamagnetic Cr^{6+} compound obtained following calcination would no longer have any line broadening effect, and so the ^{29}Si linewidth would decrease, as is observed.

In conclusion, it would seem unlikely that any of the chromium in this particular chromosilicate sample has been isomorphously substituted in the lattice, although this cannot be proven using MAS NMR.

5.2.4. Ti-silicalite/Ti-ZSM-5

Two titanium-substituted ZSM-5 samples (courtesy of Mr. John Dwyer, Department of Chemistry, UMIST) were studied together with a titanium substituted silicalite sample, synthesised by Laporte Industries Limited, Widnes. No chemical analysis details are available for either of the substituted ZSM-5 samples. The substituted silicalite sample is known to contain 2.76% Ti (equivalent to 3.3 Ti atoms per unit cell, assuming complete lattice substitution), as determined by XRF.

(1) Ti-silicalite.

Figure 5.12 shows both SPE and CP/HPD ^{29}Si MAS NMR spectra of the as-synthesised forms of the sample. The relevant ^{29}Si NMR data are collated in Table 5.11.

The ^{29}Si SPE NMR spectrum is typical of that observed for a normal silicalite sample. The presence of very small amounts of tetrahedrally coordinated aluminium is confirmed by ^{27}Al NMR (spectrum not shown). The amount of aluminium present in the sample is, however, not enough to

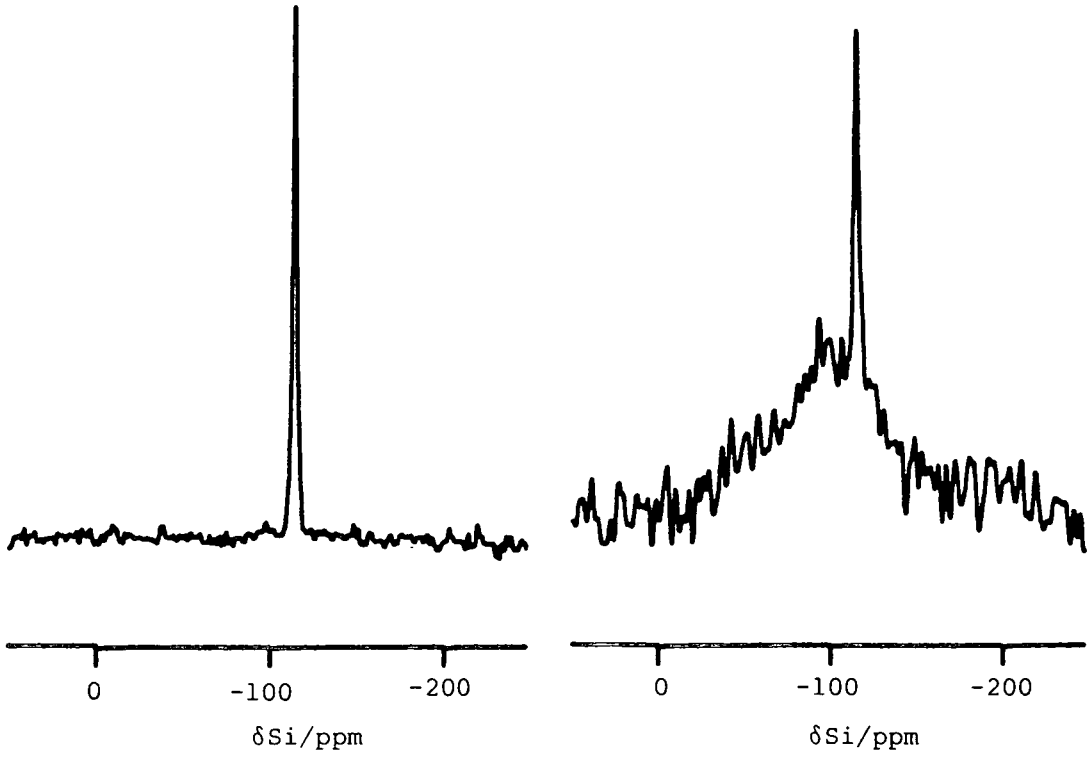

SF = 39.7 MHz; RD = 5 s; NT = 468 (SPE), 760 (CP/HPD); SI = 2 K;
CT = 10 ms; TD = 1 K; PD = 5 μs; PA = π/2; SS = 3.0 kHz; SR = 13218;
SW = 20 kHz.

Figure 5.12

SPE (left) and CP/HPD (right) ^{29}Si MAS NMR spectra of Ti-silicalite.

produce a Q^3 resonance at -102 ppm. If all the titanium were isomorphously substituted into the silicalite framework, the effects of this substitution would be clearly visible as a Q^3 resonance in the ^{29}Si NMR spectrum. The linewidth, plus the apparent fine structure in the

sample	chemical shift/(ppm) CP/HPD	SPE	linewidth (Hz) CP/HPD	SPE
Ti-silicalite	-114.1	-110.3 -113.9 -116.1	100	95

Table 5.11

^{29}Si NMR data for Ti-silicalite from Figure 5.12

SPE spectrum, and lack of a Q^3 resonance line, lead us to conclude that the ^{29}Si NMR spectrum shows no effects of titanium substitution. Thus the titanium is probably located in the pores and not in the zeolite lattice. A broad resonance is observed to high frequency of the main peak in the CP/MAS NMR spectrum, and the Q^4 [Si(4Si)] resonance must be due to the presence of protons near the Q^4 silicons. Following calcination, spectra (not shown) similar to those shown in Figure 5.12 were obtained.

(2) Ti-ZSM-5

Both samples display exactly the same ^{29}Si SPE and CP/HPD MAS NMR spectra, and so will be treated as one in the following discussion. Calcination of the samples yielded no extra information and so will not be referred to in the discussion. SPE and CP/HPD ^{29}Si MAS NMR spectra typical of that obtained for the Ti-ZSM-5 samples are presented in Figure 5.13. The NMR data for the two samples are collated in Table 5.12. Figure 5.14 shows graphs of the logarithm of the signal intensity plotted against variable ^{29}Si CP contact times for the two Ti-ZSM-5 samples.

From the two graphs it is apparent that the two resonances present in both ^{29}Si NMR spectra of both samples have common ^1H $T_{1\rho}$ values (as determined from the exponential decay part of the graphs) within experimental error. This suggests that full spin diffusion is operative in both samples. A similar graph (not shown) to those shown in Figure 5.14 is produced by ZSM-5 (SiO_2/Al_2O_3 = 80), indicating that in a non-isomorphously substituted ZSM-5 sample, common $T_{1\rho}$ (^1H) values for the two ^{29}Si resonance lines also exist. As the rate of cross-polarisation depends on the dipolar interactions between the rare

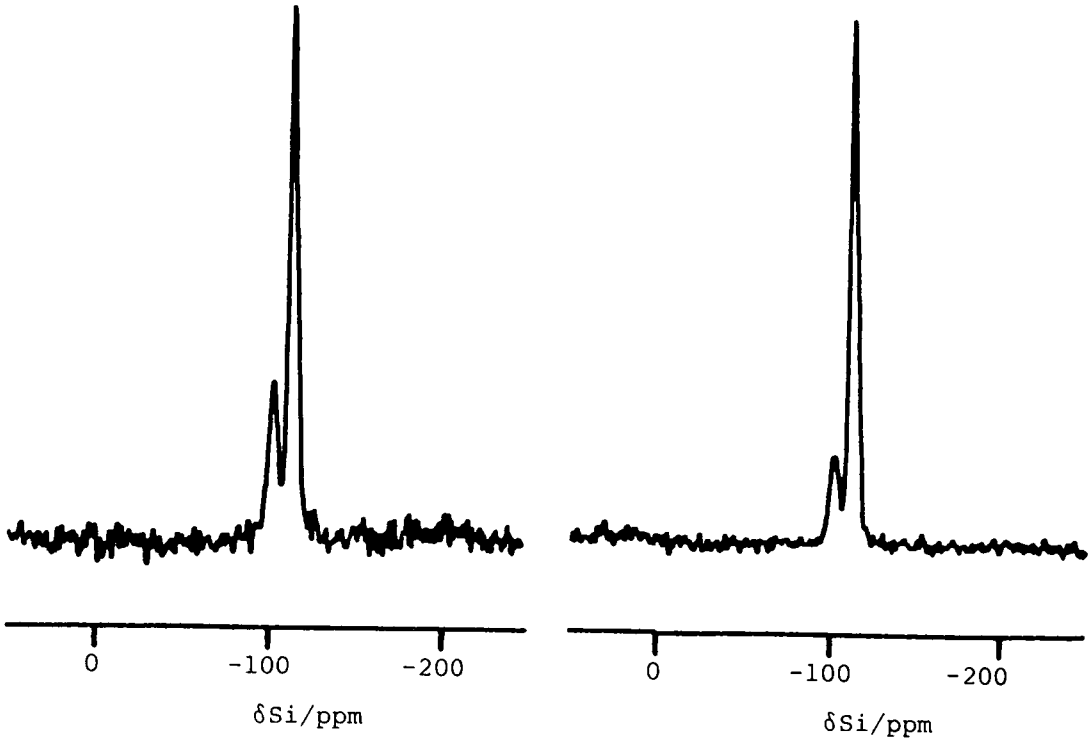

SF = 39.7 MHz; RD = 20 s (SPE), 5 s (CP/HPD); NT = 1960 (SPE), 264 (CP/HPD); SI = 2 K; CT = 5 ms; TD = 1 K; SS = 3.0 kHz; SR = -23.0; SW = 20 kHz.

Figure 5.13

SPE (left) and CP/HPD (right) ^{29}Si MAS NMR spectra of Ti-ZSM-5 (54/45)

and abundant spin systems, it is possible that substitution of a heteroatom other than silicon into a silicon-proton system might be

sample	chemical shift/(ppm) CP/HPD	SPE	linewidth (Hz) CP/HPD	SPE
54/45	-112.2 -101.9	-111.7 -101.9	200	200
54/2L	-112.2 -102.4	-112.2 -103.4	200	200

Table 5.12

^{29}Si NMR data for Ti-ZSM-5 samples

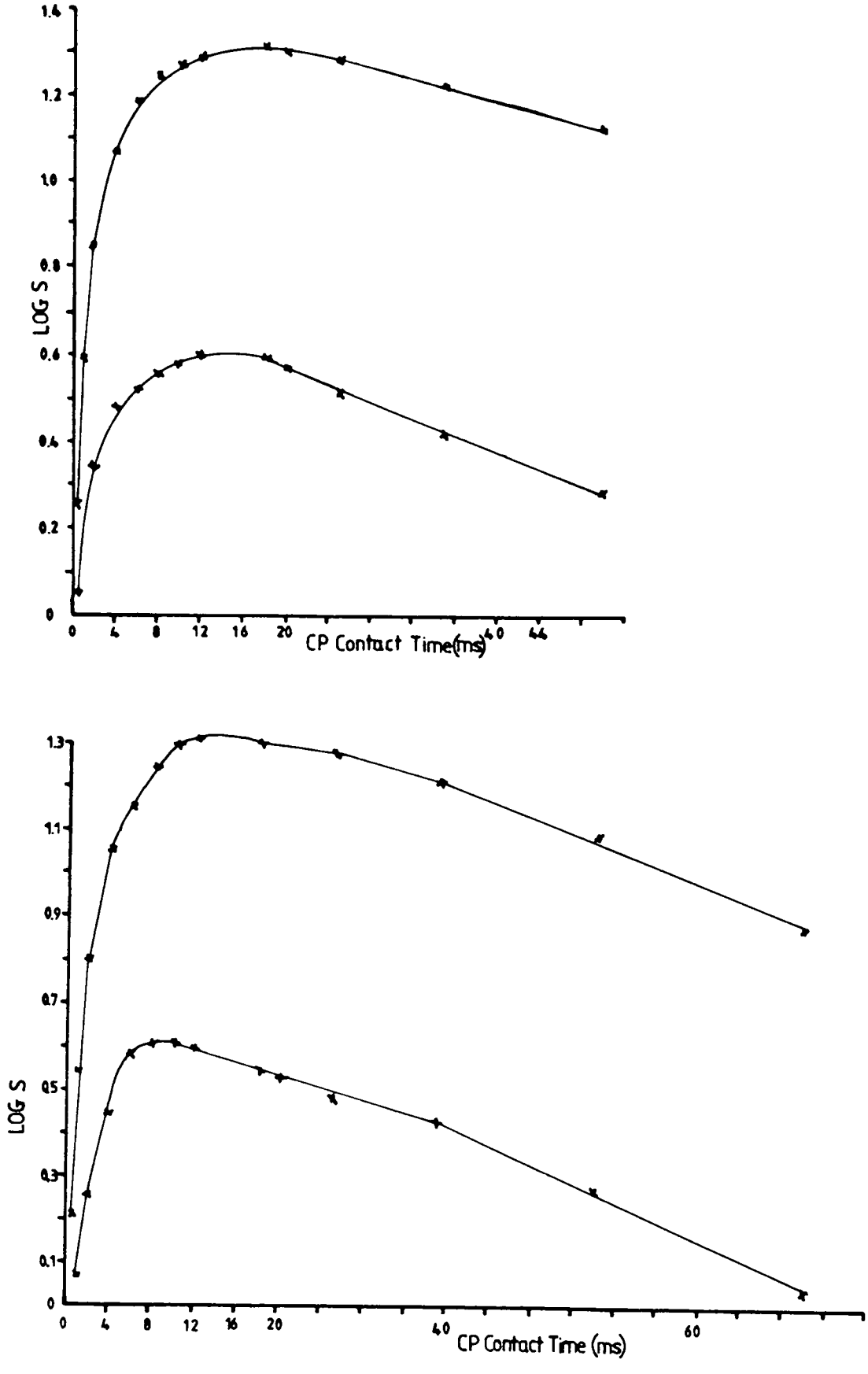

Figure 5.14

Graphs of the log of the signal intensity *versus* CP contact time (ms) for sample 54/45 (top) and 54/2L (bottom)

expected to have an effect on the cross-polarization rate. Unfortunately, it is difficult to judge whether the cross-polarization rates are affected or not from the graphs, especially as the extent of the effect will be dependent upon the substitution level, which is unknown.

In conclusion, for the Ti-ZSM-5 samples studied, MAS NMR cannot prove substitution, nor can substitution even be inferred on the basis of the ^{29}Si MAS NMR results.

5.2.5. La-ZSM-5

Only one La-ZSM-5 sample was received, HSZ-1346. The XRF results are as follows: SiO_2/La_2O_3 = 83.7 (equivalent to 2.1 La atoms per unit cell, assuming all La atoms to be substituted in the lattice).

Figure 5.15 shows the ^{29}Si SPE and CP/HPD MAS NMR spectra for the

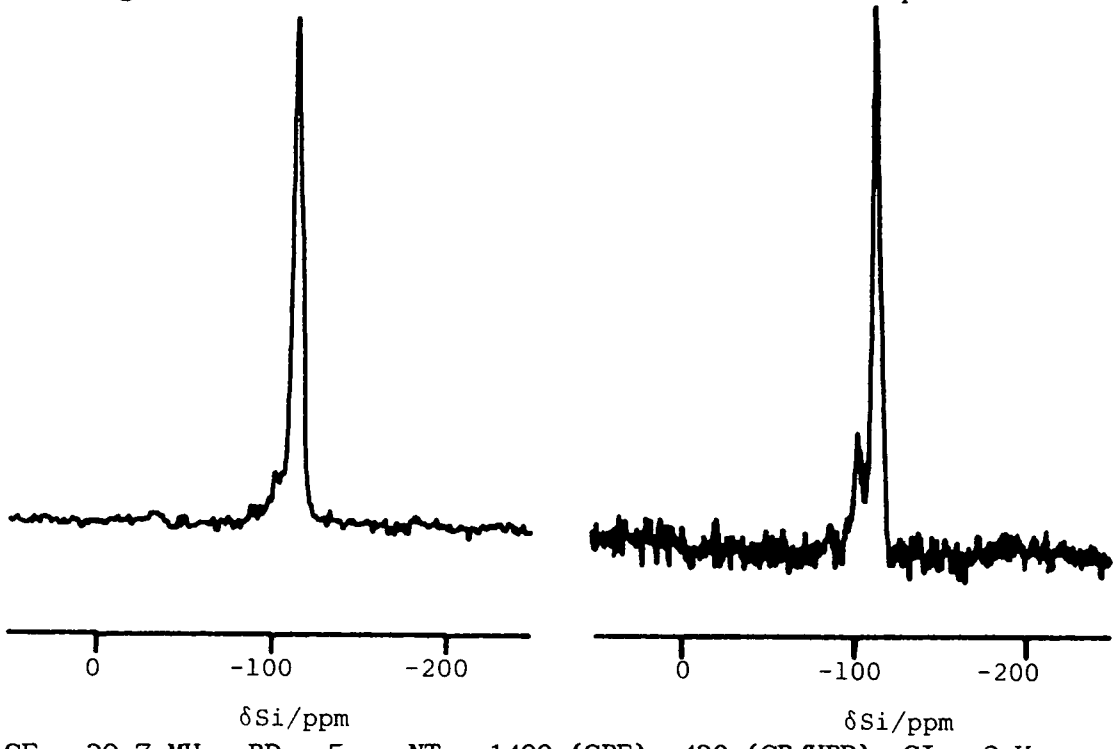

SF = 39.7 MHz; RD = 5 s; NT = 1400 (SPE), 430 (CP/HPD); SI = 2 K; CT = 5 ms; TD = 1 K; PD = 5 μs; PA = π/2; SS = 3.0 kHz; SR = 13200; SW = 20 kHz.

Figure 5.15

SPE (left) and CP/HPD (right) ^{29}Si MAS NMR spectra of La-ZSM-5

sample	chemical shift/(ppm) CP/HPD	SPE	linewidth (Hz) CP/HPD	SPE
La-ZSM-5	-112.6 -102.0	-112.6 -102.0	260 -	260 -

Table 5.13

^{29}Si NMR data for La-ZSM-5 sample from Figure 5.15

as-synthesised sample (the calcined sample gave ^{29}Si spectra similar to those in the Figure). The ^{29}Si NMR data are summarised in Table 5.13.

The ^{29}Si CP/HPD MAS NMR signal from La-ZSM-5 was strong. A graph of the logarithm of the signal intensity *versus* the CP contact time (not shown) was similar to those already presented in section 5.2.4 for Ti-ZSM-5. Thus we have a similar situation for this sample as has occurred previously for the titanium substituted ZSM-5 samples. Once again, the Q^3 (-102 ppm) peak can be assigned to ≡SiOR groups, where R = H^+, TPA^+, and Na^+ (XRF results indicate 0.33 weight % Na_2O).

An attempt was made to observe the ^{139}La resonance for this sample using the double bearing ^{29}Si probe. ^{139}La is 99.91% abundant, spin 7/2, has a quadrupole moment of 0.21 x 10^{-28} m^2 (the quadrupole moment for Al is 0.15 x 10^{-28} m^2) and resonates at 28.5 MHz (200 MHz proton). A liquid sample (an aqueous solution of $LaCl_3.7H_2O$) was used to locate a resonance. The ^{139}La NMR spectrum of the liquid was *ca.* 150 Hz broad, the spectrum of the solid being unobservable. Similarly, no ^{139}La NMR spectrum was observed for La-ZSM-5. This is undoubtedly because of the large quadrupolar broadening of the signal at 4.7 T, indicating that the lanthanum nuclei are not in a symmetrical (cubic) environment in the La-ZSM-5 sample.

On the basis of the spectroscopic evidence presented, it would seem unlikely that any of the lanthanum is substituted in the silicate

lattice, although NMR provides no direct proof for non-substitution.

5.3 Viséite

Viséite was first reported by Mélon[264] (1942) as having the following composition: $5CaO.5Al_2O_3.3SiO_2.3P_2O_5.nH_2O$ (where $30 > n > 25$). No strucutural relationship to any other known mineral was suggested by Mélon. McConnell, in an investigation into viséite[181] (1952), used powder diffraction methods to establish a structural analogy between viséite and analcime. The viséite sample from Visé, Liège, Belgium (presented to the U.S. National Museum, catalogue no. 106364), had its chemical formula rewritten by McConnell as $(Na_2Ca_{10})(AlO_2)_{20}(SiO_2)_6(PO_2)_{10}(H_3O_2)_{12}.16H_2O$ to show the proposed relationship of the structure to that of analcime. Breck[28] reported in 1974 that "a close inspection of the X-ray powder data for viséite shows it might be interpreted as being a mixture of crandallite [a calcium-aluminium phosphate of composition $CaAl_3(PO_4)_2(OH)_5.H_2O$] and analcime."

The most recent study of viséite was carried out in 1977 by Dunn and Appleman.[182] They used the original Visé sample (NMNH no. 106364) and obtained data on several others, also from Visé. They examined all the samples using powder X-ray diffraction techniques. The materials were so poorly crystalline that only a few weak, extremely broad, and diffuse diffraction lines were obtained. Dunn and Appleman report several (varying) approximate chemical formulae for their viséite samples and conclude that on the basis of their structural investigations there is insufficient evidence to characterise accurately viséite.

A sample of viséite labelled as being contaminated with trolleite [$Al_4(OH)(PO_4)_3$], was obtained from the Cureton Mineral Co., Tucson, Arizona. The sample is believed to have originated in Visé. It was crushed, separated using sieves (and also by colour as viséite is white, trolleite is green) and analysed using powder XRD, XRF, and ^{27}Al, ^{31}P, and ^{29}Si MAS NMR.

The two samples analysed as:

"viséite" fraction: $Si_{0.29}P_{0.23}Al_{0.41}(Ca_{0.04}Na_{0.03})$ - sample I

remainder: $Si_{0.21}P_{0.35}Al_{0.39}(Ca_{0.05})$ - sample II

The powder XRD traces are presented in Figure 5.16.

Sample I was identified as containing topaz, alpha-quartz, trolleite, and "viséite". Sample II was identified as containing alpha-quartz, xonotlite, trolleite, and "viséite".

The powder XRD data for viséite (from the original analysis by McConnell) is shown together with any viséite identified lines present in the XRD traces of samples I and II (from Figure 5.16), in Table 5.14.

^{31}P MAS NMR spectra relating to both samples I and II are presented in Figure 5.17. The use of HPD decreases the ^{31}P linewidth by a factor of three. This implies there is considerable ^{1}H - ^{31}P interaction in both these samples. This is demonstrated in Figure 5.18 which shows the ^{31}P CP/HPD MAS NMR spectrum of sample I (the spectrum for sample II is similar), together with ^{27}Al and ^{29}Si MAS NMR spectra of sample I. The NMR data are collated in Table 5.15.

If one accepts the structural analogy between viséite and analcime proposed by McConnell, the phosphorus, aluminium, and silicon environments (in the lattice) should be tetrahedral. The ^{31}P NMR chemical shift of the most intense resonance in the spectrum is, according to work on ^{31}P NMR chemical shifts in AlPO's and SAPO's (see

(i) McConnell viséite			(ii) Sample I		
d (Å)	2θ	I/I_{max} x 100	d (Å)	2θ	I/I_{max} x 100
5.68	13.6	4	5.91	≃15	4
4.98	17.8	1	-	-	-
3.46	25.8	5	(2.94	25.51	34)
2.92	30.6	10	2.20	40.87	10
2.20	41.0	2	2.11	42.86	3
2.11	42.9	<1	2.03	44.48	2
2.014	45.0	<1	1.90	47.83	2
1.886	48.3	3			
1.740	52.6	6	(iii) Sample II		
1.380	67.9	1			
1.323	71.3	1	d (Å)	2θ	I/I_{max} x 100
1.282	73.9	1	5.68	15.6	7
1.196	80.3	2	3.51	25.33	49
1.155	83.8	2	(2.94	30.36	38)
1.138	85.3	1	2.20	40.91	10
1.105	88.5	1	2.12	42.65	12
			2.03	44.53	10
			1.89	47.99	6

Table 5.14

Powder XRD data for samples I and II (identified viséite lines only)

Chapter Six), in agreement with that obtained for $(PO_4)^{3-}$ units. However, the major contaminant of sample I, trolleite, consists of (PO_4) tetrahedra, together with Al-O octahedra and corner-sharing hydroxyl groups. As "viséite" appears to be present only in small amounts, the most intense resonance cannot be due entirely to viséite, but is most likely to be due to trolleite. Supporting evidence for this comes from the linewidth decrease of the main phosphorus resonance on decoupling, and the strong ^{31}P CP signal - both factors attributable to ^{31}P - ^{1}H interaction, to be expected for trolleite. There are two other smaller phosphorus resonances to high frequency of the main resonance, one of which disappears in the CP spectrum (Figure 5.18). These peaks are unassigned.

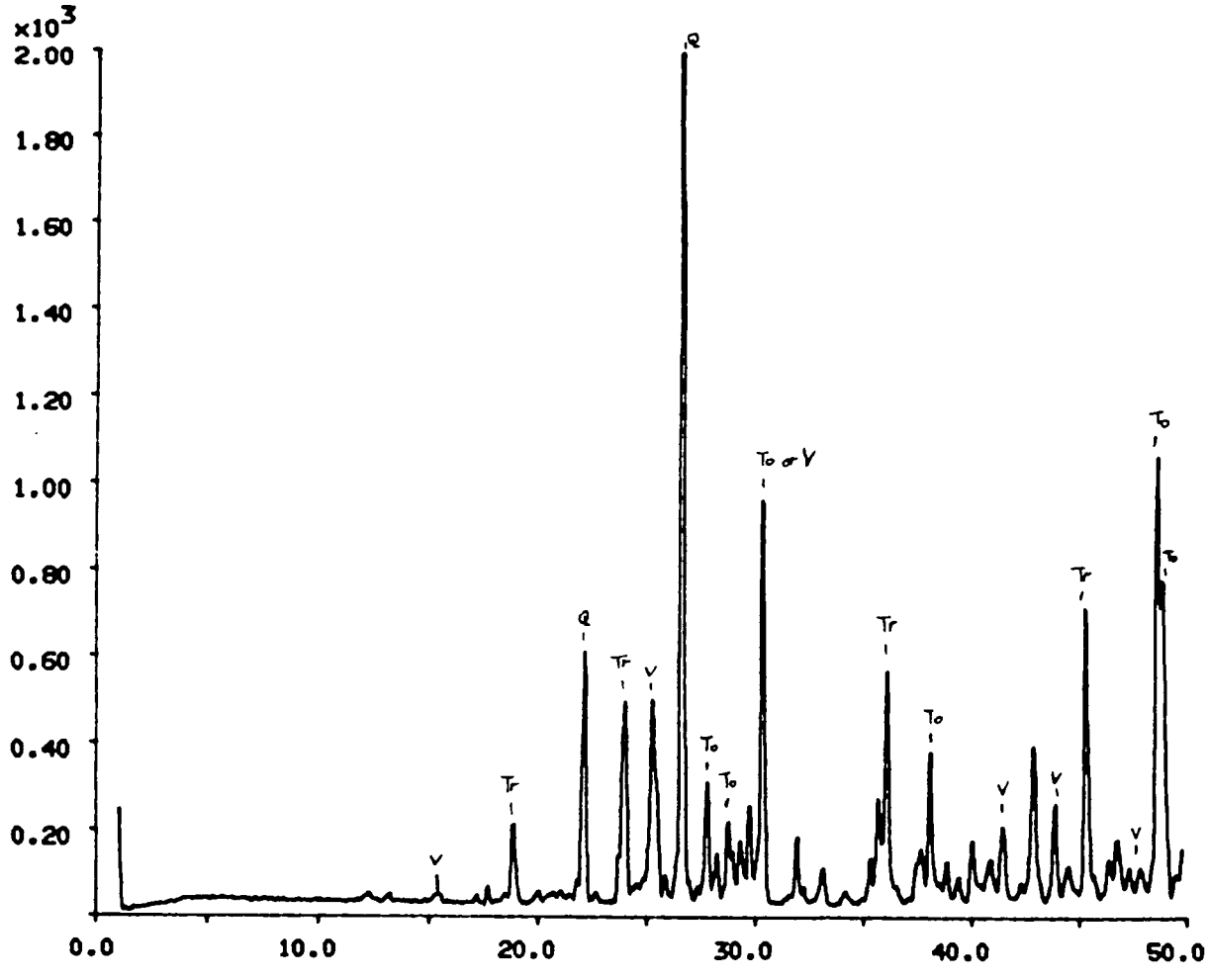

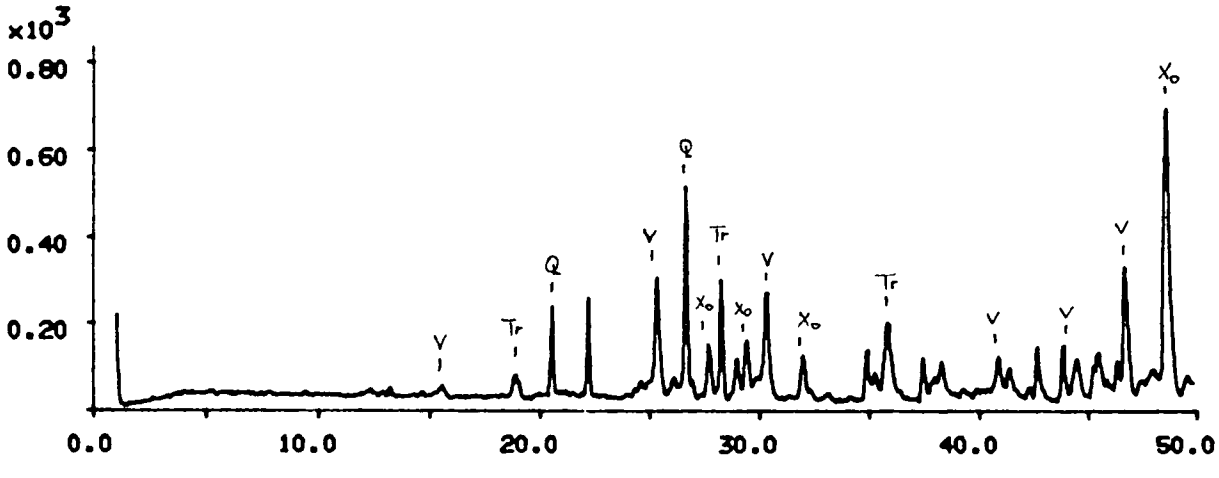

Figure 5.16

Powder XRD-traces for sample I (upper) and sample II (lower)

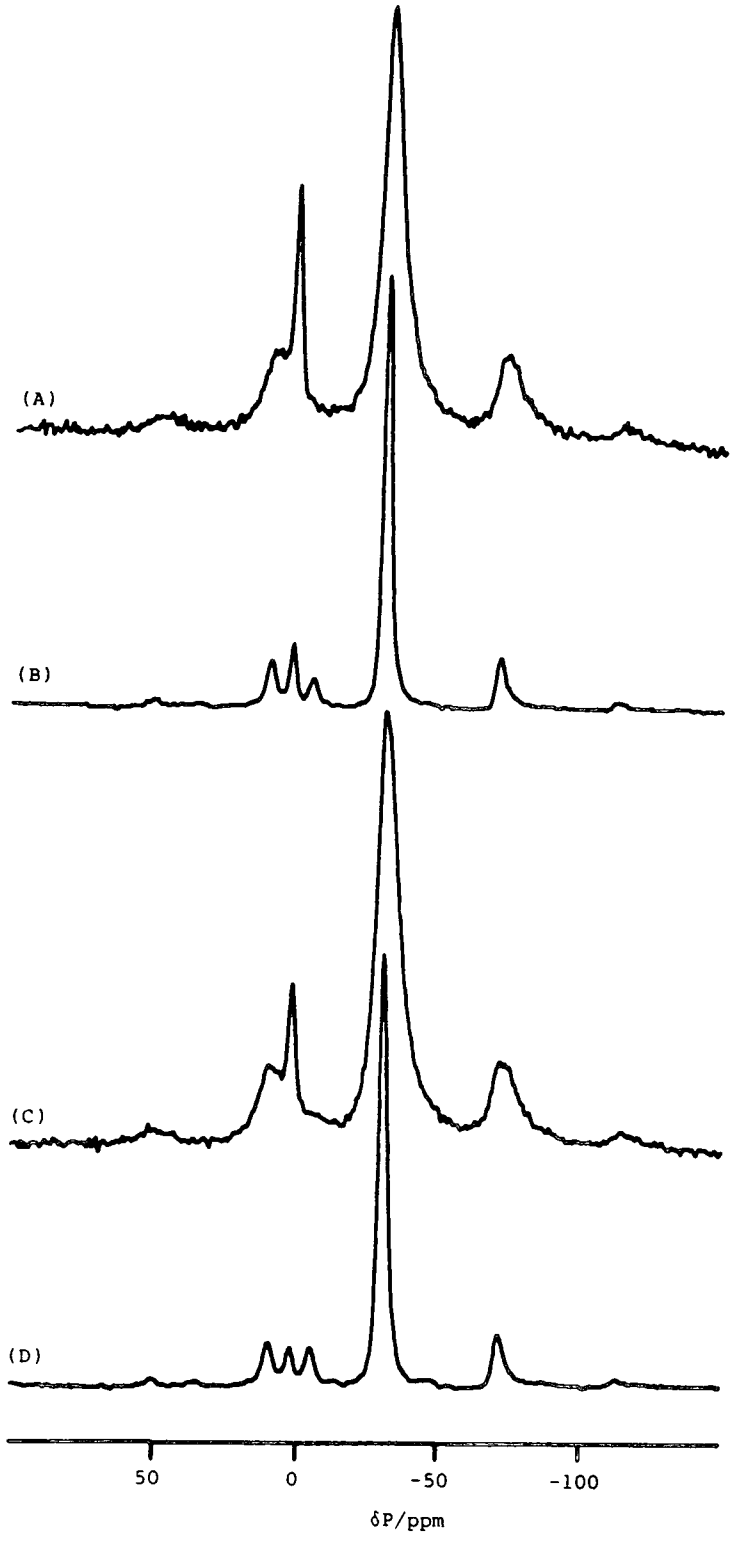

SF = 81.0 MHz; RD = 20 s; NT = 16; SI = 2 K; TD = 1 K; PD = 5 μs; PA = π/2; SS = 2.6 kHz; SR = 105.9; SW = 20 kHz.

Figure 5.17

(A), (B) ^{31}P MAS NMR spectra of sample I. (A) SPE - no HPD; (B) SPE.

(C), (D) ^{31}P MAS NMR spectra of sample II. (C) SPE - no HPD; (D) SPE.

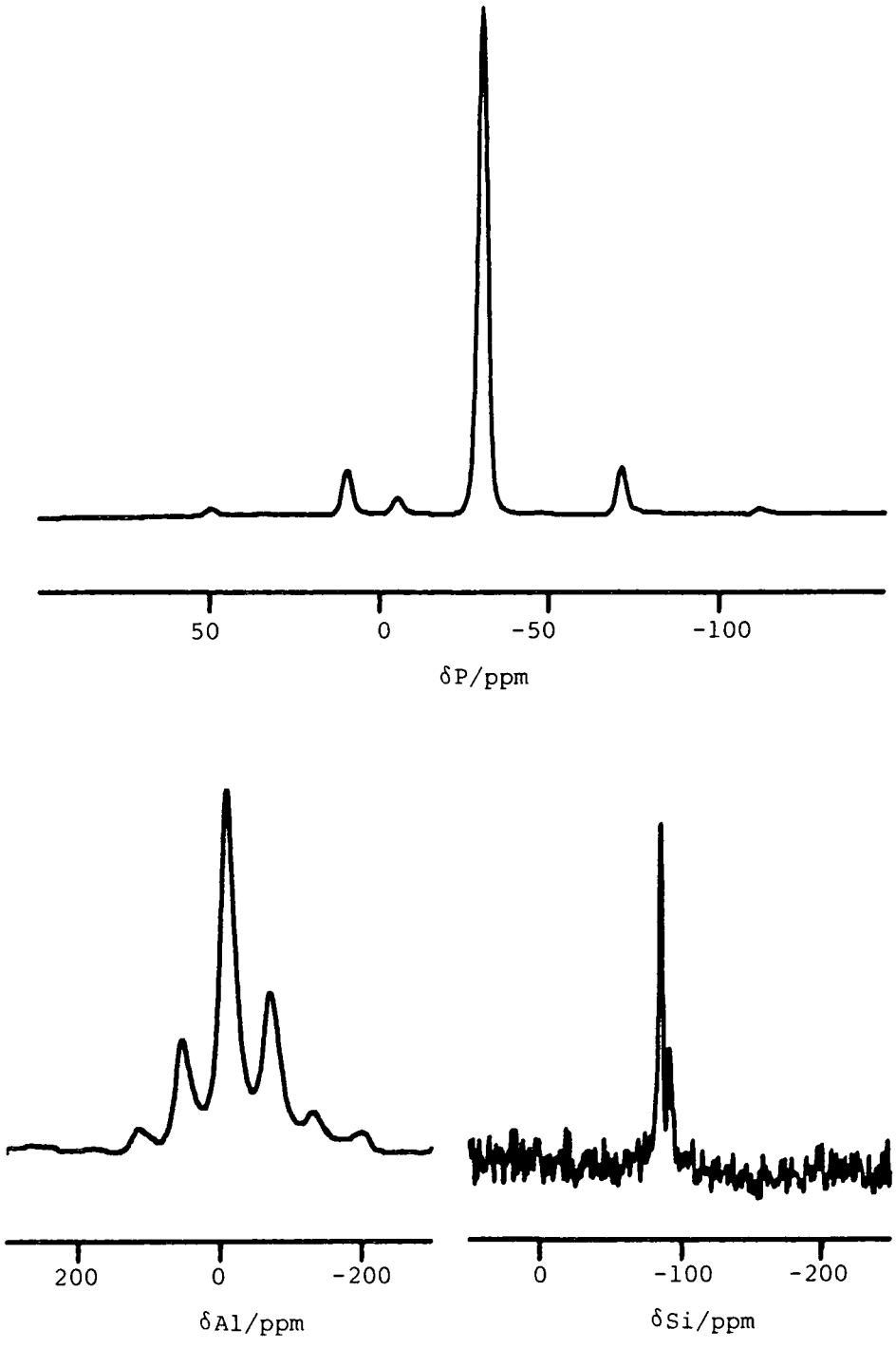

^{31}P CP/HPD: SF = 81.0 MHz; RD = 5 s; NT = 130; SI = 2 K; TD = 1 K; CT = 5 ms; 10 dB attenuation; SS = 3.4 kHz; SR = 105.9; SW = 20 kHz.

^{27}Al SPE - no HPD: SF = 52.1 MHz; RD = 1 s; NT = 100; SI = 2 K; TD = 1 K; PD = 1 μs; PA = π/6; SS = 1.8 kHz; SR = 362.3; SW = 50 kHz.

^{29}Si SPE: SF = 39.7 MHz; RD = 10 s; NT = 3752; SI = 2 K; TD = 1 K; PD = 3 μs; PA = π/4; SW = 20 kHz.

Figure 5.18

^{31}P (upper), ^{27}Al (lower left), and ^{29}Si (lower right)

MAS NMR spectra of sample I.

experiment	sample I chemical shift/ (ppm)	sample I linewidth (Hz)	sample II chemical shift/ (ppm)	sample II linewidth (Hz)
^{31}P SPE - (no HPD)	2.6 -30.3	690	2.6 -30.3	690
^{31}P SPE	2.5 -30.2 -4.6	230	2.5 -30.2 -4.6	230
^{31}P CP/HPD	-30.2 -4.6	230	-30.2 -4.6	230
^{27}Al	-5.6	1250	-5.6	1250
^{29}Si	-85.0 -91.2	130	—	—

Table 5.15

NMR data for samples I and II

The ^{27}Al NMR chemical shift of the aluminium resonance of sample I falls in the range normally assigned to octahedral aluminium. The tetrahedral shift range is obscured by the presence of spinning sidebands. Fast rotation will be needed to remove the sidebands and so determine whether or not the sample contains tetrahedral aluminium. The observed ^{27}Al NMR signal is most likely to be due to trolleite, which contains Al octahedra. The ^{29}Si NMR spectrum of sample I has two resonance lines, one at -85.0 ppm, the other at -91.2 ppm. The silicon-containing contaminants of this sample are topaz and alpha-quartz. The latter has a ^{29}Si NMR chemical shift of *ca.* -110 ppm. No such resonance is observed in the ^{29}Si NMR spectrum. However, in view of the recycle delay (10 s) and the long spin-lattice relaxation time for quartz (*ca.* 60 s), one would not expect to see the quartz resonance. The ^{29}Si NMR chemical shift of topaz is -85.6 ppm.[35] This

d (Å)	2θ	I/I_{max} x 100
5.69	14.9	37
4.97	17.8	27
3.51	25.4	38
2.99	30.0	45
2.94	30.5	100
1.90	47.9	30
1.76	52.0	-

Table 5.16

Powder XRD data for crandallite (major lines)

taken from ref. 265.

is in reasonable agreement with the resonance of the most intense peak in the ^{29}Si NMR spectrum of sample I. However, the -91.2 ppm peak remains unaccounted for and so can be tentatively assigned to silicon atoms in viséite. This chemical shift is in good agreement with the ^{29}Si NMR chemical shifts observed for silicon atoms substituted into an aluminophosphate lattice in SAPO-5 (see Chapter Six). To prove this assignment requires a pure sample of viséite. To this end, a sample of the original viséite was obtained courtesy of Dr. P.J. Dunn (NMNH no. 106364). Unfortunately, the sample size was insufficient for either MAS NMR or powder XRD investigation.

Breck[28] proposed that viséite was a mixture of crandallite and analcime. A comparison of the XRD data for McConnell's viséite and those obtained for samples I and II, with the data for crandallite[265] (Table 5.16) reveals that all the lines in the XRD trace assigned to viséite, could equally be due to crandallite.

To summarise, it would seem most unlikely that "viséite" exists as a pure enough material for conclusive spectroscopic investigation. The powder XRD data previously obtained for viséite is equally valid for

another phosphorus containing mineral, crandallite.

5.4 Conclusions and recommendations for further work.

The work presented in this chapter shows that the most conclusive evidence of isomorphous substitution of a heteroatom into the silicate lattice of a ZSM-5 type molecular sieve occurs only when MAS NMR can observe directly the substituting heteroatom. For cases where indirect observation is unavoidable, MAS NMR cannot prove substitution, or even infer the state of the substituting heteroatom. However, as in the case of the ferrisilicate samples, a great deal of information can be obtained about the system when other analytical techniques are used in conjunction with MAS NMR.

Of the heteroatoms studied, only boron can be directly proved by MAS NMR to substitute isomorphously into the lattice. Even then, as predicted using Pauling's minimum radius ratio concept,[185] the preferred coordination for boron is trigonal. This is reflected in the relative instability of the boron in Boralite (as compared to aluminium) and the ease of formation of BO_3 units, creating defect sites on thermal treatment. If one accepts the suggestion that up to 10% variation in bond lengths is allowable for isomorphous substitution,[197] then only boron, phosphorus, chromium (VI), titanium, and manganese substitution will be successful. Several attempts were made at synthesizing P-ZSM-5 during the course of these studies, although in every case the level of phosphorus incorporation proved to be too low for NMR investigation purposes. As previously mentioned, NMR cannot prove the isomorphous substitution of Cr and Ti into the silicate lattice of ZSM-5. For

Cr (III), octahedral coordination is the most stable state. The same is true of the Cr (VI) state where there are no unpaired electrons *i.e.* d^0, as opposed to d^3 for Cr (III). The most stable and common oxidation state for titanium is Ti (IV) (d^0). Thus, titanium generally forms covalent compounds, with titanium preferring a tetrahedral geometry, although Ti-O-Si bonds are known in octahedral coordination. Lanthanum has an ionic radius of over double that of aluminium (both elements being in a 3+ configuration), and so substitution would seem unlikely. However, the ionic radius of Fe (III) is 1.3 times as large as the ionic radius of Al (III), and low levels of isomorphous substitution seem possible, as observed.

Although MAS NMR combined with powder XRD is an ideal combination of analytical techniques for investigating the mineral viséite, the problem is the mineral itself. So far, all attempts to obtain reasonably pure specimens of viséite have either failed or produced very small quantities of the mineral. It is known, however, that at least one other research group is currently active in MAS NMR investigations of viséite.[266] In the light of the results in this chapter, it would seem reasonable in any further investigations of this kind to restrict the use of MAS NMR to studies of directly observable NMR-active (preferably spin I = 1/2) nuclei. Such nuclei could include ^{31}P, ^{119}Sn, ^{207}Pb, ^{205}Tl, ^{119}Hg, ^{195}Pt, ^{125}Te, ^{113}Cd, plus possibly ^{9}Be, ^{45}Sc, ^{51}V, ^{55}Mn, ^{59}Co, ^{63}Cu, ^{71}Ga, ^{87}Rb, ^{93}Nb, ^{115}In, ^{121}Sb, ^{133}Cs, and ^{187}Re, although these last spin I = n/2 nuclei would require the use of higher magnetic field strengths than 4.7 T.

Future studies into isomorphous substitution in zeolites might also consider the effects of substitution on the unit cell size as determined by powder XRD measurements. If the M-O bond length is greater than

1.62 Å (the Si-O bond length), then unit cell expansion is to be expected and *vice versa*.

Certain infrared frequencies for zeolites are reported to be sensitive to composition.[204] The use of infrared, chemical analysis, powder XRD, and MAS NMR should provide a wealth of information concerning coordination of any substituted heteroatom in a zeolite sample.

The use of probe molecules or gases such as xenon is beginning to find applications in zeolite chemistry.[170] It is possible that ^{129}Xe NMR could be used to determine whether or not isomorphous substitution has occurred, as the Xe atoms might be expected to be affected by extra-lattice material present in the pores and so the ^{129}Xe NMR spectrum obtained will be different if substitution has taken place.

In all the substituted ZSM-5 molecular sieves studied, the presence of tetrahedral aluminium was identified by ^{27}Al MAS NMR. In order to clarify the causes of the Q^3 resonance line apparent in several ^{29}Si MAS NMR spectra, it would be necessary to synthesise the samples from pure reagents in order to exclude contamination by aluminium. Such "pure" materials could also have their catalytic properties investigated unambiguously. Whatever catalytic activity they possess must then be due to acid sites created by heteroatom substitution. These acid sites could also be investigated in dehydrated samples using ^{1}H multiple pulse NMR with MAS (CRAMPS). The CRAMPS experiment has already provided evidence for the existence of acid sites in simpler non-substituted aluminosilicate zeolites.[104]

In instances where directly observable NMR-active nuclei are used for isomorphous substitution, MAS NMR could be used to investigate the crystallisation of the molecular sieve.

CHAPTER SIX - NMR RESULTS FOR VARIOUS MOLECULAR SIEVE-TYPE MATERIALS BASED ON ALUMINOPHOSPHATE FRAMEWORKS

6.1 Introduction

NMR results are presented in this chapter for a number of molecular sieve materials based on aluminium- and phosphorus-containing frameworks. Originally, the aim was to investigate the topology of these materials using NMR, and by comparing the spectra for the heteroatom substituted material with that of the analogous aluminophosphate material, elucidate the substitution mechanism. However, several samples proved impossible to obtain during the short timescale of these studies. Table 6.1 shows the various aluminophosphate and substituted aluminophosphate materials investigated.

$AlPO_4$-n	SAPO-/other-n
$AlPO_4$-5	SAPO-5 BAPO-5
$AlPO_4$-11	—
—	SAPO-20
(no Patent example)	SAPO-34

Table 6.1

AlPO's and substituted AlPO's studied

6.2 Aluminophosphates

Table 3.5 (Chapter Three, p. 93) listed the 3-D network $AlPO_4$-n structures originally synthesised by Wilson *et al.*.[221] Two of these materials, namely $AlPO_4$-5 and $AlPO_4$-11, have been studied using ^{31}P, ^{27}Al, and ^{13}C MAS NMR and the results are presented and discussed in this section.

6.2.1. $AlPO_4$-5

$AlPO_4$-5 is the most well-characterised aluminophosphate molecular sieve. Figures 6.1 and 6.2 show photographs of a model of the accepted framework structure.

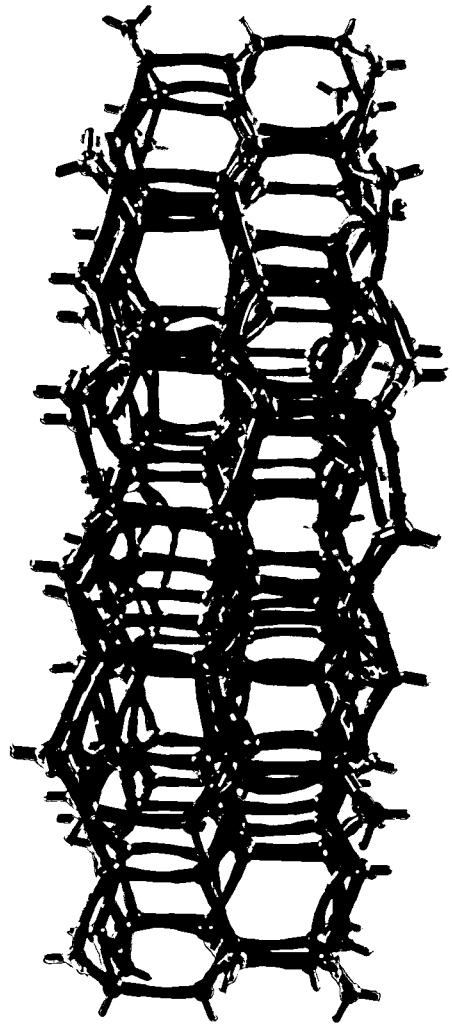

Figure 6.1

Model of $AlPO_4$-5 structure

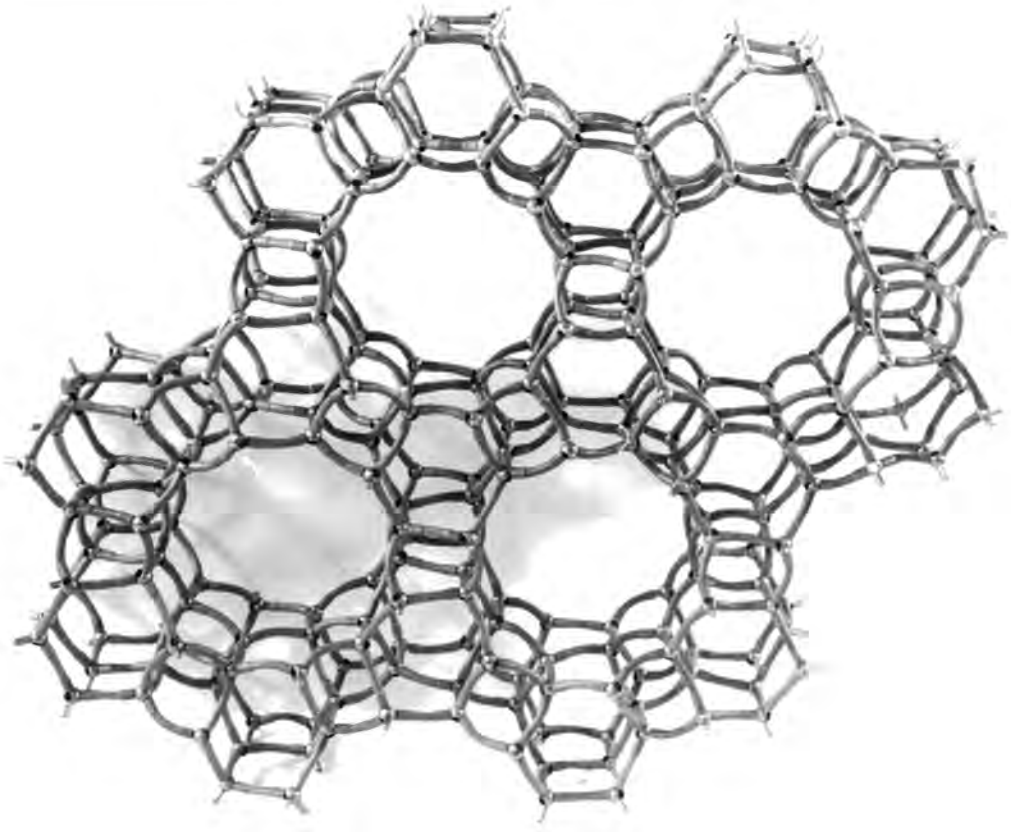

Figure 6.2

Model of $AlPO_4$-5 structure

The structure was investigated and solved by Bennett and coworkers.[227] It consists of condensed AlO_4 and PO_4 tetrahedra (the unit cell containing 12 Al and 12 P tetrahedral oxide units with Al and P atoms alternating over the tetrahedral nodes of the framework), building up 4-, 6-, and 12-membered rings. The 12-membered rings are non-connecting and parallel. The powder XRD pattern (Figure 6.3) is unique, indicating that the structure of $AlPO_4$-5 itself is novel. Typical powder XRD data for $AlPO_4$-5 (major lines only) are presented for both the Union Carbide Corporation (UCC) $AlPO_4$-5 (for comparison) and Laporte synthesised $AlPO_4$-5 in Table 6.2.

Two samples of $AlPO_4$-5 were studied. In both cases, the Al:P ratio (as determined by XRF) was close to 1.0. Both samples were investigated

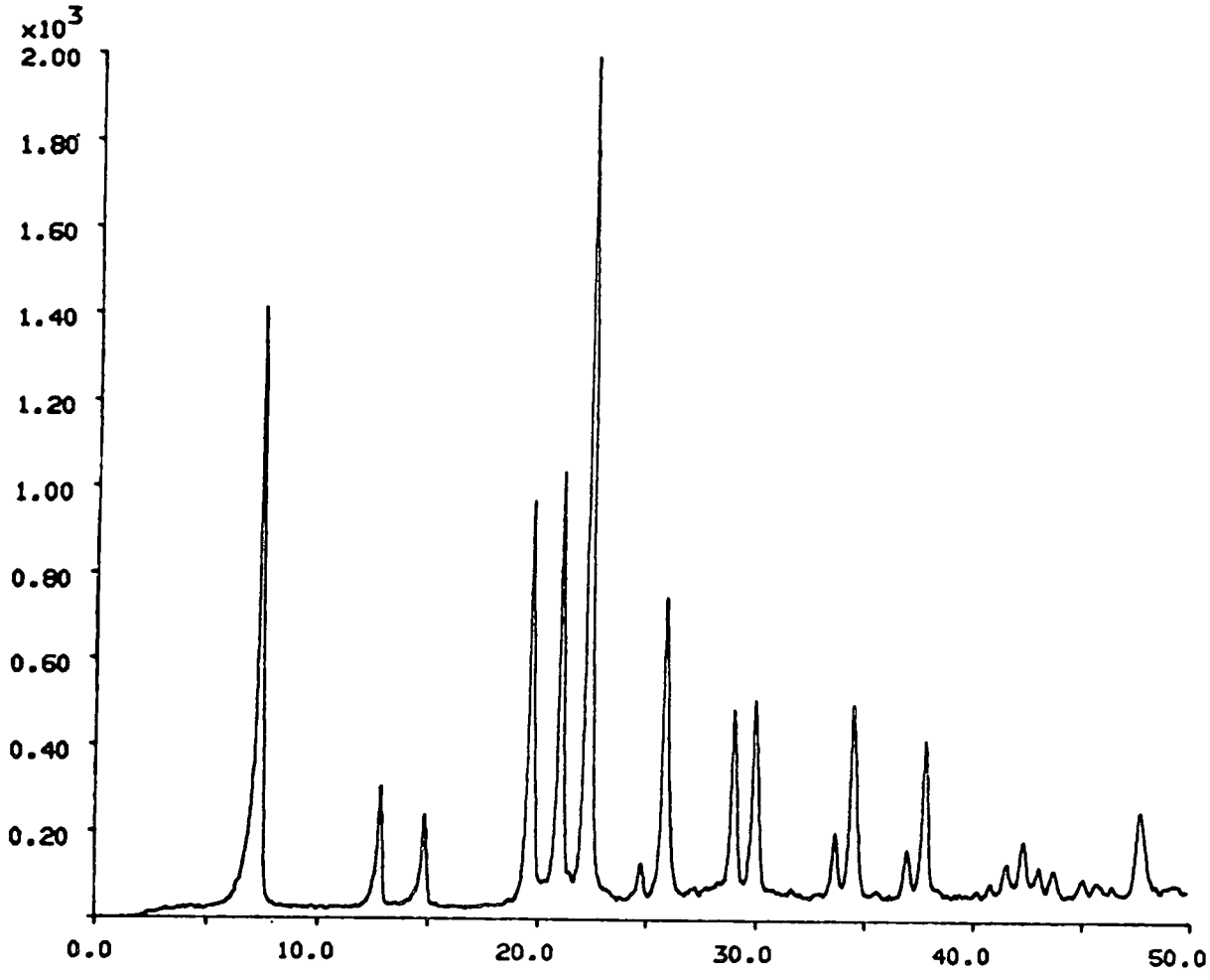

Figure 6.3

Powder XRD trace of Laporte $AlPO_4$-5

(i) UCC			(ii) Laporte		
d (Å)	2θ	I/I_{max} x 100	d (Å)	2θ	I/I_{max} x 100
11.8	7.46	100	12.1	7.32	100
6.84	12.92	11	6.92	12.80	12
5.93	14.92	28	6.00	14.76	8
4.50	19.78	66	4.52	19.63	26
4.24	21.09	63	4.23	20.98	26
3.97	22.43	94	4.00	22.20	48
3.43	25.97	37	3.46	25.73	31
3.08	29.05	21	3.09	28.90	8
2.97	30.07	22	2.99	29.94	9
2.60	34.57	19	2.62	34.27	7
2.40	37.73	13	2.39	37.68	6

Table 6.2

Powder XRD data for $AlPO_4$-5 (major lines only)

Identification number	sample	^{31}P NMR[a] chemical shift/(ppm)	^{31}P NMR[a] linewidth (Hz)	^{27}Al NMR chemical[b] shift/(ppm)	^{27}Al NMR linewidth (Hz)
HSZ-1297	Et_3N-$AlPO_4$-5	-29.0	800	35.8	1070
	$AlPO_4$-5	-28.4	550	33.4	1000
RIL003	Et_3N-$AlPO_4$-5	-29.0	740	33.6	1350
	$AlPO_4$-5	-29.3	560	31.4	1000

a) SPE or CP/HPD (contact time = 5 ms)
b) Experimental values (*i.e.* uncorrected for quadrupolar effects)

Table 6.3

^{31}P and ^{27}Al data of $AlPO_4$-5 and Et_3N-precursor

in their precursor and calcined forms and the relevant ^{31}P and ^{27}Al data are presented in Table 6.3. Figure 6.4 shows the ^{31}P and ^{27}Al MAS NMR spectra for both the precursor and calcined forms of (HSZ-1297) $AlPO_4$-5.

The appearance of only one line in both the ^{27}Al and ^{31}P NMR spectra is in agreement with the strict Al,P ordering of alternating AlO_4 and PO_4 tetrahedra in the crystal structure of $AlPO_4$-5 and its precursor Et_3N-$AlPO_4$-5. This ordering has already been inferred for the precursor TPAOH-$AlPO_4$-5 from the X-ray structure analysis carried out by Bennett *et al.*.[227]

^{27}Al MAS NMR spectra of both Et_3N-$AlPO_4$-5 and $AlPO_4$-5 (sample HSZ-1297) were also acquired at 78.2 MHz (300 MHz proton) by A.N. Wilson of K.S.L.A. (Shell Research B.V.), Amsterdam. The experimental chemical shifts and linewidths are collated in Table 6.4.

From a previous investigation of $AlPO_4$-5 carried out by Müller *et al.*,[235] the quadrupole coupling constant ($\chi = e^2qQ/h$), and asymmetry

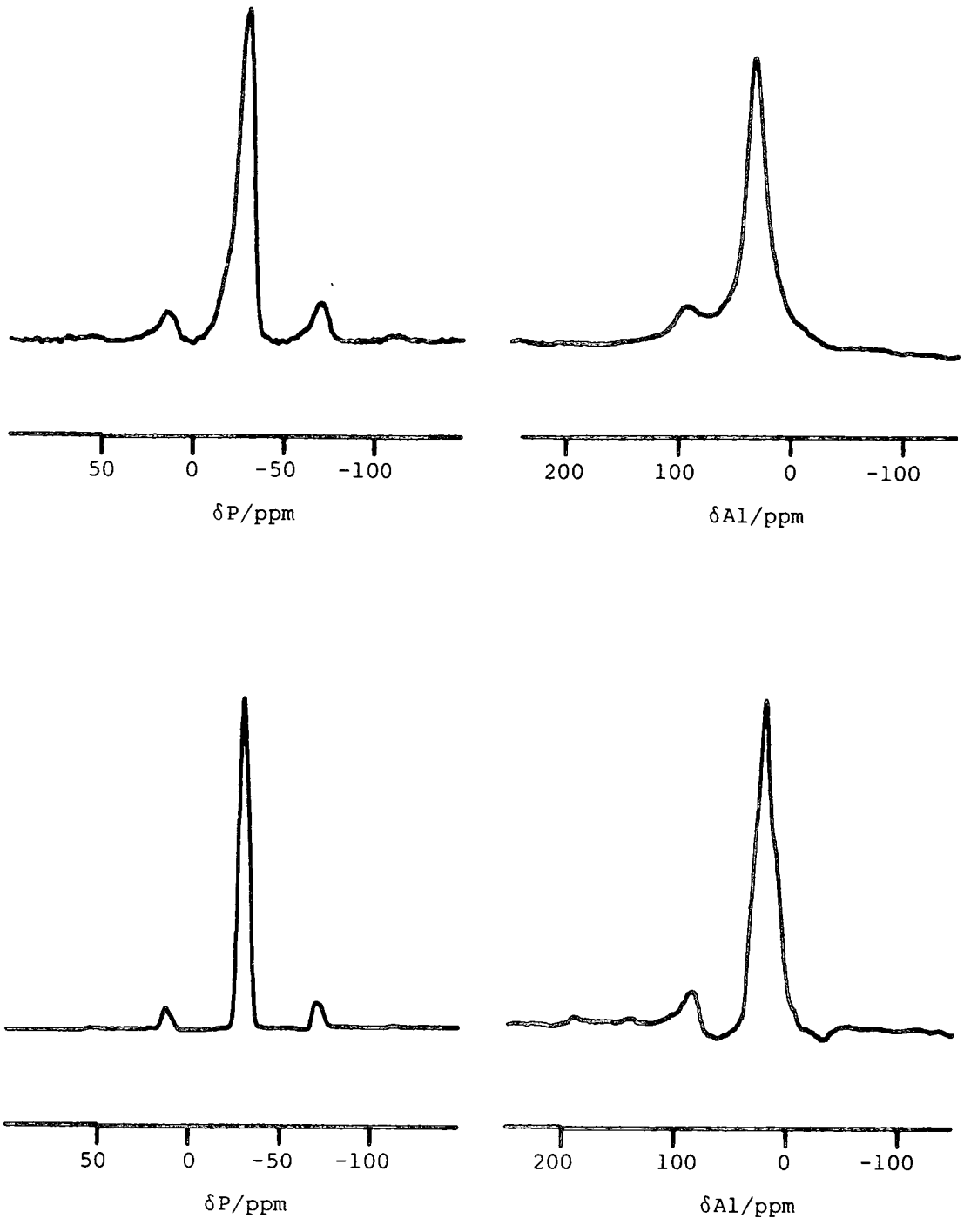

Figure 6.4

upper spectra: precursor Lower spectra: calcined

Left hand side: ^{31}P SPE MAS NMR: SF = 81.01 MHz; RD = 10 s; SW = 20 kHz; SI = 2 K; TD = 1 K; NT = 80; SS = 3.3 kHz; PD = 5 μs; PA = π/2; SR = 1005.13.

Right hand side: ^{27}Al SPE MAS NMR: SF = 52.11 MHz; RD = 1 s; SW = 50 kHz; SI = 2 K; TD = 1 K; NT = 1000; SS = 3.6 kHz; PD = 3 μs; PA = π/4; SR = 33800.

sample	experimental chemical shift/(ppm)	linewidth (Hz)
Et_3N-$AlPO_4$-5	36.8	990
$AlPO_4$-5	33.0	700

Table 6.4

78.2 MHz ^{27}Al NMR (7.0 T)

parameter (η), are known for the Al sites in $AlPO_4$-5. It is possible, knowing these two values to calculate the correction factor for the quadrupole-induced shift (QIS) contributions to the observed chemical shift, and so arrive at the true chemical shift for ^{27}Al in $AlPO_4$-5. The calculation is as:[267]

$$[\delta(Al)/ppm] = \delta_{exp} + 3 \times 10^4 \times 1/5(1 + 1/3\eta^2)(e^2qQ/h\upsilon_o)^2 \quad \ldots \quad (6.1)$$

where υ_o = 50.1 MHz (200 MHz proton), 78.2 MHz (300 MHz proton);

$\eta = 0.95$

$\chi = e^2qQ/h = 2.3$ MHz

} ref. 235

The corrected ^{27}Al chemical shifts are presented for $AlPO_4$-5 (HSZ-1297) in Table 6.5.

It is immediately obvious from equation (6.1) that as the strength of the magnetic field is increased, the correction factor decreases, until

sample	^{27}Al NMR [δ_{corr} /(ppm)]	
	50.1 MHz	78.2 MHz
Et_3N-$AlPO_4$-5	52.3	43.6
$AlPO_4$-5	49.9	39.8

Table 6.5

Corrected ^{27}Al chemical shifts at 50.1 MHz (4.7 T) and 78.2 MHz (7.0 T)

sample	experimental chemical shift/(ppm)	linewidth (Hz)
Et_3N-$AlPO_4$-5	36.8	990
$AlPO_4$-5	33.0	700

Table 6.4

78.2 MHz ^{27}Al NMR (7.0 T)

parameter (η), are known for the Al sites in $AlPO_4$-5. It is possible, knowing these two values to calculate the correction factor for the quadrupole-induced shift (QIS) contributions to the observed chemical shift, and so arrive at the true chemical shift for ^{27}Al in $AlPO_4$-5. The calculation is as:[267]

$$[\delta(Al)/ppm] = \delta_{exp} + 3 \times 10^4 \times 1/5(1 + 1/3\eta^2)(e^2qQ/h\upsilon_o)^2 \quad \ldots \quad (6.1)$$

where υ_o = 50.1 MHz (200 MHz proton), 78.2 MHz (300 MHz proton);

$\eta = 0.95$

$\chi = e^2qQ/h = 2.3$ MHz

} ref. 235

The corrected ^{27}Al chemical shifts are presented for $AlPO_4$-5 (HSZ-1297) in Table 6.5.

It is immediately obvious from equation (6.1) that as the strength of the magnetic field is increased, the correction factor decreases, until

sample	^{27}Al NMR [δ_{corr} /(ppm)]	
	50.1 MHz	78.2 MHz
Et_3N-$AlPO_4$-5	52.3	43.6
$AlPO_4$-5	49.9	39.8

Table 6.5

Corrected ^{27}Al chemical shifts at 50.1 MHz (4.7 T) and 78.2 MHz (7.0 T)

at 130.3 MHz (500 MHz proton), the correction factor is only 2.4 ppm. The ^{27}Al field-dependent chemical shifts at 4.7 T and 7.0 T are remarkably similar (see Tables 6.3 and 6.4 respectively). This suggests that no correction is necessary, as clearly, the increase in field strength has not resulted in the expected high frequency shift, closer to the true isotropic, field-independent chemical shift, as would be the case if second-order quadrupolar effects were dominant. However, the linewidths of both the precursor and calcined forms of $AlPO_4$-5 are significantly narrower at the higher field strength, implying that large second-order quadrupolar effects are present in the sample. It should be remembered, however, that precise determination of experimental chemical shifts is difficult for broad lines. In the case of ^{27}Al chemical shift determinations, the error is estimated to be $\pm$ 4 ppm. This would account for the apparently coincidental similarity of the two sets of chemical shift data at the two field strengths.

It is obvious from Table 6.5 that the correction factor applied to the field-dependent ^{27}Al chemical shifts at 4.7 T, produces chemical shifts that are grossly in error. Although other methods have been developed to obtain true chemical shifts (see Chapter Two), it is clear that the corrective process used here works reasonably only at high field strengths. It is questionable whether such a correction is worthwhile at lower field strengths.

The ^{31}P and ^{27}Al NMR results are in good agreement with those obtained by both Müller *et al.*[235] (270 MHz proton) and by Blackwell and Patton[234] (200 MHz proton).

The magnitude of the quadrupole coupling constant for $AlPO_4$-5 is apparent from the inhomogeneously broadened ^{27}Al MAS NMR spectrum and provides evidence of the presence of distorted $(AlO_4)^{5-}$ tetrahedra in

the framework structure. This is in accordance with the strong displacements of the framework oxygen atoms found by single-crystal X-ray investigation for TPAOH-$AlPO_4$-5.[227] The distortion is also apparent in the likewise inhomogeneously broadened (by incomplete averaging of the P,Al dipolar interaction with MAS) ^{31}P MAS NMR spectrum of $AlPO_4$-5.

According to the idealized chemical composition of $Et_3N.12AlPO_4$[223] and the probable location of one template molecule per two 12-membered rings[223] of alternating $(AlO_4)^{5-}$ and $(PO_4)^{3-}$ tetrahedra, it is reasonable that the Al sites (and also the P sites) of the rings are affected by the dipolar Et_3N molecule. Both resonances decrease in linewidth following calcination, suggesting some sort of interaction between the Al, P sites and the organic template. Further evidence of P site interaction with the Et_3N molecules in the channels is that cross-polarization (CP) is possible before calcination. CP is also possible (although not as efficiently, as evinced by the decrease in S/N ratio in the ^{31}P spectrum) following calcination. This suggests that the proton magnetization necessary in order for CP to occur comes from two sources: (i) the organic template, and (ii) water molecules present in the channel system.

The small peak to the high frequency side of the main ^{27}Al resonance was originally thought to be a spinning sideband. However, experiments designed to study the effect of pulse angle on ^{27}Al (quadrupolar) nuclei have shown that the peak in question is most likely to be due to the excitation of other transitions than the $(1/2 \longleftrightarrow -1/2)$ transition, as at very low pulse angles ($< \pi/6$), spinning sidebands equidistant from the main ^{27}Al resonance appear. This is shown in Figure 6.5, for (RIL003) Et_3N-$AlPO_4$-5. Figure 6.6 shows the ^{13}C CP/HPD

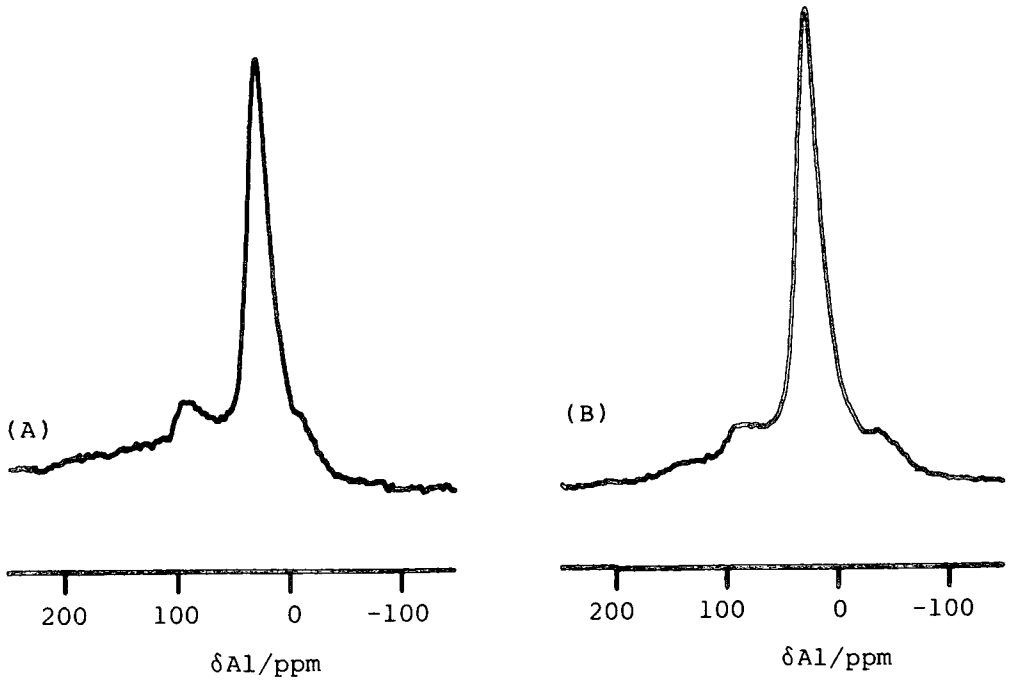

SF = 52.11 MHz; RD = 1 s; SW = 50 kHz; SI = 2 K; TD = 1 K; NT = 1000; SS = 3.0 kHz; SR = -2343.75.

Figure 6.5

Effect of pulse angle on ^{27}Al NMR spectrum of Et_3N-$AlPO_4$-5

(A) Pulse angle = $\pi/4$. (B) Pulse angle $\leq \pi/6$

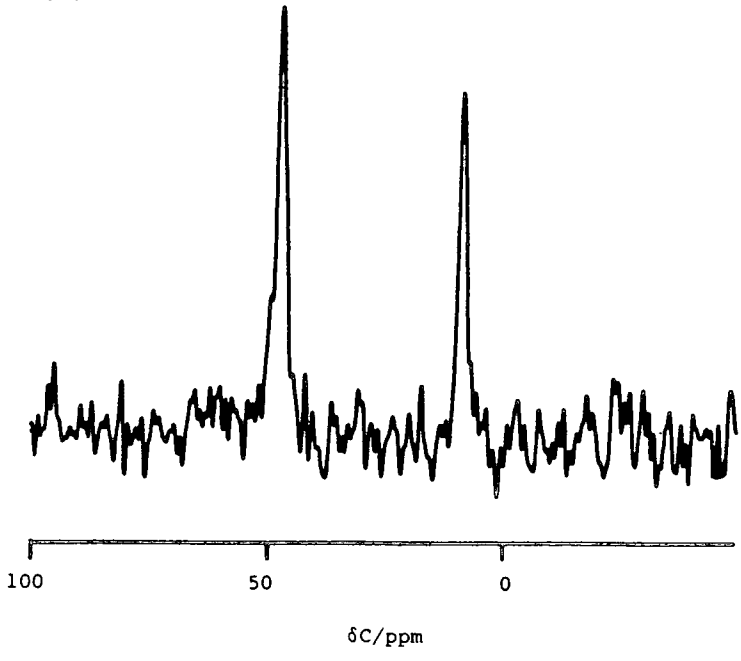

SF = 50.3 MHz; RD = 5 s; CT = 1 ms; SW = 10 kHz; SI = 2 K; TD = 1 K; NT = 320; SS = 4.0 kHz; SR = 0.382.

Figure 6.6

^{13}C CP/HPD MAS NMR spectrum of Et_3N enclathrated in $AlPO_4$-5

sample state	^{13}C shift/(ppm)		Δδ/ppm
	CH_2	CH_3	
solution	46.9	12.6	34.3
solid (Et_3N-$AlPO_4$-5)	47.7	9.3	38.4

Table 6.6

Comparison of solid-state and solution-state ^{13}C NMR shifts for Et_3N

MAS NMR spectrum of Et_3N, the organic template used in the synthesis of both $AlPO_4$-5 samples. The ^{13}C chemical shifts of both the solid form of Et_3N (enclathrated in the $AlPO_4$-5 channels) and the solution are presented in Table 6.6. The linewidths (100 Hz for the CH_3 resonance, 120 Hz for the CH_2 resonance) together with the change in chemical shift in the solid-state, suggest a significant interaction of the template with the framework.

The phosphorus spin-lattice relaxation time (T_1) was measured [using the inversion-recovery pulse sequence (with HPD)] to be 23 s. Thus in order to obtain a quantitative ^{31}P NMR spectrum for $AlPO_4$-5, it is necessary to use a recycle delay of 115 s, or alternatively, with a 10 s recycle delay cut the effective flip-angle to $\pi/4$ (pulse duration, 2.5 μs).

6.2.2. $AlPO_4$-11.

The powder X-ray diffraction pattern of $AlPO_4$-11 (Figure 6.7) is unique and represents a novel, and as yet undetermined, structure. The powder XRD data for the $AlPO_4$-11 sample investigated here are compared with those for a UCC $AlPO_4$-11 sample in Table 6.7. Figure 6.7 shows the

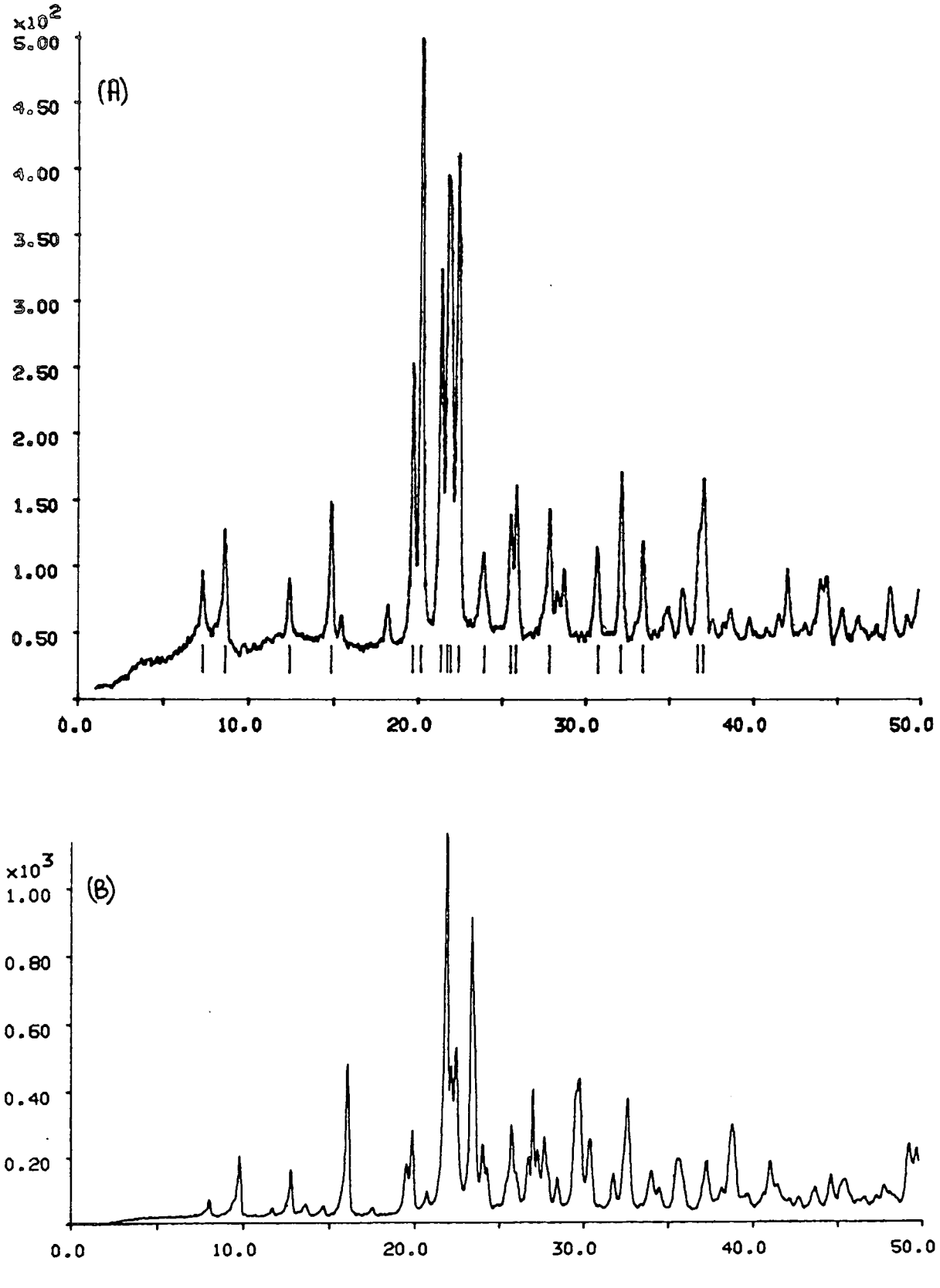

Note: scale of (B) increased fourfold relative to (A)

Figure 6.7

XRD patterns for (A) *i*-Pr_2NH-$AlPO_4$-11 and (B) $AlPO_4$-11 after calcination

(i) UCC $AlPO_4$-11			(ii) Laporte $AlPO_4$-11 (precursor)		
d (Å)	2θ	I/I_{max} x 100	d (Å)	2θ	I/I_{max} x 100
10.85	8.15	34	11.97	7.40	29
9.31	9.50	49	10.14	8.75	41
6.66	13.29	16	7.12	12.50	16
5.64	15.71	30	5.96	15.00	31
4.32	20.56	50	4.56	19.75	49
4.23	21.00	100	4.43	20.38	100
4.00	22.23	58	4.21	21.50	56
3.93	22.63	75	4.12	22.00	69
3.83	23.23	67	4.01	22.63	71
3.62	24.60	10	3.75	24.25	11
3.59	24.80	11	3.55	25.75	15
3.38	26.37	13	3.50	26.13	10
3.34	26.69	17	3.27	28.13	17
3.13,3.11	28.52,28.70	15	2.99	31.00	11
2.84	31.50	10	2.87	32.50	20
2.71	33.06	15	2.78	33.75	11
2.61	34.36	11	2.56	37.00	10
2.39,2.37	37.64,37.97	14	2.54	37.38	14

Table 6.7

X-ray powder diffraction data for UCC and Laporte $AlPO_4$-11 molecular sieves (major lines only)

powder XRD trace of calcined $AlPO_4$-11. The sample was made with diisopropylamine (i-Pr_2NH) as the template and had an Al:P ratio of 0.948:1.0 *i.e.* unity within experimental error. ^{31}P and ^{27}Al NMR spectra of both the calcined and precursor forms of $AlPO_4$-11 are presented in Figure 6.8. The experimentally determined chemical shifts and linewidths are collated in Table 6.8.

The ^{27}Al MAS NMR spectrum of the as-synthesised form of $AlPO_4$-11 is consistent with the accepted chemical shift of tetrahedral aluminium in aluminophosphate frameworks,[236] and is in agreement with that observed by Blackwell and Patton.[234] The resonance lineshape is asymmetrical, suggesting the distortion of $(AlO_4)^{5-}$ tetrahedra as was observed for $AlPO_4$-5. On calcination, two peaks are produced. It is relevant to

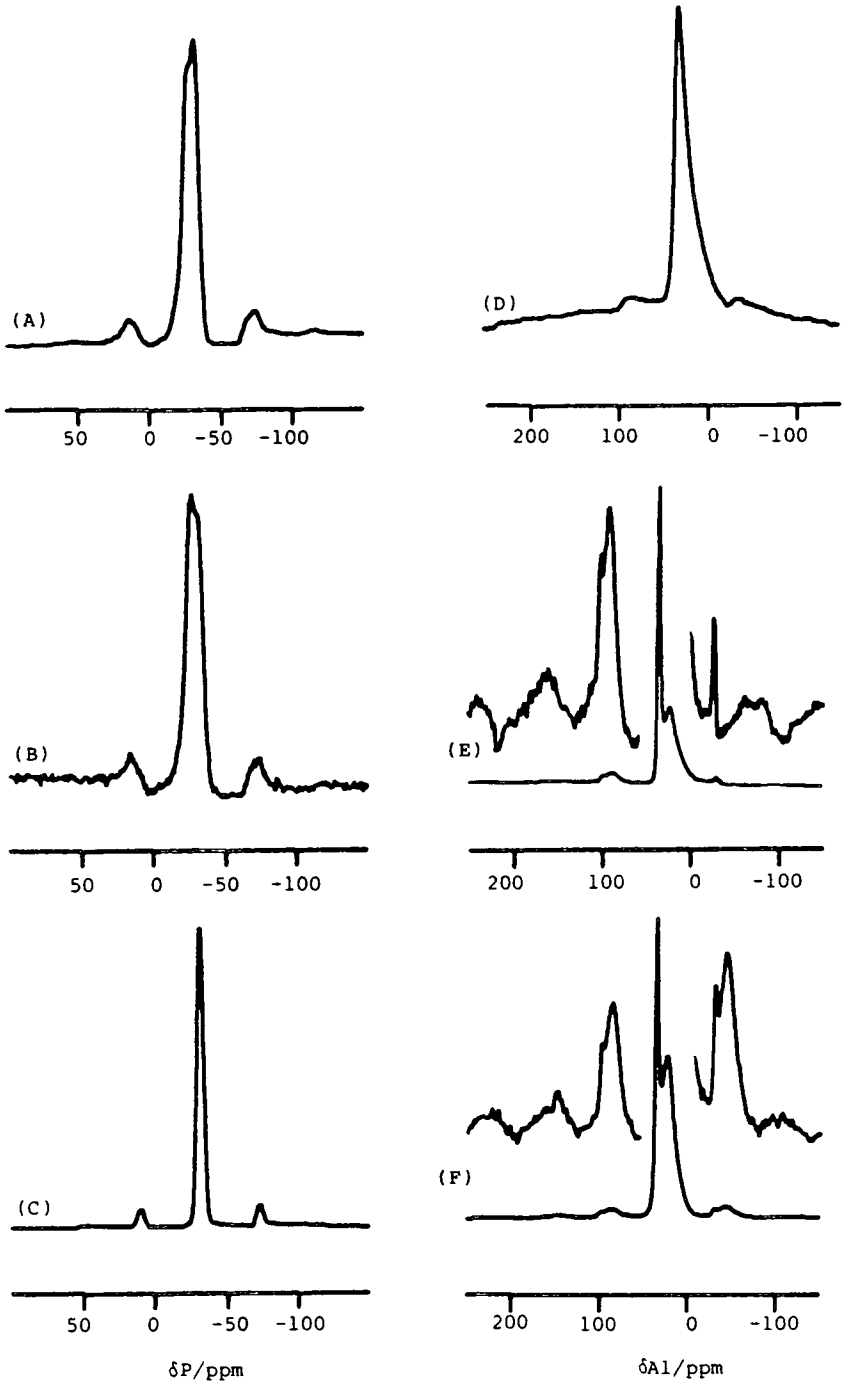

(A), (B), and (D) - precursor.

(C), (E), and (F) - calcined.

Figure 6.8

^{31}P (left hand side) and ^{27}Al SPE (right) MAS NMR spectra of $AlPO_4$-11.

(For conditions, see over)(and text)

Figure 6.8 (contd.)

Conditions for acquisition of the spectra.

(A) SPE: SF = 81.01 MHz; RD = 60 s; SW = 20 kHz; SI = 2 K; TD = 1 K;
NT = 24; SS = 3 kHz; PD = 5 μs; PA = 2π/5; SR = 105.9.

(B) CP/HPD: SF = 81.01 MHz; RD = 10 s; SW = 20 kHz; SI = 2 K; TD = 1 K;
NT = 130; CT = 10 ms; SS = 3.3 kHz; SR = 105.9.

(C) SPE: SF = 81.01 MHz; RD = 60 s; SW = 20 kHz; SI = 2 K; TD = 1 K;
NT = 24; SS = 3 kHz; PD = 4 μs; PA = 2π/5; SR = 105.9.

(D) SF = 52.1 MHz; RD = 0.5 s; SW = 50 kHz; SI = 2 K; TD = 1 K;
NT = 400; SS = 2.9 kHz; PD = 2 μs; PA = π/6; SR = -2344.

(E) SF = 52.1 MHz; RD = 0.5 s; SW = 50 kHz; SI = 2 K; TD = 1 K;
NT = 180; SS = 3.0 kHz; PD = 6 μs; PA = π/2; SR = -2344.

(F) SF = 52.1 MHz; RD = 0.5 s; SW = 50 kHz; SI = 2 K; TD = 1 K;
NT = 180; SS = 3.0 kHz; PD = 2 μs; PA = π/6; SR = -2344.

(A), (B), and (D) - precursor.

(C), (E), and (F) - calcined.

sample	^{31}P NMR		^{27}Al NMR	
	chemical shift/(ppm)	linewidth (Hz)	chemical[a] shift/(ppm)	linewidth (Hz)
i-Pr_2NH-$AlPO_4$-11	-30.8 -26.1	960	32.2	880
$AlPO_4$-11	-30.9	450	35.5 24.3	260 —

a) Experimental values (field dependent)

Table 6.8

^{31}P and ^{27}Al data of $AlPO_4$-11 and i-Pr_2NH-$AlPO_4$-11

note here that the linewidth of the ^{27}Al resonance before calcination is such that if two peaks (due to different Al containing species) with a chemical shift difference of 11.2 ppm were to exist, they would not be observable. However, this can be ruled out as the powder XRD trace for $AlPO_4$-11 shows the sample to be phase pure before calcination. The high-frequency line is substantially narrower (and more symmetrical) than the low-frequency line. Blackwell and Patton[234] reported observing virtually no change in the ^{27}Al NMR spectrum following calcination of $AlPO_4$-11. However, they note the appearance, to low frequency of the most intense resonance, of a second peak. The high-frequency ^{27}Al resonance can sensibly be assigned to Al nuclei in framework sites whose nuclear symmetry has been altered, perhaps by coordination with water molecules. However, if this were indeed the case, one would expect the chemical shift to fall in the octahedral chemical shift region, as was observed by Blackwell and Patton for $AlPO_4$-17.[234] The X-ray powder diffraction trace for calcined $AlPO_4$-11 indicates that calcination produces various $AlPO_4$ polymorphs including $AlPO_4$ versions of the SiO_2 phases α-crystobalite, quartz, dense $AlPO_4$, and possibly some $AlPO_4$-11.

Müller *et al.*[236] in a previous study of $AlPO_4$ polymorphs at 270 MHz proton (70.4 MHz ^{27}Al) recorded a chemical shift of 38.8 ppm for $AlPO_4$-T (low temperature tridymite) and 39.8 ppm for $AlPO_4$-C (low temperature crystobalite). The linewidths were 350 Hz and 390 Hz respectively. The use of a lower magnetic field (50.1 MHz) will (due to the increased second-order quadrupolar effects) reduce the chemical shift (*i.e.* move it to lower frequency of that observed at 70.4 MHz) and so an experimental chemical shift of 35.5 ppm is reasonable for such a polymorph. Thus the resonance at 35.5 ppm observed following calcination of *i*-Pr_2NH-$AlPO_4$-11 is due to structure collapse and subsequent formation of $AlPO_4$-T or $AlPO_4$-C. The broad resonance at 24.3 ppm can then be assigned to dense $AlPO_4$. ^{27}Al MAS NMR spectra acquired at higher magnetic field would be most useful in this situation, as a decrease in quadrupolar effects would be observed, perhaps simplifying interpretation of the spectrum. [It is interesting to note here that a change in the pulse width from 1 μs (18^o) to 5 μs (90^o) results in a change in the relative intensities of the two peaks and a change in the sideband pattern. This is shown on Figure 6.8, (E) and (F)].

The ^{31}P MAS NMR spectrum of the precursor form of $AlPO_4$-11 shows two peaks, with chemical shifts falling in the accepted tetrahedral (PO_4) phosphorus range. Cross-polarization is possible for both peaks, although there is a reversal of intensities compared with those observed in the SPE spectrum. Obviously, the high-frequency resonance is more strongly associated with protons (either from the template or from water molecules) than the low-frequency peak. The presence of two phosphorus sites could be due to crystallographic inequivalence in the unit cell. However, this cannot be proven as the crystal structure is undetermined.

sample state	^{13}C shifts/(ppm) (CH)	(CH_3)	$\Delta\delta_C$/(ppm)
solution	45.30	23.72	21.58
solid	54.9	22.1	32.8

Table 6.9

^{13}C solution- and solid-state chemical shifts for *i*-Pr_2NH in the precursor $AlPO_4$-11

Strong ^{31}P CP enhancement is observed for calcined $AlPO_4$-11. Blackwell and Patton observed two resonances for calcined $AlPO_4$-11 using SPE (no HPD) ^{31}P MAS NMR. They did not record ^{31}P NMR of the as-synthesised $AlPO_4$-11, and no ^{31}P NMR spectra were presented for calcined $AlPO_4$-11. The two phosphorus sites in $AlPO_4$-11 have differing T_1 values, the high-frequency peak having a T_1 of 36 s, the low-frequency peak, a T_1 of 39 s (as measured by inversion recovery). Figure 6.9 shows the ^{13}C CP/HPD NMR spectrum of the template of $AlPO_4$-11, diisopropylamine, enclathrated in the channels of $AlPO_4$-11. Table 6.9 compares solution-state ^{13}C chemical shifts with solid-state ^{13}C chemical shifts. The observed differences in chemical shift and the substantial linewidth for *i*-Pr_2NH in the solid-state (140 Hz for the high frequency peak, 120 Hz for the low frequency peak) are attributable to interactions of the template with the aluminophosphate framework.

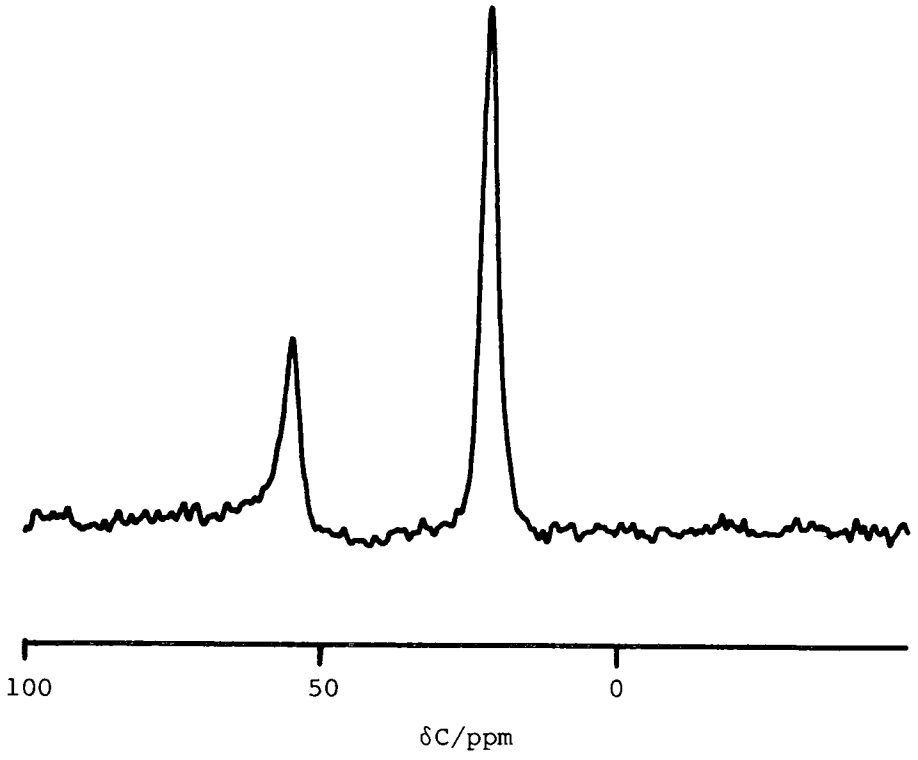

SF = 50.3 MHz; RD = 5 s; SW = 10 kHz; SI = 2 K; TD = 1 K; NT = 450; SS = 4.0 kHz; CT = 1 ms; SR = 0.382.

Figure 6.9

^{13}C CP/MAS NMR spectrum of diisopropylamine, the template for $AlPO_4$-11

6.3 Silicoaluminophosphates (SAPO-n)

Table 3.8 (Chapter Three, p. 97) listed some of the microporous SAPO molecular sieves originally synthesised by Lok *et al.*.[224] Three of these materials, namely SAPO-5 (silicon substituted $AlPO_4$-5), SAPO-20 (sodalite topology), and SAPO-34 (chabazite topology) have been studied using ^{31}P, ^{29}Si, ^{27}Al, and ^{13}C MAS NMR. The results are presented and discussed in this section. The results for SAPO-5 (HSZ-1345) are the subject of a paper.[238]

6.3.1. SAPO-5

The structure of SAPO-5 is topologically related to the novel structure type found for the aluminophosphate, $AlPO_4$-5. Table 6.10 shows the three samples studied together with details of their synthesis conditions and powder XRD-determined impurities. The powder XRD data for UCC SAPO-5 are presented together with those for the three Laporte-synthesised SAPO-5 samples in Table 6.11.

(1) SAPO-5 (HSZ-1345)

This sample of SAPO-5 was shown to be contaminated with small amounts of SAPO-11. The scanning electron micrograph (SEM) of SAPO-5 (Figure 6.10) shows 5 - 10 μm regular hexagonal blocks with some aggregates of between 20 and 100 μm across. There is some degree of intergrowth and some rectangular blocks are also present. There is no visible sign of SAPO-11.

The powder XRD pattern identifies the structure of SAPO-5 to be topologically identical to that found for $AlPO_4$-5 (see Section 6.2.1.). The sample analyses as (normalised to one mole of PO_2^+): 1.0 (PO_2^+); 0.12 (SiO_2); 1.104 (AlO_2^-). Figure 6.11 shows the ^{27}Al, ^{31}P, and ^{29}Si MAS NMR spectra of the precursor and calcined forms of SAPO-5. The data are collated in Table 6.12. The ^{31}P T_1 value for the as-synthesised SAPO-5 is 18 s (as measured by inversion-recovery using HPD).

template	sample code	contaminants (from powder XRD)	preparation details
unknown	HSZ-1345	SAPO-11	One litre preparation
TEAOH	HSZ-1206	Boehmite + amorphous	Small bomb preparation
TPAOH	019S	pure	Small bomb preparation

Table 6.10

The SAPO-5 molecular sieves investigated

(i) UCC SAPO-5

d (Å)	2θ	I/I_{max} x 100
11.8	7.5	100
6.68	12.9	12
5.91	15.0	26
4.46	19.9	61
4.21	21.1	53
3.96	22.45	77
3.59	24.8	5
3.43	26.0	30
3.07	29.1	17
2.96	30.15	19
2.66	33.65	15
2.59	34.65	16

(ii) Laporte (HSZ-1345)[a)]

d (Å)	2θ	I/I_{max} x 100
11.95	7.4	93
6.81	13.0	13
5.91	15.0	27
4.46	19.9	67
4.17	21.3	99
3.94	22.6	100
3.58	24.9	10
3.41	26.1	40
3.08	29.0	26
2.97	30.05	23
2.68	33.4	8
2.59	34.6	19

(iii) Laporte (HSZ-1206)[b)]

d (Å)	2θ	I/I_{max} x 100
11.95	7.4	100
6.81	13.0	19
5.91	15.0	35
4.46	19.9	75
4.17	21.3	62
3.94	22.6	88
3.58	24.9	5
3.41	26.1	34
3.08	29.0	22
2.97	30.05	16
2.68	33.4	5
2.59	34.6	14

(iv) Laporte (019S)[c)]

d (Å)	2θ	I/I_{max} x 100
11.95	7.4	100
6.81	13.0	12
5.91	15.0	67
4.46	19.9	81
4.17	21.3	38
3.94	22.6	69
3.58	24.9	4
3.41	26.1	39
3.08	29.0	13
2.97	30.05	39
2.68	33.4	4
2.59	34.6	22

a) Plus extra peaks at 9.4, 5.53, 4.35 Å due to SAPO-11. UCC patent example 13 is also impure.

b) Plus extra peaks at 6.1, 3.2, 2.4 Å due to boehmite + amorphous material.

c) "Pure" material.

Table 6.11

Powder X-ray data for SAPO-5 samples (major lines only)

Figure 6.10

SEM of SAPO-5 (HSZ-1345)

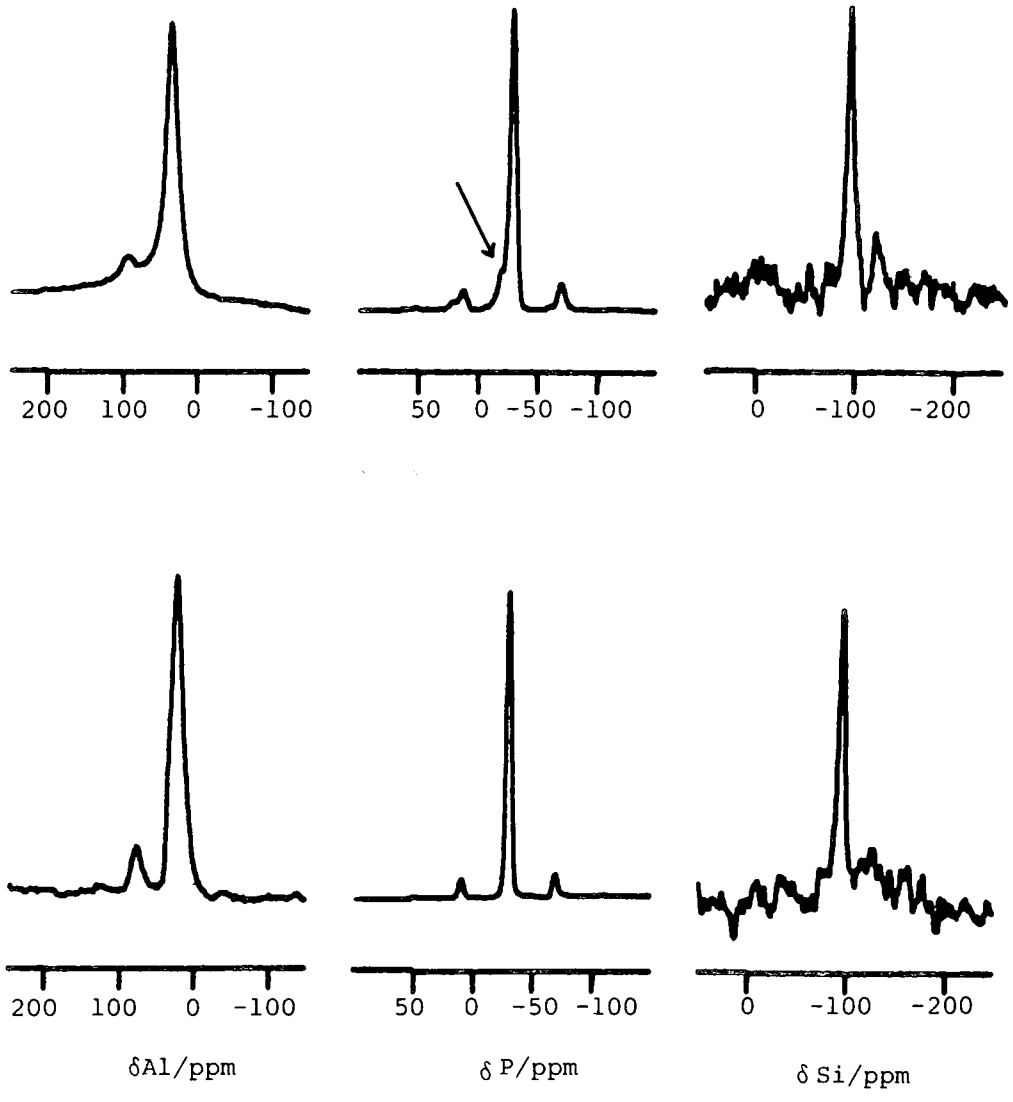

^{27}Al SPE (no HPD): SF = 52.1 MHz; RD = 2 s; SW = 50 kHz; SI = 2 K; TD = 1 K; NT = 110 (precursor), 80 (calcined); SS = 3.0 kHz; PD = 4 μs; PA = π/4; SR = 33715.

^{31}P CP/HPD: SF = 81.01 MHz; RD = 6 s; SW = 20 kHz; SI = 2 K; TD = 1 K; NT = 110 (precursor and calcined); CT = 10 ms; SS = 3.3 kHz; SR = 1005.13.

^{29}Si SPE (no HPD): SF = 39.7 MHz; RD = 10 s; SW = 20 kHz; SI = 2 K; TD = 1 K; NT = 18000 (precursor), 12000 (calcined); SS = 3.3 kHz; PD = 5 μs; LB = 100 Hz; PA = π/2; SR = 13797.

Figure 6.11

^{27}Al (left), ^{31}P (centre), and ^{29}Si (right) MAS NMR spectra for the precursor (upper) and calcined (lower) forms of SAPO-5.

(The shoulder in the ^{31}P spectrum of the precursor, mentioned in the text, is indicated by an arrow.)

	precursor SAPO-5	SAPO-5
^{27}Al chemical shift/(ppm)	33.5	32.6
Al linewidth (Hz)	1200	1100
^{31}P chemical shift/(ppm)	-28.4	-29.6
P linewidth (Hz)	540	400
^{29}Si chemical shift/(ppm)	*ca.* -92.0	*ca.* -92.0
Si linewidth (Hz)	200	260

Table 6.12

^{27}Al, ^{31}P, and ^{29}Si data for SAPO-5

The ^{27}Al and ^{31}P chemical shifts and linewidths are in good agreement with those noted previously for $AlPO_4$-5. Perhaps surprisingly, the substitution of silicon into the aluminophosphate lattice does not appear to have affected the ^{31}P or ^{27}Al NMR spectra noticeably. Once again we have single resonance lines for both the ^{27}Al and ^{31}P NMR spectra confirming the structural congruence of SAPO-5 with $AlPO_4$-5. The ^{31}P MAS NMR spectrum of the precursor SAPO-5 has a shoulder to high-frequency not previously observed for $AlPO_4$-5. This additional resonance is no longer visible after calcination suggesting that it arises from interaction of the organic template with framework phosphorus nuclei.

^{27}Al MAS NMR spectra of both the precursor and calcined SAPO-5 were also acquired at 78.2 MHz (300 MHz proton) by A.N. Wilson of K.S.L.A. (Shell Research B.V.), Amsterdam. The experimental chemical shifts and linewidths are presented in Table 6.13.

Assuming the values of the quadrupole coupling constant and the asymmetry parameter to be those of $AlPO_4$-5 (as determined by Müller *et*

sample	experimental chemical shift/(ppm)	linewidth (Hz)
precursor SAPO-5	36.8	900
SAPO-5	33.0	800

Table 6.13

^{27}Al chemical shifts (at 78.2 MHz) and linewidths for precursor SAPO-5 and SAPO-5

al.[235]) and using equation 6.1 one can calculate the corrected ^{27}Al chemical shift. The results are shown in Table 6.14. As was observed for $AlPO_4$-5 (HSZ-1297), the experimental chemical shifts determined at the two different field strengths are quite similar. The same arguments used for $AlPO_4$-5 (section 6.2.1.) can be invoked, and once again, it is questionable as to whether a correction factor is desirable at 4.7 T (50.1 MHz) as the calculated, field-independent ^{27}Al chemical shifts are grossly in error.

^{29}Si MAS NMR spectra of both the precursor and calcined forms of SAPO-5 exhibit only a single broad resonance line with a chemical shift of *ca.* -92.0 ppm. A single resonance line would be expected if the silicon atoms were preferentially substituting for either P or Al atoms,

sample	corrected ^{27}Al chemical shift/(ppm) 50.1 MHz	78.2 MHz
precursor SAPO-5	50.0	43.6
SAPO-5	47.9	39.8

Table 6.14

Corrected (field-independent) ^{27}Al chemical shifts at 50.1 and 78.2 MHz

but not *both*. Lok *et al.*[224] consider that (i) Si substitution for P and (ii) simultaneous substitution of two Si for one P and one Al are more likely to occur than (iii) Si substitution for Al. Their preparation (Lok *et al.*, Patent example 13) apparently possesses cation exchange properties. This, coupled with the small excess of Al over P, tends to support their claim for likely substitution preferences for Si atoms in SAPO-5. If route (ii) was the predominant mode of substitution, *two* ^{29}Si signals (within the limits of resolution) should be observed corresponding to the two possible environments of the Si atoms in the lattice [Si(4Al) and Si(4P)]. This appears not to be the case. (The ^{29}Si NMR resonances are broad which could be due to the strain put on the bond angles leading to distorted SiO_4 tetrahedra in the framework following Si substitution into a perfectly ordered Al,P lattice.) The absence of a signal at *ca.* -112 ppm shows there are no large clusters of SiO_2 or extra-framework silica present in the sample. One reasonable conclusion is that route (i) is the dominant route for Si substitution. The ^{29}Si chemical shift (*ca.* -92.0 ppm) is however an unusual one for silicon atoms surrounded by four aluminium atoms. [Although it is relevant to note that the ^{29}Si chemical shift (-89.1 ppm) in zeolite A is observed for Si in an Si(4Al) environment.] The unusual shift for SAPO-5 may be caused by strained angles at silicon atoms and/or by the influence of nearest neighbour phosphorus atoms (the degree of silicon substitution for phosphorus is small). It is interesting to note here that on calcination of the precursor SAPO-5 to give SAPO-5, the ^{29}Si linewidth increases from 200 Hz to 260 Hz while both the ^{31}P and ^{27}Al linewidths decrease. It would seem that whilst the structure can adopt a more comfortable configuration on removal of the template (as evinced by the decrease in the ^{27}Al and ^{31}P linewidths), the presence of silicon

causes strain in the structure. It is thus to be expected that although the level of Si substitution is known to be variable, the total lattice substitution is low. Alternatively, it is possible that route (ii) is dominant, with substitution at contiguous AlO_4 and PO_4 tetrahedra and that the resolution is inadequate to distinguish between the two Si environments. One argument against this is that as the level of Si substitution is only *ca.* 5% by weight, not all the P atoms will be substituted. Thus more than one environment might be expected for the phosphorus nuclei and therefore more than one ^{31}P MAS NMR chemical shift should be observable (although the intensity of any other peaks would probably be vanishingly small). No second phosphorus resonance is observed in the ^{31}P NMR spectrum.

To clarify the situation with regard to the mode of Si substitution, the sample of SAPO-5 in question was cation exchanged (1M KCl solution, four times at 90°C, each time for 4 h followed by thorough washing with distilled water to remove all traces of Cl^- ions - no reaction with aqueous silver nitrate). XRF analysis revealed that SAPO-5 does indeed have K^+ exchange capacity, the sample analysing as:

$$(Na,K)^+_{0.071}(SiO_2)_{0.095}(PO_2)^+_{1.000}(AlO_2)^-_{1.107}$$

with no trace of Cl^-. The excess of aluminium is roughly balanced by the amount of cations in the sample and the silicon substitution level. It therefore seems most likely that route (i) is the dominant substitution *i.e.* SiO_2 replaces PO_2^+ in the framework of SAPO-5. Figure 6.12 shows the ^{13}C CP/HPD MAS NMR spectrum of the organic template in SAPO-5. Table 6.15 lists the observed solid-state ^{13}C chemical shifts and linewidths.

The experimental ^{13}C NMR chemical shift values for the unknown

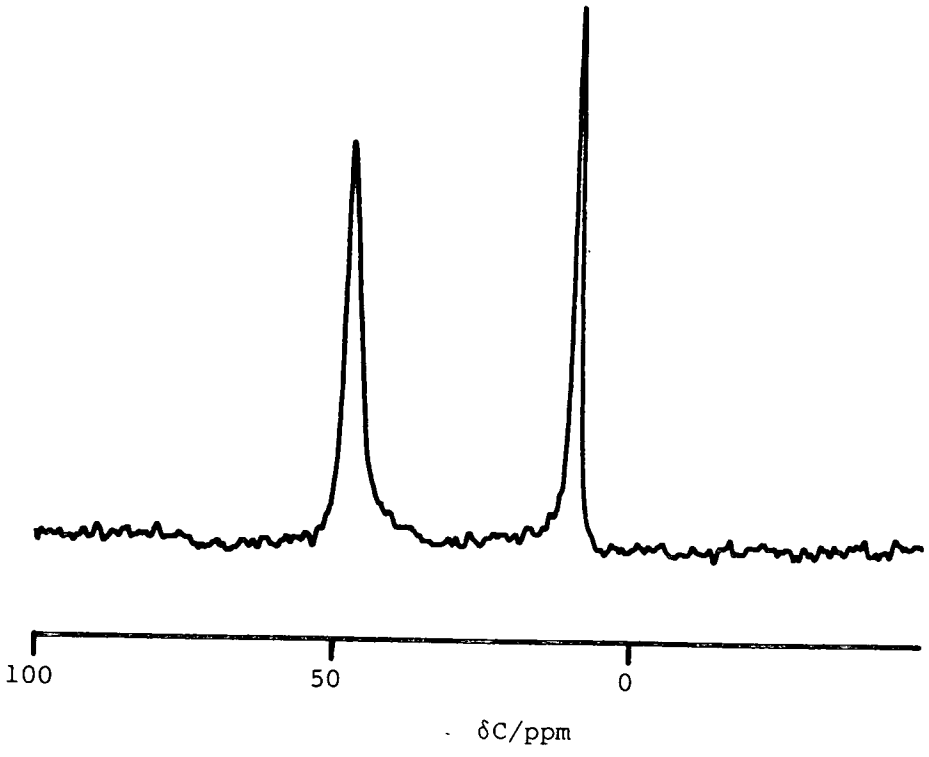

SF = 50.3 MHz; RD = 5 s; SW = 10 kHz; SI = 2 K; TD = 1 K; NT = 1200; CT = 1 ms; SS = 4.0 kHz; SR = 0.382.

Figure 6.12

^{13}C CP/HPD MAS NMR spectrum of Et_3N in Et_3N-SAPO-5

precursor of SAPO-5 (HSZ-1345) identify it to be triethylamine (Et_3N).

sample state	^{13}C chemical shift/(ppm)	
	CH_2	CH_3
Et_3N liquid	46.9	12.6
Et_3N-SAPO-5	48.0 (120 Hz)	9.6 (55 Hz)

Table 6.15

^{13}C NMR chemical shifts for Et_3N

As was observed for $AlPO_4$-5, ^{31}P CP is possible both before and after calcination and again water molecules or hydroxyl groups must be responsible for the ^{31}P CP signal following calcination.

(2) SAPO-5 (HSZ-1206)

From the XRD traces for the precursor (not shown) and calcined forms (Figure 6.13) of SAPO-5 (HSZ-1206), it is apparent that on calcination a large percentage of the structure collapsed to form an amorphous mass. However, even before calcination *i.e.* in the precursor form, the sample contained some boehmite and possibly some amorphous material. XRF measurements show the sample has a much higher silicon level in the product material compared with HSZ-1345. It analyses as (normalised to one mole of PO_2^+): 1.0(PO_2^+); 0.77(SiO_2); 1.285(AlO_2^-).

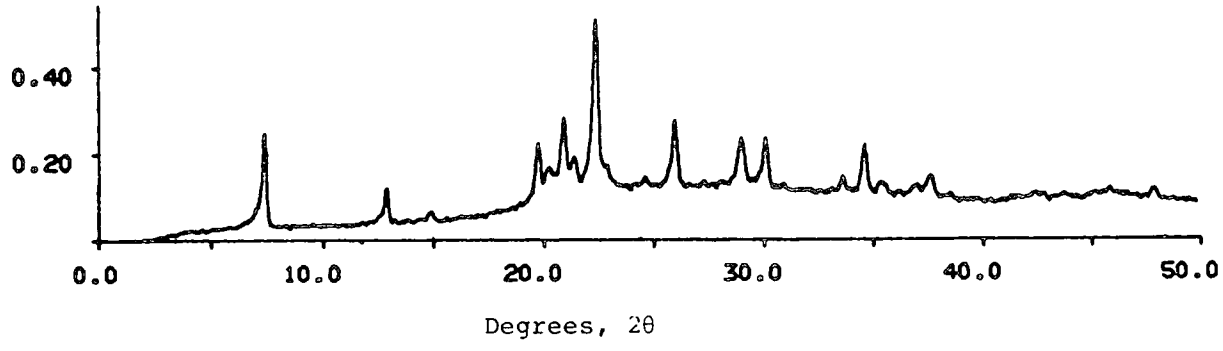

Figure 6.13

Powder XRD trace for calcined SAPO-5 (HSZ-1206)

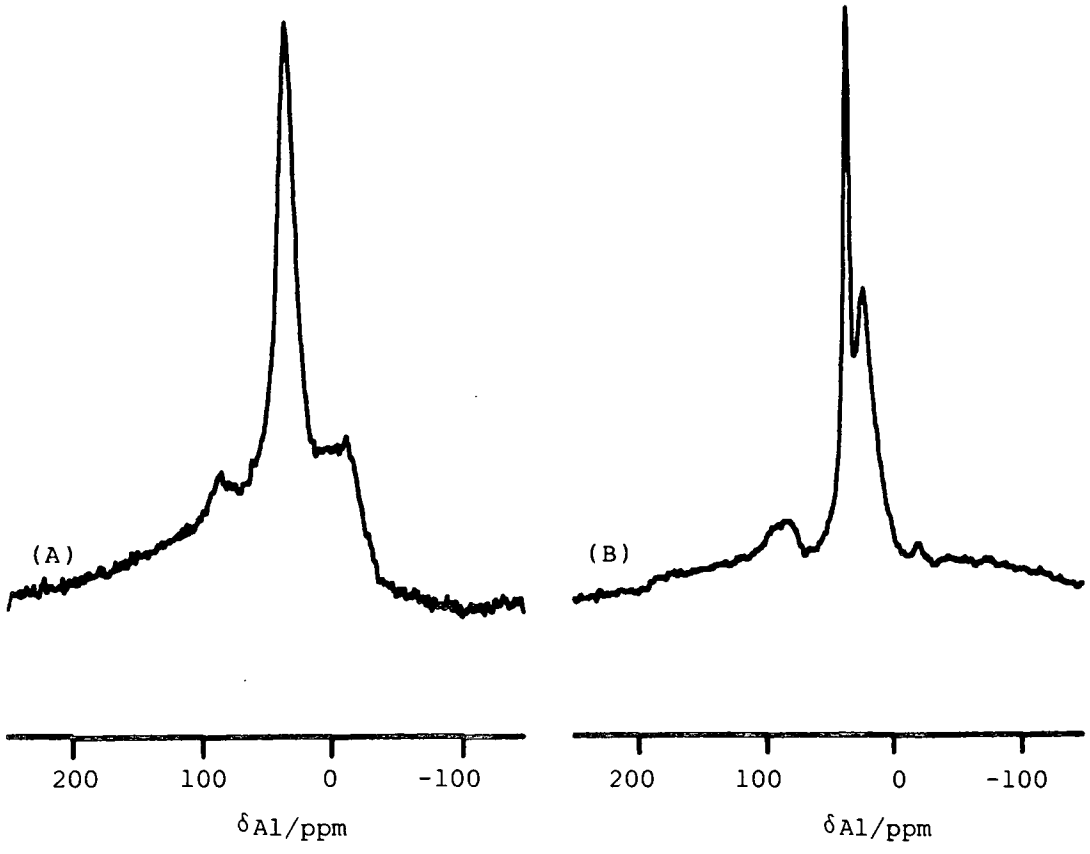

SF = 52.1 MHz; RD = 1 s; SW = 50 kHz; SI = 2 K; TD = 1 K; NT = 400 (as-synthesised), 140 (calcined); SS = 3.3 kHz; SR = 34477.

Figure 6.14

^{27}Al MAS NMR spectra of (A) as-synthesised, and (B) calcined SAPO-5 (HSZ-1206)

Figure 6.14 shows the ^{27}Al NMR spectra of TEA-SAPO-5 and SAPO-5. The NMR data for the spectra are shown in Table 6.16 together with ^{31}P NMR data (spectra not shown).

The boehmite impurity present in the precursor material is clearly discernible in the ^{27}Al NMR spectrum [Figure 6.14(A)]. Calcination of this particular sample seems to have a similar effect as was previously observed for $AlPO_4$-11 (section 6.2.2.). The ^{27}Al NMR spectrum of the

sample	^{31}P NMR		^{27}Al NMR[a)]	
	chemical shift/(ppm)	linewidth (Hz)	chemical[a)] shift/(ppm)	linewidth (Hz)
TEA-SAPO-5	-27.2	880	33.0	1070
SAPO-5	-29.6	450	36.3	300
			23.2	—

a) Experimental values (*i.e.* field dependent)

Table 6.16

^{31}P and ^{27}Al MAS NMR chemical shifts and linewidths for SAPO-5 (HSZ-1206).

calcined material is alomst identical to that recorded for calcined $AlPO_4$-11. Accordingly, the resonances can be assigned to the formation of a polymorph of $AlPO_4$ and boehmite plus possibly some remaining SAPO-5. The most intense peak in the powder XRD traces of both calcined $AlPO_4$-11 and calcined SAPO-5 (HSZ-1206) is due to $AlPO_4$-crystobalite, a dense polymorph of $AlPO_4$.

The ^{29}Si MAS NMR spectrum of the precursor form of SAPO-5 (HSZ-1206)(Figure 6.15) shows only a single, broad (linewidth = 475 Hz), featureless resonance with a chemical shift of -111.5 ppm. Therefore there has been no silicon substitution into the $AlPO_4$-5 lattice in this sample and all the silicon is present as amorphous silica. It would appear that far from increasing the level of lattice substitution on going to higher loadings of silicon in the reaction mixture, no silicon is actually substituted, and so low loadings are actually to be preferred. No template study was undertaken.

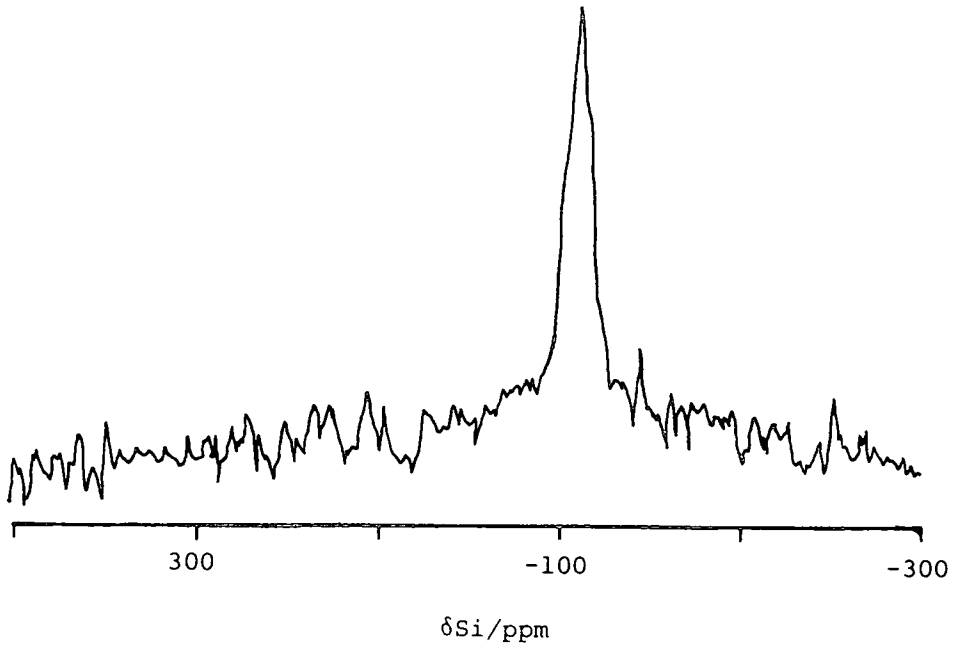

SPE; SF = 59.5 MHz (Varian VXK-360); RD = 30 s; SW = 20 kHz; SI = 2 K; TD = 1 K; NT = 1900; LB = 100.

Figure 6.15

^{29}Si MAS NMR spectrum of SAPO-5 (HSZ-1206)

(3) SAPO-5 (019S)

This sample analysed as (normalised to one mole of PO_2^+): 1.0 (PO_2^+); 0.28 (SiO_2); 1.334 (AlO_2^-), and so has a silicon loading intermediate to that of the two previous SAPO-5 samples. The sample is powder XRD "pure", that is, any impurities that may exist in the sample are below the detection limits of powder XRD techniques.

Table 6.17 collates the ^{31}P and ^{27}Al NMR data for this sample (spectra not shown). The ^{31}P and ^{27}Al MAS NMR shifts and linewidths are similar to those observed for (HSZ-1345) SAPO-5. The ^{29}Si MAS NMR spectrum however is identical to that observed for (HSZ-1206) SAPO-5.

sample	^{31}P NMR		^{27}Al NMR[a)]	
	chemical shift/(ppm)	linewidth (Hz)	chemical[a)] shift/(ppm)	linewidth (Hz)
TPAOH-SAPO-5	-29.3	710	37.5	900
SAPO-5	-29.7	500	34.7	840

a) Experimental values (*i.e.* field dependent)

Table 6.17

^{31}P and ^{27}Al MAS NMR chemical shifts and linewidths for TPAOH-SAPO-5 and SAPO-5 (019S).

The single ^{29}Si resonance line is very broad (linewidth = 500 Hz) and is centred at -110.8 ppm. It would appear that in common with the previous example, no silicon substitution has taken place and the apparent ^{29}Si signal is due to extra-lattice silicon present as amorphous silica.

The ^{27}Al NMR spectrum of fully hydrated calcined SAPO-5 (019S) is shown in Figure 6.16. The broad base is due to extra-lattice aluminium (the XRF analysis shows a large excess of AlO_2^-).

Figure 6.17 shows the ^{13}C CP/HPD MAS NMR spectrum of the template of SAPO-5 (019S), tetra-*n*-propylammonium hydroxide (TPAOH) present in SAPO-5 as the TPA^+ cation. Table 6.18 shows the solution-state and solid-state ^{13}C NMR chemical shifts.

In previous investigations using ^{13}C CP/HPD MAS NMR to investigate the structure and position of the organic template in high-silica zeolite syntheses, several research groups reported[144,145] the splitting of the CH_3 group resonance into two peaks of almost equal intensity (the splitting being *ca.* 1 ppm), apparently due to TPA ions in different environments. This splitting is not observed for TPAOH in SAPO-5

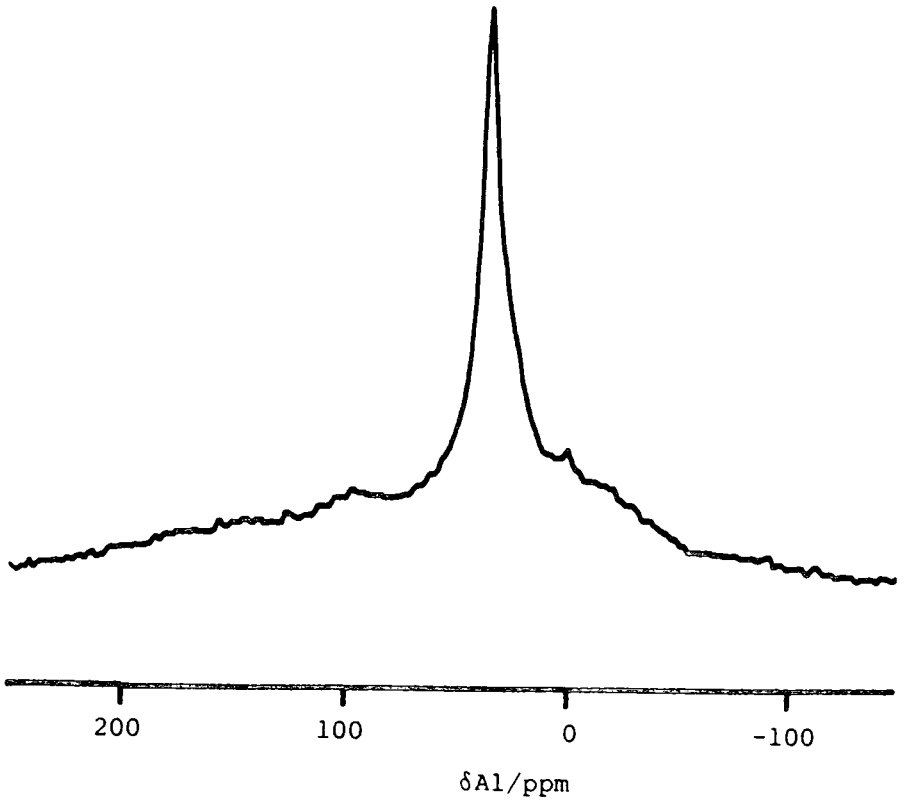

SF = 52.1 MHz; RD = 2 s; SW = 100 kHz; SI = 2 K; TD = 1 K; NT = 1100; SS = 3.0 kHz; PD = 2 μs; PA = π/6; SR = -2417.9.

Figure 6.16

^{27}Al MAS NMR spectrum of hydrated, calcined SAPO-5 (019S)

(019S). However, a splitting is not to be expected as only one type of channel, and hence one environment, exists for the TPA^+ cations in SAPO-5.

sample state	^{13}C NMR chemical shifts/(ppm) (N.CH_2)	(CH_2)	(CH_3)	Δδ/(ppm)
TPAOH (aq)	62.6	16.3	11.3	51.3
TPA in SAPO-5 (019S)	61.5	15.7	13.5	48.0
TPABr (solid)[145]	60.0	15.9	12.6	47.4

Table 6.18

^{13}C NMR chemical shifts for TPAOH

To summarize, for SAPO-5 NMR has been shown to be able to provide information on the mode of silicon substitution into the aluminophosphate lattice. NMR can also readily distinguish lattice from extra-lattice silicon even when the silica cannot be readily detected using powder XRD techniques.

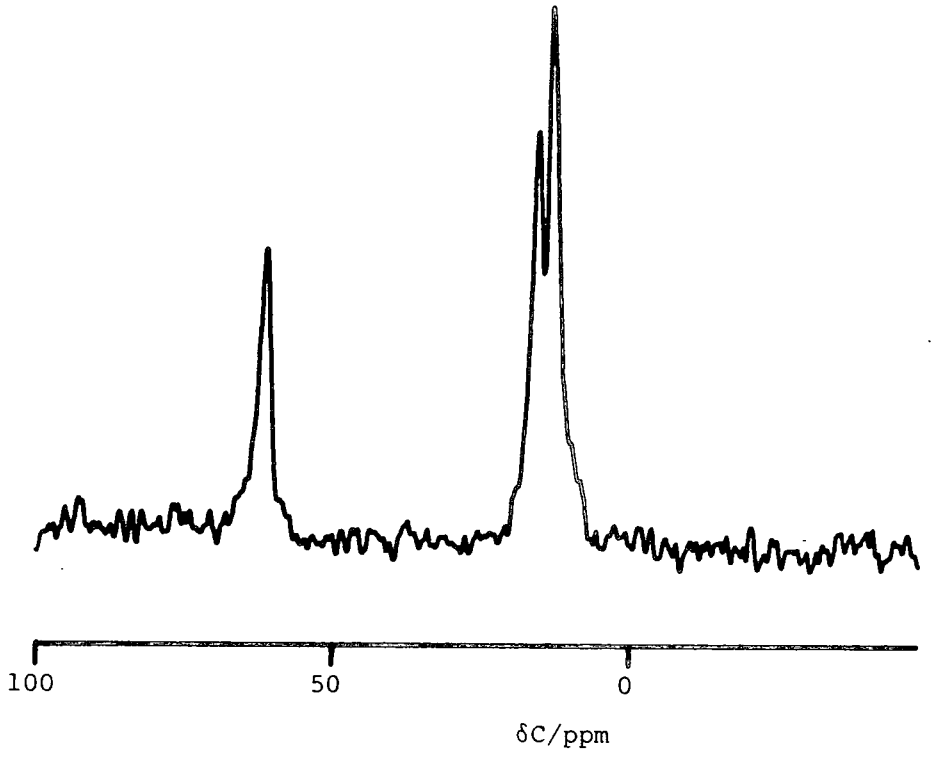

SF = 50.3 MHz; RD = 5 s; SW = 10 kHz; SI = 2 K; TD = 2 K; NT = 2350; SS = 4.0 kHz; CT = 1 ms; LB = 10 Hz; SR = 0.382.

Figure 6.17

^{13}C CP/HPD MAS NMR of TPAOH [template for SAPO-5 (019S)]

6.3.2. SAPO-20 (021S)

SAPO-20 is identified as being structurally analogous to TMA-sodalite on the basis of its similar X-ray powder diffraction pattern. Table 6.19 presents the XRD data for precursor and calcined forms of Laporte-synthesised SAPO-20 with UCC SAPO-20 and Laporte TMA-sodalite (RD 696/85).

(i) UCC SAPO-20			(ii) Precursor SAPO-20 (Laporte)		
d (Å)	2θ	I/I_{max} x 100	d (Å)	2θ	I/I_{max} x 100
6.28	14.1	40	6.4	13.7	80
4.46	19.9	41	4.5	19.4	40
4.00	22.2	5	4.04	21.9	5
3.65	24.4	100	3.69	24.1	100
3.16	28.2	13	3.18	28.0	11
2.84	31.5	11	2.85	31.4	12
2.58	34.7	14	2.60	34.4	15
2.24	40.2	4	2.25	39.9	4
2.11	42.9	6	2.12	45.5	6
1.91	47.7	5	1.92	47.4	4

(iii) calcined SAPO-20 (Laporte)			(iv) TMA-sodalite (Laporte RD 696/85)		
d (Å)	2θ	I/I_{max} x 100	d (Å)	2θ	I/I_{max} x 100
6.40	13.7	83	6.63	13.2	33
4.50	19.4	38	4.60	19.2	43
4.04	21.9	8	—	—	—
3.69	24.1	100	3.75	23.7	100
3.18	28.0	23	3.23	27.6	19
2.85	31.4	21	2.87	31.1	24
2.60	34.4	26	2.58	34.1	24
2.25	39.9	9	2.27	39.7	8
2.12	45.5	8	2.13	42.5	16
1.92	47.4	14	1.92	47.2	12

Table 6.19

Powder X-ray data for SAPO-20 samples

and TMA-sodalite (major lines only)

It is relevant to note here that although there are some variations in relative intensities between the samples of SAPO-20, many of the major lines match closely in d-spacings. The differences may be due to ordering of the Al and Si/P in the framework and the different extra-framework constituents in the two compositions.

In common with TMA-sodalite, the organic template used in the synthesis of SAPO-20 (also $AlPO_4$-20) is the tetramethylammonium ion. This appears to be the only template with which SAPO-20 can be made. The framework structure of sodalite (see Figure 3.2c, p. 35) consists entirely of sodalite units packed together. Each sodalite cage is bounded by 4- and 6-rings. As the TMA^+ ion is much too large to enter the framework after crystallization, it must be trapped or enclathrated by the crystallizing sodalite cages.

The Laporte sample analyses as (normalised to one mole of PO_2^+): 1.0 (PO_2^+); 0.37 (SiO_2); 1.28 (AlO_2^-). The ^{31}P and ^{27}Al MAS NMR spectra for SAPO-20 are shown in Figure 6.18. The data relevant to this discussion are presented in Table 6.20. According to powder XRD,

	^{31}P NMR		^{27}Al NMR[a)]	
sample	chemical shift/(ppm)	linewidth (Hz)	chemical[a)] shift/(ppm)	linewidth (Hz)
TMA-SAPO-20	-34.0 -23.8 (-17.0)	320	30.9 15.9	1850
SAPO-20	-35.2	550	29.8	1850

a) Experimental values (*i.e.* field dependent)

Table 6.20

^{31}P and ^{27}Al MAS NMR chemical shifts and linewidths for SAPO-20.

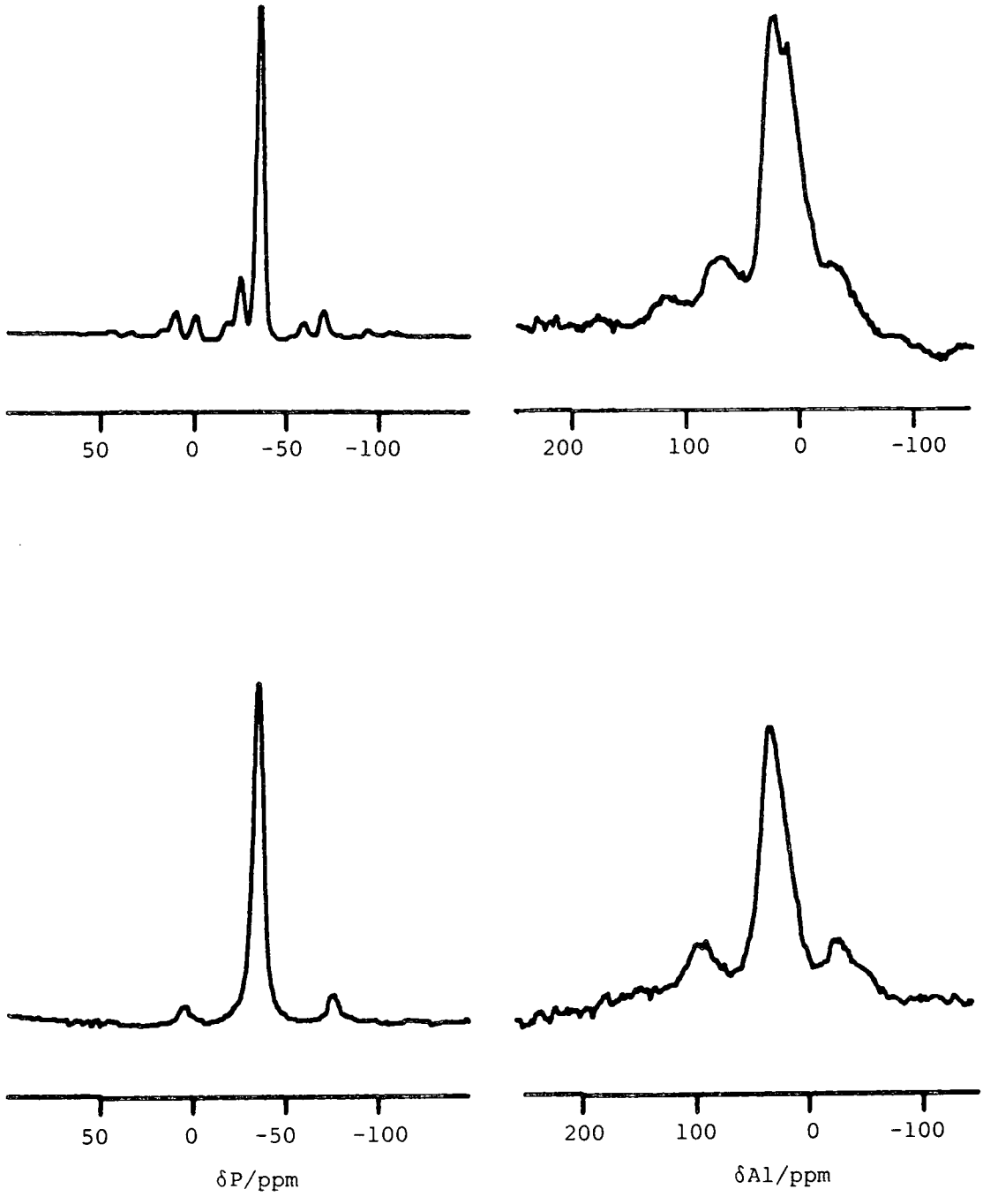

^{31}P CP/HPD: SF = 81.01 MHz; RD = 6 s; SW = 20 kHz; SI = 2 K; TD = 1 K; NT = 16; SS = 3.0 kHz; CT = 2 ms; SR = 856 (precursor), 105.9 (calcined)

^{27}Al SPE: SF = 52.1 MHz; RD = 1 s; SW = 50 kHz; SI = 2 K; TD = 1 K; NT = 4000 (precursor), 1500 (calcined); SS = 3.0 kHz; PD = 1 μs; PA = π/6; SR = -2350.

Figure 6.18

^{31}P (left) and ^{27}Al (right) MAS NMR spectra of precursor (upper) and calcined (lower) forms of SAPO-20

^{31}P resonance/(ppm)	T_1 value (s)
-34.0	52.0
-23.8	47.9

Table 6.21

^{31}P spin-lattice relaxation times for TMA-SAPO-20.

calcination does not destroy the lattice of SAPO-20. However, changes are observed in both the ^{27}Al and ^{31}P NMR spectra of the calcined form of SAPO-20 relative to the as-synthesised form. The most striking change is the formation of only one phosphorus site following calcination. This resonance is slightly shifted to lower frequency and is substantially broader than the most intense resonance observed for TMA^+-SAPO-20. This change in the ^{31}P NMR spectrum is unexplained.

The shoulder visible to lower frequency of the most intense peak in the ^{27}Al NMR spectrum is no longer visible following calcination. In order to clarify whether this shoulder is actually the manifestation of quadrupolar effects on the ^{27}Al resonance, or a separate ^{27}Al signal, higher magnetic field experiments would need to be performed. Calcination does not seem to affect significantly the linewidth of the ^{27}Al NMR resonance line.

The phosphorus spin-lattice relaxation times (T_1) were determined for the precursor compound using the inversion-recovery pulse sequence. The values are presented in Table 6.21. It would appear that, in common with the T_1 values as found for $AlPO_4$-5, $AlPO_4$-11, and SAPO-5, the phosphorus T_1 values for the phosphorus sites in SAPO-20 are quite long. These long T_1 values pose little problem to the NMR spectroscopist

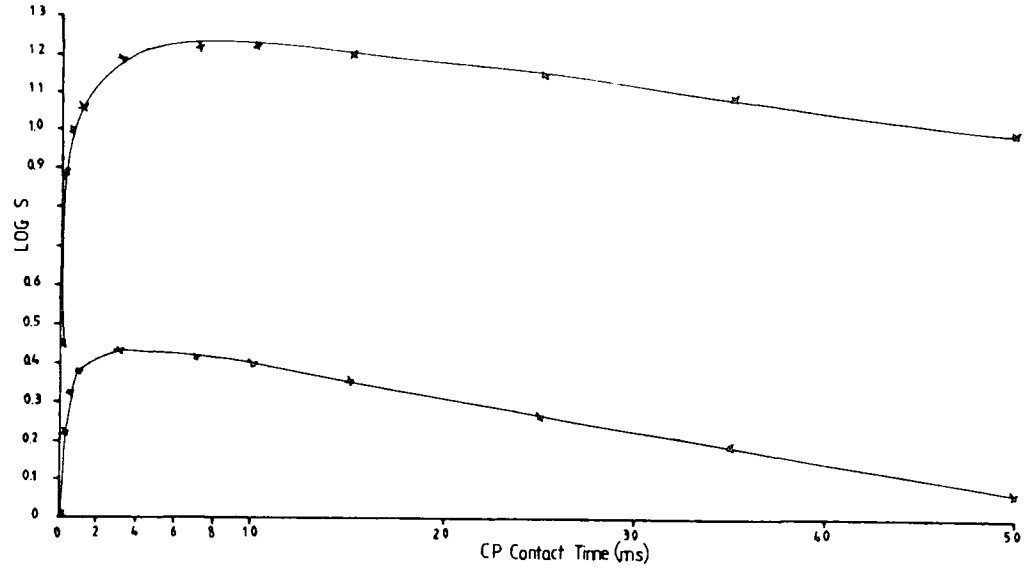

Figure 6.19

Plot of the log of the ^{31}P CP/HPD signal *versus* CT (ms)

however, as (i) the flip-angle (α_ϵ) can be reduced according to:

$$\cos \alpha_\epsilon = \exp (-RD/T_1)$$

and (ii), ^{31}P CP is possible with SAPO-20 (the recycle delay depends then, not on T_1 of the ^{31}P nucleus, but on that of the abundant nucleus, (I), in this case, the proton. Figure 6.19 shows a graph of the logarithm of the ^{31}P CP/HPD signal intensity plotted against the varying CP contact time (CT). The graph shows that the cross-polarization rates (T_{CP}^{-1}) appear to be similar for both the (major) phosphorus resonances, and that the (^1H) $T_{1\rho}$ values for the two resonances are similar, though apparently not identical. Direct measurement of the proton relaxation time in the rotating frame using wide-line NMR techniques in conjunction with a computer program (developed by Mr. B.J. Say and Dr. A. Kenwright) that allows fitting of the data according to a multi-exponential decay

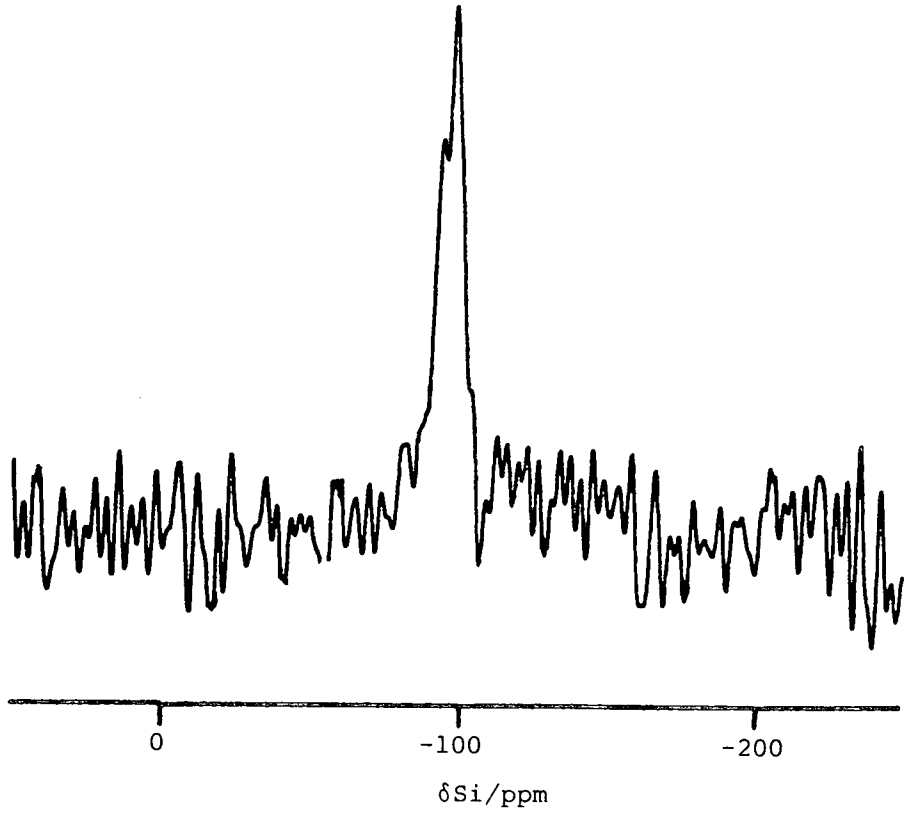

SF = 39.7 MHz; RD = 60 s; SW = 20 kHz; SI = 2 K; TD = 1 K; NT = 586; SS = 3.8 kHz; PD = 3 μs; PA = π/3; LB = 20 Hz; SR = 13200.

Figure 6.20

^{29}Si SPE MAS NMR spectrum of TMA-SAPO-20.

using an iterative least squares fitting procedure, showed that the signal from the sample could best be fitted to two components. This surprising result indicates that the sample does not possess full proton spin diffusion.

Figure 6.20 shows the ^{29}Si SPE MAS NMR spectrum for as-synthesised SAPO-20. There appear to be at least two silicon sites in the spectrum. The chemical shifts of the two clearly discernible resonances (-92.3, -97.2 ppm) are similar to those observed for SAPO-5. Unfortunately no crystal structure has been published for SAPO-20. However, it is

possible that inequivalent silicon sites exist in the unit cell, as is observed for SAPO-34 (*vide infra*).

Figure 6.21 shows the ^{13}C CP/HPD MAS NMR spectrum of the template (TMAOH) of SAPO-20. Table 6.22 presents the ^{13}C data for TMA^+ in solution and in sodalite, as well as in SAPO-20.

The symmetrical nature and linewidth of TMA^+ in SAPO-20 suggests that SAPO-20 has β-cages of a similar size to sodalite and that there is little interaction of the template with the framework. ^{31}P CP is probably therefore due to framework-water molecule interactions.

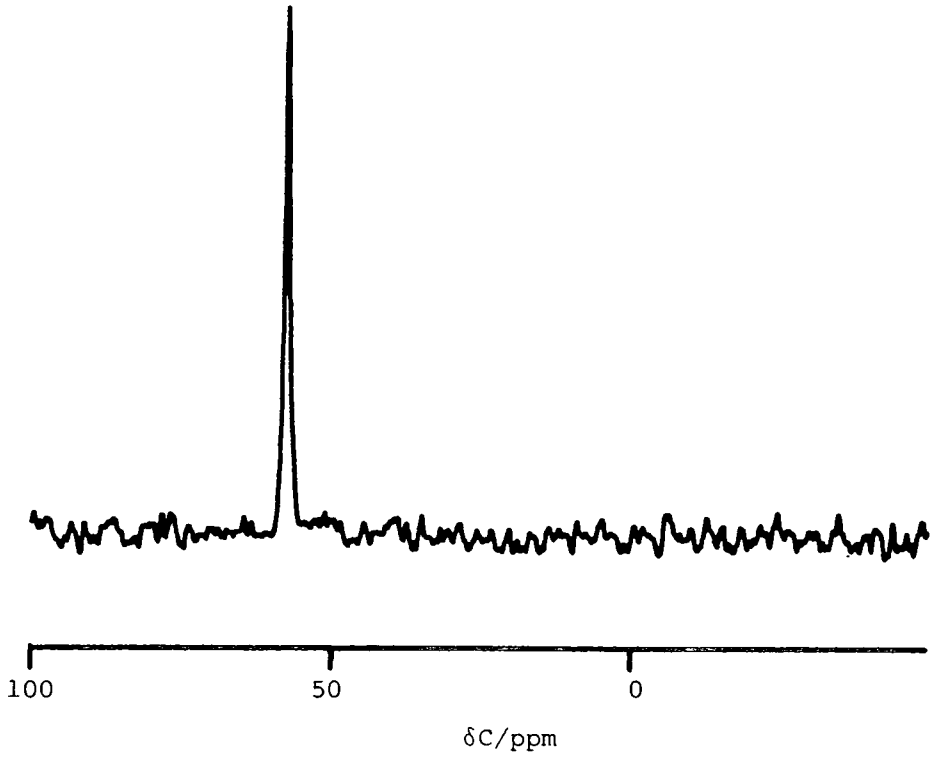

SF = 50.3 MHz; RD = 5 s; SW = 10 kHz; SI = 2 K; TD = 2 K; NT = 440; SS = 3.7 kHz; CT = 1 ms; SR = 0.382.

Figure 6.21

^{13}C CP/HPD MAS NMR spectrum of TMA^+ in SAPO-20.

	^{13}C NMR	
sample	chemical shift/(ppm)	linewidth (Hz)
TMA (aq)	56.4	—
SAPO-20	58.3	23
sodalite	58.5	22

Table 6.22

^{13}C NMR data for TMA^+.

6.3.3. SAPO-34 (057)

SAPO-34 is, by comparison of the X-ray powder diffraction patterns, structurally analogous to the natural zeolite, chabazite (see Figure 3.4). Table 6.23 lists the XRD data obtained for Laporte-synthesised SAPO-34 and compares it with that of U.C.C. SAPO-34. Figure 6.22 shows the powder XRD traces for the precursor and calcined forms of SAPO-34. The Laporte SAPO-34 sample analysed as (normalised to one mole of PO_2^+): 1.0 (PO_2^+); 0.06 (SiO_2); 1.25 (AlO_2^-).

Figure 6.23 shows the ^{31}P and ^{27}Al MAS NMR spectra for both the precursor and calcined forms of SAPO-34. The NMR data are presented in Table 6.24.

It is obvious from Figure 6.22 that, on calcination, the microporous structure of the precursor form of SAPO-34 collapses and the sample becomes amorphous. This structure change is reflected in the chemical shift and linewidth changes in both the ^{31}P and ^{27}Al MAS NMR spectra. The two ^{31}P resonances collapse or rearrange to give one shifted resonance following calcination. The single ^{27}Al NMR resonance line is also shifted and its linewidth doubled. It is most likely that a polymorph of $AlPO_4$ has been formed on calcination as was observed for

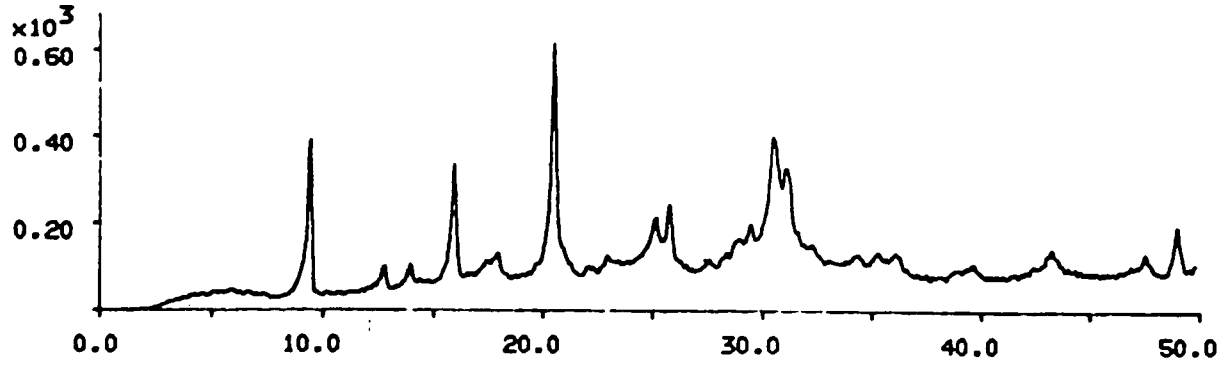

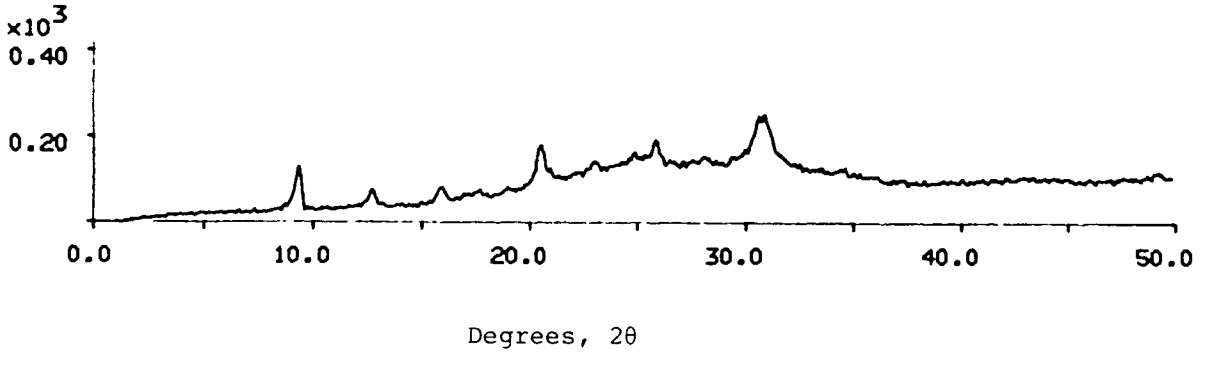

Figure 6.22

Powder XRD-traces for SAPO-34, (A) precursor, (B) calcined.

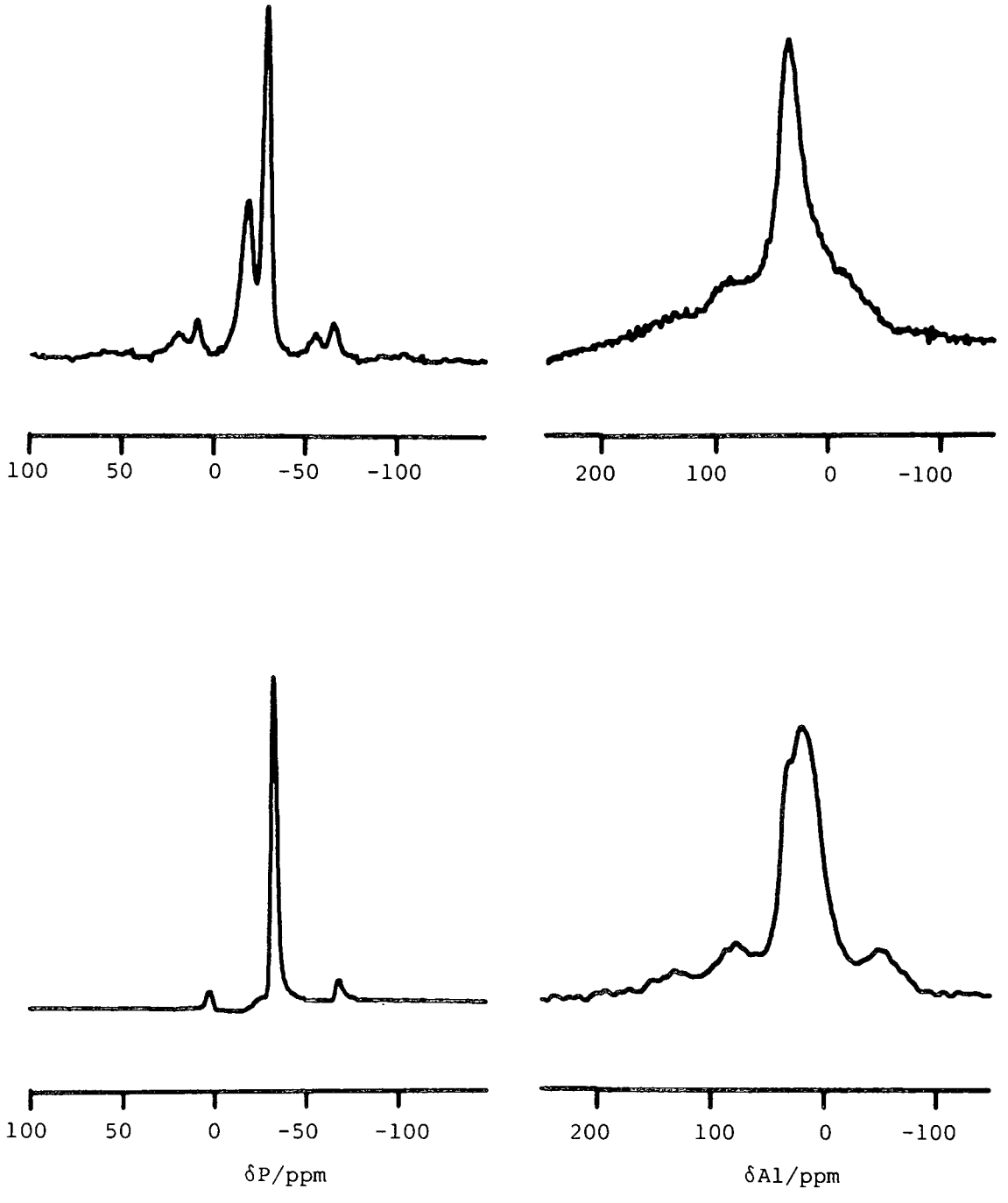

^{31}P SPE (no HPD): SF = 81.01 MHz; RD = 30 s; SW = 30 kHz; SI = 2 K; TD = 1 K; NT = 12; SS = 3.0 kHz; PD = 4 μs; PA = 2π/5; SR = 218 (precursor), 105.9 (calcined).

^{27}Al: SF = 52.1 MHz; RD = 0.5 s; SW = 50 kHz; SI = 2 K; TD = 1 K; NT = 500 (precursor), 4000 (calcined); SS = 3.3 kHz; PD = 1 μs; PA = π/6; SR = -2344.

Figure 6.23

^{31}P (left) and ^{27}Al (right) MAS NMR spectra of the precursor (upper) and calcined (lower) forms of SAPO-34

(i) U.C.C. SAPO-34			(ii) Precursor SAPO-34 (Laporte)		
d (Å)	2θ	I/I_{max} x 100	d (Å)	2θ	I/I_{max} x 100
9.31	9.5	100	9.20	9.6	100
6.86	12.9	11	6.91	12.8	11
6.30	14.0	10	6.32	14.0	8
5.52	16.0	50	5.53	16.0	44
4.93	18.0	11	4.92	18.0	8
4.31	20.6	73	4.31	20.6	68
3.53	25.2	14	3.53	25.2	10
3.45	29.5	14	3.45	25.8	14
3.03	29.5	4	3.03	29.5	5
2.93	30.5	24	2.92	30.6	19
2.87	31.2	18	2.86	31.3	14

Table 6.23

Powder XRD data for SAPO-34

$AlPO_4$-11 and SAPO-5 (HSZ-1206).

^{31}P Cross-polarization is possible both before and after calcination. Figure 6.24 shows a plot of the logarithm of the intensity of the two ^{31}P CP resonances in the precursor material *versus* CP contact time (ms). Both resonances appear to have similar CP efficiencies. However, as was observed for SAPO-20, the ^{1}H $T_{1\rho}$ values (determined from the slope of the exponential decay part of the graph) appear to differ.

	^{31}P NMR		^{27}Al NMR[a)]	
sample	chemical shift/(ppm)	linewidth (Hz)	chemical[a)] shift/(ppm)	linewidth (Hz)
TEA-SAPO-34	-23.8	400	35.5	1200
	-17.9	480		
SAPO-34	-29.9	360	18.7	2400

a) Experimental values (*i.e.* field dependent)

Table 6.24

^{31}P CP/HPD and ^{27}Al MAS NMR chemical shifts and linewidths for SAPO-34.

Direct ^{1}H $T_{1\rho}$ measurement confirms that this is indeed the case, and the data could again best be fitted to two components.

In the ^{29}Si MAS NMR spectrum of as-synthesised SAPO-34 two inequivalent ^{29}Si resonances are apparently discernible (see Figure 6.25). The ^{29}Si chemical shifts are of the same magnitude as those observed for SAPO-5 (HSZ-1345), suggesting that silicon substitutes for phosphorus in the SAPO-34 structure.

The crystal structure for the SAPO molecular sieve structurally related to chabazite has recently been published by Ito *et al.*.[237] They report the crystal structure of $H_3O^+.Al_4SiP_3O_{16}^-.nH_2O$. The sample was crystallised using morpholine as the template, but the topology is the same as that of SAPO-34. Ito *et al.* report that the Si atoms are distributed exclusively on the P sites and that there are two inequivalent P sites, and hence two inequivalent Si sites (see Figure 6.26). [It is interesting to note that the $AlPO_4$ version of SAPO-34, $AlPO_4$-34, does not exist (there is no patent example for it). It is

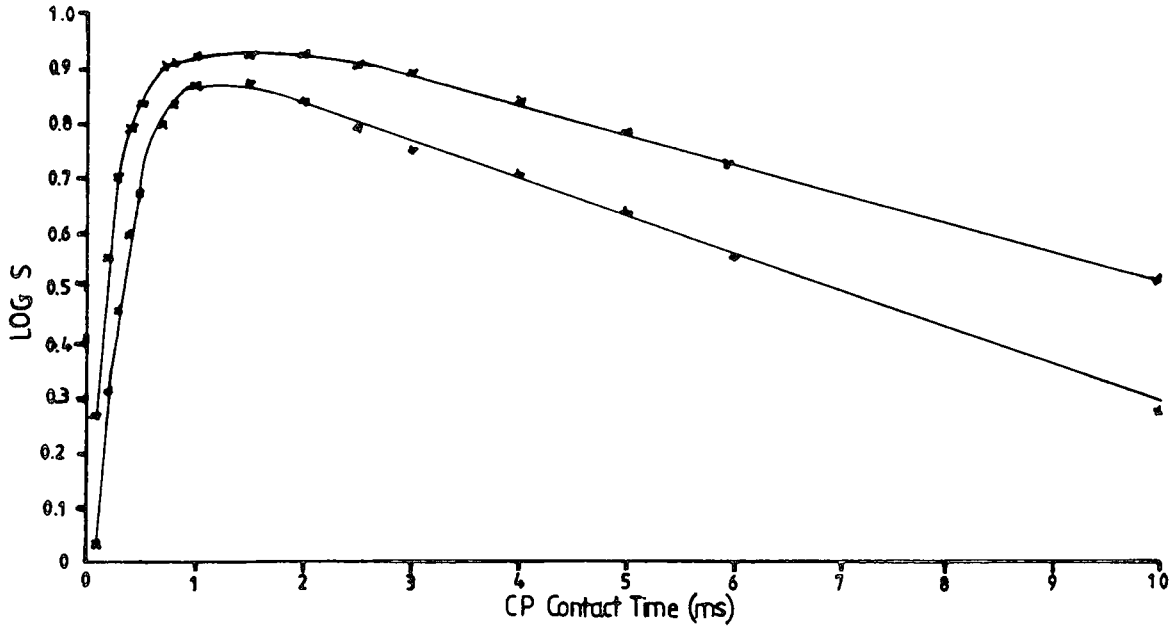

Figure 6.24

Plot of log (signal intensity) versus CP_{CT} (ms)

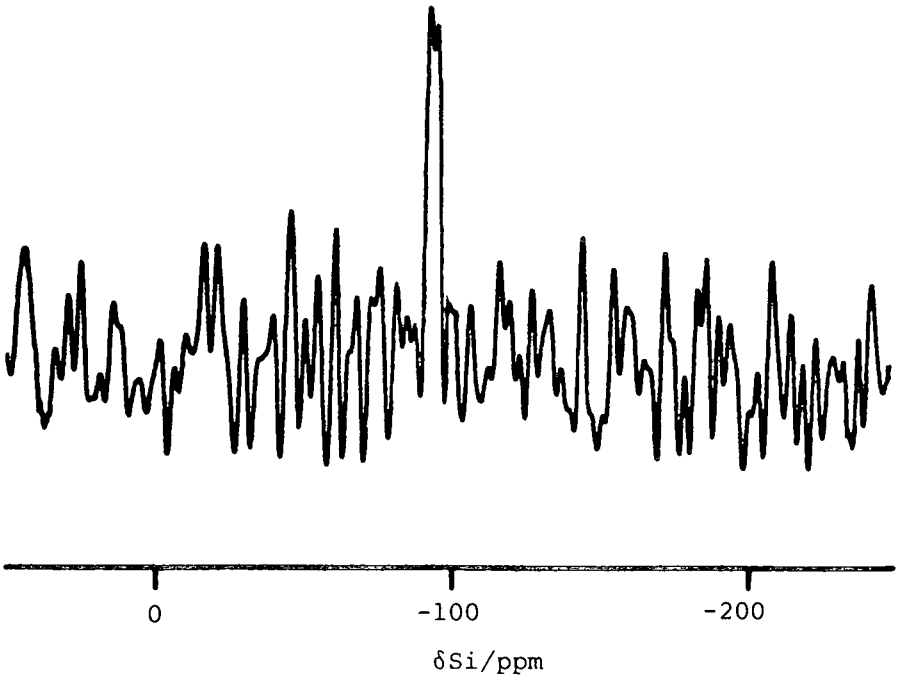

SPE; SF = 39.7 MHz; RD = 60 s; SW = 20 kHz; SI = 2 K; TD = 1 K;
NT = 1900; SS = 3.7 kHz; PD = 5 μs; PA = π/2; LB = 50; SR = 13200.

Figure 6.25

^{29}Si MAS NMR spectrum of TEAOH-SAPO-34

therefore, perhaps, surprising that SAPO-34 exists at all in view of the already discussed strain-inducing effect of silicon substitution into the AlPO lattice - this particular sample of SAPO-34 has an extremely small amount of silicon in the lattice - and not surprising that the sample becomes amorphous on calcination.]

Ito *et al.* quote the "occupancy factors" of the Si atoms on the P sites as 0.1 for P(1) and 0.2 for P(2). These occupancy factors disagree with the ^{29}Si MAS NMR spectrum which indicates almost equal Si occupancy of the two P sites. It should be remembered, however, that the ^{29}Si spin-lattice relaxation times are unknown for SAPO-34 and so it is conceivable that a recycle delay of 60 s is too short and that one or

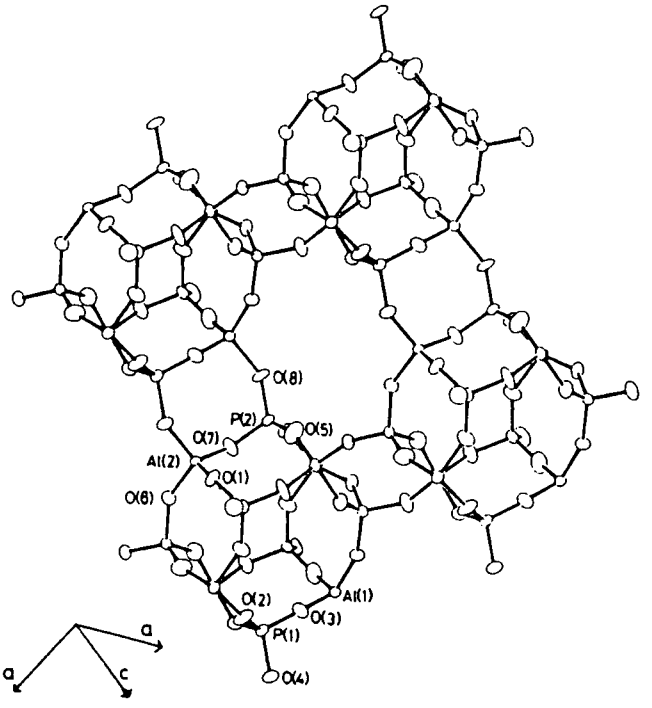

Figure 6.26

ORTEP diagram of the four double hexagonal ring units in SAPO-34. The unique atoms only are labelled. From ref. 237.

other of the two Si sites is being attenuated. The occupancy factors will also, of course, be reflected in the ^{31}P SPE MAS NMR spectrum. The integrated intensities of the two sites are in a ratio of 2:3 (high-frequency *versus* low frequency). The low Si substitution level (*ca.* 5%) cannot be responsible for the difference in intensities of the two phosphorus resonances. From the published space group (Trigonal, R3), one would expect equal populations of phosphorus atoms in the two inequivalent sites before substitution. Thus the ^{31}P MAS NMR data appear to conflict with the XRD data (accepting that the XRF analysis is correct for the Laporte SAPO-34 sample).

Ito *et al.* also report that the substitution of Si for P in framework sites results in an excess of -1e per atom. This may be

charge balanced by protonated water (H_3O^+).

In the Laporte-synthesised SAPO-34, there is a sensible excess of AlO_2^- over PO_2^+ indicating Si substitution for P on framework sites as already discussed. It seems most likely that the excess negative charge is compensated for either by protonated water or by the template TEA^+ cations. The ^{13}C CP/HPD MAS NMR spectrum of the organic template used in the synthesis of SAPO-34 is shown in Figure 6.27. The solid-state ^{13}C chemical shifts are compared to those obtained in solution-state in Table 6.25. The chemical shift difference ($\Delta\delta$) is sufficiently small as to make template interaction with the framework unlikely. Therefore the proton magnetization necessary for ^{31}P CP and compensation for framework

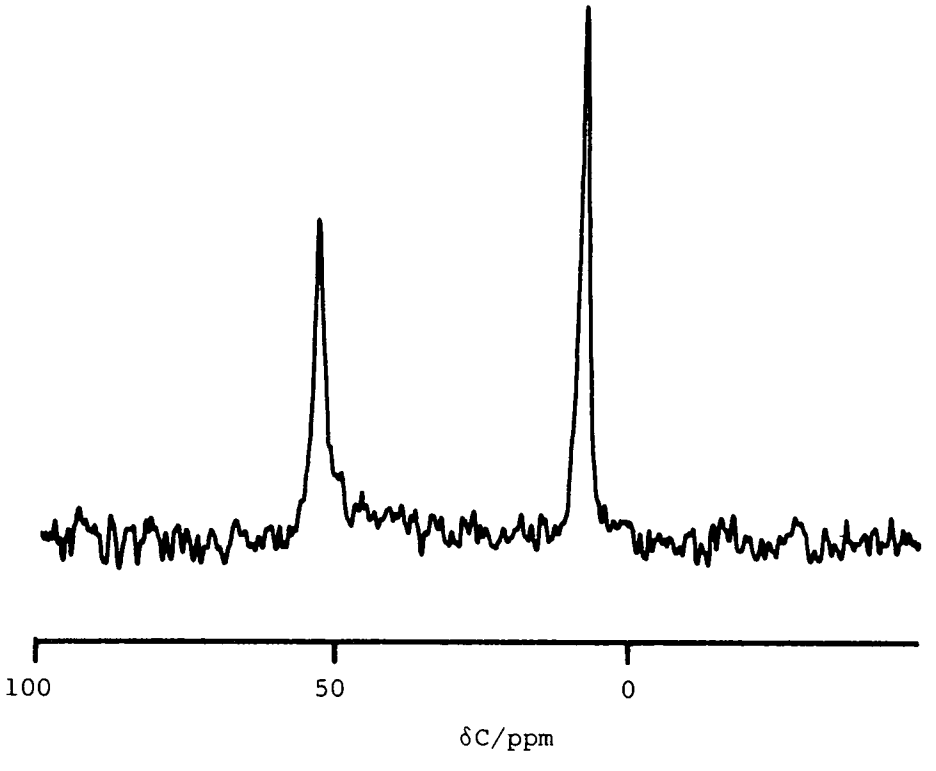

SF = 50.3 MHz; RD = 5 s; SW = 10 kHz; SI = 2 K; TD = 1 K; NT = 1650; SS = 4.0 kHz; CT = 1 ms; SR = 0.382.

Figure 6.27

^{13}C CP/HPD MAS NMR spectrum of TEAOH in SAPO-34.

charge imbalance probably comes from zeolitic water present in the cages of SAPO-34. The T_1 values for the phosphorus atoms are as follows: for the high-frequency peak, 9.7 s, and for the low-frequency peak, 18.1 s (as measured by inversion-recovery).

sample state	^{13}C chemical shifts/(ppm)		$\Delta\delta$/(ppm)
	CH_2	CH_3	
TEAOH (aq)	52.9	7.0	45.9
TEAOH-SAPO-34	53.0	7.4	45.6

Table 6.25

^{13}C NMR chemical shifts for TEAOH

6.4 Other substituted $AlPO_4$ molecular sieves

Recently, Union Carbide have patented various types of molecular sieves having the framework structure composed of MO_2, AlO_2, and PO_2 tetrahedral oxide units. Here M represents at least one element capable of forming framework tetrahedral oxides. They claim the following group of elements can form tetrahedral oxides: arsenic, beryllium, boron, chromium, gallium, germanium, lithium, and vanadium. In the following section, studies of BAPO-5, the boron-substituted analogue of $AlPO_4$-5 using MAS NMR are discussed.

6.4.1. BAPO-5

Two BAPO-5 samples were studied. In the synthesis of HSZ-1337

equal molar quantities of Al_2O_3, B_2O_3, and P_2O_5 were used. For the 032A sample, the molar ratio of Al_2O_3, B_2O_3, and P_2O_5 was 1:1:2. The results discussed for BAPO-5 (HSZ-1337) form the basis of a paper which has recently been accepted for publication.[268]

(1) BAPO-5 (HSZ-1337)

From the powder XRD trace (not shown), BAPO-5 is clearly topologically related to $AlPO_4$-5. Table 6.26 lists the XRD data and uses a U.C.C. BAPO-5 for comparison.

The sample analysed as (normalised to one mole of PO_2^+): 0.05 (BO_2^-); 0.98 (AlO_2^-); 1.00 (PO_2^+). It is relevant to note here that B is not seen in the normal multi-element scan (MES) XRF analysis. Therefore, the MES analysis is normalised to 100% PO_2 and AlO_2 oxides and the B analysis is done by titration on a separate (weighed) sample. The amounts of PO_2 and AlO_2 oxides were recalculated to take the BO_2 into account.

Figure 6.28 shows the ^{27}Al and ^{31}P MAS NMR spectra of both the precursor and calcined/rehydrated forms of BAPO-5. Experimental chemical shifts and linewidths are collated in Table 6.27.

The data are in good agreement with those reported in previous studies on $AlPO_4$-5,[235] confirming the structural congruence of BAPO-5 with $AlPO_4$-5. Substitution of boron into the $AlPO_4$ lattice does not appear to have affected the ^{27}Al or ^{31}P MAS NMR spectra noticeably. This was also the case with SAPO-5, with silicon substituted into the $AlPO_4$ framework.[238] In both the as-synthesised and calcined/rehydrated forms of BAPO-5, there is an additional resonance to the low frequency side of the main ^{27}Al peak. The chemical shift and broad nature of this resonance, especially apparent in the ^{27}Al NMR spectrum of the calcined sample, indicates that there is some amorphous material present in the

(i) U.C.C. BAPO-5			(ii) Laporte BAPO-5 (HSZ-1337)		
d (Å)	2θ	I	d (Å)	2θ	I/I_{max} x 100
12.1 - 11.56	7.3 - 7.65	m - vs	11.8	7.5	85
4.55 - 4.46	19.5 - 19.95	m - s	6.84	12.9	20
4.25 - 4.17	20.9 - 21.3	m - vs	5.93	14.9	26
4.00 - 3.93	22.2 - 22.6	w - vs	4.5	19.8	73
3.47 - 3.40	25.7 - 26.15	w - m	4.24	21.1	84
			3.99	22.4	100
			3.43	26.0	40
w = weak			3.08	29.0	23
m = medium			2.97	30.1	22
s = strong			2.60	34.6	19
vs = very strong			2.40	37.7	15

Table 6.26

Powder XRD data for BAPO-5

sample. This could be due to unreacted starting material and/or to structural degradation produced on calcination.[235] The latter possibility is supported by the increase in ^{27}Al NMR linewidth of the calcined form relative to the as-synthesised form of BAPO-5.

The presence of only one phosphorus resonance confirms that the phosphorus atoms are in an unique environment. Although the ^{31}P NMR CP

	^{31}P NMR		^{27}Al NMR[a)]	
sample	chemical shift/(ppm)	linewidth (Hz)	chemical[a)] shift/(ppm)	linewidth (Hz)
Et_3N-BAPO-5	-28.7	850	32.6	1200
BAPO-5	-27.0	850	34.6	1500

a) Experimental values (*i.e.* field dependent)

Table 6.27

^{31}P and ^{27}Al MAS NMR data for Et_3N-BAPO-5 and BAPO-5.

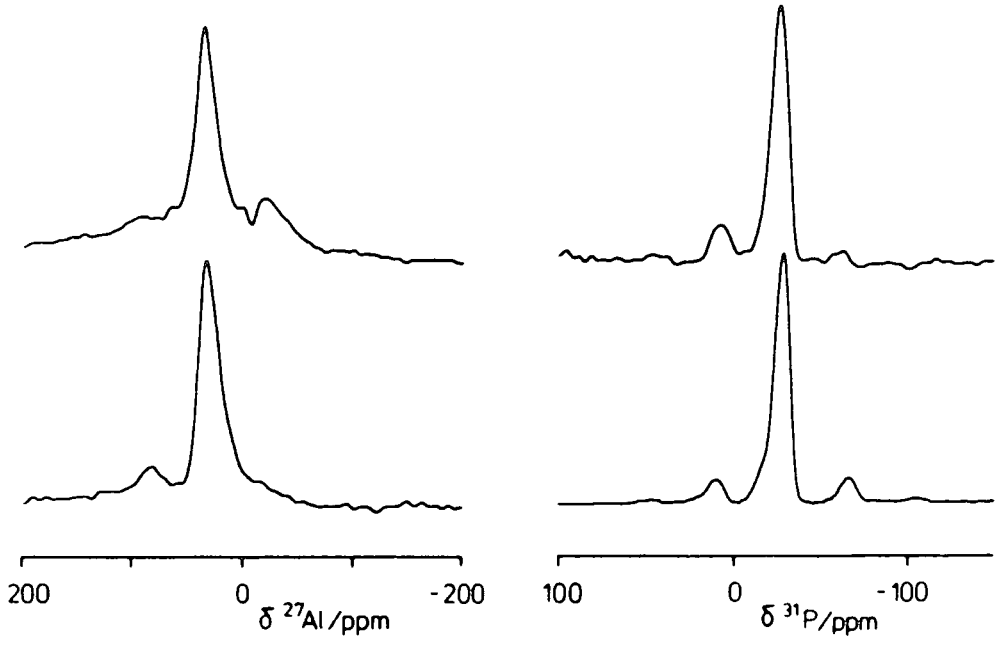

^{27}Al SPE (no HPD): SF = 52.1 MHz; RD = 2 s; SW = 50 kHz; SI = 2 K; TD = 1 K; NT = 140 (precursor), 310 (calcined); SS = 3.0 kHz; PD = 1 μs; PA = π/6; SR = -2344.

^{31}P CP/HPD: SF = 81.01 MHz; RD = 4 s (precursor), 6 s (calcined); SW = 20 kHz; SI = 2 K; TD = 1 K; NT = 32 (precursor), 556 (calcined); SS = 3.0 kHz; CT = 6 ms; SR = 1005.13.

Figure 6.28

^{27}Al (left) and ^{31}P (right) MAS NMR spectra of Et_3N-BAPO-5 (lower) and BAPO-5 (upper)

signal is weaker after calcination of the sample (as evinced by the increased number of transients necessary to achieve comparable S/N ratios in the precursor and calcined forms of BAPO-5), that it is possible to cross-polarize at all is indicative of some residual proton-phosphorus interaction following calcination and subsequent rehydration. Because removal of the template does not appear to affect the ^{31}P NMR linewidth, the proton magnetization necessary for CP is most likely to have come from water molecules present in the channel system.

Figure 6.29 shows ^{11}B MAS NMR spectra of the precursor (CP/HPD) and calcined (SPE) forms of BAPO-5. The presence of a single narrow (linewidth = 200 Hz) resonance line and the chemical shift of this resonance (-1.1 ppm) indicate that the substituted boron atoms are tetrahedrally coordinated *i.e.* present in the $AlPO_4$ framework. An ^{11}B spectrum (not shown) similar to that for the calcined material is

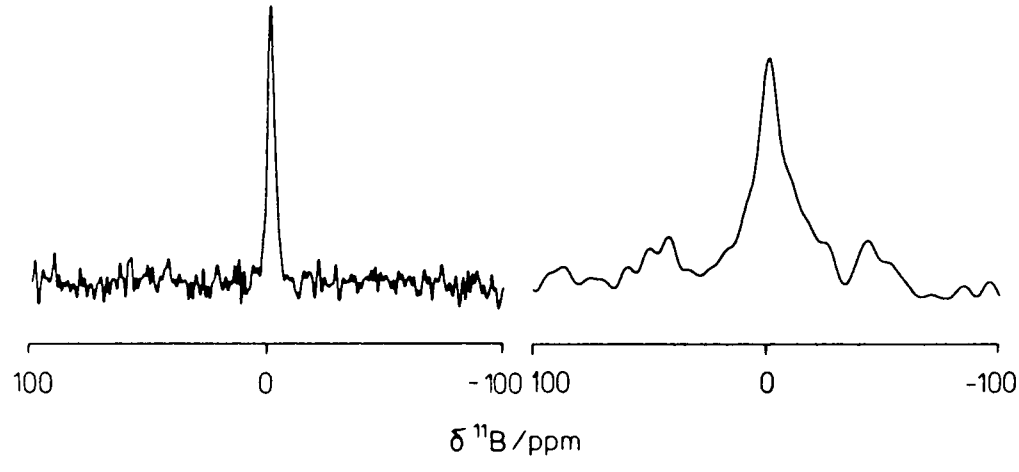

SF = 64.2 MHz; RD = 5 s (CP/HPD), 20 s (SPE); SW = 20 kHz; SI = 2 K; TD = 2 K; NT = 1800; SS = 3.3 kHz; PD = 4 μs; PA = π/4; LB = 100 (calcined); SR = -10352.

Figure 6.29

^{11}B MAS NMR spectra of precursor (left) and calcined (right) forms of BAPO-5

obtained for the *precursor* material without CP *i.e.* with HPD only. Since on removal of the template, ^{11}B CP for the calcined form of BAPO-5 is not possible, ^{11}B CP for the precursor form of BAPO-5 must occur because of interaction of template molecules with framework boron atoms. Thus several environments may exist for boron atoms in BAPO-5. The substantial linewidth of the SPE ^{11}B NMR signal in the calcined material, as compared with the CP/HPD spectrum of the precursor material supports this claim. Alternatively, the presence of amorphous material in the channels may distort the boron environment such that the lineshape is asymmetrical and broad in comparison to the CP spectrum. It should be remembered that boron-11 is a quadrupolar nucleus and so the linewidth is very sensitive to distortion effects. It should also be noted that from the ^{11}B NMR spectra shown in Figure 6.29, the presence of tetrahedrally coordinated boron compounds in the pores cannot be ruled out. This would seem unlikely, however, as the preferred coordination for boron outside of tetrahedrally coordinated oxide lattices is trigonal.[179,180] If the boron atoms were in a trigonal coordination, the ^{11}B spectrum would no longer be a narrow single resonance line, but a quadrupolar powder pattern (see section 5.2.1.). This decrease in symmetry would then be clearly visible from the ^{11}B MAS NMR spectrum.

To summarise, ^{11}B NMR can prove directly that some of the boron present in this particular BAPO-5 sample has substituted in the aluminophosphate framework. Unfortunately, unlike in the case of silicon substitution in SAPO-5,[238] no preferred mode of substitution can be elucidated from the ^{11}B NMR results as the tetrahedral chemical shift range for boron atoms is narrow.

The ^{13}C CP/HPD MAS NMR chemical shifts and linewidths for the

template of BAPO-5 (Et_3N) are identical with those obtained for $AlPO_4$-5 (section 6.1.1.). It is thus possible to conclude that there appears to be significant template-framework interaction in this sample of BAPO-5.

(2) BAPO-5 (032A)

The ^{31}P and ^{27}Al MAS NMR spectra (not shown) are similar to those shown in Figure 6.4 for $AlPO_4$-5 (section 6.2.1.). No evidence for the presence of extra-lattice aluminium is found in the ^{27}Al NMR spectra. The ^{11}B MAS NMR spectra are presented in Figure 6.30.

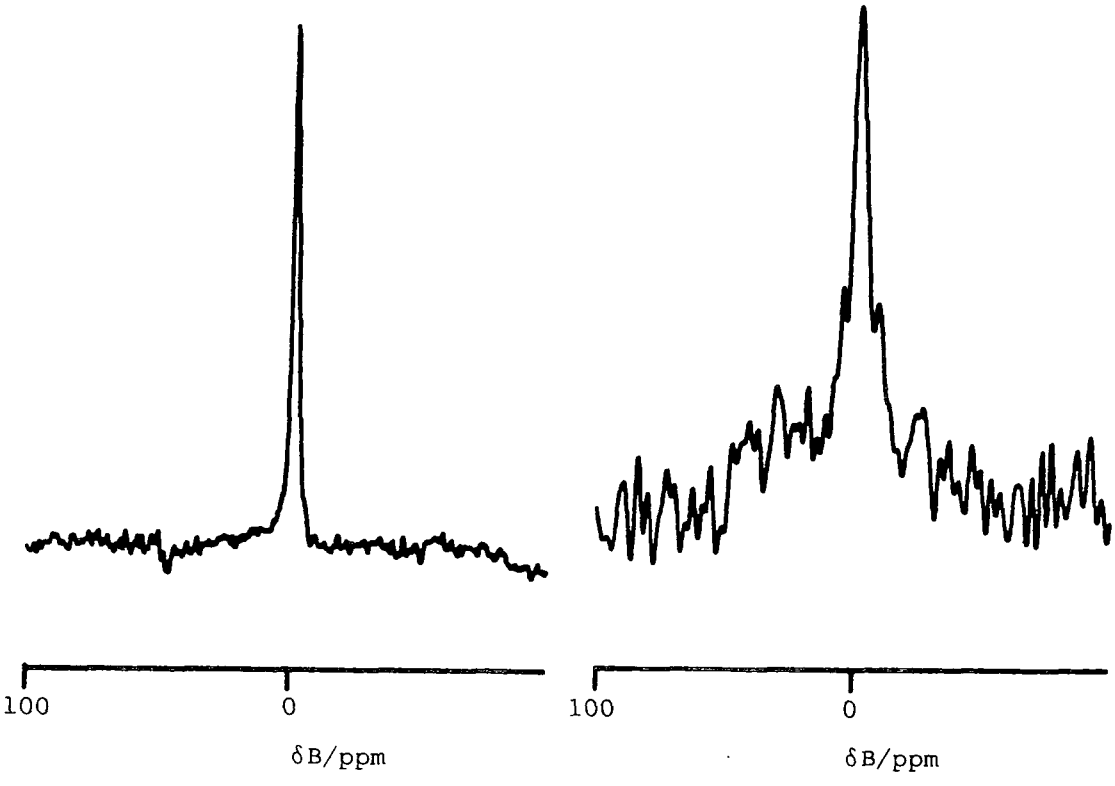

CP/HPD: SF = 64.2 MHz; RD = 5 s; SW = 20 kHz; NT = 1200; SS = 3.3 kHz; CT = 1 ms.
SPE: RD = 20 s; SW = 20 kHz; NT = 1646; SS = 3.3 kHz; PD = 4 μs; PA = π/4; LB = 50 Hz; SR = -10352.2.

Figure 6.30

^{11}B MAS NMR spectra of precursor form of BAPO-5 (032A)

CP/HPD (left) and SPE (right)

The ^{11}B CP/HPD MAS NMR spectra for the two BAPO-5 samples resemble each other closely. The chemical shift and linewidth values are in good agreement. Thus boron atoms have substituted into the $AlPO_4$ lattice. The SPE spectrum in Figure 6.30 shows some fine structure. The linewidth (450 Hz) is also considerably less than was observed in the previous BAPO-5 sample. Thus the possibility of more than one environment existing for the boron atoms in this BAPO-5 sample also exists.

BAPO-5 (032A), like HSZ-1337, has a small ion-exchange capability, as confirmed following ion-exchange (see section 6.3.1. for method) with 1M KCl solution and subsequent MES XRF analysis. The small cation exchange capacity means that the molar oxide amounts of B and Al must exceed those of P. On charge-balancing grounds, it is most likely that boron will substitute for aluminium in the $AlPO_4$ lattice. However, if this were the case, no ion-exchange capacity would be expected. It is therefore suggested that boron substitutes for both aluminium and phosphorus and so at least two boron environments may exist in BAPO-5.

6.5 General discussion of results

^{31}P and ^{27}Al MAS NMR chemical shifts are consistent with tetrahedral $(PO_4)^{3-}$ and $(AlO_4)^{5-}$ units respectively, in all as-synthesised forms of the aluminophosphates and substituted aluminophosphates studied. The substitution of a heteroatom does not appear to affect significantly the ^{31}P or ^{27}Al NMR spectra of the samples studied (see Table 6.28). For isomorphous substitution to occur the substitution level should apparently be low. High substitution

sample	^{31}P chemical shift/(ppm)
Et_3N-$AlPO_4$-5	-29.0
i-Pr_2NH-$AlPO_4$-11	-30.8
	-26.1
Et_3N-SAPO-5	-28.4
TEA-SAPO-5	-27.2
TPA-SAPO-5	-29.3
TMA-SAPO-20	-34.0
	-23.8
TEA-SAPO-34	-28.2
	-17.9
Et_3N-BAPO-5	-28.7

Table 6.28

^{31}P MAS NMR chemical shifts for $AlPO_4$-5, $AlPO_4$-11 SAPO-5, SAPO-20, SAPO-34, and BAPO-5 (precursor form).

levels lead to none of the substituent being incorporated in the lattice. The charge imbalance produced on substitution of a heteroatom such as silicon which is electronically neutral in the SiO_2 form, can be compensated for by protonated water molecules or by the organic template. The general mode of substitution for silicon is isomorphous replacement of phosphorus for silicon (as determined by the ^{29}Si chemical shift in the SAPO spectrum). No preferential substitution sites (*i.e.* preferred *phosphorus* sites for substitution) can be identified using ^{29}Si MAS NMR.

The ^{27}Al MAS NMR lineshapes are asymmetrical and, in general, broad, indicating the presence of distorted $(AlO_4)^{5-}$ tetrahedra and the presence of sizeable quadrupole coupling constants. This asymmetry manifests itself in the unusually large ^{31}P MAS NMR linewidths. This

suggests that heteroatom substitution occurs isomorphously only at low levels because of existing lattice distortion effects.

For those substituted molecular sieves having the $AlPO_4$-5 structure, the range of ^{31}P chemical shifts is -27.2 to -29.3 ppm (relative to 85% H_3PO_4 solution). The total ^{31}P chemical shift range for all samples studied is -17.9 to -34.0 ppm.

Note that a table of ^{27}Al chemical shifts would be meaningless for the purposes of comparison as the chemical shift reported corresponds to the centre of gravity of the line rather than the true isotropic chemical shift.

Calcination (in air at 550°C) is seen to affect considerably the NMR spectra of all the samples studied. Some remain crystalline (notably those with lower substitution levels) and others collapse to form a dense $AlPO_4$ phase (or phases). This structure collapse is visible in the powder X-ray diffraction patterns, but also from the NMR spectra.

Many of the syntheses result in the formation of impure AlPO's and SAPO's. The contaminant is normally a reactant, a dense polymorph of $AlPO_4$, or another type of molecular sieve AlPO or SAPO. MAS NMR is able to detect all forms of contaminants. The usual contaminant in the preparations with high levels of substituent silicon, is finely dispersed silica. Powder X-ray diffractometry is unable to detect this at low levels, whereas, using ^{29}Si MAS NMR, it is immediately recognizable from its characteristic ^{29}Si chemical shift.

For several SAPO molecular sieves, NMR is able to detect crystallographically inequivalent sites. SAPO-34 for instance, has two inequivalent phosphorus sites (and hence two inequivalent silicon sites). ^{31}P and ^{29}Si MAS NMR results are able to confirm the presence

of these sites.

The quadrupole coupling constants and asymmetry parameters for the Al sites are not known for any of the $AlPO_4$-n or SAPO-n molecular sieves, with the exception of $AlPO_4$-5. Consequently, the ^{27}Al chemical shifts quoted are uncorrected for quadrupole induced shifts and so no correlation between ^{27}Al chemical shift and Al-O distance or Al-O-P bond angle can be made. Although several $AlPO_4$-n crystal structures have been published, there is insufficient data to undertake similar correlations for ^{31}P chemical shifts for either $AlPO_4$-n or SAPO-n samples.

In general, ^{31}P CP/HPD MAS NMR is possible for both as-synthesised and calcined forms of AlPO's and SAPO's. ^{13}C NMR studies indicate that, in general, there is considerable template-framework interaction (as evinced by the broad, asymmetric lineshapes and shifted chemical shifts with respect to those observed in ^{13}C solution-state NMR). ^{31}P CP NMR following calcination and removal of the template is probably due to framework-phosphorus interaction with water molecules.

Several ^{27}Al NMR spectra display quadrupolar splittings at 52.1 MHz. It is expected that going to higher fields will improve the ^{27}Al NMR spectra (because of the decrease in second-order quadrupolar effects), and so help to clarify the Al nuclear environment. Higher magnetic fields will also affect (decrease) the ^{31}P NMR linewidths (broadening of the lines is due to dipolar couplings to quadrupolar ^{27}Al nuclei, which will be reduced at higher fields). The phosphorus T_1 times for the AlPO and SAPO molecular sieves studied range from 7 s to 50 s. In the cases where more than one phosphorus resonance is observed, the T_1 values can be substantially different. It is therefore important to measure the T_1 values prior to any quantitative investigation. Long recycle delays will thus be necessary for SPE ^{31}P

NMR studies of these materials. However, the regular delays necessary for ^{31}P CP/HPD MAS NMR will be much less, 5 s normally being sufficient.

6.6 Conclusions and recommendations for further work

The main conclusion is that, as is the case for aluminosilicate zeolites, MAS NMR spectroscopy is an extremely powerful analytical tool ideal for the structural investigation and characterisation of these new molecular sieve-type materials. However, the full investigative potential of MAS NMR will only be realised when used in conjunction with other well-established analytical techniques such as powder XRD (preferably single-crystal XRD), and chemical analysis techniques such as X-ray fluorescence spectroscopy.

MAS NMR spectroscopy has proved itself to be the analytical method of choice for many inorganic fine-powder systems. It is non-destructive, requires reasonably small amounts of sample, is both qualitative and (under the correct conditions) quantitative. The vast majority of the results shown in Chapters Five and Six however, would have benefitted from the use of a higher static magnetic field. This applies not only to the obvious case of quadrupolar nuclei such as ^{27}Al, but also to ^{29}Si and ^{31}P where the increased spread of chemical shifts at higher fields might allow the resolution of otherwise overlapping resonance lines.

Before the new catalyst materials can be used in industrial processes, the organic template and any other occluded material must first be removed from the channels of the sample. The process of burning out the template at elevated temperatures (calcination) is thus

an extremely important one. Many of the samples investigated during the course of these studies became amorphous due to structure collapse following calcination. The channel system which was to give rise to molecular sieve, ion-exchange or catalyst properties is thus no longer intact, rendering the material defunct. It is, therefore, extremely important to know the conditions under which the structure remains intact, whilst, at the same time, removing the occluded template. A thorough investigation using different temperatures, different atmospheres, different heating times, and different methods of calcination (deep-bed, shallow-bed, under vacuum *etc.*) is called for. Powder XRD would then be used to determine the crystallinity of the sample. Fourier transform IR could be used to see if all the template had in fact been removed.

The crystal structures of several AlPO's apart from $AlPO_4$-5 have now been reported ($AlPO_4$-12, $AlPO_4$-15, $AlPO_4$-17, and $AlPO_4$-21). It would be most interesting to investigate these materials using MAS NMR and to compare the ^{31}P and ^{27}Al NMR results with the NMR results for their silicon (or other heteroatom) substituted analogues. The investigation of AlPO's with known crystal structures will allow the maximum information to be extracted from the MAS NMR spectra. Several of these aluminophosphates are reported to have inequivalent phosphorus sites as well as different aluminium coordination units (see Table 3.5) and so their NMR spectra should prove interesting. $AlPO_4$-21 changes structure on thermal treatment to become $AlPO_4$-25. MAS NMR could perhaps be used to follow this metamorphosis.

Comparatively little is known about the aluminophosphate and silicoaluminophosphate gels that form prior to hydrothermal crystallisation of AlPO's and SAPO's. MAS NMR could be used to investigate the early stages of development of a molecular sieve such as

an AlPO or a SAPO. Moreover, ^{13}C MAS NMR studies might provide otherwise unobtainable information on the role of the template during crystallisation.

The determination of precise isotropic chemical shift values for half-integer quadrupolar nuclei, such as ^{27}Al , is very important as, to date, most of the ^{27}Al chemical shifts reported for AlPO's and SAPO's (and indeed aluminosilicate zeolites) are field-dependent and simply correspond to the line centres of gravity. It is, however, possible to determine accurately the true (corrected) ^{27}Al chemical shift. Correlations could then undoubtedly be established between ^{27}Al chemical shifts and Al-O-P bond angles or Al-O bond distances, thus aiding structure elucidation in these materials.

Brønsted acid sites can be created in AlPO-n molecular sieves by heteroatom substitution. This has already been shown to be the case for divalent cobalt substitution into $AlPO_4$-5 and $AlPO_4$-11, and zinc substitution into $AlPO_4$-5. Multiple-pulse ^1H MAS NMR could be used to investigate the acid sites in these materials. Careful dehydration and removal of the orgainc template would be essential in any multiple-pulse ^1H experiment. Further studies of the acidic character of these materials could include adsorption and subsequent MAS NMR analysis of various bases such as ammonia and triethylamine.

The heteroatom substitution level in aluminophosphates has been shown to be necessarily low. For SAPO molecular sieves, this invariably makes the investigation of the mode of substitution of the silicon atoms a very time-consuming experiment. Future work might consider the possibility of using a ^{29}Si enriched silica source, so decreasing the time required to produce an adequate signal-to-noise ratio in the ^{29}Si MAS NMR spectrum.

PUBLICATIONS, COLLOQUIA, AND CONFERENCES

List of Publications

1. I.P. Appleyard, R.K. Harris, and F.R. Fitch, *Chem. Lett.*, 1985, 1747.

2. I.P. Appleyard, R.K. Harris, and F.R. Fitch, accepted for publication in *Zeolites*, 1986.

3. M.J. Hey, A. Nock, R. Rudham, I.P. Appleyard, G.A. Haines, and R.K. Harris, accepted for publication in *J. Chem. Soc., Faraday Trans. 1*, 1986.

COLLOQUIA AND CONFERENCES

The Board of Studies in Chemistry requires that each postgraduate research thesis contains an appendix listing:

(A) all research colloquia, research seminars, and lectures arranged by the Department of Chemistry during the period of the author's residence as a postgraduate student;

(B) all research conferences attended and papers presented by the author during the period when research for the thesis was carried out.

RESEARCH COLLOQUIA, SEMINARS, AND LECTURES

(A) Lectures and Seminars organised by the Department of Chemistry during the period 1984-1986.

19.10.84 Dr. A. Germain (Languedoc, Montpellier)
"Anodic Oxidation of Perfluoro Organic Compounds in Perfluoroalkane Sulphonic Acids"

24.10.84 * Prof. R.K. Harris (Durham)
"N.M.R. of Solid Polymers"

28.10.84 Dr R. Snaith (Strathclyde)
"Exploring Lithium Chemistry: Novel Structures, Bonding, and Reagents"

7.11.84 * Prof. W.W. Porterfield (Hampden-Sydney College, USA)
"There is no Borane Chemistry (only Geometry)"

7.11.84 * Dr. H.S. Munro (Durham)
"New Information from ESCA Data"

21.11.84 * Mr. N. Everall (Durham)
Picosecond Pulsed Laser Raman Spectroscopy"

27.11.84 Dr. W.J. Feast (Durham)
" A Plain Man's Guide to Polymeric Organic Metals"

28.11.84 Dr. T.A. Stephenson (Edinburgh)
"Some recent Studies in Platinum Metal Chemistry"

12.12.84 * Dr. K.B. Dillon (Durham)
"^{31}P NMR Studies of some Anionic Phosphorus Complexes"

11. 1.85 Emeritus Prof. H. Suchitzky (Salford)
"Fruitful Fissions of Benzofuroxanes and Isobenzimidazoles (umpolung of *o*-phenylenediamine)"

13. 2.85 Dr. G.W.J. Fleet (Oxford)
"Synthesis of some Alkaloids from Carbohydrate"

19. 2.85 * Dr. D.J. Mincher (Durham)
"Stereoselective Syntheses of Some Novel Anthracyclinones Related to the Anti-cancer Drug Adriamycin and to the Steffimycin Antibiotics"

27. 2.85 * Dr. R.E. Mulvey (Durham)
"Some Unusual Lithium Complexes"

6. 3.85 Dr. P.J. Kocienski (Leeds)
"Some Synthetic Applications of Silicon-Mediated Annulation Reactions"

7. 3.85 Dr. P.J. Rodgers (I.C.I. plc Agricultural Division, Billingham)
"Industrial Polymers from Bacteria"

12. 3.85 * Prof. K.J. Packer (B.P. Ltd./East Anglia)
"NMR Investigations of the Structure of Solid Polymers"

14. 3.85 * Prof. A.R. Katritzky F.R.S. (Florida)
"Some Adventures in Heterocyclic Chemistry"

20. 3.85 Dr. M. Poliakoff (Nottingham)
New Methods for Detecting Organometallic Intermediates in Solution"

28. 3.85 Prof. H. Ringsdorf (Mainz)
"Polymeric Liposomes as Models for Biomembranes and Cells"

24. 4.85 Dr. M.C. Grossel (Bedford College, London)
"Hydroxypyridine Dyes - Bleachable One-Dimensional Metals?"

25. 4.85 Major S.A. Shackelford (U.S. Air Force)
"*In Situ* Mechanistic Studies on Condensed Phase Thermochemical Reaction Processes: Deuterium Isotope Effects in HMX Decomposition, Explosives and Combustion"

1. 5.85 Dr. D. Parker (I.C.I plc, Petrochemical and Plastics Division, Wilton)
"Applications of Radioisotopes in Industrial Research"

7. 5.85 Prof. G.E. Coates (formerly of Wyoming, U.S.A.)
"Chemical Education in England and America: Successes and Deficiencies"

8. 5.85 Prof. D. Tuck (Windsor, Ontario)
"Lower Oxidation State Chemistry of Indium"

8. 5.85 Prof. G. Williams (U.C.W., Aberwystwyth)
"Liquid Crystalline Polymers"

9. 5.85 * Prof. R.K. Harris (Durham)
"Chemistry in a Spin: Nuclear Magnetic Resonance"

14. 5.85 Prof. J. Passmore (New Brunswick, U.S.A.)
The Synthesis and Characterisation of some Novel Selenium-Iodine Cations, aided by 77-Se NMR Spectroscopy"

15. 5.85 Dr. J.E. Packer (Auckland, New Zealand)
"Studies of Free Radical Reactions in Aqueous Solution Using Ionising Radiation"

17. 5.85 Prof. I.D. Brown (McMaster University, Canada)
"Bond Valence as a Model for Inorganic Chemistry"

21. 5.85 * Dr. D.L.H. Williams (Durham)
"Chemistry in Colour"

22. 5.85 Dr. M. Hudlicky (Blacksburg, U.S.A.)
Preferential Elimination of Hydrogen Fluoride from Vicinal Bromofluorocompounds"

22. 5.85 Dr. R. Grimmett (Otago, New Zealand)
"Some Aspects of Nucleophilic Substitution in Imidazoles"

4. 6.85 * Dr. P.S. Belton (Food Research Institute, Norwich)
"Analytical Photoacoustic Spectroscopy"

13. 6.85 Dr. D. Woolins (Imperial College, London)
"Metal - Sulphur - Nitrogen Complexes"

14. 6.85 Prof. Z. Rappoport (Hebrew University, Jerusalem)
"The Rich Mechanistic World of Nucleophilic Vinylic Substitution"

19. 6.85 * Dr. T.N. Mitchell (Dortmund)
"Some Synthetic and NMR-Spectroscopic Studies of Organotin Compounds"

26. 6.85 Prof. G. Shaw (Bradford)
"Synthetic Studies on Imidazole Nucleosides and the Anitbiotic Coformycin"

12. 7.85 Dr. K. Laali (Hydrocarbon Research Institute, University of Southern California, U.S.A.)
"Recent Developments in Superacid Chemistry and Mechanistic Considerations in Electrophilic Aromatic Substitutions: A Progress Report"

13. 9.85 Dr. V.S. Parmar (Delhi)
"Enzyme Assisted ERC Synthesis"

17.10.85 * Dr. C.J. Ludman (Durham)
"Some Thermochemical Aspects of Explosions"

24.10.85 * Dr. J. Dewing (UMIST)
"Zeolites - Small Holes, Big Opportunities"

30.10.85 Dr. S.N. Whittleton (Durham)
"An Investigation of a Reaction Window"

31.10.85 Dr. P. Timms (Bristol)
"Some Chemistry of Fireworks"

5.11.85 Prof. M.J. O'Donnell (Indiana-Purdue University, U.S.A.)
"New Methodology for the Synthesis of Amino Acids"

7.11.85 * Prof. G. Ertl (Munich, W. Germany)
"Heterogeneous Catalysis"

14.11.85 * Dr. S.G. Davies (Oxford)
"Chirality Control and Molecular Recognition"

20.11.85 Dr. J.A.H. McBride (Sunderland Polytechnic)
"A Heterocyclic Tour on a Distorted Tricycle - Biphenylene"

21.11.85 * Prof. K.H. Jack (Newcastle)
"Chemistry of Si-Al-O-N Engineering Ceramics"

28.11.85 * Dr. B.A.J. Clark (Kodak Ltd.)
"Chemistry and Principles of Colour Photography"

28.11.85 * Prof. D.J. Waddington (York)
"Resources for the Chemistry Teacher"

15. 1.86 * Prof. N. Sheppard (East Anglia)
"Vibrational and Spectroscopic Determinations of the Structures of Molecules Chemisorbed on Metal Surfaces"

23. 1.86 Prof. Sir Jack Lewis (Cambridge)
"Some More Recent Aspects in the Cluster Chemistry of Ruthenium and Osmium Carbonyls"

29. 1.86 Dr. J.H. Clark (York)
"Novel Fluoride Ion Reagents"

30. 1.86 * Dr. N.J. Phillips (Loughborough)
"Laser Holography"

12. 2.86 Dr. J. Yarwood (Durham)
"The Structure of Water in Liquid Crystals"

12. 2.86 Dr. O.S. Tee (Concordia University, Montreal, Canada)
"Bromination of Phenols"

13. 2.86 * Prof. R. Grigg (Queen's, Belfast)
"Thermal Generation of 1,3-Dipoles"

19. 2.86 Prof. G. Procter (Salford)
"Approaches to the Synthesis of Some Natural Products"

20. 2.86 * Dr. C.J.F. Barnard (Johnson Matthey Group)
"Platinum Anti-Cancer Drug Development"

26. 2.86 * Ms. C. Till (Durham)
"ESCA and Optical Emission Studies of the Plasma Polymerisation of Perfluoroaromatics"

27. 2.86 * Prof. R.K. Harris (Durham)
"The Magic of Solid State NMR"

5. 3.86 Dr. D. Hathway (Durham)
"Herbicide Selectivity"

5. 3.86 Dr. M. Schroder (Edinburgh)
"Studies on Macrocyclic Compounds"

6. 3.86 * Dr. B. Iddon (Salford)
"The Magic of Chemistry"

12. 3.86 * Dr. J.M. Brown (Oxford)
"Chelate Control in Homogeneous Catalysis"

14. 5.86 Dr. P.R.R. Langridge-Smith (Edinburgh)
"Naked Metal Clusters - Synthesis, Characterisation, and Chemistry"

9. 6.86 Prof. R. Schmutzler (Braunschweig, W. Germany)
"Mixed Valence Diphosphorus Compounds"

23. 6.86 Prof. R.E. Wilde (Texas Technical University, U.S.A.)
"Molecular Dynamic Processes from Vibrational Bandshapes"

* Indicates colloquia attended by the author.

(B) Conferences Attended

1. British Zeolite Association Seventh Annual Meeting, July, 1984, Chislehurst, Kent.

2. BZA, Eighth Annual Meeting, July, 1985, Chester College.
Poster presented: Solid-state NMR studies of Aluminophosphate and Silicoaluminophosphate molecular sieves.

3. BZA, Ninth Annual Meeting, Royal Holloway College, London, March, 1986.
Lecture presented: Multinuclear Magic-angle Rotation Magnetic Resonance Studies of Zeolites and Related Materials.

4. Seventh Annual Meeting NMR Spectroscopy, University of Cambridge, July, 1985.
Poster presented: Solid-state NMR studies of SAPO-5.

5. British Radiofrequency Spectroscopy Group, High Resolution NMR in Solids, University of Oxford, April, 1986.
Poster presented: Solid-state NMR studies of BAPO-5, the boron substituted analogue of SAPO-5.

6. Graduate Symposium, Durham, March, 1985.

7. Graduate Symposium, Durham, March, 1986.
Lecture presented: Solid-state NMR of New Catalyst and Molecular Sieve-Type Materials.

REFERENCES

1. E.M. Flanigen, Proceeds of the Fifth International Conference on Zeolites, 1980, 760-780, and *op. cit.*.

2. J.C. Vedrine, ACS Symposium Series, 1985, vol. 279, pp. 257-274, and *op. cit.*.

3. M. Mehring, "High Resolution NMR Spectroscopy in Solids", Springer-Verlag, New York, second ed., 1983.

4. U. Haeberlen, "High Resolution NMR in Solids, Selective Averaging", Academic Press, New York, 1976.

5. C.P. Slichter, "Principles of Magnetic Resonance", Springer-Verlag, New York, second ed., 1978.

6. A. Abragam, "The Principles of Nuclear Magnetism", Oxford University Press, London, 1961.

7. R.K. Harris, "Nuclear Magnetic Resonance Spectroscopy: a Physicochemical View", Longman Scientific and Technical, England, 1986.

8. E.R. Andrew, *Prog. NMR Spectrosc.*, 1971, 8, 1; E.R. Andrew, *Int. Rev. Phys. Chem.*, 1981, 1, 195.

9. M.H. Cohen and F. Reif, "Solid State Physics", Ed. F. Seitz and D. Turnbull, vol. 5, Academic Press, New York, 1957.

10. J.F. Baugher, P.C. Taylor, T. Oja, and P.J. Bray, *J. Chem. Phys.*, 1969, 50, 4914.

11. K. Narita, J.-I. Umeda, and H. Kusumoto, *J. Chem. Phys.*, 1966, 44, 2719.

12. E. Kundla, A. Samoson, and E. Lippmaa, *Chem. Phys. Lett.*, 1981, 83, 229.

13. S. Schramm and E. Oldfield, *J. Chem. Soc., Chem. Commun.*, 1982, 980.

14. S. Ganapathy, S. Schramm, and E. Oldfield, *J. Chem. Phys.*, 1982, 77, 4360.

15. A. Samoson, E. Kundla, and E. Lippmaa, *J. Magn. Reson.*, 1982, 49, 350.

16. A. Samoson, *Chem. Phys. Lett.*, 1985, 119, 29.

17. E. Lippmaa, A. Samoson, and M. Mägi, *J. Am. Chem. Soc.*, 1986, 108, 1730.

18. D. Freude, J. Haase, J. Klinowski, T.A. Carpenter, and G. Roniker, *Chem. Phys. Lett.*, 1985, 119, 365.

19. A. Samoson and E. Lippmaa, *Phys. Rev.*, 1983, B28, 6567.

20. A. Samoson and E. Lippmaa, *Chem. Phys. Lett.*, 1983, 100, 205.

21. A. Pines, M.G. Gibby, and J.S. Waugh, *J. Chem. Phys.*, 1973, 59, 569.

22. S.R. Hartmann and E.L. Hahn, *Phys. Rev.*, 1962, 128, 2042.

23. J. Tegenfeldt and U. Haeberlen, *J. Magn. Reson.*, 1979, 36, 453.

24. E.O. Stejskal and J. Schaefer, *J. Magn. Reson.*, 1975, 18, 560.

25. C.A. Fyfe, J.M. Thomas, J. Klinowski, and G.C. Gobbi, *Angew. Chem., Int. Ed. Engl.*, 1983, 22, 259.

26. J. Klinowski, *Prog. Nucl. Magn. Reson. Spectrosc.*, 1984, 16, 237.

27. J.M. Thomas and J. Klinowski, *Adv. Catal.*, 1985, 33, 199.

28. D.W. Breck, "Zeolite Molecular Sieves", Wiley, New York, 1974.

29. R.M. Barrer, "Zeolites and Clay Minerals as Sorbents and Molecular Sieves", Academic Press, London, 1978.

30. R.M. Barrer, "Hydrothermal Chemistry of Zeolites", Academic Press, London, 1982.

31. A.Fr. Cronstedt, *Kongl. Svenska. Vetenskaps Acad. Handlingar*, 1756, 17, 120.

32. W. Loewenstein, *Am. Mineral.*, 1954, 39, 92.

33. E. Lippmaa, M. A. Alla, T.J. Pehk, and G. Engelhardt, *J. Am. Chem. Soc.*, 1978, 100, 1929.

34. G. Engelhardt, D. Kunath, M. Mägi, A. Samoson, M. Tarmak, E. Lippmaa, Poster from Workshop on Adsorption of Hydrocarbons in Zeolites, Berlin-Adlershof, 1979, vol. 11, 19-22; G. Engelhardt, D. Zeigen, E. Lippmaa, and M. Mägi, *Z. Anorg. Allg. Chem.*, 1980, 468, 35.

35. E. Lippmaa, M. Mägi, A. Samoson, G. Engelhardt, and A.-R. Grimmer, *J. Am. Chem. Soc.*, 1980, 102, 4889.

36. M. Mägi, E. Lippmaa, A. Samoson, G. Engelhardt, and A.-R. Grimmer, *J. Phys. Chem.*, 1984, 88, 1518.

37. E. Lippmaa, M. Mägi, A. Samoson, M. Tarmak, and G. Engelhardt, *J. Am. Chem. Soc.*, 1981, 103, 4992.

38. V. Gramlich and W.M. Meier, *Z. Kristallogr.*, 1971, 133, 134.

39. J.J. Pluth and J.V. Smith, *J. Am. Chem. Soc.*, 1980, 102, 4704.

40. L.A. Bursill, E.A. Lodge, J.M. Thomas, and A.K. Cheetham, *J. Phys. Chem.*, 1981, 85, 2409.

41. L.A. Bursill, E.A. Lodge, and J.M. Thomas, *Nature (London)*, 1981, 291, 265.

42. T. Rayment and J.M. Thomas, *Zeolites*, 1983, 3, 2.

43. A.K. Cheetham, M.M. Eddy, D.A. Jefferson, and J.M. Thomas, *Nature (London)*, 1982, 299, 24.

44. A.K. Cheetham, C.A. Fyfe, J.V. Smith, and J.M. Thomas, *J. Chem. Soc., Chem. Commun.*, 1982, 823.

45. J.M. Thomas, C.A. Fyfe, S. Ramdas, J. Klinowski, and G.C. Gobbi, *J. Phys. Chem.*, 1982, 86, 3061.

46. M.T. Melchior, D.E.W. Vaughan, R.H. Jarman, and A.J. Jacobson, *Nature (London)*, 1982, 298, 455.

47. J. Klinowski, S. Ramdas, J.M. Thomas, C.A. Fyfe, and J.S. Hartman, *J. Chem. Soc., Faraday Trans. 2*, 1982, 78, 1025.

48. G. Engelhardt, U. Lohse, E. Lippmaa, M. Tarmak, and M. Magi, *Z. Anorg. Allg. Chem.*, 1981, 482, 49.

49. D.E.W. Vaughan, M.T. Melchior, and A.J. Jacobson, "Intrazeolite Chemistry", ed. G.D. Stucky and F.G. Dwyer, ACS Symposium Series No. 218, Washington D.C., 1983, p. 231.

50. J.M. Thomas, J. Klinowski, S. Ramdas, M.W. Anderson, C.A. Fyfe, and G.C. Gobbi, ref. 49, p. 159.

51. M. O'Keefe and B.G. Hyde, "Structure and Bonding in Crystals", ed. M. O'Keefe and A. Navrotsky, Academic Press, New York, 1981, vol. 1, p. 277.

52. (a). S. Hayashi, K. Suzuki, S. Shin, K. Hayamizu, and O. Yamamoto, *Bull. Chem. Soc. Jpn*, 1985, 58, 52; (b). L. X.-Sheng and J.M. Thomas, *J. Chem. Soc., Chem. Commun.*, 1985, 1544.

53. J.M. Thomas, J. Klinowski, and M.W. Anderson, *Chem. Lett.*, 1983, 1555.

54. C.A. Fyfe, G.C. Gobbi, J. Klinowski, J.M. Thomas., and S. Ramdas, *Nature (London)*, 1982, 296, 530.

55. D.G. Hay, H. Jaeger, and G.W. West, *J. Phys. Chem.*, 1985, 89, 1070.

56. C.A. Fyfe, G.J. Kennedy, G.T. Kokotailo, J.R. Lyerla, and W.W. Fleming, *J. Chem. Soc., Chem. Commun.*, 1985, 740.

57. C.A. Fyfe, G.J. Kennedy, C.T. de Schutter, and G.T. Kokotailo, *J. Chem. Soc., Chem. Commun.*, 1984, 541.

58. G.W. West, *Aust. J. Chem.*, 1984, 37, 455.

59. P.F. Barron, R.L. Frost, and O.J. Skjemstad, *J. Chem. Soc., Chem. Commun.*, 1983, 581.

60. (a). T. Watanabe, H. Shimizu, A. Masuda, and H. Saito, *Chem. Lett.*, 1983, 1293; (b). J.H. Iwamiya and B.C. Gerstein, *Zeolites*, 1986, 6, 181; (c). G. Debras, A. Gourgue, J.B. Nagy, and G. Clippeleir, *Zeolites*, 1986, 6, 161.

61. D.J. Cookson and B.E. Smith, *J. Magn. Reson.*, 1985, 63, 217.

62. J.B. Nagy, Z. Gabelica, and E.G. Derouane, *Chem. Lett.*, 1982, 1105.

63. G. Engelhardt, U. Lohse, A Samoson, M. Mägi, M. Tarmak, and E. Lippmaa, *Zeolites*, 1982, 2, 59.

64. G. Boxhoorn, A.G.T.G. Kortbeek, G.R. Hays, and N.C.M. Alma, *Zeolites*, 1984, 4, 15.

65. G.L. Woolery, L.B. Alemany, R.M. Dessau, and A.W. Chester, *Zeolites*, 1986, 6, 14.

66. G. Engelhardt, B. Fahlke, M. Mägi, and E. Lippmaa, *Z. Phys. Chemie, (Leipzig)*, 1985, 266, 239.

67. J.B. Nagy, Z. Gabelica, E.G. Derouane, and P.A. Jacobs, *Chem. Lett.*, 1982, 2006.

68. C.A. Fyfe, G.T. Kokotailo, G.J. Kennedy, and C. de Schutter, *J. Chem. Soc., Chem. Commun.*, 1985, 306.

69. A.-R. Grimmer, F. von Lampe, M. Tarmak, and E. Lippmaa, *Chem. Phys. Lett.*, 1983, 97, 185.

70. R.H. Jarman, *J. Chem. Soc., Chem. Commun.*, 1983, 512.

71. J.M. Thomas, J. Klinowski, S. Ramdas, B.K. Hunter, and D.T.B. Tennakoon, *Chem. Phys. Lett.*, 1983, 102, 158.

72. S. Ramdas and J. Klinowski, *Nature (London)*, 1984, 308, 521.

73. R. Radeglia and G. Engelhardt, *Chem. Phys. Lett.*, 1985, 114, 28.

74. J.V. Smith and C.S. Blackwell, *Nature (London)*, 1983, 303, 223.

75. G. Engelhardt, R. Radeglia, U. Lohse, A. Samoson, and E. Lippmaa, *Z. Chem.*, 1985, 7, 252.

76. D.H. Olson, G.T. Kokotailo, S.L. Lawton, and W.M. Meier, *J. Phys. Chem.*, 1981, 85, 2238.

77. A.-R. Grimmer, *Chem. Phys. Lett.*, 1985, 119, 416.

78. N. Janes and E. Oldfield, *J. Am. Chem. Soc.*, 1985, 107, 6769.

79. P.J. Grobet, W.J. Mortier, and K. van Genechten, *Chem. Phys. Lett.*, 1985, 119, 361.

80. C.A. Fyfe, G.T. Kokotailo, J.D. Graham, C. Browning, G.C. Gobbi, M. Hyland, G.J. Kennedy, and C.T. de Schutter, *J. Am. Chem. Soc.*, 1986, 108, 522.

81. M.T. Melchior, ref. 49, p. 243.

82. C.A. Fyfe, G.C. Gobbi, W.J. Murphy, R.S. Ozubko, and D.A. Slack, *J. Am. Chem. Soc.*, 1984, 106, 4435.

83. J.W. Akitt and W.J. Gessner, *J. Chem. Soc., Dalton Trans.*, 1984, 147, and *op. cit.*.

84. D. Müller, W.J. Gessner, H.-J. Behrens, and G. Scheler, *Chem. Phys. Lett.*, 1981, 79, 59.

85. D. Freude and H.-J. Behrens, *Cryst. Res. Technol.*, 1981, 16, 36.

86. C.A. Fyfe, G.C. Gobbi, J.S. Hartman, J. Klinowski, and J.M. Thomas, *J. Phys. Chem.*, 1982, 86, 1247.

87. (a). E.T. Lippmaa, A.V. Samoson, V.V. Brei, and Yu.I. Gorlov, *Dokl. Akad. Nauk SSSR*, 1981, 259, 403; (b). M.C. Cruickshank, L.S. Dent-Glasser, S.A.I. Barri, and I.J.F. Poplett, *J. Chem. Soc., Chem. Commun.*, 1986, 23.

88. D. Freude, T. Fröhlich, H. Pfeifer, and G. Scheler, Second Workshop on Adsorption of Hydrocarbons in Microporous Sorbents, Eberswalde, G.D.R., November 1982, vol. 2, p. 9.

89. J.B. Nagy, Z. Gabelica, G. Debras, E.G. Derouane, J.-P. Gilson, and P.A. Jacobs, *Zeolites*, 1984, 4, 133.

90. J. Klinowski, M.W. Anderson, and J.M. Thomas, *J. Chem. Soc., Chem. Commun.*, 1983, 525.

91. E.M. Flanigen, J.M. Bennet, R.W. Grose, J.P. Cohen, R.L. Patton, R.M. Kirchner, and J.V. Smith, *Nature (London)*, 1978, 271, 512.

92. A.P.M. Kentgens, K.F.M.G.J. Scholle, and W.S. Veeman, *J. Phys. Chem.*, 1983, 87, 4357.

93. F.M.M. Geurts, A.P.M.Kentgens, and W.S. Veeman, *Chem. Phys. Lett.*, 1985, 120, 206.

94. C.V. McDaniel and P.K. Maher, "Molecular Sieves", Society of Chemical Industry, London, 1968, p. 186.

95. C.V. McDaniel and P.K. Maher, "Zeolite Chemistry and Catalysis", ACS Monograph No. 171, 1976, p. 285.

96. C.V. McDaniel and P.K. Maher, U.S.P.3 449 070/1969.

97. G.T. Kerr, "Molecular Sieves", ed. W.M. Meier and J.B. Utterhoeven, ACS Advances in Chemistry Series No. 121, Washington D.C., 1974.

98. J. Klinowski, J.M. Thomas, C.A. Fyfe, and G.C. Gobbi, *Nature (London)*, 1982, 296, 533.

99. I.E. Maxwell, W.A. van Erp, G.R. Hays, T. Couperus, R. Huis, and A.D.H. Clague, *J. Chem. Soc., Chem. Commun.*, 1982, 523.

100. G. Engelhardt, U. Lohse, V. Patzelová, M. Mägi, and E. Lippmaa, *Zeolites*, 1983, 3, 233.

101. G. Engelhardt, U. Lohse, V. Patzelová, M. Mägi, and E. Lippmaa, *Zeolites*, 1983, 3, 239.

102. V. Bosácek, D. Freude, T. Fröhlich, H. Pfeifer, and H. Schmiedel, *J. Colloid Interface Sci.*, 1982, 85, 502.

103. D. Freude, T. Fröhlich, H. Pfeifer, and G. Scheler, *Zeolites*, 1983, 3, 171.

104. D. Freude, T. Fröhlich, M. Hunger, H. Pfeifer, and G. Scheler, *Chem. Phys. Lett.*, 1983, 98, 263.

105. D. Freude, M. Hunger, and H. Pfeifer, *Chem. Phys. Lett.*, 1982, 91, 307.

106. D.R. Corbin, R.D. Farlee, and G.D. Stucky, *Inorg. Chem.*, 1984, 23, 2920.

107. D. Freude, J. Haase, H. Pfeifer, D. Prager, and G. Scheler, *Chem. Phys. Lett.*, 1985, 114, 143.

108. M. Pruski, H. Ernst, H. Pfeifer, and B. Staudte, *Chem. Phys. Lett.*, 1985, 119, 412.

109. T.M. Duncan and C. Dybowski, *Surf. Sci. Reports*, 1981, 1, 157.

110. (a). J.B. Nagy, G. Engelhardt, and D. Michel, *Adv. Colloid Interface Sci.*, 1985, 23, 67; (b). H. Pfeifer, D. Freude, and M. Hunger, *Zeolites*, 1985, 5, 274.

111. D. Freude, M. Hunger, and H. Pfeifer, *Chem. Phys. Lett.*, 1982, 91, 307.

112. K.F.M.G.J. Scholle, A.P.M. Kentgens, W.S. Veeman, P. Frenken, and G.P.M. van der Velden, *J. Phys. Chem.*, 1984, 88, 5.

113. K.F.M.G.J. Scholle, W.S. Veeman, J.G. Post, and J.H.C. van Hooff, *Zeolites*, 1983, 3, 214.

114. D. Michel, A. Germanus, D. Scheller, and B. Thomas, *Z. Phys. Chem. (Leipzig)*, 1981, 262, 113.

115. D. Michel, A. Germanus, and H. Pfeifer, *J. Chem. Soc., Faraday Trans. 1*, 1982, 78, 237.

116. I. Jünger, W. Meiler, and H. Pfeifer, *Zeolites*, 1982, 2, 310.

117. J.H. Lunsford, W.P. Rothwell, and W.J. Shen, *J. Am. Chem. Soc.*, 1985, 107, 1540.

118. J.B. Utterhoeven, L.G. Christner, and W.K. Hall, *J. Chem. Phys.*, 1965, 69, 2177.

119. R.D. Shannon, K.H. Gardner, R.H. Staley, G. Bergeret, P. Gallezot, and A. Auroux, *J. Phys. Chem.*, 1985, 89, 4778.

120. H.K. Beyer and I. Belenykaja, in "Catalysis by Zeolites", ed. B. Imelik *et al.*, Elsevier, Amsterdam, 1980, p. 203.

121. U. Lohse, H. Stack, H. Thamm, W. Schirmer, A.A. Isirikjan, N.I. Regent, and M.M. Dubinin, *Z. Anorg. Allg. Chem.*, 1980, 460, 179.

122. J. Klinowski, J.M. Thomas, M. Audier, S. Vasudevan, C.A. Fyfe, and J.S. Hartman, *J. Chem. Soc., Chem. Commun.*, 1981, 570.

123. J.Klinowski, J.M. Thomas, C.A. Fyfe, G.C. Gobbi, and J.S. Hartman, *Inorg. Chem.*, 1983, 22, 63.

124. J. Klinowski, J.M. Thomas, M.W. Anderson, C.A. Fyfe, and G.C. Gobbi, *Zeolites*, 1983, 3, 5.

125. J. Klinowski, C.A. Fyfe, and G.C. Gobbi, *J. Chem. Soc., Faraday Trans. 1*, 1985, 81, 3003.

126. G.R. Hays, W.A. van Erp, N.C.M. Alma, P.A. Couperus, R. Huis, and A.E. Wilson, *Zeolites*, 1984, 4, 377.

127. H.K. Beyer, I.M. Belenykaja, F. Hange, M. Tielen, P.J. Grobet, and P.A. Jacobs, *J. Chem. Soc., Faraday Trans. 1*, 1985, 81, 2889.

128. P.J. Grobet, P.A. Jacobs, and H.K. Beyer, *Zeolites*, 1986, 6, 47.

129. C.A. Fyfe, G.C. Gobbi, and G.J. Kennedy, *J. Phys. Chem.*, 1984, 88, 3248.

130. C.A. Fyfe, G.J. Kennedy, G.T. Kokotailo, and C.T. de Schutter, *J. Chem. Soc., Chem. Commun.*, 1984, 1093.

131. J. Scherzer, ACS Symposium Series, 1984, vol. 248, p. 157.

132. D.W. Breck and G.W. Skeels, Proceedings of the Fifth International Conference on Zeolites, ed. L.V.C. Rees, Heyden, London, 1980, p. 335.

133. D.W. Breck and G.W. Skeels, Proceedings of the Sixth International Congress on Catalysis, Heyden, London, 1977, vol. 2, p. 645.

134. G. Engelhardt and U. Lohse, *J. Catal.*, 1984, 88, 513.

135. C.D. Chang, C.T.-W. Chu, J.N. Maile, R.F. Bridger, and R.B. Calvert, *J. Am. Chem. Soc.*, 1984, 106, 8143.

136. R.M. Dessau and G.K. Kerr, *Zeolites*, 1984, 4, 315.

137. M.W. Anderson, J. Klinowski, and X. Liu, *J. Chem. Soc., Chem. Commun.*, 1984, 1596.

138. D.S. Shihabi, W.E. Garwood, P. Chu, J.N. Miale, R.M. Lago, C.T.-W. Chu, and C.D. Chang, *J. Catal.*, 1985, 93, 471.

139. C.D. Chang, S.D. Hellring, J.N. Miale, and K.D. Schmidt, *J. Chem. Soc., Faraday Trans. 1*, 1985, 81, 2215.

140. G. Engelhardt, B. Fahlke, M. Mägi, and E. Lippmaa, *Zeolites*, 1983, 3, 292.

141. G. Engelhardt, B. Fahlke, M. Mägi, and E. Lippmaa, *Zeolites*, 1985, 5, 49.

142. K.F.M.G.J. Scholle, W.S. Veeman, P. Frenken, and G.P.M. van der Velden, *J. Phys. Chem.*, 1984, 88, 3395.

143. K.F.M.G.J. Scholle, W.S. Veeman, P. Frenken, and G.P.M. van der Velden, *Appl. Catal.*, 1985, 17, 233.

144. G. Boxhoorn, R.A. van Santen, W.A. van Erp, G.R. Hays, R. Huis, and A.D.H. Clague, *J. Chem. Soc., Chem. Commun.*, 1982, 264.

145. J.B. Nagy, Z. Gabelica, and E.G. Derouane, *Zeolites*, 1983, 3, 43.

146. R.H. Jarman and M.T. Melchior, *J. Chem. Soc., Chem. Commun.*, 1984, 414.

147. M.T. Melchior, D.E.W. Vaughan, A.J. Jacobson, and R.H. Jarman, presented at the 26th. Rocky Mountain Conference, 1984.

148. H. Lechert, ACS Advances in Chemistry Series, "Molecular Sieves", Washington, 1973, p. 74.

149. H. Lechert, and H.W. Henneke, ACS Symposium Series No. 40, "Molecular Sieves II", 1977, p. 53.

150. H. Lechert, *Catal. Rev.*, 1976, 14, 1.

151. D. Freude, A. Hauser, H. Pankau, and H. Schmiedel, Z. *Phys. Chemie (Leipzig)*, 1972, 251, 13.

152. D. Freude, U. Lohse, H. Pfeifer, W. Schirmer, H. Schmiedel, and H. Stack, Z. *Phys. Chem. (Leipzig)*, 1974, 255, 443.

153. G.W. West, *Zeolites*, 1981, 1, 150.

154. W.D. Basler, *Coll. Surf.*, 1984, 12, 59.

155. M. Hunger, Z. *Phys. Chemie (Leipzig)*, 1985, 266, 135.

156. M.T. Melchior, D.E.W. Vaughan, A.J. Jacobson, and C.F. Pectroski, Proceedings of the Sixth International Zeolite Conference, ed. D. Olson and A. Bisio, Butterworths, Guildford, 1984, p. 684.

157. W.D. Basler, *J. Chem. Phys.*, 1985, 82, 5297.

158. H.A. Resing, *Advances in Molecular Relaxation Processes*, 1967-1968, 1, 109.

159. K.J. Packer, *Prog. Nucl. Magn. Reson. Spectrosc.*, 1967, 3, 87.

160. H.A. Resing, *Advances in Molecular Relaxation Processes*, 1972, 3, 199.

161. H. Pfeifer, in "NMR: Basic Principles and Progress", ed. P. Diehl, E. Fluck, and R. Kosfeld, Springer-Verlag, Berlin, vol. 7, p. 53.

162. H.A. Resing and J.K. Thompson, "Molecular Sieve Zeolites I", ACS Advances in Chemistry Series No. 101, 1971, p. 473.

163. H. Pfeifer, A. Gutsze, and S.P. Zhdanov, *Z. Phys. Chem. (Leipzig)*, 1976, 275, 721 and 735.

164. E.B. Whipple, P.J. Green, M. Ruta, and R.L. Bujalski, *J. Phys. Chem.*, 1976, 80, 1350.

165. P.H. Kasai and P.M. Jones, *J. Mol. Catal.*, 1984, 27, 81.

166. D. Deininger and D. Michel, *Wiss. Z. Karl Marx Univ. Leipzig, Math. Naturwiss. Reihe*, 1973, 22, 551.

167. D. Michel, *Z. Phys. Chem. (Leipzig)*, 1973, 252, 263.

168. D. Michel, *Surf. Sci.*, 1974, 42, 453.

169. D. Freude, H. Pfeifer, W. Ploss, and B. Staudte, *J. Mol. Catal.*, 1981, 12, 1.

170. T. Ito and J.P. Fraissard, ref. 131, p. 510.

171. L.-C. de Menorval, T. Ito, and J.P. Fraissard, *J. Chem. Soc., Faraday Trans. 1*, 1982, 78, 403.

172. J.A. Ripmeester, *J. Am. Chem. Soc.*, 1982, 104, 289.

173. J.A. Ripmeester, *J. Magn. Reson.*, 1984, 56, 247.

174. L.-C. de Menorval, J. Fraissard, T. Ito, and M. Primet, *J. Chem. Soc., Faraday Trans. 1*, 1985, 81, 2855.

175. M. Primet, L.-C. de Menorval, J. Fraissard, and T. Ito, *J. Chem. Soc., Faraday Trans. 1*, 1985, 81, 2867.

176. T. Ito and H. Mori, *Acta Crystallogr.*, , 1953, 6, 24.

177. C. Dunbar and F. Machatschki, *Z. Kristallogr.*, 1930, 76, 133.

178. G. Johansson, *Acta Crystallogr.*, , 1959, 12, 522.

179. E.L. Muetterties, "The Chemistry of Boron and its Compounds", Wiley and Sons, New York, 1967.

180. R.M. Adams, "Boron, Metallic Boron Compounds, and Boranes", Interscience, New York, 1964.

181. D. McConnell, *Am. Mineral.*, 1952, 37, 609.

182. P.J. Dunn and D.E. Appleman, *Mineral. Mag.*, 1977, 41, 437.

183. J. Ward, Ref. 132. p. 3.

184. J.A. Rabo, "Zeolite Chemistry and Catalysis", ACS Monograph, Washington D.C., 1976, p. 118.

185. L. Pauling, "The Nature of the Chemical Bond", Cornell University Press, third. ed..

186. K. Tanabe, *Catal. Sci. Tech.*, 1981, 2, 232.

187. M.R. Klotz, U.S.P.4 268 420/1981.

188. L. Marosi, J. Stabenow, and M. Schwarzmann, E.P.Appl.010 572/ 1980.

189. M.R. Klotz, U.S.P.4 405 504/1983.

190. M. Taramasso, G. Perego, and B. Notari, B.P.Appl.2 071 071/ 1981.

191. M. Taramasso, G. Manara, V. Fattore, and B. Notari, B.P.Appl.2 024 790/1980.

192. M. Tielen, M. Ceelen, and P.A. Jacobs, Proceedings of Conference, Hungary, 1985, pp. 1-18.

193. A. Cotton and G. Wilkinson, "Advanced Inorganic Chemistry", Interscience, New York, Third Edition, p. 52.

194. R.D. Shannon, *Acta Crystallogr.*, , 1976, B32, 751.

195. K.G. Ione, L.A. Vostrikova, and V.M. Mastikhin, *J. Mol. Catal.*, 1985, 31, 355.

196. V.N. Romannikov, L.S. Chumachenko, V.M. Mastikhin, and K.G. Ione, *J. Catal.*, 1985, 94, 508.

197. B.L. Meyers, S.R. Ely, N.A. Kutz, J.A. Kaduk, and E. van der Bossche, *J. Catal.*, 1985, 91, 352.

198. B.D. Cullity, "Elements of X-Ray Diffraction", Addison-Wesley, Reading, Mass., 1967, p. 352.

199. J.V. Smith, *Acta Crystallogr.*, , 1954, 7, 479.

200. D.E. Appleman and J.R. Clark, *Am. Mineral.*, 1965, 59, 1827.

201. Ref. 30, p. 293.

202. J. Krogh-Moe, *Acta Crystallogr.*, 1972, B28, 169.

203. S. Meslin and F. Santoni, *Acta Crystallogr.*, 1972, B28, 3559.

204. E.M. Flanigen, ref. 184, p. 80.

205. Z. Gabelica, J.B. Nagy, P. Bodart, and G.Debras, *Chem. Lett.*, 1984, 1059.

206. Z. Gabelica, G. Debras, and J.B. Nagy, *Stud. Surf. Sci. Catal.*, 1984, 19, 113.

207. K.F.M.G.J. Scholle and W.S. Veeman, *Zeolites*, 1985, 5, 118.

208. L.A. Vostrikova, K.G. Ione, V.M. Mastikhin, and A.V. Petrova, *React. Kinet. Catal. Lett.*, 1984, 26, 291.

209. E.G. Derouane, L. Baltusis, R.M. Dessau, and K.D. Schmitt, in "Catalysis by Acids and Bases", ed. B. Imelik, Elsevier, Amsterdam, 1985, p. 135.

210. C.T.-W. Chu, G.H. Kuehl, R.M. Lago, and C.D. Chang, *J. Catal.*, 1985, 93, 451.

211. C.T.-W. Chu and C.D. Chang, *J. Phys. Chem.*, 1985, 89, 1569.

212. M.G. Howden, *Zeolites*, 1985, 5, 334.

213. W.W. Kaeding, C.T.-W. Chu, W.B. Young, B. Weinstein, and S.A. Butler, *J. Catal.*, 1981, 67, 159.

214. E.G. Derouane, S. Detremmerie, Z. Gabelica, and N. Blom, *Appl. Catal.*, 1981, 1, 201.

215. W.J. Dell, P.J. Bray, and S.Z. Xiao, *J. Non-Cryst. Solids*, 1983, 58, 1, and *op. cit.*.

216. B.E. Mann, "NMR and the Periodic Table", ed. R.K. Harris and B.E. Mann, Academic Press, London, 1978, p. 92.

217. G. Artoli, J.J. Pluth, and J.V. Smith, *Acta Crystallogr.*, 1984, C40, 214.

218. E.M. Flanigen and R.W. Grose, ref. 162, p. 76.

219. D. McConnell, *Min. Mag.*, 1964, 33, 799.

220. L.D. Rolleman and E.W. Valyocsik, *Inorg. Synth.*, 1983, 22, 61.

221. S.T. Wilson, B.M. Lok, C.A. Messina, T.R. Cannan, and E.M. Flanigen, *J. Am. Chem. Soc.*, 1982, 104, 1146.

222. S.T. Wilson, B.M. Lok, E.M. Flanigen, U.S.P.4 310 440/1982.

223. S.T. Wilson, B.M. Lok, C.A. Messina, T.R. Cannan, and E.M. Flanigen, "Intrazeolite Chemistry", ACS Symposium Series, 1983, vol. 218, p. 79.

224. B.M. Lok, C.A. Messina, R.L. Patton, R.T. Gajek, T.R. Cannan, and E.M. Flanigen, *J. Am. Chem. Soc.*, 1984, 106, 6092.

225. B.M. Lok, C.A. Messina, R.L. Patton, R.T. Gajek, T.R. Cannan, and E.M. Flanigen, U.S.P.4 440 871/1984.

226. E.M. Flanigen, B.M. Lok, R.L. Patton, and S.T. Wilson, E.P.Appl.0 158 976/1985.

227. J.M. Bennett, J.P. Cohen, E.M. Flanigen, J.J. Pluth, and J.V. Smith, ref. 223, p. 109.

228. J.B. Parise, *J. Chem. Soc., Chem. Commun.*, 1984, 1449.

229. J.B. Parise, *Acta Crystallogr.*, 1984, C40, 1641.

230. J.J. Pluth, J.V. Smith, and J.M. Bennett, *Acta Crystallogr.*, 1986, C42, 2008.

231. J.J. Pluth, J.V. Smith, J.M. Bennett, and J.P. Cohen, *Acta Crystallogr.*, 1986, C42, 283.

232. J.B. Parise, *Acta Crystallogr.*, 1985, C41, 515.

233. J.M. Bennett, J.M. Cohen, G. Artioli, J.J. Pluth, and J.V. Smith, *Inorg. Chem.*, 1985, 24, 188.

234. C.S. Blackwell and R.L. Patton, *J. Phys. Chem.*, 1984, 88, 6135.

235. D. Müller, E. Jahn, B. Fahlke, G. Ladwig, and U. Haubenreisser, *Zeolites*, 1985, 5, 53.

236. D. Müller, E. Jahn, G. Ladwig, and U. Haubenreisser, *Chem. Phys. Lett.*, 1984, 109, 332.

237. M. Ito, Y. Shimoyama, Y. Saito, Y. Tsurita, and M. Otake, *Acta Crystallogr.*, 1985, C41, 1698.

238. I.P. Appleyard, R.K. Harris, and F.R. Fitch, *Chem. Lett.*, 1985, 1747.

239. G.C. Bond, M.R. Gelsthorpe, K.S.W. Sing, and C.R. Theocharis, *J. Chem. Soc., Chem. Commun.*, 1985, 1056.

240. N.J. Tapp, N.B. Milestone, and L.J. Wright, *J. Chem. Soc., Chem. Commun.*, 1985, 1801.

241. R.S. Aujla, R.K. Harris, K.J. Packer, N. Parameswaran, B.J. Say, A. Bunn, and M.E.A. Cudby, *Polym. Bull.*, 1982, 8, 253.

242. R.K. Harris, in ref. 7, p. 81.

243. J.S. Frye and G.E. Maciel, *J. Magn. Reson.*, 1982, 48, 125.

244. R.K. Harris, *Analyst*, 1985, 110, 649.

245. J. Schaefer and E.O. Stejskal, *J. Magn. Reson.*, 1974, 15, 173.

246. C.H.A. Seiler, G.W. Feigenson, S.I.Chan, and M.-C. Hsu, *J. Am. Chem. Soc.*, 1972, 94, 2535.

247. J.H. Davis, K.R. Jeffrey, M. Bloom, and M.I. Valic, *Chem. Phys. Lett.*, 1976, 42, 390.

248. D. Canet, J. Brondeau, J.P. Marechal, and B. Robin-Cherbier, *Org. Magn. Reson.*, 1982, 20, 51.

249. S.L. Patt, *J. Magn. Reson.*, 1982, 49, 161.

250. J. Cox, Ph.D. Thesis, 1984, University of East Anglia.

251. M.J. Hey, A. Nock, R. Rudham, I.P. Appleyard, G.A. Haines, and R.K.Harris, accepted for publication in *J. Chem. Soc., Faraday Trans. 1*, 1986.

252. P. Richat, R. Beaumont, and D. Berthoneuf, *J. Chem. Soc., Faraday Trans. 1*, 1974, 70, 1402.

253. P.A. Jacobs, "Carboniogenic Activity of Zeolites", Amsterdam, 1977, p. 99.

254. P.A. Jacobs, M. Tielen, amd J.B. Uytterhoeven, *J. Catalysis*, 1977, 50, 98.

255. R. Rudham and A. Stockwell, *Acta Phys. Chem.*, 1978, 26, 281.

256. R. Rudham and A. Stockwell, ref. 120, p. 113.

257. N.C.M. Alma, personal communication, 1984.

258. V.H. Schmidt, "Pulsed Magnetic and Optical Resonance", Proceedings of the Ampere International Summer School II, September, 1971, ed. R. Blinc, Ljublijana, Yugoslavia, pp. 75-83.

259. K.C. Lal and H.E. Petch, *J. Chem. Phys.*, 1965, 43, 178.

260. P.J. Bray, J.O. Edwards, J.G. O'Keefe, V.F. Ross, and I. Tatsuzaki, *J. Chem. Phys.*, 1961, 35, 435

261. G.L. Turner, K.A. Smith, R.J. Kirkpatrick, and E. Oldfield, *J. Magn. Reson.*, 1986, 67, 544.

262. E. Oldfield, R.A. Kinsey, K.A. Smith, J.A. Nichols, and R.J. Kirkpatrick, *J. Magn. Reson.*, 1983, 51, 325.

263. E.G. Derouane, M. Mestdagh, and L. Vielvoye, *J. Catalysis*, 1974, 33, 169.

264. J. Mélon, *Ann. Soc. Geol. Belg.*, 1942, 66, 53.

265. A.M. Blount, *Am. Mineral.*, 1974, 59, 41.

266. Z. Gabelica, private communication.

267. D. Müller, *Ann. Physik (Leipzig)*, 1983, 39, 451.

268. I.P. Appleyard, R.K. Harris, and F.R. Fitch, accepted for publication in *Zeolites*.